Universiteit
Leiden
The Netherlands

# Design, synthesis and application of paramagnetic NMR ptobes for protein strucutre studies

Miao, Q.

**Citation**

Miao, Q. (2019, November 28). *Design, synthesis and application of paramagnetic NMR ptobes for protein strucutre studies*. Retrieved from https://hdl.handle.net/1887/81086

| | |
|---|---|
| Version: | Publisher's Version |
| License: | Licence agreement concerning inclusion of doctoral thesis in the Institutional Repository of the University of Leiden |
| Downloaded from: | https://hdl.handle.net/1887/81086 |

**Note:** To cite this publication please use the final published version (if applicable).

Cover Page

Universiteit Leiden

The handle http://hdl.handle.net/1887/81086 holds various files of this Leiden University dissertation.

**Author**: Miao, Q.
**Title**: Design, synthesis and application of paramagnetic NMR ptobes for protein strucutre studies
**Issue Date**: 2019-11-28

# Design, synthesis and application of paramagnetic probes for protein structure studies

Proefschrift

ter verkrijging van
de graad van Doctor aan de Universiteit Leiden,
op gezag van Rector Magnificus prof.mr. C.J.J.M. Stolker,
volgens besluit van het College voor Promoties
te verdedigen op donderdag 28 november 2019
klokke 10:00

door

Qing Miao

geboren te Xi'an, China in 1988

**Design, synthesis and application of paramagnetic probes for protein structure studies**

**Qing Miao**

Doctoral thesis, Leiden University, 2019

Cover image: Model of Co(II)-TraNP1 attached to T4Lys and structures of TraNP1, TraNP2 and HMDOTA (front cover)

Model of T4Lys tagged with Gd(III)-CLaNP13 (back cover)

Printed by RIDDERPRINT

**Promotor:** Prof. Dr. M. Ubbink

**Copromotor:** Dr. M. Overhand

| | |
|---|---|
| **Promotiecommissie:** | Prof. Dr. H. S. Overkleeft (voorzitter) |
| | Prof. Dr. G. A. van der Marel (secretaris) |
| **Overige commissieleden:** | Prof. Dr. M. Zweckstetter (University of Göttingen, Duitsland) |
| | Prof. Dr. S. Hirota (Nara Institute of Science and Technology, Japan) |
| | Dr. M. I. Huber |

The research described in this thesis was performed in the Macromolecular Biochemistry Department of Leiden Institute of Chemistry at the University Leiden in Leiden, the Netherlands.

The research described in this thesis was financially supported by the Chinese Scholarship Council (No. 201506870013).

路漫漫其修远兮，吾将上下而求索

*The road ahead will be long, I shall search*

-屈原(Quyuan)，《楚辞·离骚》

*To my family and friends*

# Contents

***List of abbreviations*** ..... ***8***

***List of symbols*** ..... ***10***

***Chapter I***

*Introduction and thesis outline* ..... ***13***

***Chapter II***

*A double armed, hydrophilic, transition metal complex as paramagnetic NMR probe* ..... ***55***

***Chapter III***

*A hydrophilic paramagnetic NMR probe for lanthanoid ions and 3d-block ions* ..... ***81***

***Chapter IV***

*Rigidified and hydrophilic DOTA-like lanthanoid ligands: Design, synthesis, NMR studies and molecular modeling* ..... ***93***

***Chapter V***

*A two-armed probe for in-cell DEER measurements on protein* ..... ***121***

***Chapter VI***

*General discussion, conclusions and prospects* ..... ***141***

***English summary*** ..... ***147***

***Nederlandse samenvatting*** ..... ***149***

***Appendices*** ..... ***151***

***List of publications*** ..... ***166***

***Curriculum vitae*** ..... ***167***

# List of abbreviations

| | |
|---|---|
| TraNP | transition metal ion NMR probe |
| CLaNP | caged lanthanoid NMR probe |
| PCS | pseudocontact shifts |
| RDC | residue dipolar couplings |
| PRE | paramagnetic relaxation enhancements |
| NOE | nuclear Overhauser effect |
| BMS | bulk magnetic susceptibility shifts |
| T4Lys | T4 Lysozyme |
| BCX | Bacillus circulans xylanase |
| Cys | cysteine |
| His | histidine |
| DCM | dichloromethane |
| MeOH | methanol |
| EtOH | ethanol |
| ACN | acetonitrile |
| DMF | *N*,*N*-dimenthylformamide |
| DMSO | dimethylsulfoxide |
| TFA | trifluoroacetic acid |
| DIPEA | diisopropylethyl amine |
| Boc | *tert*-butyloxycarbonyl |
| DOTA | 1,4,7,10-tetraazacyclododecane-1,4,7,10-tetraacetate |
| EDTA | ethylenediaminetetraacetic acid |
| DTT | dithiothreitol |
| EDCI | 1-ethyl-3-(3-dimethyl-aminopropyl)-carbodiimide |
| MsCl | methanesulfonylchloride |
| NHS | *N*-hydroxysuccinimide |
| MTSL | (S-(1-oxyl-2,2,5,5-tetramethyl-2,5-dihydro-1H-pyrrol-3-yl)methyl methanesulfonothioate |
| MST | methanethiosulfonate |
| Ln | lanthanoid |
| Ln(III) | lanthanoid +3 ions |
| FTIR | Fourier transform InfraRed |
| HPLC | high performance liquid chromatography |
| HRMS | high resolution mass spectrometry |
| LC-MS | liquid chromatography-mass spectrometry |
| *m/z* | mass-to-charge ratio |
| NMR | nuclear magnetic resonance |
| paraNMR | paramagnetic nuclear magnetic resonance |

| | |
|---|---|
| HSQC | heteronuclear singular quantum correlation |
| COSY | correlation spectroscopy |
| EXSY | exchange spectroscopy |
| MRI | magnetic resonance imaging |
| EPR | electron paramagnetic resonance |
| DEER | double electron–electron resonance |
| SAP | square antiprismatic |
| TSAP | twisted square antiprismatic |
| Hz | hertz |
| **δ** | chemical shift |
| *J* | coupling constant |
| Å | Ångström |
| *aq* | aqueous |
| calcd. | calculated |
| K | kelvin |
| Da | dalton |
| equiv. | molar equivalent |
| h | hour(s) |
| min | minute(s) |
| ms | millisecond(s) |
| ppm | parts per million |
| s | singlet |
| d | double |
| dd | double doublet |
| t | triplet |
| q | quartet |
| m | multiplet |
| br | broad |
| rt | room temperature |
| sat. | saturated |
| eq. | equation |
| TLC | thin layer chromatography |
| o/n | over night |

# List of symbols

| | |
|---|---|
| $B_0$ | magnetic field |
| $\chi$ | magnetic susceptibility tensor |
| $\chi_x$ | susceptibility values along the tensor framework X axes |
| $\chi_y$ | susceptibility values along the tensor framework Y axes |
| $\chi_z$ | susceptibility values along the tensor framework Z axes |
| $\Delta\chi$ | anistropic magnetic susceptibility tensor |
| $\Delta\chi_{ax}$ | axial components of the $\Delta\chi$-tensor |
| $\Delta\chi_{rh}$ | rhombic components of the $\Delta\chi$-tensor |
| $r_{IM}$ | distance between the nucleus and paramagnetic center |
| I | observed nuclei I |
| J | observed nuclei J |
| $\boldsymbol{\gamma}_I$ | nuclear gyromagnetic ratio of nucleus I |
| $\boldsymbol{\gamma}_J$ | nuclear gyromagnetic ratio of nucleus J |
| T | absolute temperature |
| h | Planck constants |
| $k_B$ | Boltzmann constants |
| $r_{IJ}$ | internuclear distance |
| $R_{1,dip}^{para}$ | longitudinal nuclear relaxation rate due to Solomon mechanism |
| $R_{2,dip}^{para}$ | transverse nuclear relaxation rate due to Solomon mechanism |
| $\tau_c$ | total correlation time, $\tau_c^{-1} = \tau_r^{-1} + \tau_s^{-1}$ |
| $\tau_r$ | rotational correlation time of the molecule, |
| $\tau_s$ | electronic relaxation time |
| S | total electron spin quantum number |
| $\mu_B$ | the Bohr magneton |
| $\boldsymbol{\omega}_I$ | the Larmor frequency of the nucleus |
| $\mu_0$ | the permeability of vacuum |
| $R_{2,curie}^{para}$ | transverse nuclear relaxation rate due to Curie mechanism |
| $g_e$ | electronic g-factor |
| h | Plank's constant |
| $I_{dia}$ | peak intensity in the diamagnetic spectrum |
| $I_{para}$ | peak intensity in the paramagnetic spectrum |
| $I_{para}/I_{dia}$ | intensity ratio |
| $R_{2,para}$ | paramagnetic contribution to the longitudinal relaxation |
| $R_{2,para}$ | diamagnetic contribution to the longitudinal relaxation |
| $\chi_P$ | corrected paramagnetic molar susceptibility |
| $\chi_D$ | diamagnetic susceptibility |
| $\Delta f$ | chemical shift difference of the inert compound in the presence and absence of the paramagnetic compound |

| | |
|---|---|
| C | molar concentration |
| M | molecular mass |

# Chapter I

# Introduction and thesis outline

# *Chapter I*

## 1 Paramagnetic NMR for protein studies

### 1.1 General introduction

Understanding protein structures at the atomic level is essential for investigating protein function. Nuclear magnetic resonance (NMR) is one of the prominent techniques that can obtain structure information with atomic resolution. The NMR observable most frequently used for structure determination is the nuclear Overhauser effect (NOE), which can generate structure information up to 5 Å because it depends on dipolar interactions between protons.[1,2]

Longer distance interactions were found by the study of metalloproteins, containing unpaired electrons.[3,4] The interactions between the unpaired electron and a nucleus are referred to as paramagnetic effects, and thus the studies of these effects by NMR are called paramagnetic NMR (paraNMR). The magnetic moment of the unpaired electron is about 658 times stronger than that of a proton. Consequently, the paramagnetic effects can be observed over distances up to 100 Å, offering long-range distance information for structural studies. Because of the anisotropic properties of paramagnetic effects, they provide not only distance but also orientation restraints.

Paramagnetic effects depend on the magnetic susceptibility ($\chi$) as well as the relaxation time of the unpaired electrons. The magnetic susceptibility can either be isotropic or anisotropic and is the cause of peak shifts in the NMR spectrum by paramagnetism, called the hyperfine shift. It consists of two parts, the contact shift and pseudocontact shift (PCS). The contact shift is a consequence of the delocalization of unpaired spin density on the nucleus and is thus only observed for nuclei very close to the paramagnetic center. If the $\chi$ tensor has an anisotropic component (described by the $\Delta\chi$-tensor), also the dipolar interaction between the (time-averaged) unpaired electron spin(s) and the nucleus leads to shifts, the pseudocontact shift (PCS). The dipolar interaction can be quite strong and can cause shifts for nuclei up to 100 Å away from the electron spin, providing long-range distance and orientation information. For systems with an anisotropic magnetic susceptibility, molecules in solution will be partially aligned in a magnetic field, resulting in residual dipolar couplings (RDC) between nuclei, for example $^{1}H$ and $^{15}N$ in amide groups. Such alignment affects the entire molecule equally, assuming it is rigid, so the location of the paramagnetic center relative to the nucleus is irrelevant. Thus, RDC is independent of the distance between the nuclei and the electron spin, and is determined by the size and orientation of the alignment tensor ($\Delta\chi$-tensor).

Paramagnetic centers, both with isotropic and anisotropic magnetic susceptibilities, also cause enhanced relaxation of nuclear spins, a phenomenon called paramagnetic relaxation enhancement (PRE). It decreases with the sixth power of the distance between the unpaired electron and nucleus. The large size of the PRE at short distances and the strong distance dependence together make the PRE a sensitive tool

to detect minor states in which the nucleus gets close to the unpaired electron, e.g. in dynamic proteins. PRE depends on the electronic relaxation time and the number of the unpaired electrons. Fast electronic relaxation (> $10^{11}$ $s^{-1}$) leads to weaker PRE than slow electronic relaxation (~ $10^{9}$ $s^{-1}$), because the latter are in the range of nuclear transitions (Larmor frequencies). Two types of relaxation mechanism, Solomon relaxation[5,6] and Curie relaxation[7,8], are distinguished. In general, the Solomon mechanism is dominant for electron spins with a long relaxation time and it is the main contribution to PRE in isotropic paramagnetic species. The Curie mechanism is dominant for electrons that have a fast relaxation time, and it is the main contribution to PRE in anisotropic paramagnetic systems.

Many transition metal ions contain unpaired electrons, leading to paramagnetism. The paramagnetism of 3d-block and 4f-block ions is the best studied.[9,10] Manganese(II) has an isotropic $\chi$ tensor and a long electronic relaxation time, thus causes no PCS but strong PRE. High-spin cobalt(II) can generate large PCS with weak PRE, compared with other 3d-block ions. Iron is stable in +2 and +3 oxidation states. In the case of iron(II), it can be paramagnetic or diamagnetic, depending on its ligands. For iron(III), the paramagentism can be either large or small, depending on the coordination environment. The 4f-block elements are referred to as lanthanoids, with the general symbol Ln. Unlike 3d-block ions, lanthanoids are not found in biological processes. Lutetium(III) and lanthanum(III) have no unpaired electrons, the rest of Ln(III) series is paramagnetic. Gadolinium(III) has a strong isotropic magnetic susceptibility, with seven unpaired electrons, yielding no PCS but very strong PRE. Other Ln(III) have anisotropic susceptibilities of varying strength, causing PCS and PRE. Not only transition ions have unpaired electrons, radicals can also be used as paramagnetic center. Stable nitroxide radicals are often used. They do not cause PCS, but yield sizable PRE.

All the paramagnetic effects are observed by comparison with a diamagnetic species. Therefore, it is very important to use a diamagnetic reference that is as similar to the paramagnetic sample as possible. Lanthanoids are chemically similar, thus, the diamagnetic reference can be easily obtained by substitution of the paramagnetic ion with Lu(III) or La(III). Although nitroxide is stable under common conditions, it can be reduced with ascorbic acid to obtain diamagnetic reference. Alternatively, diamagnetic control probes can be used that are chemically similar to the nitroxide probes. Because 3d-block ions usually have different properties, no perfect diamagnetic reference exists. However, zinc(II) is commonly used diamagnetic reference for cobalt(II) and manganese(II), because charge and size are similar.

### 1.2 Paramagnetic effects

Three types of paramagnetic effects are most frequently used, PCS, RDC and PRE. The first two types are measured as peak shifting (ppm) and splitting (Hz), respectively. PCS

and RDC are dependent on the size of the Δχ-tensor, which is related to the electron g-tensor. Generally, a paramagnetic center with more unpaired electrons will generate stronger PCS and RDC. PRE can be observed in any paramagnetic system as line-broadening and is related to the electronic relaxation time, $\tau_s$, which is the longitudinal relaxation time of the unpaired electron, as well as the rotational correlation time of the molecule, $\tau_r$.

### 1.2.1 The pseudocontact shift (PCS)

The PCS can easily be measured with high accuracy. It can be described by the position of the nucleus in the frame defined by the Δχ-tensor, equation 1.1 and Figure 1.1 A:

$$\mathrm{PCS} = \frac{1}{12\pi r_{IM}^3}\left[\Delta\chi_{ax}(3cos^2\theta - 1) + \frac{3}{2}\Delta\chi_{rh}(sin^2\theta cos2\Omega)\right] \quad 1.1$$

$$\Delta\chi_{ax} = \chi_z - \frac{\chi_x+\chi_y}{2} \quad \text{and} \quad \Delta\chi_{rh} = \chi_x - \chi_y \quad 1.2$$

where $r_{IM}$ is the distance between the unpaired electron and nucleus, θ, and Ω are the polar coordinates of the nucleus with respect to the principal axes of the Δχ-tensor, $\Delta\chi_{ax}$ and $\Delta\chi_{rh}$ are the axial and rhombic components of the Δχ tensor, respectively, as defined by equation 1.2, $\chi_x$, $\chi_y$, and $\chi_z$ are the susceptibility values along the tensor framework axes (Figure 1.1A). Euler angles describe the tensor frame orientation relative to the laboratory frame, e.g. the frame defined in a PDB file. The position of the paramagnetic center, the three Euler angles and the sizes of $\Delta\chi_{ax}$ and $\Delta\chi_{rh}$ are the eight parameters that define the Δχ tensor. They can be obtained by fitting the measured PCS to equation 1.1 with a protein structure. Several software packages[11–14] are available for tensor calculation. The one used in this thesis is Numbat[11]. In principle, one can determine the Δχ tensor with eight PCS, however, to get an accurate result, generally at least three times more PCS are needed.

### 1.2.2 The residual dipolar coupling (RDC)

In isotropic solutions, internuclear dipolar couplings average to zero due to fast molecular tumbling. Partial alignment of a molecule in a magnetic field will cause the nucleus to experience RDC due to dipolar coupling with nearby nuclei.[15] The RDC caused by alignment due to a paramagnetic center with anisotropic magnetic susceptibility is described by equation 1.3[3,16] and Figure 1.1 B

$$RDC = -\frac{B_0^2}{15k_BT}\frac{\gamma_I\gamma_J h}{16\pi^3 r_{IJ}^3}\left[\Delta\chi_{ax}(3cos^2\theta - 1) + \frac{3}{2}\Delta\chi_{rh}sin^2\theta cos2\Omega\right] \quad 1.3$$

where I and J are the observed nuclei, and $\gamma_I$ and $\gamma_J$ are the nuclear gyromagnetic ratio of nucleus I and J, respectively. θ and Ω determine the orientation of the I–J vector relative to Δχ tensor (Figure 1.1B), $r_{IJ}$ is the internuclear distance, T is the absolute temperature, h and $k_B$ are the Planck and Boltzmann constants, respectively. One can see that RDC yields information about the orientation of the internuclear vector in the frame of the Δχ tensor, but not the distance of the nuclei to the paramagnetic center. Like with PCS, the

tensor frame can be fitted on the basis of observed RDC and a protein structure, or if the tensor frame is already known, the RDC can be used to establish a bond vector orientation within a protein structure. Also, mobility of the bond vector is readily detected by reduction of the RDC due to averaging. RDC thus find application in the study of protein dynamics.

### 1.2.3 The paramagnetic relaxation enhancement (PRE)

Spin-spin interactions are a dominant source of nuclear spin relaxation. Like with nuclear spin interactions, also electron-nuclear spin interactions contribute to relaxation. Apart from the dipole-dipole interaction, also the rapid flipping of the electron spin is a source of nuclear relaxation. Two mechanisms, referred to as Solomon mechanism[5,6] and Curie spin mechanism[7,8], cause PRE. Solomon relaxation is caused by the dipole–dipole coupling of the electron spin and nearby nucleus. It is caused by both the rapid electron spin flipping due to the fast longitudinal relaxation and the variation in the dipolar interaction due to molecular tumbling in the magnetic field. It affects both the longitudinal ($R_{1,dip}$) and transverse ($R_{2,dip}$) relaxation rates according to equations 1.4 and 1.5:

$$R_{1,dip}^{para} = \frac{2}{15}\left(\frac{\mu_0}{4\pi}\right)^2 \frac{\gamma_I^2 g_e^2 \mu_B^2 S(S+1)}{r_{IM}^6}\left(\frac{3\tau_c}{1+\omega_I^2\tau_c^2}\right) \qquad 1.4$$

$$R_{2,dip}^{para} = \frac{1}{15}\left(\frac{\mu_0}{4\pi}\right)^2 \frac{\gamma_I^2 g_e^2 \mu_B^2 S(S+1)}{r_{IM}^6}\left(4\tau_c + \frac{3\tau_c}{1+\omega_I^2\tau_c^2}\right)$$

$$\text{and } \tau_c^{-1} = \tau_r^{-1} + \tau_s^{-1} \qquad 1.5$$

Where $R_{1,dip}^{para}$ and $R_{2,dip}^{para}$ are the longitudinal and transverse nuclear relaxation rate, $g_e$ is the electron g-factor, β is the electron Bohr magneton, S is the total electron spins quantum number, $\mu_0$ is the permeability of vacuum and $\omega_I$ the Larmor frequency of the nucleus. For electron spin having slow longitudinal relaxation, such as $Gd^{3+}$ and $Mn^{2+}$,[10,17] the Solomon mechanism is dominant. As the PRE is proportional to the inverse sixth power of $r_{IM}$, it is very sensitive to the change in $r_{IM}$, making it a powerful restraint for the study of lowly populated states or complexes of proteins in solution.[18–20]

Curie spin relaxation is the dipolar coupling between the time-averaged magnetic moment of the unpaired electron(s) with the nucleus. In this case, only the rotational correlation time ($\tau_r$) is a source of time-dependent modulation contributing mostly to transverse ($R_{2,curie}$) relaxation, shown in equation 1.6 (list of the symbols at beginning of this thesis):[9]

$$R_{2,curie}^{para} = \frac{1}{5}\left(\frac{\mu_0}{4\pi}\right)^2 \frac{\omega_I^2 g_e^4 \mu_B^4 S^2(S+1)^2}{(3kT)^2 r_{IM}^6}\left(4\tau_r + \frac{3\tau_r}{1+\omega_I^2\tau_r^2}\right) \qquad 1.6$$

Thus, this type of relaxation is mainly important for large systems in a strong magnetic field, when $\tau_r$ and $\omega_I$ are large.[21]

## 2. Sources of paramagnetism

In this section, a brief overview of the most used paramagnetic resources is presented.

### 2.1 3d-Block transition metal ions

Transition metals in the 3d-block of the periodic table have various oxidation states with different numbers of unpaired electrons occupying the d-orbitals.[23] Thus these cations are great candidates generating various paramagnetic effects. They are frequently found in proteins. It was estimated that more than 25% of the known proteins contain one or more transition metal ions.[24] A heme protein with a low-spin iron(III) was the first example to be studied by paramagnetic NMR.[25] From then on, studies on other transition metal ions in proteins became popular. Among them, iron, cobalt, manganese, copper and nickel ions are found most frequently and those are discussed hereafter.

Transition metal ion complexes of 3d-block elements are stable with 4 to 6 electron donor sites. According to the number of coordination sites, transition metal ions have mainly three types of coordination geometries, tetrahedral, square pyramidal and octahedral (Figure 1.2). The magnetic properties of 3d-block complexes can be strongly affected by the ligands, the environments and the coordination geometries. Some properties are shown in Table 1.1. The unpaired electrons will be partially delocalized to the ligand orbitals, affecting the magnetic properties. Iron is a good example. Fe(III) and

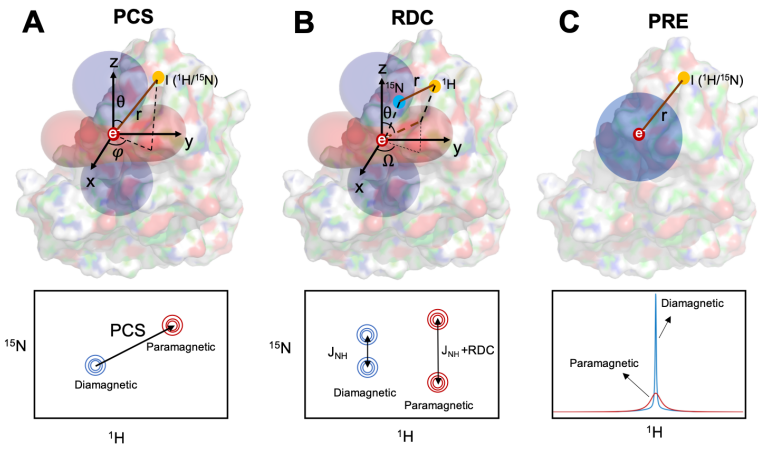


**Figure 1.1** Schematic representation of the paramagnetic effects (adapted from reference [22]). Definitions in a structure (top) and its effect on the NMR spectrum (bottom). **A)** PCS; **B)** RDC; **C)** PRE.

Fe(II) are the most stable and commonly found oxidation states of iron. Both of them have high and low-spin states. With weak axial ligands, Fe(III) is in a high-spin state. With strong ligands, Fe(III) turns into a low-spin state. High-spin Fe(III) contains five unpaired electrons, and its electronic relaxation time can vary from $10^{-9}$ to $10^{-11}$ s.[26,27] Therefore, it can generate sizeable PCS and PRE, depending on the ligands. The magnetic properties of low-spin state Fe(III) are quite different due to its short electronic relaxation time, $<10^{-11}$ s.[26,27] As a result, low-spin Fe(III) mainly generates PCS. Fe(II) has six electrons occupying d-orbitals, so when these electrons are paired, Fe(II) is diamagnetic. Its high-spin state has up to four unpaired electrons with a short electronic relaxation time ($10^{-12}$ s), mainly causing PCS.[23] Proteins containing iron ions have been well studied by paramagnetic NMR, for example cytochrome *c*, rubredoxin and hemoglobin.[28]

Cobalt(II), with an electronic configuration of $3d^7$ can be in a high-spin state containing three unpaired electrons or a low-spin state containing one unpaired electron. However, for low-spin Co(II), the electronic relaxation time is longer than for the high-spin state, thus low-spin Co(II) causes strong PRE and small PCS. In contrast, high-spin Co(II) can generate the largest PCS among 3d-block ions with weak PRE. Manganese (II) harbours one of its five unpaired electrons in each of the d-orbitals and has a long electronic relaxation time, causing the strongest PRE of all 3d-block ions. Copper(II) is the most stable ionic state of copper. There are three types of copper(II) in proteins, depending on its coordination. Consequently, various paramagnetic effects were observed for Cu(II).[29] Cu(II) contains one unpaired electron, generating small PCS, but strong PRE, because of its relatively small $\Delta\chi$ tensor but long electronic relaxation time. Therefore, Cu(II) is outstanding for PRE and it is widely used in electron paramagnetic resonance (EPR).[30,31] The divalent ion of nickel has two unpaired electrons, generating small PCS with sizeable PRE.

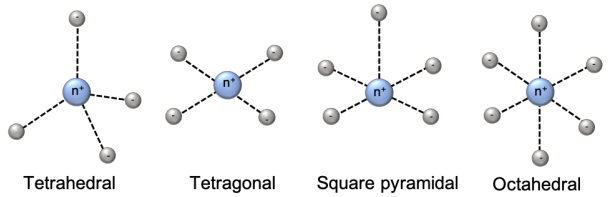


**Figure 1.2** Schematic diagrams of 3d-block ions coordination geometries.

### 2.2 Lanthanoid ions

Lanthanoid ions, especially +3 oxidation ions (Ln(III)), have been used as chemical shift monitors and line broadening agents in NMR for bio-molecules studies since several decades.[32] Their chemical properties are similar because the 4f-orbitals are shielded by 5s and 5p subshells, and thus these electrons are essentially inert in the coordination interactions with the ligands. Thus, complexes that bind Ln(III), generally have similar

affinities for all lanthanoid ions. Consequently, the ions without unpaired electrons, Lu(III) and La(III), are ideal diamagnetic references.

An overview of the paramagnetic properties of paramagnetic lanthanide ions (excluding promethium, which is radioactive) is presented in Table 1.1. Among these ions, Gd(III) has seven unpaired electrons, distributed over each of the f-orbitals, producing an isotropic magnetic susceptibility tensor with a long electronic relaxation time. Therefore, it causes strong PRE. Gd(III) enjoys an increasing popularity in EPR as spin label.[33] The remaining paramagnetic lanthanoid ions generate anisotropic tensors, producing all the paramagnetic effects discussed above. However, the extremely short electronic relaxation times make their PRE effect complicated and rarely studied. In general, Tb(III) and Dy(III) generate the strongest $\Delta\chi$-tensor, causing the largest PCS, Tm(III) and Ho(III) produce medium PCS and sizable PCS can also be observed with Yb(III) and Er(III). Other lanthanoid ions are barely used for protein paramagnetic NMR because the $\Delta\chi$-tensor is weaker.[17]

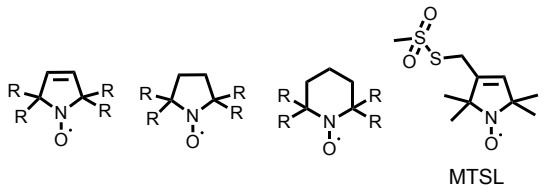


**Figure 1.3** Structure of nitroxides, R represents a bulky group

### 2.3 Nitroxide radicals

Nitroxides are organic molecules with five- or six- membered heterocyclic rings containing a radical that is protected by bulky groups (Figure 1.3). With an unpaired electron and small size, nitroxides are the most frequently used paramagnetic centers in NMR to generate PRE up to 20 Å.[36] This popularity is also due to localized paramagnetic effect of the unpaired electron. The stability of the radical depends on the size of the ring and the α-position substituents. Generally, nitroxides with a five-membered ring are more stable than six-membered one and larger bulky groups at α-position offering stronger steric shielding, increasing the stability. The most applied nitroxide for protein labeling is MTSL (S-(1-oxyl-2,2,5,5-tetramethyl-2,5-dihydro-1H-pyrrol-3-yl)methyl methanesulfonothioate, Figure 1.3), which is commercially available.

## 3 General overview of natural and artificial paramagnetic centers

Paramagnetism of biomolecules can exist naturally or introduced artificially by different strategies. Metalloproteins with paramagnetic ions can readily be studied by paraNMR. For diamagnetic metalloproteins, the diamagnetic center can be replaced by paramagnetic ions. However, not all of the diamagnetic metalloproteins are suitable for metal ion substitution and, obviously, this approach also does not work for non-

**Table 1.1** Magnetic properties of 3d-block and 4f-block ions

| Ion | Conf.[a] | J[b] | $\tau_s$[c] | range[d] | PCS[e] | PRE[e] | RDC[e] |
|---|---|---|---|---|---|---|---|
| $Fe^{3+}$ (HS) | $[Ar]3d^5$ | 5/2 | $10^{-9}$-$10^{-13}$ | 20 | + | ++ | / |
| $Fe^{3+}$ (LS) | $[Ar]3d^5$ | 1/2 | $10^{-11}$-$10^{-13}$ | 15 | ++ | + | / |
| $Mn^{2+}$ | $[Ar]3d^5$ | 5/2 | $10^{-8}$ | 25 | / | ++ | / |
| $Fe^{2+}$ (HS) | $[Ar]3d^6$ | 2 | $10^{-12}$ | 15 | + | + | / |
| $Co^{2+}$ (LS) | $[Ar]3d^7$ | 1/2 | $10^{-9}$-$10^{-10}$ | 20 | + | ++ | / |
| $Co^{2+}$ (HS) | $[Ar]3d^7$ | 3/2 | $10^{-12}$ | 25 | ++ | + | / |
| $Ni^{2+}$ | $[Ar]3d^8$ | 1 | $10^{-10}$-$10^{-12}$ | 15 | + | + | / |
| $Cu^{2+}$ | $[Ar]3d^9$ | 1/2 | $10^{-8}$-$10^{-9}$ | 20 | + | ++ | / |
| $Ce^{3+}$ | $[Xe]4f^1$ | 5/2 | $10^{-13}$ | 10 | + | + | / |
| $Pr^{3+}$ | $[Xe]4f^2$ | 4 | $10^{-13}$ | 20 | + | + | / |
| $Nd^{3+}$ | $[Xe]4f^3$ | 9/2 | $10^{-13}$ | 10 | + | + | / |
| $Sm^{3+}$ | $[Xe]4f^5$ | 5/2 | $10^{-13}$ | 7 | + | + | / |
| $Eu^{3+}$ | $[Xe]4f^6$ | 0 | $10^{-13}$ | 15 | + | + | / |
| $Gd^{3+}$ | $[Xe]4f^7$ | 7/2 | $10^{-8}$ | 25 | / | +++ | / |
| $Tb^{3+}$ | $[Xe]4f^8$ | 6 | $10^{-13}$ | 45 | ++++ | + | +++ |
| $Dy^{3+}$ | $[Xe]4f^9$ | 15/2 | $10^{-13}$ | 45 | ++++ | + | +++ |
| $Ho^{3+}$ | $[Xe]4f^{10}$ | 8 | $10^{-13}$ | 35 | +++ | + | ++ |
| $Er^{3+}$ | $[Xe]4f^{11}$ | 15/2 | $10^{-13}$ | 30 | ++ | + | + |
| $Tm^{3+}$ | $[Xe]4f^{12}$ | 6 | $10^{-12}$-$10^{-13}$ | 50 | +++ | ++ | ++ |
| $Yb^{3+}$ | $[Xe]4f^{13}$ | 7/2 | $10^{-13}$ | 25 | ++ | + | + |
| Nitr. | / | 1/2 | $10^{-7}$ | 15 | / | ++ | / |

[a]Conf. is the electron configuration of the ions; [b]J is the total angular momentum quantum number; [c]$\tau_s$ electronic relaxation time (in second) based on references[10,34,35]; [d]paramagnetic effects range (in Å) based on references [17,23]; [e]+ indicates the intensity of the three effects based on references[17,23], / indicates non-applicable or small.

metalloproteins. Consequently, various methods have been investigated to introduce

paramagnetic centers. Two types of approaches can be distinguished. Paramagnetic centers can be added to the solution, resulting in solvent-PRE, PRE of protein nuclei caused by non-specific interactions with paramagnetic relaxation agents in the solution. Such agents tumble freely and independently of the protein molecules, so any anisotropy of the paramagnetic center will average to zero and no PCS or RDC are expected, only PRE. Solvent PRE are not discussed here further, but recent reviews have been published.[37,38] Alternatively, a paramagnetic center can be attached covalently at a specific site on the protein.

The two main methods of the covalent approach are the introduction of a genetically encoded metal binding site in the target protein and the chemical attachment of a paramagnetic center to the protein. Several principles need to be followed in the design of a suitable protein paramagnetic center. (i) The target protein structure and properties should be interfered with as little as possible. A highly charged or hydrophobic paramagnetic center as well as the choice of improper binding sites can cause unfolding and result in precipitation of the target protein. Thus small probes with low charge and high polarity are preferred. (ii) The paramagnetic center needs to be rigid relative to the target protein, as the anisotropic effects decrease dramatically with the mobility of a paramagnetic center relative to the protein. Furthermore, movement of paramagnetic center leads to averaged paramagnetic effects, which hampers the translation into structural information. (iii) The paramagnetic center should exist in a single conformation. Many metal complexes show exchange of coordinating groups or flexibility of parts of the coordinating cage. Such coordination states can result in different orientations of the $\Delta\chi$-tensor and thus more than one set of PCS or RDC (in the slow exchange) or line broadening (in the intermediate exchange regime) will be observed. (iv) For probes that are linked via two identical tethers (e.g. Cys residues) to a protein, $C_2$ symmetry is important to avoid that attachment results in different isomers, each with its own $\Delta\chi$-tensor. (v) The metal affinity needs to be high, the probe needs to easily available (e.g. straightforward synthesis) and stable.

### 3.1 Metalloproteins

#### 3.1.1 Paramagnetic metalloproteins

Among the metalloproteins with paramagnetic properties the iron and copper proteins are the best studied by paraNMR. Iron often occurs in either iron-sulfur clusters, like found in ferredoxin[26,39] or in heme, like in cytochromes.[40] In FeS clusters, iron is bound to sulfurs from cysteine and inorganic sulfur, in heme, the iron is coordinated with the macrocycle as a tetradentate and additional axial ligands. Only high-spin Fe(II) and Fe(III) can generate paramagnetic effects of sufficient quality for structural studies. Bertini *et al.* extensively studied iron proteins by paraNMR.[41–46] Oxidized *Saccharomyces cerevisiae* iso-1-cytochrome *c*, containing a low-spin Fe(III) was the first paramagnetic metalloprotein for which the structure was refined with paramagnetic restraints. The

strategy used there was to start with a known structure based on other restraints, often NOE, to calculate the tensor of the paramagnetic center. Then based on the measured NOEs and PCS, the structure is recalculated and, based on the new structure, the tensor is recalculated. This iteration method finally gives a more accurate structure.[25,47]

### 3.1.2 Metalloproteins with paramagnetic substitution

In many cases, metals are either not paramagnetic or have inconvenient paramagnetic properties. In such cases, substituting the metal with another that also has affinity for the metal binding site can be a solution. For proteins containing Cu(II), the metal ions are ligated by histidine, cysteine, aspartic acid or tyrosine residues, or by sulfide.[48,49] Because Cu(II) mainly generates PRE, signals of the coordinating residues are broadened. Therefore, investigation of copper protein structures has been done by substituting the Cu(II) with Co(II) or Zn(II). By substitution with Co(II), Vila *et al.* investigated the metal binding site of stellacyanin, and it was found for the first time that a Gln was involved in Cu(II) coordination.[50] Also Ln(III) are used for substitution if the metal ion has a similar ionic radius and coordination chemistry as a lanthanoid.[51] Calcium binding sites are particularly useful in this respect. Therefore, Ln(III) was successfully substituted for Ca(II) in the EF-hand motif.[52,53] For most calcium proteins, the EF-motif appears as a pair, yet simultaneous substitution with two Ln(III) ions is unfavorable, due to strong electrostatic repulsion. Calbindin $D_{9k}$, which bears two Ca(II) binding sites, is suitable for Ln(III) substitution. Moreover, one of the binding sites can be selectively substituted by Ln(III) at EF-hand motif.[54] Using this as a model protein, the whole lanthanoid group was incorporated in this way, yielding an interesting comparative study of the paramagnetic effects.[55] Calmodulin, with four calcium binding sites is also a good example that has been studied by paramagnetic NMR.[54,56,57]

## 3.2 Genetically encoded metal binding sites

### 3.2.1 Natural amino acids or peptides

Paramagnetism based structural restraints were developed with paramagnetic metalloproteins and extended to diamagnetic metalloproteins. How about non-metalloproteins? Inspired by the strategy of Ln(III) EF-hand substitution, lanthanoid-binding peptides (LBPs) have been proposed for furnishing a paramagnetic center to a protein. Initially, LBPs which comprise an EF-hand like motif were engineered to proteins at the N-terminus.[58] With peptide screening, lanthanoid ion binding affinity was substantially improved and the number of residues decreased to 17.[59–61] Later, double-lanthanoid-binding tags that enable to binding two Ln(III) simultaneously were reported with less than 40 residues.[62,63] However, due to the high mobility of terminal tags, the paramagnetic effects were largely reduced in the result of averaging. Thus, a LBP was successfully inserted into interleukin-1β (IL1β) at three different loops and the tag structure was confirmed by X-ray diffraction results.[64] Such tags coordinated with Gd(III)

can also be used in EPR to determine the distance between two labels.[63] This approach does have some disadvantages. The sites of paramagnetic centers are limited to the N/C terminus or loops and by co-expression, the LBPs are also isotope labelled, which complicates the NMR spectra, especially for the diamagnetic spectra. Also, this approach requires that the structure of the target protein is well known and still it is difficult to predict the location of the lanthanoid beforehand.

Subsequently, to overcome these drawbacks, LBPs were developed that can be attached by linking them to the protein chemically. Generally, these tags contain free thiol groups for attachment to cysteine residues.[64] They can be introduced anywhere by introducing a cysteine on the protein surface. Su *et al* designed a series of LBPs either with one D-chiral cysteine for tag linkage or with different cysteine positions on the LBP. Using ArgN as model protein, large paramagnetic effects were obtained for all Ln(III) loaded LBTs with different tensor rotations for each of the tags.[66] Unfortunately, the mobility of LBP decreases the paramagnetic effects, similar to the LBP fusion method.[63,65] Reduction of LBP mobility can be achieved by anchoring the tag with two sites.[67,68] The first double anchored LBP was designed by Saio *et al.* and comprised a combination between a N-terminal fusion LBP and a chemically linked LBP via a disulfide bond. First, the LBP construction with a free thiol group was fused to N-terminal of GB1 (B1 immunoglobulin binding domain of protein G), containing one cysteine residue. Then the cysteine was activated by using DTNB to form the second linkage between the LBP cysteine and GB1 cysteine, achieving double linkage (referred as L2GB). Large PCS and $\Delta\chi$-tensor were observed for L2GB, compared with the same sequence LBP but singly attached (referred as L1GB). The $\Delta\chi_{rh}$ of L2GB is larger than of L1BG, while the PCS of both tags were similar, because the metal ion position of L1BG is closer to the protein. This result indicates that double-anchoring can rigidify the LBP relatively to the protein.[67]

An alternative, simple approach is to use the metal binding propensity of the canonical amino acids, like histidine, aspartic acid, and tyrosine to bind metals. The His tag, used in protein purification, is an example. It has been used also for paramagnetic NMR, but like the N-terminal fusion LBP, it is too mobile to yield good paraNMR properties.[69] Di-histidine motives can be engineered to generate metal ion binding sites, initially reported for EPR measurements with Cu(II).[70–72] A recent study successfully extended this approach to paramagnetic NMR studies, in which Co(II) was sandwiched by a di-histidine motif either on an $\alpha$-helix or a $\beta$-sheet, with low ion dissociation. Sizeable PCS were detected for Co(II) loaded di-histidine motifs in various proteins.[73]

### 3.2.2 Unnatural amino acids

A number of unnatural amino acids (UAA) with a wide variety of side chains, featuring different functions, were designed and synthesized for the purpose of extending protein building blocks.[74,75] Among these, some possess relatively strong metal ion binding

properties. Bipyridylalanine (BpyAla, Figure 1.4, **2**) is one of the frequently encoded UAA for protein function modification, mainly due to its specific metal binding affinity.[76–78] Paramagnetic transition metal ions, such as Co(II), which require less coordination sites than Ln(III), can be coordinated by BpyAla. A West Nile virus NS2B-NS3 protease (WNVpro) mutant with a BpyAla residue at a loop can coordinate a Co(II) ion, generating a single set of PCS. Additional coordination was required from proximal side chains, as was demonstrated by mutation of nearby residues.[79] This is mainly due to the small size of BpyAla with few coordination sites. HQA (2-amino-3-(8-hydroxyquinolin-3-yl)propanoic acid, Figure 1.4, **3**) is equally suited and thus has been used as metal ion binding motif as well.[80] So far, only Mn(II) was captured by HQA mutated membrane proteins to generate PRE.[80] As discussed in section 2, not only paramagnetic ions can lead paramagnetism, but also nitroxide radicals can also cause PRE. Therefore, a mutated protein with an UAA containing a nitroxide radical (Figure 1.4, **4**) was reported but it was only used for EPR studies.[81–83]

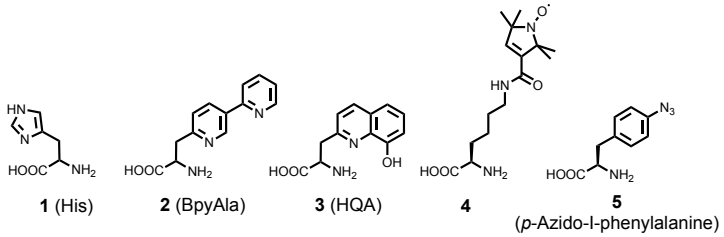


**Figure 1.4** Structures of some natural and unnatural amino acids. **2-5** are unnatural amino acids.

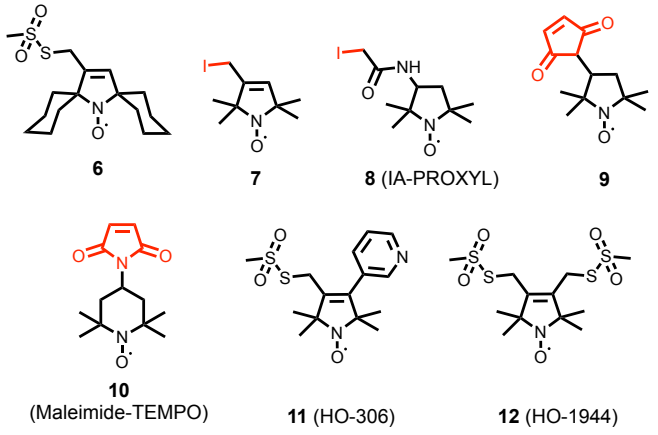


**Figure 1.5** Structures of nitroxide probes. The functional groups for covalent attachment to cysteine via a thioether are drawn in red. Probe **6** is derived from MTSL; probe **7** and **8** are iodide functionalized nitroxides; probe **10** and **11** are maleimide functionalized nitroxides; probe **12** is two-anchored nitroxide.

### 3.3 Synthetic tags

#### 3.3.1 Nitroxide probes

Nitroxides as spin-labels are extensively used in EPR and NMR spectroscopy for determining biomolecular structures, like protein conformations,[84–87] protein-DNA complexes[88,89] and protein-RNA complexes.[90,91] Two main factors need to be considered for the design and application of nitroxides in biosystems. First, the stability of the unpaired electron in relation to tag linkage. Nitroxides are stable under most non-reducing conditions, nonetheless, they still can be oxidized to an oxammonium or reduced to a hydroxiamine. To connect the label to biomolecules, the most efficient way is to activate a free thiol group by methanethiosulfonate (MST)[92] or pyridylthio groups[93] that can form disulfide bonds with cysteine residues. Such bonds are cleavable under reducing conditions. Several ways have been proposed to stabilize nitroxides. Based on MTSL, a more stable nitroxide with longer electronic relaxation time was reported, in which the methyl groups are replaced by cycloalkanes (Figure 1.5, **6**).[94] Since thioether bonds compared with disulfide bonds are more stable under reducing conditions, iodide[90,95] and/or maleimide nitroxides[95,96] show advantages by forming thioether with free thiols (Figure 1.5, **7-10**).

Secondly, the internal rotation of the label is another factor that strongly affects EPR spectra, although less so for NMR spectra. As shown in Figure 1.6 A, the linker of the tag can undergo several internal rotations, causing problems for the interpretation of inter-spin distances measured by EPR in terms of structural restraints.[97–100] Reduction of these movements can be achieved by substitution with bulky groups (Figure 1.5, **11**),[101] introduction of a second attachment group (Figure 1.5, **12**),[102–104] or encoding UAA containing free radical (Figure 1.4, **4**).[105]

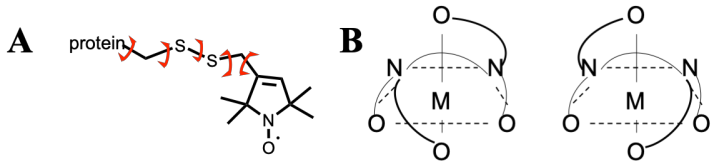


**Figure 1.6 A)** MSTL linkage rotation. The arrows indicate the rotation. **B)** Schematic representation of EDTA complex coordination enantiomers, M represents the metal ion, O represents carboxyl groups, curves indicate the ethylene groups, dashed lines indicate the coordination plane.

#### 3.3.2 Aminopolycarboxylic acid based probes

##### 3.3.2.1 EDTA based probes

EDTA is a widely used ligand for a broad range of metal ions, due to its high metal ion binding affinity with four carboxylic acids and two amine groups. Its complexes with

paramagnetic ions can be linked to proteins via disulfide bond by functionalizing them with MST and pyridylthio groups. The first EDTA based protein paramagnetic probe, S-(2-pyridylthio)cysteaminyl-EDTA (Figure 1.7, **13**), was reported by Ebright *et al.* in 1992.[106] Soon, this probe became commercially available and its various metal ion complexes were used for protein paramagnetic NMR studies.[107–109] According to these studies, two sets of PCS were detected with a Co(II) loaded probe **13**, due to the presence of stereoisomers of the complexes (Figure 1.6 B).[107] Further works introduced chiral centers and a rigid attachment group to Ln(III)-EDTA, resulting in single sets of PCS but with a small $\Delta\chi$-tensor (Figure 1.7, **14**).[109,110]

#### 3.3.2.2 DTPA, DTTA and TAHA based probes

DTPA (diethylenetriaminepentaacetic acid) has a similar structure as EDTA, but with a higher metal binding affinity.[111] DTPA functionalized with two MST groups, CLaNP1 (caged lanthanoids NMR probe # 1, Figure 1.7, **15**), was published as protein paramagnetic probe, using Yb(III) and Y(III) as paramagnetic metal ion and diamagnetic reference, respectivly.[112] Yb(III) loaded CLaNP1 bound to pseudoazurin (Paz) caused large PCS. However, multiple sets of PCS were observed for each amide. Three $\Delta\chi$-tensors were determined based on three main resonance shifts, demonstrating the conformational exchange of the probe. A crystal structure of Paz linked to Y(III)-CLaNP1 was obtained in the same work, showing that the attachment arms of probe were ill-defined and the coordination cage was present in multiple conformations. DTPA coordinates lanthanoids in an octadentate geometry and forms a pair of enantiomers.[113] Once Ln(III)-CLaNP1 was tied to the protein, the symmetry of the ligand was broken, resulting in more isomers with different tenor properties. Later, a $C_3$-symmetric TAHA based probe, Cys-Ph-TAHA,[114] was produced (Figure 1.7, **16**). The paramagnetic properties of lanthanoid loaded Cys-Ph-TAHA were determined by using two ubiquitin mutants (T12C and S57C). PCS and RDC were observed. However, two minor species were observed for Cys-Ph-TAHA labeled T12C ubiquitin, but not for S57C ubiquitin.

Two DTTA (diethylene-triamine-tetraacetate) based protein probes (DTTA-C3-yne and DTTA-C4-yne, Figure 1.7, **17** and **18**)[115] were reported with alkynyl as attachment group. By genetically encoding an UAA (Figure 1.4, **5**) into the protein for specific probe ligation, the two probes were linked to the protein via 'click' chemistry to form a triazole linker. $Tb^{3+}$ or $Tm^{3+}$ loaded probes conjugated to ubiquitin mutants generated single set of PCS with a good correlation between experimental and back-calculated values. The triazole ring linker limits the rotation of the probes relative to the protein. The triazole is coplanar with the phenyl ring of the unnatural residue side chain. The PCS signs of the two probes were opposite. DTTA-C3-yne, which has the shorter linker, showed a larger $\Delta\chi$-tensor than did DTTA-C4-yne. DTTA-C3-yne was applied for structure determination of a transient protein complex.[115]

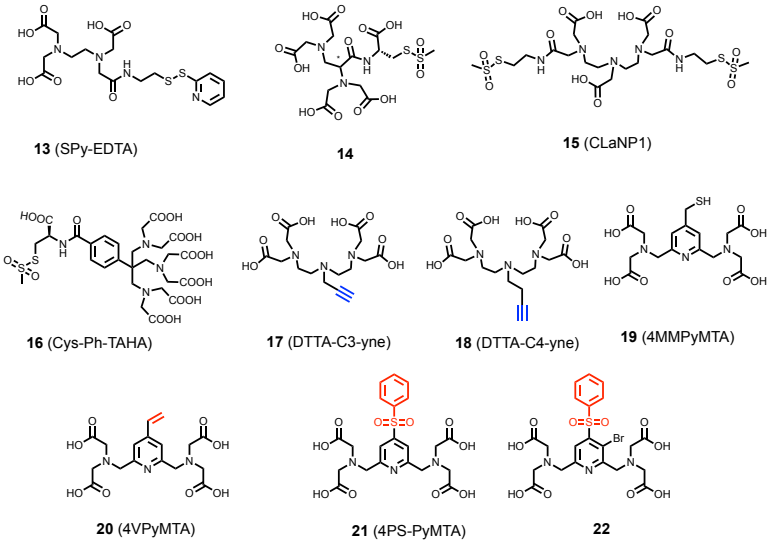


**Figure 1.7** Structures of EDTA and PyMTA based probes. The functional groups for covalent attachment to protein cysteine via thioethers are drawn in red. The alkyne groups for attachment to an azide group on an unnatural amino acid via 'click' reaction are in blue. Probe **13** and **14** are EDTA based probes. Probe **14** has two chiral centers. Probe **15** is double-anchoring probe. Probe **19-22** are PyMAT based probe. The asterisks identify the chiral carbons.

#### 3.3.2.3 PyMAT based probes

Instead of a linear structure of EDTA, PyMTA has a pyridine core with di-azanediyldiacetic acid at position 2 and 6. Its Ln(III) complexes are popular in luminescence and MRI.[116,117] 4MMPyMTA (Figure 1.7, **19**)[118] was designed and investigated as a lanthanoid paramagnetic probe to study the structures of protein minor states. 4VPyMTA (Figure 1.7, **20**)[119] was reported as a Ln(III) paramagnetic probe with a vinyl group at position 4, which forms a thioether bond with cysteine. After successful attachment of 4VPyMTA to ubiquitin, small PCS were observed.[119] Further work introduced phenylsulfonated pyridine at position 4 as a protein conjugation group (Figure 1.7 **21**).[113] Compared with probe **19** and **20**, probe **21** yielded larger PCS due to the short and rigid thioether attachment, but with a low reaction rate, even under harsh conditions. Subsequently, probe **22** (Figure 1.7 **22**)[121] was published with high reaction activity and selectivity.

### 3.3.3 Cyclen based tags

Cyclen (1,4,7,10-tetraazacyclododecane) is a cyclic ring molecule of tetraethyleneamine, which can be suitably modified to obtain various metal binding complexes, especially for lanthanoid ions. DOTA (1,4,7,10-tetraazacyclododecane-1,4,7,10-tetraacetic acid) is one of the most used cyclen derivatives and is a strong chelator of Ln(III). It was first synthesized in 1976.[122] DOTA complexes are thermally stable and the metal ion is tightly bound.[123] It is important to point out that Ln(III)-DOTA complexes undergo conformational exchange of cyclen ring flipping, combined with tetracarboxylic acid arms reorientation (Figure 1.8). The pendant arms can coordinate clockwise (Λ) or anticlockwise (Δ) and the cylcen ring has two conformations (λλλλ and δδδδ). Consequently, two pairs of enantiomeric species (square antiprism (SAP) and twisted square antiprism (TSAP)) appear in Ln(III)-DOTA in solution, which potentially can cause averaging of the magnetic effects, especially in the case of anisotropic paramagnetism.[124–126] In order to get large paramagnetic effects, the probes described below attempt to freeze the probe into one conformation by adding bulky groups on the cyclen ring and/or pendent arms.

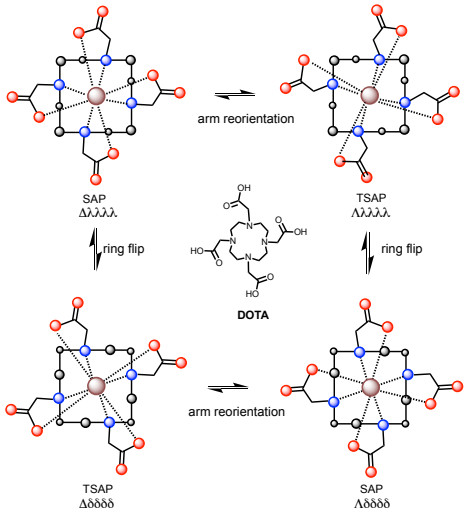


**Figure 1.8.** Schematic representation of DOTA lanthanoid complex conformational exchange. The cyclen ring is shown as a square in solid lines; nitrogens, oxygens and carbons of cyclen ring are shown as blue, red and black spheres, respectively; the metal ion is shown as brown sphere.

### 3.3.3.1 Double sites attachment

The first reported cyclen based protein paramagnetic probe was CLaNP3 (caged lanthanoid NMR probe #3, Figure 1.9, **23**)[127] which uses Ln(III) as paramagnetic center. By functionalizing two of the tetracarboxylic acid arms of DOTA with MST groups, CLaNP3 can be anchored to a protein via two disulfide-bridges, immobilizing the metal

ion relative to the protein. For Yb(III)-CLaNP3 loaded Paz, PCS up to 35 Å could be detected. However, peak doubling was observed for some resonances,[127] suggesting that more than one conformation with different $\Delta\chi$-tensors is still accessible to this complex.

Subsequently, CLaNP5 (Figure 1.9, **24**)[128,129] was published and became one of the most used lanthanoid probes. In CLaNP5 the two remaining acetate pendant arms of CLaNP3 were replaced with pyridyl-N-oxides, which reduce the presence of the TSAP conformation of cyclen based lanthanoid complexes. For Paz linked to Yb(III)-CLaNP5, a single set of large PCS was observed. In contrast, CLaNP5 attached through a single arm yielded small PCS due to its mobility causing averaging effects.[128] Further studies demonstrated that magnetic properties of CLaNP5 are not influenced to a large degree by the attachment site and, thus, it is possible to predict the $\Delta\chi$-tensor parameters and Ln position for a known protein structure with reasonable accuracy.[129] CLaNP5 is very suitable for structural studies of ground states of proteins and protein complexes. However, it was shown that it is not suitable for detecting minor states through relaxation dispersion (RD) experiments because minor conformations of the complex were detected that can lead to probe-induced RD effects.[20,130] Some other disadvantages of CLaNP5 are the high charge (+3), making it less favorable for some proteins or protein complexes and the disulfide ligation, which is liable to reduction and can cause probe loss over a period of several weeks.

CLaNP7[133] and CLaNP9[134] were produced with the aim of counteracting these disadvantages. To decrease the charge, CLaNP7 (Figure 1.9, **25**) was designed with two phenolic groups to lower the net charge to +1 by deprotonation of phenol hydroxyls.[131] CLaNP7 has a yellow color, which is convenient during the tag labelling reaction and protein purification. Similar to CLaNP5, it induced a single set of PCS in Paz, with a $\Delta\chi$-tensor value that was slightly smaller than that of CLaNP5. Interestingly, two sets of PCS were observed specifically for Yb(III)-CLaNP7 linked cytochrome *c* and this peak doubling was pH-dependent. By mutation of histidine 39, which was close to the probe attachment site, to alanine, it was demonstrated that an interaction with this residue was the cause of the peak doubling. The proposed explanation was that the Ln(III) is coordinated in the ninth coordination position by a water molecule, which forms a hydrogen bond with the imidazole ring of histidine 39, thus breaking the symmetry of the probe, causing diastereoisomers and peak doubling. The protonation and deprotonation of the imidazole ring caused the pH dependence.

Since disulfide bonds can easily be reduced, CLaNP9 (Figure 1.9, **26**)[132], was designed as variation of CLaNP5, featuring two bromoacetanilide groups to react with cysteine residues to form chemically stable thioether bonds. Using T4 lysozyme (T4Lys) and Paz as model proteins, Yb(III) loaded CLaNP9 yielded single sets of PCS under reducing conditions, indicating the high stability of this probe. However, it is difficult to

get the protein 100% tagged, due to fast hydrolysis of the bromoacetanilide groups in aqueous solutions.

CLaNPs are not the only double-armed, cyclen based tags, T1 and T2 (Figure 1.9, **27**)[133] were reported as double-anchored probes using MST as attachment groups. T1 and T2 are enantiomers, whereas their two coordination arms are chiral isopropanol moieties. Large $\Delta\chi$-tensors were found for these lanthanoid complexes linked to *Staphylococcus aureus* 6-hydroxymethyl-7,8-dihydropterin pyrophosphokinase (HPPK).[133]

The tags described above are all lanthanoid based cyclen probes. In chapter II and III of this thesis, we report several novel two-armed transition metal ions probes, TraNPs (Transition metal ion NMR Probes), e.g. Figure1.9, **28**).

#### 3.3.3.2 Single site attachment

DOTA-M8 (Figure 1.9, **29**)[134] is one of the most well-known single-armed lanthanoid probes. Its structure is based on M4DOTMA.[135] Yb(III) loaded M4DOTMA complex exhibits a single conformation, due to the bulkiness of the ligand, which has eight chiral methyl substitutions on the cyclen ring and acetate acid pendent arms, forming sterically crowded lanthanoid ion complexes.[136] Therefore, with one pendent acetate acid arm modified as attachment arm, the DOTA-M8 lanthanoid ion complex also features this rigidity. A single set of large PCS was reported for Dy(III)-DOTA-M8 labelled ubiquitin. Dy(III) is tightly bound to DOTA-M8, even under harsh chemical or physical conditions.[134] However, a minor species (15-20%) was observed in the NMR spectra and this ratio was increased to 50% by heating the tagged protein solution to 323 K. This minor species has a similar tensor value and slightly different tensor orientation and metal ion position. Further studies reported slow conformational exchange between the two coordination geometries of Ln(III)-DOTA-M8, which caused two sets of paramagnetic effects, moreover, the exchange rate is dependent on ionic radius of the lanthanoid.[137,138]

DOTA-M8 is ligated to the protein via a disulfide bond, which is unstable under reducing conditions. Efforts to link DOTA-M8 to proteins by different attachment chemistries have been proposed. Instead of the pyridylthio-crosslinker in DOTA-M8, a propyliodoacetamide ($AC_3H_6NHCOCH_2I$) group was introduced to DOTA-M8 to form the chemically more stable thioether bond after reaction with cysteine. This new tag was referred to as M8-CAM-I (Figure 1.9, **30**),[139] and can be used for in-cell NMR measurements. Due to the longer linker, a smaller $\Delta\chi$-tensor was obtained compared to DOTA-M8.[139] Another DOTA-M8 derivative, referred as DOTA-M7Py, was also used for in-cell NMR measurement (Figure 1.9, **31**).[140] In comparison with DOTA-M8 and M8-CAM-I, using 4-(Phenylsulfonyl)pyridine as attachment active group, DOTA-M7Py forms a more rigid and shorter linkage to the protein.[140] But the reaction activity of DOTA-M7Py is low, and thus, DOTA-M7FPy (Figure 1.9, **32**)[141] and DOTA-M7PyThiazole (Figure

1.9, **33**)[141] were produced. Both of them can react with cysteine with high selectivity and efficiency. DOTA-M7PyThiazole generates an even larger Δχ-tensor than DOTA-M8.[141]

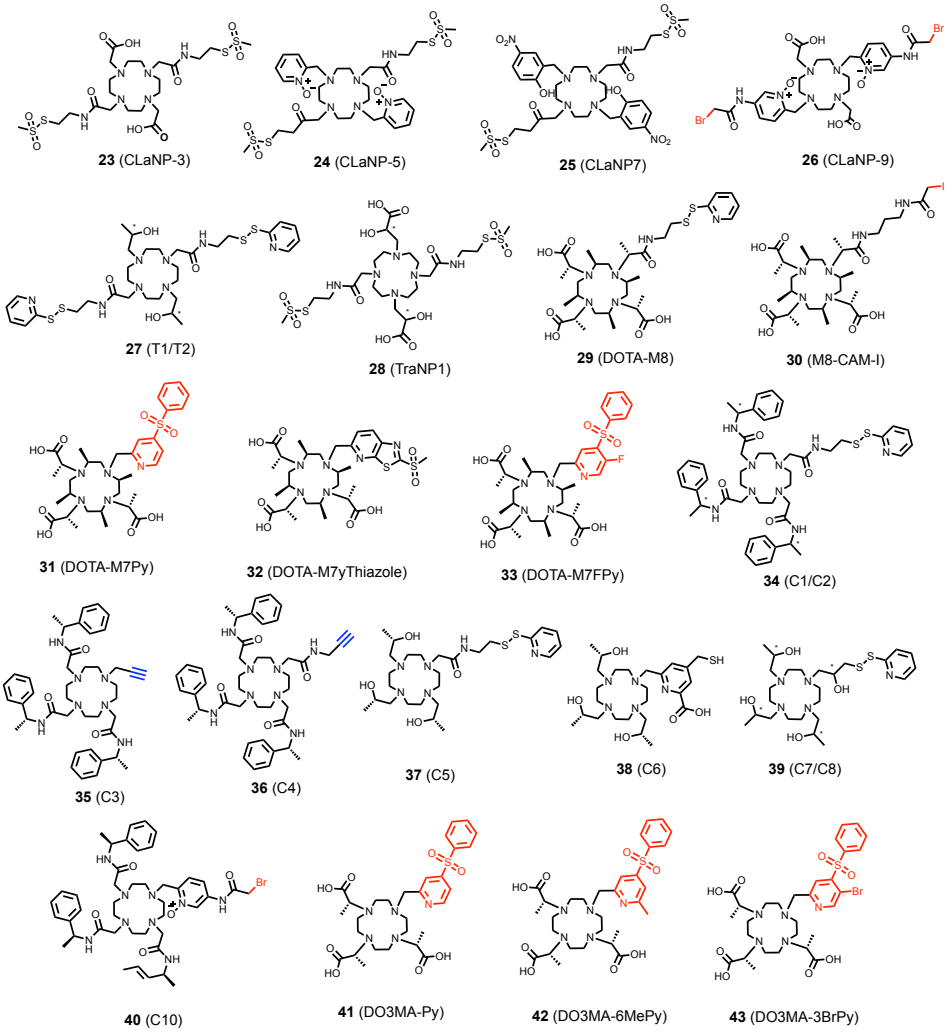


**Figure 1.9** Structures of cyclen based paramagnetic probes. The functional groups for attachment to cysteine via a thioether bond are drawn in red. The functional groups for attachment to an unnatural amino acid nitrite group via 'click' reaction are in blue. **23-28** are two-armed probes. Asterisks identify chiral carbons.

Another example of a rigid DOTA based probe for protein paraNMR studies is C1 (Figure 1.9, **34**).[142] In C1, amides are involved in metal ion chelation instead of carboxyl groups. Harsh condition were required to induce Ln(III) into C1, so after Ln(III) was captured by C1, the ions are tightly bound. With three chiral bulky pendent arms, C1 generated single sets of PCS when attached to ubiquitin or ArgN. According to $^{1}$H

spectra of Yb(III) loaded C1, only one conformation is present. C2 (Figure 1.9, **34**) is the enantiomer of C1, generating a slightly different tensor orientation.[142] Several variants of C1 were developed with alkynyl as attachment groups, C3 and C4, (Figure 1.9, **35**, **36**).[143] C3 and C4 were ligated via a 'click' reaction to ubiquitin genetically encoded with the UAA *p*-azido-L-phenylalanine (AzF, Figure 1.4, **5**).[143] The PCS of C4 are smaller than C3 due to its longer linker.

C1 and its variants contain aromatic rings, which are highly hydrophobic, causing serious protein precipitation. Subsequently, several probes with hydrophilic chiral pendent arms were produced. C5 (Figure 1.9, **37**)[144] has three chiral (S)-2-hydroxypropyl groups as pendent arms. In addition, variants of C5 containing different attachment linkers were also reported, C6 (Figure 1.9, **38**)[144] with a rigid picolinic acid linker, C7 (Figure 1.9, **39**)[144] with the same ligation group as C5 but with a higher symmetry for lanthanoid ion coordination, and C8 (Figure 1.9, **40**),[144] an enantiomer of C7. In general, these tags exhibit large $\Delta\chi$-tensors, similar to C1 and C2. As shown in a study using three proteins and attachments at different sites, the $\Delta\chi$-tensor of C7 is highly affected by the protein environment, which is unexpected for lanthanoid based probes (see section 2.2).[144] Recently, DO3MA-Py (Figure 1.9, **41**)[145], DO3MA-6MPy (Figure 1.9, **42**)[145] and DO3MA-3BrPy (Figure 1.9, **43**)[146] were reported, which contain methyl substituted carboxylic acid as pendent arms and phenylsulfonated pyridine with different substitution groups on pyridine ring as functional group for attachment. These lanthanoid ion complexes have a zero net charge and form thioether bonds with cysteine residues. Large PCSs were detected with these three probes. While the ligation rates of DO3MA-Py and DO3MA-6MPy are slow, even under high pH and temperature, DO3MA-3BrPy, with the Br substitution, decreased the reaction time to 6 h at ambient temperature. DO3MA-3BrPy loaded with Gd(III) was applied for in cell distance measurements by EPR, reporting a narrow distance distribution.[146]

### 3.3.4 Small molecule tags

Small molecules like dipicolinic acid (DPA), iminodiacetic acid (IDA) and nitrilotriacetic acid (NTA) are also popular for protein paraNMR probes design. This popularity derives from their small size, having potentially minimal impact on the protein structure. These small probes usually require additional coordination, from either buffer molecules or protein side chains, especially in the case of lanthanoids, which need seven to nine coordination sites for tightly binding. Metal ions are added after probe attachment, so the probe needs to have a high affinity for the metal ions.

#### 3.3.4.1 DPA and HQA tags

DPA (dipicolinic acid) coordinates metal ions in non-chiral geometry, avoiding possible peak doubling, and its affinity for lanthanoids can be up to nanomolar.[147] 4MMDPA (Figure 1.10, **44**)[148] was the first DPA developed tag featuring good immobilization of the

metal ion relative to the protein by invoking additional side chain coordination. A free thiol group was engineered to DPA at position 4 forming 4MMDPA for protein attachment via a disulfide bond. 4MMDPA was linked to ArgN and could chelate Ln(III) with additional coordination from a Glu, located close to the attachment site. Dissociation of the metal ion was observed with a rate of 0.1 $s^{-1}$, no peak doubling was observed and the $\Delta\chi$-tensor was smaller than found with cyclen based tags. Subsequently, 3MDPA (Figure 1.10, **45**)[149] and probe **46** (Figure 1.10)[150] were produced as variants of 4MMDPA. 3MDPA has a free thiol group at position 3 and a shorter linker. Compared to 4MMDPA, a different tensor orientation, with a smaller $\Delta\chi$-tensor (especially $\Delta\chi_{ax}$), was found for Ln(III)-3MDPA linked ArgN, whereas residue Glu 21 was likely still involved in the coordination. 3MDPA also showed good affinity for Co(II). Probe **46**, containing a vinyl group, was produced to link the probe to the protein via a Michael reaction, forming a thioether linker. The Michael reaction avoids the problem of maleimide functioned tags (Figure 1.10, **47**) which create a new chiral center upon reaction with a thiol group.[150] This functional group was also used for a HQA based probe, 2V-8HQA (Figure 1.10, **48**),[151] for binding transition metal ions, Co(II) and Mn(II), generating the largest observed $\Delta\chi$-tensor for Co(II).[151] A DPA derivative with a phenylsulfonated pyridine functional group (Figure 1.10, **49**)[152] was reported to generate a stable, rigid and short tether with a thioether bond to a cysteine.

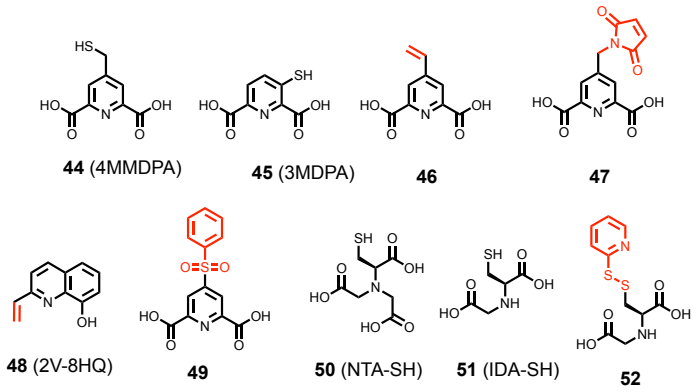


**Figure 1.10** Structures of small molecule probes. The functional groups for attachment via thioether bonds are drawn in red. **44-47**, **49,** DPA based; **48** HQA based; **50** NTA based; **51-52** IDA based.

### 3.3.4.2 NTA and IDA tags

Nitrilotriacetic acid (NTA) based probes need extra coordination from the surroundings, just like DPA tags. The first NTA based probe that can bind lanthanoids, NTA-SH (Figure 1.10, **50**),[153] was obtained by modifying one of three acetate acid groups with a free thiol group. Its lanthanoid complexes induce a single set of PCS, either with one or a pair of

tags on a protein. With a single NTA-SH tagged to ubiquitin or ArgN, different sizes of $\Delta\chi$-tensor and tensor orientations were observed, suggesting additional coordination by side-chains. That makes the paramagnetism of NTA-SH tags unpredictable. This variation can be reduced by simultaneously anchoring two tags at position of i and i+4 of an $\alpha$-helix.[153] The metal ion affinity is not very high, so the ion can be exchanged by adding EDTA to remove it and then introducing a another metal ion.

Iminodiacetic acid (IDA), which only contains two acetic acid groups, represents an even smaller tag. The IDA-SH (Figure 1.10, **51**)[154] probe was reported to yield a single set of PCS after chelating lanthanoid ions. However, this tag also functions by additional coordination of protein side chains.[154] Unexpectedly, by anchoring two of IDA-SH at position i and i+4 of an $\alpha$-helix, instead of lanthanoids, Co(II) can be coordinated, yielding sizeable PCS.[151] Further study of this tag showed a second set of PCS and only partial metal binding (see this thesis chapter II).

## 4 Examples of applications of paramagnetic NMR for protein studies

Paramagnetic effects encoding long-range distance and angular restraints provide structural and dynamic information of biomolecules. For example, by measuring PCS, protein domain rotation, conformational exchange and protein-protein complexes can be studied. Herein, several examples of the application of paramagnetic probes in protein resonance assignment, structure determination, protein-protein complex studies, protein-ligand binding and characterization of lowly-populated states are discussed.

### 4.1 NMR resonance assignment

For protein structural studies with NMR spectroscopy, the assignment of the resonances to the nuclei is a basic requirement. Heteronuclear multidimensional (3D/4D) measurements generally are sufficient for the assignment of small, isotope labeled proteins. For large proteins, complete assignment is challenging because of line broadening and crowding. Paramagnetic NMR can relief crowding by shifting the overlapped peaks to a different extend, based on the distance between the nucleus and the paramagnetic center, and creating more dispersion. For methyl group spectra in particular, this is useful.[155] PCS that are generated by a characterized paramagnetic probe that is rigid relative to the protein (e.g. a double-armed probe) in a protein with known structure, can be predicted to good approximation. By comparing the calculated PCS with the experimental value, an assignment can obtained in principle. However, nuclei located at different positions relative to the paramagnetic center can have the same PCS, making this strategy more complicated. Thus, data from more than one paramagnetic centers at different sites on the protein are required to lift this degeneracy. Several software packages, like PLATYPUS,[156] PARAssign,[157] and Echidna,[158] were developed for resonance assignment using paramagnetic restraints.

For instance, by attaching CLaNP5 (Figure 1.9, **24**) at several sites, resonances of methyl groups of the N-terminal domain (ntd) of HSP90 could be assigned using PARAssign for the calculations.[159] Three sets of $^{1}H$ PCS of methyl groups were obtained by tagging Yb(III)-CLaNP5 to three positions (50C/54C, 101C/105C and 149C/187C) of ntd-HSP90 and used as input data for PARAssign. The starting tensor parameters were based on previously reported values. A Hungarian method[160] was applied for minimal cost assignment of resonances. Then, in an iterative fashion, the tensors were recalculated and the assignment procedure repeated until the assignments did not change anymore. With a combination of two sets of data (50C/54C, 101C/105C), over 60% of methyl groups of an Ile/Leu/Val methyl labelled sample could be assigned and for the remaining observed PCS the choice of possible methyl groups was reduced to two or three possible assignments. The choice of tagging sites turned out to be important. The tensor orientations of the 50C/54C and 149C/187C mutants happened to be almost parallel, which strongly reduces the information content, because the two data sets are then highly correlated.

**4.2 Protein structure determination**

The combination of paramagnetic NMR structural restraints with information obtained from other methods, such as X-ray crystallography, cryo-electron microscopy, EPR and diamagnetic NMR, can improve the accuracy of the protein structure. PCS is the most applied paramagnetic effect for protein structure determination because they are readily measured with high accuracy by simple one or two-dimensional spectra. RDC is independent from the distance to the paramagnetic center, thus it can offer information about domain orientation. Softwares, like CYANA,[161] Xplor-NIH,[12,162,163] and PCS-Rosetta,[164] were developed for protein structure computation using paramagnetic restraints.

The first example of protein structure refinement was done with a paramagnetic metalloprotein, by an iterative method, as described in section 3.1.1. Furthermore, PCS restraints were used for membrane protein structure refinement. It is challenging to obtain adequate structure restraints from diamagnetic NMR for membrane protein structures with high accuracy because such proteins are often large assemblies and in a membrane-mimicking environment. Crick *et al.* were the first to apply PCS restraints for structure refinement of a membrane protein, 7TM phototactic receptor sensory rhodopsin II (pSRII), which comprises seven α-helices in the membrane. Initially, the pSRII structure was determined on the basis of NOE restraints, and the data collection and resonance assignment were very laborious. By labeling pSRII with paramagnetic probe C1 (Figure 1.9, **31**), at four positions, the global fold of the protein could be derived by only using PCS restraints, and when combined with NOE restraints derived only from leucine methyl groups, the calculated structure showed a backbone RMSD (root-mean-

square deviation) of 2.6 Å in comparison with the structure determined by classical NMR methods.[165]

For understanding enzyme function, the elucidation of the structures of intermediates can be crucial, yet few approaches are available to study such transient states. Recently, the structure of an unstable intermediate, so far only detectable by mass spectrometry, was determined on the basis paramagnetic restraints.[166] *S. aureus* sortase A (SrtA) transforms a backbone amide of a substrate peptide into a thioester with its cysteine residue (Cys184) in the active-site. The thioester intermediate could be observed in the presence of calcium or in the absence of 1.0 mM tri-glycine, yet with a low concentration and short life time. A disulfide-bond-linked intermediate analogue (SrtA–QALPECG-$NH_2$), which showed similarity in chemical shifts in $^{15}N$-$^{1}H$ HSQC spectra to the thioester intermediate with $Ca^{2+}$, was produced to obtain the assignment of thioester intermediate. Then, the probes **21** and **22** (Figure 1.7) loaded with one of four lanthanoids, $Dy^{3+}$, $Tb^{3+}$, $Tm^{3+}$ and $Lu^{3+}$, were linked to SrtA. After addition of QALPETG-$NH_2$ peptide in the present of 1.0 mM $Ca^{2+}$, the thioester intermediate was formed, and thus PCS were recorded. In comparison with the PCS obtained from free SrtA, the side chain of residue Trp194, displayed a clear difference. Using the PCS as input for Xplor-NIH, a structure of the thioester intermediate was calculated, yielding an ensemble of ten low-energy structure with a RMSD of 1.1 Å. Therefore, paramagnetic NMR is also a powerful tool for protein minor state structure determination.

Like structure determination of membrane proteins and protein intermediates, also the characterization of protein structure in cellular conditions is challenging. X-ray crystallography and single-particle EM cannot be used, and NMR approaches are limited by the short live time of the sample, the low protein concentration and the poor spectral quality, making it difficult to obtain sufficient structural restraints. Therefore, paramagnetic effects that can be observed in simple spectra in a short time are good candidates for in-cell protein NMR measurements. Müntener *et al.* solved the structure of protein G B1 domain (GB1), by using in-cell paramagnetic NMR spectroscopy.[167] DOTA-M7Py (Figure 1.9, **28**), loaded with one of three lanthanoids, $Tb^{3+}$, $Tm^{3+}$ and $Lu^{3+}$, was used as paramagnetic center. PCS and RDC were recorded after the labeled protein transferred into *Xenopus laevis* oocytes. Based on the observed paramagnetic effects from the in-cell sample, the 3D structure was obtained with a Cα RMSD of 1.1 Å for the ensemble of the ten lowest energy structures, using Rosetta software.[164]

Recently, cobalt(II) was also utilized for protein structure determination.[168] Cobalt(II) binding sites (double-histidine, dHis, motif) was inserted at three different positions in ERp29, one at a time.[73] PCS generated by Co(II) of the backbone amides were used for structure calculation.

### 4.3 Protein-protein interaction

Protein-protein interactions (PPI) are based on non-covalent forces, such as long-range charge-charge attractions and hydrophobic interactions. The formation of a stereospecific protein-protein complex is preceded by the formation of an encounter complex. These weak and dynamic complexes are essential for rapid complex formation, yet are difficult to be characterized by traditional techniques.[169,170] Paramagnetic NMR opens a new avenue to investigate PPI. PRE in particular are sensitive to minor states in which a nucleus is closer to a paramagnetic center than in the major state, usually the stereospecific complex. Attaching a paramagnetic probe on one of the interacting proteins, the paramagnetic effects can be recorded for the partner protein to determine the relative orientation(s) of the two proteins (Figure 1.11).[171]

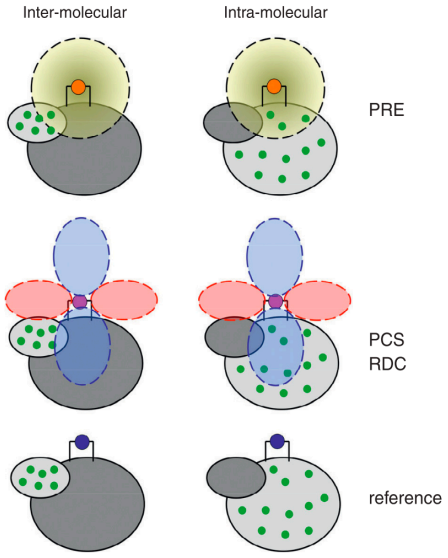


**Figure 1.11** Idealized strategy for measuring PRE, PCS and RDC for structure determination of protein–protein complexes. Six independent samples are produced. PRE are extracted from a complex tagged with an isotropic paramagnetic center, for example, $Gd^{3+}$. PCS and RDC are obtained from a complex tagged with an anisotropic paramagnetic center, for example, $Tm^{3+}$. A diamagnetically tagged complex, for example, with $Lu^{3+}$, serves a reference. In order to decrease signal overlap the intermolecular and intra-molecular are determined independently from different samples in which either one of the proteins is isotope labeled (green dots). The intra-molecular restraints are used to position the paramagnetic center and orient the magnetic susceptibility tensor. A combination of ten 2D spectra (such as TROSY and HSQC) is sufficient to obtain a complete set of intermolecular and intra-molecular PRE, RDC, and PCS. Reprinted with permission from reference [171]. Copyright (2014) Elsevier.

The electron transfer complex of yeast iso-1-cytochrome *c* (Cc) and yeast cytochrome *c* peroxidase (CcP) is one of the comprehensively characterized electron transfer complexes by paramagnetic NMR. Both proteins contain a paramagnetic heme group, but the intermolecular PCS are too small to be suitable for structural studies (M. Ubbink, personal communication). Thus, a paramagnetic tag, MSTL (Figure 1.3), was linked at different locations on the CcP surface to record PRE for Cc. The observed PRE restraints were utilized for docking of Cc on CcP, yielding a stereospecific complex similar to the crystal structure. Furthermore, it was demonstrated that the encounter complex represented no less than 30% of the complex and is localized close to the binding site for the stereospecific complex.[172–174] Cytochrome P450cam (cytP450cam), which is another well studied electron transfer protein, catalyzes the stereo- and regiospecific hydroxylation of camphor to 5-exo-hydroxycamphor by two one-electron reduction steps, in which putidaredoxin (Pdx) functions as the electron donor.[175,176] Hiruma *et al.* applied paramagnetic NMR to investigate the cytP450cam-Pdx complex structure using CLaNP7 (Figure 1.9, **25**) loaded with $Tb^{3+}$ or $Gd^{3+}$ to obtain intermolecular PCS, RDC and PRE. A well-defined putidaredoxin position was obtained, shown to be in good agreement with crystal structures that were obtained independently.[176,177] The study emphasized the need to combine the different types of paramagnetic information to get a good structure. The NMR data also provided evidence for the presence of a lowly populated encounter complex. Using additional paramagnetic restraints and the maximum occurrence of regions methodology,[178] it could be shown that in this encounter complex Pdx in fact visits a large area of the surface of cytP450cam.

PCS based structure studies of protein-protein complexes have been performed by using a two-point anchored LBP.[68] Two mutants of p62 PB1, dubbed as DR and KE, were produced to form dimer. The LBP was only incorporated at DE N-terminal to coordinate with lanthanoids. Using the observed PCS of the DE mutant, the lanthanoid position that related to the DE mutant was calculated. Then a rigid body minimization protocol in Xplor-NIH[12,162,163] was applied for docking of KE subunit. In this protocol, the positions of the metal ion and DR mutant were fixed, and the KE mutant was allowed to orient freely as a rigid body, with the measured PCS and contact-surface shifts of the KE mutant as structural restrains. However, the $\Delta\chi$-tensor symmetry causes multiple solutions. This degeneration could not be solved by adding other lanthanoid ions in the same position, but could be resolved by adjusting the length of the LBP, which was reported in later work.[179]

### 4.4 Protein ligand binding

NMR spectroscopy is very suited to study protein-ligand interactions for drug design because NMR can provide atomic level information about the binding site and ligand orientation. Paramagnetic NMR provides a new approach for such studies.

Fragment-based ligand screening, a method that searches for very small molecules binding weakly to proteins, was explored by paramagnetic NMR with a two-anchoring lanthanide-binding peptide tag (LBT).[180] Binding of the ligand was monitored with PRE caused by $Gd^{3+}$ in the LBT by studying line broadening of the $^1H$ signals in 1D spectra of the ligand with $T_{1\rho}$ relaxation experiments. Provided the ligand exchanges between free and bound state faster than the transverse relation rate, the line broadening due to the proximity of the paramagnetic center in the bound state is transferred to the spectrum of the free ligand, causing a transferred PRE (tPRE), analogous to the transferred NOE and saturation transfer. The size of the tPRE reflects the distance between the ligand nucleus in the bound state and the paramagnetic center. Analogously, also transferred PCS (tPCS) can be used for the characterization of protein-ligand complexes. These were obtained for the same system by loading the LBT with $Tb^{3+}$, $Tm^{3+}$ and $Dy^{3+}$. Another example of the use of tPCS was provided by the work of Guan *et al*.[181] The drug target protein FKBP12 was used as a model to demonstrate that the location and orientation of a ligand could be determined solely using tPCS, provided that the ligand is in fast exchange between bound and free states relative to the size of the PCS (expressed in rad/s). In such experiments, the free ligand is in excess, so only a small fraction of the ligand is bound. By placing the paramagnetic center, Ln(III)-CLaNP5 (Figure 1.9 **24**), at three positions, one at a time, on the target protein surface (Figure 1.12) a PCS based triangulation approach can be used to capture the ligand site of binding and its orientation relative to the protein. The structure of the complex was also determined independently using assignment of all $^1H$ resonances and NOE analysis, which verified the structure obtained via tPCS. The full structure analysis is much more

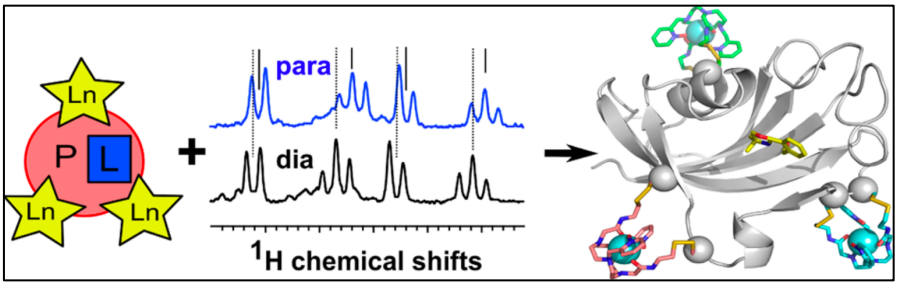


**Figure 1.12 Left**: A model of a protein (P)-ligand (L) complex tagged at several sites with a paramagnetic center; **Middle**: $^1H$ 1D NMR spectra of ligand that experiences transferred PCS during the time of the small fraction bound to the protein. The ligand is in fast exchange between the free and bound states; **Right**: Model of the structure of three paramagnetic centers (show in sticks) linked to FKBP12 (show in ribbon representation) and a bound ligand (show in yellow sticks). Reprinted (adapted) with permission from reference [181]. Copyright (2013) American Chemical Society.

laborious because it requires elaborate assignment work. However, using the tPCS, a second site was found that fitted the PCS data but left the ligand suspended "in mid air", i.e. not bound to the protein. This "ghost" site is a consequence of the degeneracy of the PCS. A PCS does not uniquely define a place in tensor space and even with triangulation using three probes, two sites can be found that fit the data. The ghost site can be discarded as it is non-physiological and clearly an artefact of the method.

It can also be of interest to study whether the weak interaction with a ligand causes changes in the structure of the protein. In general, such binding will has little or no effect on the backbone, but side chains in the active site may adjust their position to accommodate the ligand, representing a modest form of induced fit. A recent study investigated methyl group reorientation in a protein upon ligand binding by observing the PCS of the methyl groups.[182] The targeted protein was labeled with Ln(III)-CLaNP5 (Figure 1.9, **24**) at three positions and selectively isotope labeled with Leu-$\boldsymbol{\delta}_1$-$\boldsymbol{\delta}_2$/Val-$\boldsymbol{\gamma}_1$-$\boldsymbol{\gamma}_2$-[$^{13}CH_3$] residues. Significant PCS differences between free protein and ligand-protein complex were found for the residues that were located at the binding sites, proving the sensitivity of PCS to movements of the methyl group in the range of 1–5 Å. This work presents a new strategy for protein-ligand interaction research by paramagnetic NMR spectroscopy.

### 4.5 Protein dynamics

Protein folding, enzyme catalysis and other functions require conformational exchange, involving excited-states with low populations and short lifetimes (microseconds to milliseconds). The structures of these lowly populated states can usually not be solved by X-ray crystallography. Carr-Purcell-Meiboom-Gill sequence (CPMG) and $T_{1\rho}$ relaxation dispersion experiments as well as chemical exchange saturation transfer (CEST) experiments are uniquely suitable NMR methods for the study of such high-energy states of proteins.[183–185]

Relaxation dispersion experiments can yield the absolute chemical shift difference for a nucleus between the minor and major states. In combination with RDC restraints, obtained in an external alignment medium, the structure of a minor state can be determined in favorable cases.[186,187] However, it is still difficult to convert the limited information into a 3D structure. It would be beneficial if PCS of minor states could be determined because they would provide powerful structural restraints that could help to determine the structure of the minor state. PCS show a gradient across the protein so, for example, if an α-helix moves between major and minor states, all nuclei in the helix would display a change in PCS consistent with such a move. The PCS change is equivalent to a chemical shift change, so a relaxation dispersion experiment will yield the sum of both, whereas the diamagnetic control sample would only produce the chemical shift change.[130] For this application, the rigidity of the paramagnetic center is absolutely

essential to obtain accurate structural restraints. The relaxation dispersion studies of cardiac troponin C substituted with lanthanoids ($Ce^{3+}$ or $Pr^{3+}$) indicated that the motions of the paramagnetic center are very likely modulating the observed PCS.[188] One can avoid this problem by anchoring the probe at a rigid segment, provided also the probe itself is rigid on millisecond timescale. CLaNP5 was the first probe for which its rigidity was tested by relaxation dispersion experiments. CLaNP5 was loaded with $Tm^{3+}$, $Yb^{3+}$, or $Lu^{3+}$ and linked to two well-known rigid proteins, Paz and Cc. The probe was linked to Paz in a loop region, and to Cc on a short β-strand. $^{1}H$ CPMG relaxation dispersion experiment showed that dispersion effects were observed, but it turned out that these effects were caused by the movement of the tag rather than protein.[130] This was further investigated with CLaNP5 linked to adenylate kinase. Similarly, it was found that the probe caused relaxation dispersion and it could be deduced that a minor state of the probe exists in which the $\Delta\chi$ tensor is rotated by 20° relative to the one from the major state. This work showed simultaneously the great power of paramagnetic NMR for the study of minor states and the significant problem of finding a probe that has no exchange ongoing in the millisecond timescale whatsoever. In particular, the ring flips of the cyclen ring are hard to suppress.[189]

Alternatively, the protein structure of minor state can be derived from chemical exchange saturation transfer (CEST) experiments. A recently proposed method, PCS-CEST, demonstrated the study of a minor conformation of a slow-exchange system, Abp1p SH3-Ark1p, with a paramagnetic center.[118] 4MMPyMTA (Figure 1.7, **19**) bounded $Tb^{3+}$ was attached to a SH3 domain. Several $^{15}N$ PCS of the exited states, which were obtained by adding 3% Ark1p peptide, were measured from CEST experiments and shown to be in agreement with the 100% Abp1p SH3-Ark1p complex. This approach, with the same paramagnetic center, was utilized to study the pre-existing folding transitional conformations of HYPA/FBP11 FF domain. In comparison with the ground state, smaller PCS magnitudes were found by the PCS-CEST experiment for the minor state, indicating the domain is in exchange with a small population of less ordered protein.

## 5 Conclusions

The development and improvement of paramagnetic probes, especially site-specific paramagnetic probes, open a wide range of protein structure investigation methods. By engineering a LBT, His residue pairs or UAA, a metal binding motif or a radical can be introduced. Alternatively, chemical probes can be attached to the protein surface. A double-anchoring strategy provides the least flexible paramagnetic centers. While the current probes are excellent for the study of ground state structures, for the study of minor state structures the development of completely rigid probes, or probes that at least are not mobile on the millisecond timescale, remains a challenge.[20] Rigid and non-reducible attachment allow the probes to be used under reducing conditions, for

instance for studies in-cells. Avoiding disulphide chemistry is not straightforward, because for many other attachment methods, hydrolysis competes with cysteine attachment. In comparison with lanthanoid probes, 3d-block metal ion based probes have not been developed extensively. These could find application in the study of local effects, such as changes in an active site. Therefore, finding new rigid chelators remains an important goal for the future.

Recently, the study of conformations of carbohydrates by paramagnetic NMR was reported.[190,191] Here, representing the paramagnetic center was engineered on the oligosaccharide, dedicating a new, alternative way for paramagnetic NMR to study protein–ligand interactions.[192] Furthermore, paramagnetic probes are becoming increasingly used in EPR spectroscopy in which distances can be measured between two unpaired-electron spin labels, for example $Mn^{2+}$ and $Gd^{3+}$, by DEER (double electron–electron resonance) experiments.[33,193] Both NMR and EPR are based on spin interactions and it is only logical that paramagnetic systems bring these two fields closer together. The combination of these spectroscopies can provide a more complete picture of the world of proteins.

## 6 Thesis outline

The aim of this thesis was to design and synthesize new paramagnetic complexes as probes for protein structure studies. **Chapter I** presents a general overview of paramagnetic NMR, sources of paramagnetism, published paramagnetic probes and examples of applications for protein structural studies. **Chapter II** describes the synthesis of several new probes for 3d-block ions, referred to as TraNPs. The magnetic properties of these probes were investigated by linking the probes to three proteins. **Chapter III** describes the synthesis and characterization of a cyclen derivative as ligand for 3d-block ions and lanthanoid ions. **Chapter IV** describes the synthesis of rigidified DOTA analogues and the study of the conformational exchange of its lanthanoid complexes. **Chapter V** describes a rigid Gd(III) probe for measuring protein distances by EPR *in vitro* and in-cells. **Chapter VI** provides a general discussion, conclusions and some perspectives in relation to the work described in this thesis.

## References

(1) Overhauser, A. W. Polarization of Nuclei in Metals. *Phys. Rev.* **1953**, *92* (2), 411–415.

(2) Schweiler, R. B. R.; Case, D. A. Charaterization Of Biomolecular Structure and Dynamics by NMR Cross Relaxation. *Prog. NMR Spectrosc.* **1994**, *26*, 27–58.

(3) Bertini, I.; Luchinat, C.; Parigi, G. Magnetic Susceptibility in Paramagnetic NMR. *Prog. Nucl. Magn. Reson. Spectrosc.* **2002**, *40* (3), 249–273.

(4) Banci, L.; Bertini, I.; Eltis, L. D.; Felli, I. C.; Kastrau, D. H. W.; Luchinat, C.; Piccioli, M.; Pierattelli, R.; Smith, M. The Three-Dimensional Structure in Solution of the Paramagnetic High-Potential Iron-Sulfur Protein I from Ectothiorhodospira Halophila through Nuclear Magnetic Resonance. *Eur. J. Biochem.* **1994**, *225* (2), 715–725.

(5) Solomon, I. 200 and More NMR Experiment. *Phys. Rev.* **1955**, *99* (8), 559.

(6) Solomon, I. Relaxation Processes in a System of Two Spins. *Phys. Rev.* **1955**, *99* (2), 559–565.

(7) Gueron, M. Nuclear Relaxation in Macromolecules by Paramagnetic Ions: A Novel Mechanism. *J. Magn. Reson.* **1975**, *19* (1), 58–66.

(8) Vega, A. J.; Fiat, D. Nuclear Relaxation Processes of Paramagnetic Complexes the Slow-Motion Case. *Mol. Phys.* **1976**, *31* (2), 347–355.

(9) Bertini, I.; Turano, P.; Vila, A. J. Nuclear Magnetic Resonance of Paramagnetic Metalloproteins. *Chem. Rev.* **1993**, *93* (8), 2833–2932.

(10) Otting, G. Protein NMR Using Paramagnetic Ions. *Annu. Rev. Biophys.* **2010**, *39* (1), 387–405.

(11) Schmitz, C.; Stanton-Cook, M. J.; Su, X.-C.; Otting, G.; Huber, T. Numbat: An Interactive Software Tool for Fitting Delta Chi-Tensors to Molecular Coordinates Using Pseudocontact Shifts. *J. Biomol. NMR* **2008**, *41* (3), 179–189.

(12) Schwieters, C. D.; Kuszewski, J. J.; Tjandra, N.; Clore, G. M. The Xplor-NIH NMR Molecular Structure Determination Package. *J. Magn. Reson.* **2003**, *160* (1), 65–73.

(13) Meiler, J.; Peti, W.; Griesinger, C. DipoCoup : A Versatile Program for 3D-Structure Homology Comparison Based on Residual Dipolar Couplings and Pseudocontact Shifts. *J. Biomol. NMR* **2000**, *17* (4), 283–294.

(14) Banci, L.; Bertini, I.; Cavallaro, G.; Giachetti, A.; Luchinat, C.; Parigi, G. Paramagnetism-Based Restraints for Xplor-NIH. *J. Biomol. NMR* **2004**, *28* (3), 249–261.

(15) Tolman, J. R.; Ruan, K. NMR Residual Dipolar Couplings as Probes of Biomolecular Dynamics. *Chem. Rev.* **2006**, *106* (5), 1720–1736.

(16) Tolman, J. R.; Flanagan, J. M.; Kennedy, M. A.; Prestegard, J. H. Nuclear Magnetic Dipole Interactions in Field-Oriented Proteins: Information for Structure Determination in Solution. *Proc. Natl. Acad. Sci.* **1995**, *92* (20), 9279–9283.

(17) Bertini, I.; Luchinat, C.; Parigi, G.; Ravera, E.; Chapter 8. Lanthanoids and Actinoids: Shift and Relaxation. In *NMR of Paramagnetic Molecules: Applications to Metallobiomolecules and Models*; 2017; pp 255–276.

(18) Clore, G. M. Visualizing Lowly-Populated Regions of the Free Energy Landscape of Macromolecular Complexes by Paramagnetic Relaxation Enhancement. *Mol. Biosyst.* **2008**, *4* (11), 1058–1069.

(19) Madl, T.; Felli, I. C.; Bertini, I.; Sattler, M. Structural Analysis of Protein Interfaces from $^{13}C$ Direct-Detected Paramagnetic Relaxation Enhancements. *J. Am. Chem. Soc.* **2010**, *132* (21), 7285-7287.

(20) Phung, L. A.; Otten, R.; Agafonov, R. V.; Hass, M. A. S.; Liu, W.-M.; Kern, D.; Schilder, J. T.; Ubbink, M. A Minor Conformation of a Lanthanide Tag on Adenylate Kinase Characterized by Paramagnetic Relaxation Dispersion NMR Spectroscopy. *J. Biomol. NMR* **2015**, *61* (2), 123–136.

(21) Bertini, I.; Luchinat, C.; Parigi, G. Chapter 3 Relaxation. In *Current Methods in Inorganic Chemistry;* 2001; pp 75-118.

(22) Saio, T.; Ishimori, K. Accelerating Structural Life Science by Paramagnetic Lanthanide Probe Methods. *BBA-Gen. Subj.* **2019**, doi.org/10.1016/j.bbagen.2019.03.018.

(23) Bertini, I.; Luchinat, C.; Parigi, G.; Ravera, E. Transition Metal Ions: Shift and Relaxation. In *Solution NMR of Paramagnetic Molecules*; 2016; pp 175–253.

(24) Andreini, C.; Bertini, I.; Rosato, A. A Hint to Search for Metalloproteins in Gene Banks. *Bioinformatics* **2004**, *20* (9), 1373–1380.

(25) Banci, L.; Bertini, I.; Bren, K. L.; Cremonini, M. A.; Gray, H. B.; Luchinat, C.; Turano, P. The Use of Pseudocontact Shifts to Refine Solution Structures of Paramagnetic Metalloproteins: Met80Ala Cyano-Cytochrome *c* as an Example. *J. Biol. Inorg. Chem.* **1996**, *1* (2), 117–126.

(26) Sands, R. H.; Dunham, W. R. Spectroscopic Studies on Two-Iron Ferredoxins. *Q. Rev. Biophys.* **1974**, *7* (4), 443–504.

(27) Bryar, T. R.; Daughney, C. J.; Knight, R. J. Paramagnetic Effects of Iron(III) Species on Nuclear Magnetic Relaxation of Fluid Protons in Porous Media. *J. Magn. Reson.* **2000**, *142* (1), 74–85.

(28) Bertini, I.; Turano, P.; Vila, A. J. Nuclear Magnetic Resonance of Paramagnetic Metalloproteins. *Chem. Rev.* **1993**, *93* (8), 2833–2932.

(29) Bertini, I.; Luchinat, C.; Parigi, G.; Pierattelli, R. NMR Spectroscopy of Paramagnetic Metalloproteins. *ChemBioChem* **2005**, *6* (9), 1536–1549.

(30) Roser, P.; Schmidt, M. J.; Drescher, M.; Summerer, D. Site-Directed Spin Labeling of Proteins for Distance Measurements in *Vitro* and in Cells. *Org. Biomol. Chem.* **2016**, *14* (24), 5468–5476.

(31) Fielding, A. J.; Concilio, M. G.; Heaven, G.; Hollas, M. A. New Developments in Spin Labels for Pulsed Dipolar EPR. *Molecules* **2014**, *19* (10), 16998–17025.

(32) Dwek, R. A.; Richards, R. E.; Morallee, K. G.; Nieboer, E.; Williams, R. J. P.; Xavier, A. V. The Lanthanide Cations as Probes in Biological Systems: Proton Relaxation Enhancement Studies for Model Systems and Lysozyme. *Eur. J. Biochem.* **1971**, *21* (2), 204–209.

(33) Goldfarb, D. $Gd^{3+}$ Spin Labeling for Distance Measurements by Pulse EPR Spectroscopy. *Phys. Chem. Chem. Phys.* **2014**, *16* (21), 9685–9699.

(34) Rubinstein, M.; Baram, A.; Luz, Z. Electronic and Nuclear Relaxation in Solutions of Transition Metal Ions with Spin S= 3/2 and 5/2. *Mol. Phys.* **1971**, *20* (1), 67–80.

(35) Eaton, D. R. The Nuclear Magnetic Resonance of Some Paramagnetic Transition Metal Acetylacetonates. *J. Am. Chem. Soc.* **1965**, *87* (14), 3097–3102.

(36) Haugland, M. M.; Lovett, J. E.; Anderson, E. A. Advances in the Synthesis of Nitroxide Radicals for Use in Biomolecule Spin Labelling. *Chem. Soc. Rev.* **2018**, *47* (3), 668–680.

(37) Hocking, H. G.; Zangger, K.; Madl, T. Studying the Structure and Dynamics of Biomolecules by Using Soluble Paramagnetic Probes. *ChemPhysChem* **2013**, *14* (13), 3082–3094.

(38) Gong, Z.; Schwieters, C. D.; Tang, C. Theory and Practice of Using Solvent Paramagnetic Relaxation Enhancement to Characterize Protein Conformational Dynamics. *Methods* **2018**, *148*, 48–56.

(39) Fukuyama, K. Structure and Function of Plant-Type Ferredoxins. *Photosynth. Res.* **2004**, *81* (3), 289–301.

(40) Reedy, C. J.; Gibney, B. R. Heme Protein Assemblies. *Chem. Rev.* **2004**, *104* (2), 617–650.

(41) Bertini, I.; Luchinat, C.; Parigi, G. Hyperfine Shifts in Low-Spin Iron(III) Hemes: A Ligand Field Analysis. *Eur. J. Inorg. Chem.* **2000**, *12*, 2473–2480.

(42) Antonkine, M. L.; Bentrop, D.; Bertini, I.; Luchinat, C.; Shen, G. Z.; Bryant, D. A.; Stehlik, D.; Golbeck, J. H. Paramagnetic $^{1}$H NMR Spectroscopy of the Reduced, Unbound Photosystem I Subunit PsaC: Sequence-Specific Assignment of Contact-Shifted Resonances and Identification of Mixed- and Equal-Valence Fe-Fe Pairs in [4Fe-4S] Centers $F_{A}^{-}$ and $F_{B}^{-}$. *J. Biol. Inorg. Chem.* **2000**, *5* (3), 381–392.

(43) Bertini, I.; Luchinat, C.; Turano, P.; Battaini, G.; Casella, L. The Magnetic Properties of Myoglobin as Studied by NMR Spectroscopy. *Chem. Eur. J.* **2003**, *9* (10), 2316–2322.

(44) Dilg, A. W. E.; Capozzi, F.; Mentler, M.; Iakovleva, O.; Luchinat, C.; Bertini, I.; Parak, F. G. Comparison and Characterization of the $[Fe4S4]^{2+/3+}$ Centre in the Wild-Type and C77S

Mutated HiPIPs from Chromatium Vinosum Monitored by Mossbauer, $^{57}$Fe ENDOR and EPR Spectroscopies. *J. Biol. Inorg. Chem.* **2001**, *6* (3), 232–246.

(45) Banci, L.; Bertini, I.; Felli, I. C.; Sarrou, J. Backbone-Only Restraints for Fast Determination of the Protein Fold: The Role of Paramagnetism-Based Restraints. Cytochrome b562 as an Example. *J. Magn. Reson.* **2005**, *172* (2), 191–200.

(46) Bertini, I.; Luchinat, C.; Macinai, R.; Martinuzzi, S.; Pierattelli, R.; Viezzoli, M. S. Isolation and Characterization of Cytochrome *c* from Rhodopseudomonas Palustris. *Inorganica Chim. Acta* **1998**, *269* (1), 125–134.

(47) Banci, L.; Bertini, I.; Bren, K. L.; Gray, H. B.; Sompornpisut, P.; Turano, P. Solution Structure of Oxidized Saccharomyces Cerevisiae Iso-1-Cytochrome *c*. *Biochemistry* **1997**, *36* (29), 8992–9001.

(48) Adman, E. T. Copper Protein Structures. *Adv. Protein Chem.* **1991**, *42*, 145–197.

(49) Crowley, J. D.; Traynor, D. A.; Weatherburn, D. C. Enzymes and Proteins Containing Manganese: An Overview. *Met. Ions Biol. Syst.* **2000**, *37*, 209–278.

(50) Bertini, I.; Fernandez, C. O.; Karlsson, B. G.; Leckner, J.; Luchinat, C.; Malmstrom, B. G.; Nersissian, A. M.; Pierattelli, R.; Shipp, E.; Valentine, J. S.; et al. Structural Information through NMR Hyperfine Shifts in Blue Copper Proteins. *J. Am. Chem. Soc.* **2000**, *122* (15), 3701–3707.

(51) Pidcock, E.; Moore, G. R. Structural Characteristics of Protein Binding Sites for Calcium and Lanthanide Ions. *J. Biol. Inorg. Chem.* **2001**, *6* (5–6), 479–489.

(52) Snyder, E. E.; Buoscio, B. W.; Falke, J. J. Calcium(II) Site Specificity: Effect of Size and Charge on Metal Ion Binding to an EF-Hand-like Site. *Biochemistry* **1990**, *29* (16), 3937–3943.

(53) Lee, L.; Sykes, B. D. Use of Lanthanide-Induced Nuclear Magnetic Resonance Shifts for Determination of Protein Structure in Solution: EF Calcium Binding Site of Carp Parvalbumin. *Biochemistry* **1983**, *22* (19), 4366–4373.

(54) Bertini, I.; Donaire, A.; Jiménez, B.; Luchinat, C.; Parigi, G.; Piccioli, M.; Poggi, L. Paramagnetism-Based versus Classical Constraints: An Analysis of the Solution Structure of Ca Ln Calbindin D9k. *J. Biomol. NMR* **2001**, *21* (2), 85–98.

(55) Bertini, I.; B. L. Janik, M.; Lee, Y.-M.; Luchinat, C.; Rosato, A. Magnetic Susceptibility Tensor Anisotropies for a Lanthanide Ion Series in a Fixed Protein Matrix. *J. Am. Chem. Soc.* **2001**, *123* (18), 4181–4188.

(56) Bertini, I.; Gupta, Y. K.; Luchinat, C.; Parigi, G.; Peana, M.; Sgheri, L.; Yuan, J. Paramagnetism-Based NMR Restraints Provide Maximum Allowed Probabilities for the Different Conformations of Partially Independent Protein Domains. *J. Am. Chem. Soc.* **2007**, *129* (42), 12786–12794.

(57) Bertini, I.; Gelis, I.; Katsaros, N.; Luchinat, C.; Provenzani, A. Tuning the Affinity for Lanthanides of Calcium Binding Proteins. *Biochemistry* **2003**, *42* (26), 8011–8021.

(58) Ma, C.; Opella, S. J. Lanthanide Ions Bind Specifically to an Added "EF-Hand" and Orient a Membrane Protein in Micelles for Solution NMR Spectroscopy. *J. Magn. Reson.* **2000**, *146* (2), 381–384.

(59) Franz, K. J.; Nitz, M.; Imperiali, B. Lanthanide-Binding Tags as Versatile Protein Coexpression Probes. *ChemBioChem* **2003**, *4* (4), 265–271.

(60) Nitz, M.; Franz, K. J.; Maglathlin, R. L.; Imperiali, B. A Powerful Combinatorial Screen to Identify High-Affinity Terbium(III)-Binding Peptides. *ChemBioChem* **2003**, *4* (4), 272–276.

(61) Nitz, M.; Sherawat, M.; Franz, K. J.; Peisach, E.; Allen, K. N.; Imperiali, B. Structural Origin of the High Affinity of a Chemically Evolved Lanthanide-Binding Peptide. *Angew. Chemie.*

*Int. Ed.* **2004**, *43* (28), 3682–3685.

(62) Silvaggi, N. R.; Martin, L. J.; Schwalbe, H.; Imperiali, B.; Allen, K. N. Double-Lanthanide-Binding Tags for Macromolecular Crystallographic Structure Determination. *J. Am. Chem. Soc.* **2007**, *129* (22), 7114–7120.

(63) Barthelmes, D.; Gränz, M.; Barthelmes, K.; Allen, K. N.; Imperiali, B.; Prisner, T.; Schwalbe, H. Encoded Loop-Lanthanide-Binding Tags for Long-Range Distance Measurements in Proteins by NMR and EPR Spectroscopy. *J. Biomol. NMR* **2015**, *63* (3), 275–282.

(64) Barthelmes, K.; Reynolds, A. M.; Peisach, E.; Jonker, H. R. A.; DeNunzio, N. J.; Allen, K. N.; Imperiali, B.; Schwalbe, H. Engineering Encodable Lanthanide-Binding Tags into Loop Regions of Proteins. *J. Am. Chem. Soc.* **2011**, *133* (4), 808–819.

(65) Su, X. C.; Huber, T.; Dixon, N. E.; Otting, G. Site-Specific Labelling of Proteins with a Rigid Lanthanide-Binding Tag. *ChemBioChem* **2006**, *7* (10), 1599–1604.

(66) Su, X. C.; McAndrew, K.; Huber, T.; Otting, G. Lanthanide-Binding Peptides for NMR Measurements of Residual Dipolar Couplings and Paramagnetic Effects from Multiple Angles. *J. Am. Chem. Soc.* **2008**, *130* (5), 1681–1687.

(67) Saio, T.; Ogura, K.; Yokochi, M.; Kobashigawa, Y.; Inagaki, F. Two-Point Anchoring of a Lanthanide-Binding Peptide to a Target Protein Enhances the Paramagnetic Anisotropic Effect. *J. Biomol. NMR* **2009**, *44* (3), 157–166.

(68) Saio, T.; Yokochi, M.; Kumeta, H.; Inagaki, F. PCS-Based Structure Determination of Protein-Protein Complexes. *J. Biomol. NMR* **2010**, *46* (4), 271–280.

(69) Jensen, M. R.; Lauritzen, C.; Dahl, S. W.; Pedersen, J.; Led, J. J. Binding Ability of a HHP-Tagged Protein towards $Ni^{2+}$ Studied by Paramagnetic NMR Relaxation: The Possibility of Obtaining Long-Range Structure Information. *J. Biomol. NMR* **2004**, *29* (2), 175–185.

(70) Voss, J.; Salwinski, L.; Kaback, H. R.; Hubbell, W. L. A Method for Distance Determination in Proteins Using a Designed Metal Ion Binding Site and Site-Directed Spin Labeling: Evaluation with T4 Lysozyme. *Proc. Natl. Acad. Sci.* **2006**, *92* (26), 12295–12299.

(71) Cunningham, T. F.; Putterman, M. R.; Desai, A.; Horne, W. S.; Saxena, S. The Double-Histidine $Cu^{2+}$-Binding Motif: A Highly Rigid, Site-Specific Spin Probe for Electron Spin Resonance Distance Measurements. *Angew. Chemie. Int. Ed.* **2015**, *54* (21), 6330-6334.

(72) Lawless, M. J.; Ghosh, S.; Cunningham, T. F.; Shimshi, A.; Saxena, S. On the Use of the $Cu^{2+}$ Iminodiacetic Acid Complex for Double Histidine Based Distance Measurements by Pulsed ESR. *Phys. Chem. Chem. Phys.* **2017**, *19* (31), 20959–20967.

(73) Bahramzadeh, A.; Jiang, H.; Huber, T.; Otting, G. Two Histidines in an α-Helix: A Rigid $Co^{2+}$ -Binding Motif for PCS Measurements by NMR Spectroscopy. *Angew. Chemie. Int. Ed.* **2018**, *57* (21), 6226–6229.

(74) Link, A. J.; Mock, M. L.; Tirrell, D. A. Non-Canonical Amino Acids in Protein Engineering. *Curr. Opin. Biotechnol.* **2003**, *14* (6), 603–609.

(75) Wang, L.; Schultz, P. G. Expanding the Genetic Code. *Angew. Chemie. Int. Ed.* **2004**, *44* (1), 34–66.

(76) Hyun, S. L.; Schultz, P. G. Biosynthesis of a Site-Specific DNA Cleaving Protein. *J. Am. Chem. Soc.* **2008**, *130* (40), 13194–13195.

(77) Xie, J.; Liu, W.; Schultz, P. G. A Genetically Encoded Bidentate, Metal-Binding Amino Acid. *Angew. Chemie. Int. Ed.* **2007**, *46* (48), 9239–9242.

(78) Luo, X.; Wang, T. S. A.; Zhang, Y.; Wang, F.; Schultz, P. G. Stabilizing Protein Motifs with a Genetically Encoded Metal-Ion Chelator. *Cell Chem. Biol.* **2016**, *23* (9), 1098–1102.

(79) Nguyen, T. H. D.; Ozawa, K.; Stanton-Cook, M.; Barrow, R.; Huber, T.; Otting, G. Generation of Pseudocontact Shifts in Protein NMR Spectra with a Genetically Encoded

Cobalt(II)-Binding Amino Acid. *Angew. Chemie. Int. Ed.* **2011**, *123*, 718–720.

(80) Park, S. H.; Wang, V. S.; Radoicic, J.; De Angelis, A. A.; Berkamp, S.; Opella, S. J. Paramagnetic Relaxation Enhancement of Membrane Proteins by Incorporation of the Metal-Chelating Unnatural Amino Acid 2-Amino-3-(8-Hydroxyquinolin-3-yl)Propanoic Acid (HQA). *J. Biomol. NMR* **2015**, *61* (3–4), 185–196.

(81) Schmidt, M. J.; Borbas, J.; Drescher, M.; Summerer, D. A Genetically Encoded Spin Label for Electron Paramagnetic Resonance Distance Measurements. *J. Am. Chem. Soc.* **2014**, *136* (4), 1238–1241.

(82) Schmidt, M. J.; Fedoseev, A.; Bücker, D.; Borbas, J.; Peter, C.; Drescher, M.; Summerer, D. EPR Distance Measurements in Native Proteins with Genetically Encoded Spin Labels. *ACS Chem. Biol.* **2015**, *10* (12), 2764–2771.

(83) Widder, P.; Berner, F.; Summerer, D.; Drescher, M. Double Nitroxide Labeling by Copper-Catalyzed Azide-Alkyne Cycloadditions with Noncanonical Amino Acids for Electron Paramagnetic Resonance Spectroscopy. *ACS Chem. Biol.* **2019**, *14* (5), 839–844.

(84) Pavićević, A.; Luo, J.; Popović-Bijelić, A.; Mojović, M. Maleimido-Proxyl as an EPR Spin Label for the Evaluation of Conformational Changes of Albumin. *Eur. Biophys. J.* **2017**, *46* (8), 773–787.

(85) Liang, B.; Bushweller, J. H.; Tamm, L. K. Site-Directed Parallel Spin-Labeling and Paramagnetic Relaxation Enhancement in Structure Determination of Membrane Proteins by Solution NMR Spectroscopy. *J. Am. Chem. Soc.* **2006**, *128* (13), 4389–4397.

(86) Tang, C.; Schwieters, C. D.; Clore, G. M. Open-to-Closed Transition in Apo Maltose-Binding Protein Observed by Paramagnetic NMR. *Nature* **2007**, *449*, 1078–1082.

(87) Gillespie, J. R.; Shortle, D. Characterization of Long-Range Structure in the Denatured State of Staphylococcal Nuclease. I. Paramagnetic Relaxation Enhancement by Nitroxide Spin Labels. *J. Mol. Biol.* **1997**, *268* (1), 158–169.

(88) Cai, S.; Zhu, L.; Zhang, Z.; Chen, Y. Determination of the Three-Dimensional Structure of the Mrf2-DNA Complex Using Paramagnetic Spin Labeling. *Biochemistry* **2007**, *46* (17), 4943–4950.

(89) Folkers, P. J. M.; van Duynhoven, J. P. M.; van Lieshout, H. T. M.; Harmsen, B. J. M.; Konings, R. N. H.; Hilbers, C. W.; van Boom, J. H.; Tesser, G. I. Exploring the DNA Binding Domain of Gene V Protein Encoded by Bacteriophage M13 with the Aid of Spin-Labeled Oligonucleotides in Combination with $^{1}$H NMR. *Biochemistry* **1993**, *32* (36), 9407–9416.

(90) Geometry, R.; Analysis, G. Nitroxyls; VII1. Synthesis and Reactions of Highly Reactive 1-oxyl-2,2,5,5-tetramethyl-2,5-dihydro-pyrrole-3-ylmethyl Sulfonates. *Synthesis* **1980**, 91, 914–916.

(91) Ramos, A.; Varani, G. A New Method to Detect Long-Range Protein-RNA Contacts: NMR Detection of Electron-Proton Relaxation Induced by Nitroxide Spin-Labeled RNA. *J. Am. Chem. Soc.* **1998**, *120* (42), 10992–10993.

(92) Smith, D. J.; Maggio, E. T.; Kenyon, G. L. Simple Alkanethiol Groups for Temporary Blocking of Sulfhydryl Groups of Enzymes. *Biochemistry* **1975**, *14* (4), 766–771.

(93) Zecherle, G. N.; Oleinikov, A.; Traut, R. R. The Proximity of the C-Terminal Domain of Escherichia Coli Ribosomal Protein L7/L12 to L10 Determined by Cysteine Site-Directed Mutagenesis and Protein-Protein Cross-Linking. *J. Biol. Chem.* **1992**, *267* (9), 5889–5896.

(94) Kirilyuk, I. A.; Polienko, Y. F.; Krumkacheva, O. A.; Strizhakov, R. K.; Gatilov, Y. V.; Grigor'ev, I. A.; Bagryanskaya, E. G. Synthesis of 2,5-bis(Spirocyclohexane)-substituted nitroxides of Pyrroline and Pyrrolidine Series, including Thiol-Specific Spin Label: An Analogue of MTSSL with Long Relaxation Time. *J. Org. Chem.* **2012**, *77* (18), 8016–8027.

(95) Berliner, L. J.; Grunwald, J.; Hankovszky, H. O.; Hideg, K. A Novel Reversible Thiol-Specific Spin Label: Papain Active Site Labeling and Inhibition. *Anal. Biochem.* **1982**, *119* (2), 450–455.

(96) Griffith, O. H.; McConnell, H. M. A Nitroxide-Maleimide Spin Label. *Proc. Natl. Acad. Sci.* **1966**, *55* (1), 8–11.

(97) Columbus, L.; Hubbell, W. L. A New Spin on Protein Dynamics. *Trends Biochem. Sci.* **2002**, *27* (6), 288–295.

(98) Lietzow, M. A.; Hubbell, W. L. Motion of Spin Label Side Chains in Cellular Retinol-Binding Protein: Correlation with Structure and Nearest-Neighbor Interactions in an Antiparallel **β**-Sheet. *Biochemistry* **2004**, *43* (11), 3137–3151.

(99) Columbus, L.; Kálai, T.; Jekö, J.; Hideg, K.; Hubbell, W. L. Molecular Motion of Spin Labeled Side Chains in α-Helices: Analysis by Variation of Side Chain Structure. *Biochemistry* **2001**, *40* (13), 3828–3846.

(100) Mchaourab, H. S.; Lietzow, M. A.; Hideg, K.; Hubbell, W. L. Motion of Spin-Labeled Side Chains in T4 Lysozyme. Correlation with Protein Structure and Dynamics. *Biochemistry* **1996**, *35* (24), 7692–7704.

(101) Fawzi, N. L.; Fleissner, M. R.; Anthis, N. J.; Kalai, T.; Hideg, K.; Hubbell, W. L.; Clore, G. M. A Rigid Disulfide-Linked Nitroxide Side Chain Simplifies the Quantitative Analysis of PRE Data. *J. Biomol. NMR* **2011**, *51* (1–2), 105–114.

(102) Nguyen, P. H.; Popova, A. M.; Hideg, K.; Qin, P. Z. A Nucleotide-Independent Cyclic Nitroxide Label for Monitoring Segmental Motions in Nucleic Acids. *BMC Biophys.* **2015**, *8* (1), 1–8.

(103) Kálai, T. Synthesis and Reactions of a Symmetric Paramagnetic Pyrrolidine Diene. *Synthesis* **1999**, *1999* (06), 973–980.

(104) Fleissner, M. R.; Bridges, M. D.; Brooks, E. K.; Cascio, D.; Kálai, T.; Hideg, K.; Hubbell, W. L. Structure and Dynamics of a Conformationally Constrained Nitroxide Side Chain and Applications in EPR Spectroscopy. *Proc. Natl. Acad. Sci.* **2011**, *108* (39), 16241–16246.

(105) Wegner, J.; Valora, G.; Halbmair, K.; Kehl, A.; Worbs, B.; Bennati, M.; Diederichsen, U. Semi-Rigid Nitroxide Spin Label for Long-Range EPR Distance Measurements of Lipid Bilayer Embedded **β**-Peptides. *Chem. Eur. J.* **2019**, *25* (9), 2203–2207.

(106) Ebright, Y. W.; Chen, Y.; Pendergrast, P. S.; Ebright, R. H. Incorporation of an EDTA-Metal Complex at a Rationally Selected Site within a Protein: Application to EDTA-Iron DNA Affinity Cleaving with Catabolite Gene Activator Protein (CAP) and Cro. *Biochemistry* **1992**, *31* (44), 10664–10670.

(107) Pintacuda, G.; Moshref, A.; Leonchiks, A.; Sharipo, A.; Otting, G. Site-Specific Labelling with a Metal Chelator for Protein-Structure Refinement. *J. Biomol. NMR* **2004**, *29* (3), 351–361.

(108) Gaponenko, V.; Altieri, A. S.; Li, J.; Byrd, R. A. Breaking Symmetry in the Structure Determination of (Large) Symmetric Protein Dimers. *J. Biomol. NMR* **2002**, *24* (2), 143–148.

(109) Ikegami, T.; Verdier, L.; Sakhaii, P.; Grimme, S.; Pescatore, B.; Saxena, K.; Fiebig, K. M.; Griesinger, C. Novel Techniques for Weak Alignment of Proteins in Solution Using Chemical Tags Coordinating Lanthanide Ions. *J. Biomol. NMR* **2004**, *29* (3), 339–349.

(110) Leonov, A.; Voigt, B.; Rodriguez-Castañeda, F.; Sakhaii, P.; Griesinger, C. Convenient Synthesis of Multifunctional EDTA-Based Chiral Metal Chelates Substituted with an S-Mesylcysteine. *Chem. Eur. J.* **2005**, *11* (11), 3342–3348.

(111) Hart, J. R. Ethylenediaminetetraacetic Acid and Related Chelating Agents. *Ullmann's Encyclopedia of Industrial Chemistry* **2000**, 574-578.

(112) Prudêncio, M.; Rohovec, J.; Peters, J. A.; Tocheva, E.; Boulanger, M. J.; Murphy, M. E. P.; Hupkes, H. J.; Kosters, W.; Impagliazzo, A.; Ubbink, M. A Caged Lanthanide Complex as a Paramagnetic Shift Agent for Protein NMR. *Chem. Eur. J.* **2004**, *10* (13), 3252–3260.

(113) Parker, D.; Dickins, R. S.; Puschmann, H.; Crossland, C.; Howard, J. A. K. Being Excited by Lanthanoid Coordination Complexes: Aqua Species, Chirality, Excited-State Chemistry, and Exchange Dynamics. *Chem. Rev.* **2002**, 102 (6), 1977-2010.

(114) Peters, F.; Maestre-Martinez, M.; Leonov, A.; Kovačič, L.; Becker, S.; Boelens, R.; Griesinger, C. Cys-Ph-TAHA: A Lanthanide Binding Tag for RDC and PCS Enhanced Protein NMR. *J. Biomol. NMR* **2011**, *51* (3), 329–337.

(115) Jiang, W.-X.; Gu, X.-H.; Dong, X.; Tang, C. Lanthanoid Tagging via an Unnatural Amino Acid for Protein Structure Characterization. *J. Biomol. NMR* **2017**, *67* (4), 273–282.

(116) Bonnet, C. S.; Buron, F.; Caillé, F.; Shade, C. M.; Drahoš, B.; Pellegatti, L.; Zhang, J.; Villette, S.; Helm, L.; Pichon, C.; et al. Pyridine-Based Lanthanide Complexes Combining MRI and NIR Luminescence Activities. *Chem. Eur. J.* **2012**, *18* (5), 1419–1431.

(117) Pellegatti, L.; Zhang, J.; Drahos, B.; Villette, S.; Suzenet, F.; Guillaumet, G.; Petoud, S.; Tóth, É. Pyridine-Based Lanthanide Complexes: Towards Bimodal Agents Operating as near Infrared Luminescent and MRI Reporters. *Chem. Commun.* **2008**, No. 48, 6591–6593.

(118) Ma, R. S.; Li, Q. F.; Wang, A. D.; Zhang, J. H.; Liu, Z. J.; Wu, J. H.; Su, X. C.; Ruan, K. Determination of Pseudocontact Shifts of Low-Populated Excited States by NMR Chemical Exchange Saturation Transfer. *Phys. Chem. Chem. Phys.* **2016**, *18* (20), 13794–13798.

(119) Yang, Y.; Li, Q.-F.; Cao, C.; Huang, F.; Su, X.-C. Site-Specific Labeling of Proteins with a Chemically Stable, High-Affinity Tag for Protein Study. *Chem. Eur. J.* **2013**, *19* (3), 1097–1103.

(120) Yang, Y.; Wang, J. T.; Pei, Y. Y.; Su, X. C. Site-Specific Tagging Proteins via a Rigid, Stable and Short Thiolether Tether for Paramagnetic Spectroscopic Analysis. *Chem. Commun.* **2015**, *51* (14), 2824–2827.

(121) Chen, J. L.; Wang, X.; Yang, F.; Cao, C.; Otting, G.; Su, X. C. 3D Structure Determination of an Unstable Transient Enzyme Intermediate by Paramagnetic NMR Spectroscopy. *Angew. Chemie. Int. Ed.* **2016**, *55* (44), 13744–13748.

(122) Stetter, H., Frank, W. Complex Formation with Tetraazac Ycloalkane-N, N′, N′′, N′′′-Tetraacetic Acids as a Function of Ring Size. *Angew. Chem. Int. Ed.* **1976**, *15* (11), 686.

(123) Izatt, R. M.; Pawlak, K.; Bradshaw, J. S.; Bruening, R. L. Thermodynamic and Kinetic Data for Macrocycle Interaction with Cations and Anions. *Chem. Rev.* **1991**, *91* (8), 1721–2085.

(124) Tóth, I.; Rodríguez-Blas, T.; Baranyai, Z.; Bányai, I.; Platas-Iglesias, C.; de Blas, A.; Purgel, M. An NMR and DFT Investigation on the Conformational Properties of Lanthanide(III) 1,4,7,10-Tetraazacyclododecane-1,4,7,10-Tetraacetate Analogues Containing Methylenephosphonate Pendant Arms. *Inorg. Chem.* **2010**, *49* (9), 4370–4382.

(125) Jacques, V.; Desreux, J. F. Quantitative Two-Dimensional EXSY Spectroscopy and Dynamic Behavior. *Inorg. Chem.* **1994**, *33* (8), 4048–4053.

(126) Opina, A. C. L.; Strickland, M.; Lee, Y. S.; Tjandra, N.; Andrew Byrd, R.; Swenson, R. E.; Vasalatiy, O. Analysis of the Isomer Ratios of Polymethylated-DOTA Complexes and the Implications on Protein Structural Studies. *Dalt. Trans.* **2016**, *45* (11), 4673–4687.

(127) Vlasie, M. D.; Comuzzi, C.; Van Den Nieuwendijk, A. M. C. H.; Prudêncio, M.; Overhand, M.; Ubbink, M. Long-Range-Distance NMR Effects in a Protein Labeled with a Lanthanide-DOTA Chelate. *Chem. Eur. J.* **2007**, *13* (6), 1715–1723.

(128) Keizers, P. H. J.; Desreux, J. F.; Overhand, M.; Ubbink, M. Increased Paramagnetic Effect of a Lanthanide Protein Probe by Two-Point Attachment. *J. Am. Chem. Soc.* **2007**, *129* (30),

9292–9293.

(129) Keizers, P. H. J.; Saragliadis, A.; Hiruma, Y.; Overhand, M.; Ubbink, M. Design, Synthesis, and Evaluation of a Lanthanide Chelating Protein Probe: CLaNP-5 Yields Predictable Paramagnetic Effects Independent of Environment. *J. Am. Chem. Soc.* **2008**, *130* (44), 14802–14812.

(130) Hass, M. A. S.; Keizers, P. H. J.; Blok, A.; Hiruma, Y.; Ubbink, M. Validation of a Lanthanide Tag for the Analysis of Protein Dynamics by Paramagnetic NMR Spectroscopy. *J. Am. Chem. Soc.* **2010**, *132* (29), 9952–9953.

(131) Liu, W.-M.; Keizers, P. H. J.; Hass, M. A. S.; Blok, A.; Timmer, M.; Sarris, A. J. C.; Overhand, M.; Ubbink, M. A pH-Sensitive, Colorful, Lanthanide-Chelating Paramagnetic NMR Probe. *J. Am. Chem. Soc.* **2012**, *134* (41), 17306–17313.

(132) Liu, W.-M.; Skinner, S. P.; Filippov, D. V.; Blok, A.; Ubbink, M.; Timmer, M.; Overhand, M.; Hass, M. A. S. A Two-Armed Lanthanoid-Chelating Paramagnetic NMR Probe Linked to Proteins via Thioether Linkages. *Chem. Eur. J.* **2014**, *20* (21), 6256–6258.

(133) Lee, M. D.; Dennis, M. L.; Swarbrick, J. D.; Graham, B. Enantiomeric Two-Armed Lanthanide-Binding Tags for Complementary Effects in Paramagnetic NMR Spectroscopy. *Chem. Commun.* **2016**, *52* (51), 7954–7957.

(134) Häussinger, D.; Huang, J. R.; Grzesiek, S. DOTA-M8: An Extremely Rigid, High-Affinity Lanthanide Chelating Tag for PCS NMR Spectroscopy. *J. Am. Chem. Soc.* **2009**, *131* (41), 14761–14767.

(135) Laboratories, E. F. Polymethylated DOTA Ligands. 1. Synthesis of Rigidified Ligands and Studies on the Effects of Alkyl Substitution on Acid−Base Properties and Conformational Mobility. *Inorg. Chem.* **2002**, *41* (7), 6846–6855.

(136) Ranganathan, R. S.; Raju, N.; Fan, H.; Zhang, X.; Tweedle, M. F.; Desreux, J. F.; Jacques, V. Polymethylated DOTA Ligands. 2. Synthesis of Rigidified Lanthanide Chelates and Studies on the Effect of Alkyl Substitution on Conformational Mobility and Relaxivity. *Inorg. Chem.* **2002**, *41* (25), 6856–6866.

(137) Opina, A. C. L.; Strickland, M.; Lee, Y. S.; Tjandra, N.; Andrew Byrd, R.; Swenson, R. E.; Vasalatiy, O. Analysis of the Isomer Ratios of Polymethylated-DOTA Complexes and the Implications on Protein Structural Studies. *Dalt. Trans.* **2016**, *45* (11), 4673–4687.

(138) Strickland, M.; Schwieters, C. D.; Göbl, C.; Opina, A. C. L.; Strub, M. P.; Swenson, R. E.; Vasalatiy, O.; Tjandra, N. Characterizing the Magnetic Susceptibility Tensor of Lanthanide-Containing Polymethylated-DOTA Complexes. *J. Biomol. NMR* **2016**, *66* (2), 125–139.

(139) Hikone, Y.; Hirai, G.; Mishima, M.; Inomata, K.; Ikeya, T.; Arai, S.; Shirakawa, M.; Sodeoka, M.; Ito, Y. A New Carbamidemethyl-Linked Lanthanoid Chelating Tag for PCS NMR Spectroscopy of Proteins in Living HeLa Cells. *J. Biomol. NMR* **2016**, *66* (2), 99–110.

(140) Müntener, T.; Häussinger, D.; Selenko, P.; Theillet, F.-X. In-Cell Protein Structures from 2D NMR Experiments. *J. Phys. Chem. Lett.* **2016**, *7* (14), 2821–2825.

(141) Müntener, T.; Kottelat, J.; Huber, A.; Häussinger, D. New Lanthanide Chelating Tags for PCS NMR Spectroscopy with Reduction Stable, Rigid Linkers for Fast and Irreversible Conjugation to Proteins. *Bioconjug. Chem.* **2018**, *29* (10), 3344–3351.

(142) Barlow, N.; Yagi, H.; Loh, C. T.; Swarbrick, J. D.; Jia, X.; Pintacuda, G.; Shin, J.; Chhabra, S.; Huber, T.; Graham, B.; et al. DOTA-Amide Lanthanide Tag for Reliable Generation of Pseudocontact Shifts in Protein NMR Spectra. *Bioconjug. Chem.* **2011**, *22* (10), 2118–2125.

(143) Loh, C. T.; Ozawa, K.; Tuck, K. L.; Barlow, N.; Huber, T.; Otting, G.; Graham, B. Lanthanide Tags for Site-Specific Ligation to an Unnatural Amino Acid and Generation of Pseudocontact Shifts in Proteins. *Bioconjug. Chem.* **2013**, *24* (2), 260–268.

(144) Lee, M. D.; Loh, C. T.; Shin, J.; Chhabra, S.; Dennis, M. L.; Otting, G.; Swarbrick, J. D.; Graham, B. Compact, Hydrophilic, Lanthanide-Binding Tags for Paramagnetic NMR Spectroscopy. *Chem. Sci.* **2015**, *6* (4), 2614–2624.

(145) Yang, F.; Wang, X.; Pan, B. Bin; Su, X. C. Single-Armed Phenylsulfonated Pyridine Derivative of DOTA is Rigid and Stable Paramagnetic Tag in Protein Analysis. *Chem. Commun.* **2016**, *52* (77), 11535–11538.

(146) Yang, Y.; Yang, F.; Gong, Y.-J.; Chen, J.-L.; Goldfarb, D.; Su, X.-C. A Reactive, Rigid $Gd^{III}$ Labeling Tag for In-Cell EPR Distance Measurements in Proteins. *Angew. Chemie. Int. Ed.* **2017**, *56* (11), 2914–2918.

(147) Pettinari, C.; Marchetti, F.; Drozdov, A. Higher Denticity Ligands. *Compr. Coord. Chem. II* **2004**, *1*, 211–251.

(148) Su, X.-C.; Man, B.; Beeren, S.; Liang, H.; Simonsen, S.; Schmitz, C.; Huber, T.; Messerle, B. A.; Otting, G. A Dipicolinic Acid Tag for Rigid Lanthanide Tagging of Proteins and Paramagnetic NMR Spectroscopy. *J. Am. Chem. Soc.* **2008**, *130* (32), 10486–10487.

(149) Man, B.; Su, X.-C.; Liang, H.; Simonsen, S.; Huber, T.; Messerle, B. A.; Otting, G. 3-Mercapto-2,6-Pyridinedicarboxylic Acid: A Small Lanthanide-Binding Tag for Protein Studies by NMR Spectroscopy. *Chem. Eur. J.* **2010**, *16* (12), 3827–3832.

(150) Li, Q. F.; Yang, Y.; Maleckis, A.; Otting, G.; Su, X. C. Thiol-Ene Reaction: a Versatile Tool in Site-Specific Labelling of Proteins with Chemically Inert Tags for Paramagnetic NMR. *Chem. Commun.* **2012**, *48* (21), 2704–2706.

(151) Swarbrick, J. D.; Ung, P.; Dennis, M. L.; Lee, M. D.; Chhabra, S.; Graham, B. Installation of a Rigid EDTA-like Motif into a Protein α-Helix for Paramagnetic NMR Spectroscopy with Cobalt(II) Ions. *Chem. Eur. J.* **2016**, *22* (4), 1228–1232.

(152) Yang, Y.; Wang, J.-T.; Pei, Y.-Y.; Su, X.-C. Site-Specific Tagging Proteins via a Rigid, Stable and Short Thiolether Tether for Paramagnetic Spectroscopic Analysis. *Chem. Commun.* **2015**, *51* (14), 2824–2827.

(153) Swarbrick, J. D.; Ung, P.; Su, X. C.; Maleckis, A.; Chhabra, S.; Huber, T.; Otting, G.; Graham, B. Engineering of a Bis-Chelator Motif into a Protein α-Helix for Rigid Lanthanide Binding and Paramagnetic NMR Spectroscopy. *Chem. Commun.* **2011**, *47* (26), 7368–7370.

(154) Swarbrick, J. D.; Ung, P.; Chhabra, S.; Graham, B. An Iminodiacetic Acid Based Lanthanide Binding Tag for Paramagnetic Exchange NMR Spectroscopy. *Angew. Chemie. Int. Ed.* **2011**, *50* (19), 4403–4406.

(155) Sattler, M.; Fesik, S. W. Resolving Resonance Overlap in the NMR Spectra of Proteins from Differential Lanthanide-Induced Shifts. *J. Am. Chem. Soc.* **1997**, *119* (33), 7885–7886.

(156) Pintacuda, G.; Keniry, M. A.; Huber, T.; Park, A. Y.; Dixon, N. E.; Otting, G. Fast Structure-Based Assignment of $^{15}$N HSQC Spectra of Selectively $^{15}$N-Labeled Paramagnetic Proteins. *J. Am. Chem. Soc.* **2004**, *126* (9), 2963–2970.

(157) Skinner, S. P.; Moshev, M.; Hass, M. A. S.; Ubbink, M. PARAssign-Paramagnetic NMR Assignments of Protein Nuclei on the Basis of Pseudocontact Shifts. *J. Biomol. NMR* **2013**, *55* (4), 379–389.

(158) Schmitz, C.; John, M.; Park, A. Y.; Dixon, N. E.; Otting, G.; Pintacuda, G.; Huber, T. Efficient -Tensor Determination and NH Assignment of Paramagnetic Proteins. *J. Biomol. NMR* **2006**, *35* (2), 79–87.

(159) Lescanne, M.; Skinner, S. P.; Blok, A.; Timmer, M.; Cerofolini, L.; Fragai, M.; Luchinat, C.; Ubbink, M. Methyl Group Assignment Using Pseudocontact Shifts with PARAssign. *J. Biomol. NMR* **2017**, *69* (4), 183–195.

(160) Munkres, J. Algorithms for the Assignment and Transportation Problems. *J. Soc. Ind. Appl.*

*Math.* **1957**, *5* (1), 32–38.

(161) Güntert, P. Automated NMR Structure Calculation With CYANA. In *Protein NMR Techniques*; Downing, A. K., Ed.; Humana Press: Totowa, NJ, 2004; pp 353–378.

(162) Schwieters, C. D.; Kuszewski, J. J.; Tjandra, N.; Clore, G. M. The Xplor-NIH NMR Molecular Structure Determination Package. *J. Magn. Reson.* **2003**, *160* (1), 65–73.

(163) Schwieters, C. D.; Kuszewski, J. J.; Clore, G. M. Using Xplor–NIH for NMR Molecular Structure Determination. *Prog. Nucl. Magn. Reson. Spectrosc.* **2006**, *48* (1), 47–62.

(164) Schmitz, C.; Vernon, R.; Otting, G.; Baker, D.; Huber, T. Protein Structure Determination from Pseudocontact Shifts Using ROSETTA. *J. Mol. Biol.* **2012**, *416* (5), 668–677.

(165) Crick, D. J.; Wang, J. X.; Graham, B.; Swarbrick, J. D.; Mott, H. R.; Nietlispach, D. Integral Membrane Protein Structure Determination Using Pseudocontact Shifts. *J. Biomol. NMR* **2015**, *61* (3–4), 197–207.

(166) Chen, J. L.; Wang, X.; Yang, F.; Cao, C.; Otting, G.; Su, X. C. 3D Structure Determination of an Unstable Transient Enzyme Intermediate by Paramagnetic NMR Spectroscopy. *Angew. Chemie. Int. Ed.* **2016**, *55* (44), 13744–13748.

(167) Müntener, T.; Häussinger, D.; Selenko, P.; Theillet, F. X. In-Cell Protein Structures from 2D NMR Experiments. *J. Phys. Chem. Lett.* **2016**, *7* (14), 2821-2825.

(168) Bahramzadeh, A.; Huber, T.; Otting, G. Three-Dimensional Protein Structure Determination Using Pseudocontact Shifts of Backbone Amide Protons Generated by Double-Histidine $Co^{2+}$-Binding Motifs at Multiple Sites. *Biochemistry* **2019**. doi.org/10.1021/acs.biochem.9b00404

(169) Teichmann, S. A. Principles of Protein-Protein Interactions. *Bioinformatics* **2002**, *18*, 13–20.

(170) de Las Rivas, J.; Fontanillo, C. Protein-Protein Interactions Essentials: Key Concepts to Building and Analyzing Interactome Networks. *PLoS Comput. Biol.* **2010**, *6* (6), 1–8.

(171) Hass, M. A. S.; Ubbink, M. Structure Determination of Protein-Protein Complexes with Long-Range Anisotropic Paramagnetic NMR Restraints. *Curr. Opin. Struct. Biol.* **2014**, *24* (1), 45–53.

(172) Volkov, A. N.; Worrall, J. A. R.; Holtzmann, E.; Ubbink, M. Solution Structure and Dynamics of the Complex between Cytochrome *c* and Cytochrome *c* Peroxidase Determined by Paramagnetic NMR. **2006**, *103* (50).

(173) Bashir, Q.; Volkov, A. N.; Ullmann, G. M.; Ubbink, M. Visualization of the Encounter Ensemble of the Transient Electron Transfer Complex of Cytochrome c and Cytochrome *c* Peroxidase. *J. Am. Chem. Soc.* **2010**, *132* (1), 241–247.

(174) Schilder, J.; Loehr, F.; Schwalbe, H.; Ubbink, M. The Cytochrome c Peroxidase and Cytochrome *c* Encounter Complex: The Other Side of the Story. *FEBS Lett.* **2014**, *588* (10), 1873–1878.

(175) *Fifty Years of Cytochrome*; Yamazaki, H., Ed.; Springer Tokyo Heidelberg new York Dordrecht London, 2012.

(176) Tripathi, S.; Li, H.; Poulos, T. L. Structural Basis for Effector Control and Redox Partner Recognition in Cytochrome P450. *Science* **2013**, *340* (6137), 1227–1230.

(177) Hiruma, Y.; Hass, M. A. S.; Kikui, Y.; Liu, W.-M.; Olmez, B.; Skinner, S. P.; Blok, A.; Kloosterman, A.; Koteishi, H.; Loehr, F.; et al. The Structure of the Cytochrome P450cam-Putidaredoxin Complex Determined by Paramagnetic NMR Spectroscopy and Crystallography. *J. Mol. Biol.* **2013**, *425* (22), 4353–4365.

(178) Andrałojć, W.; Luchinat, C.; Parigi, G.; Ravera, E. Exploring Regions of Conformational Space Occupied by Two-Domain Proteins. *J. Phys. Chem. B* **2014**, *118* (36), 10576–10587.

(179) Kobashigawa, Y.; Saio, T.; Ushio, M.; Sekiguchi, M.; Yokochi, M.; Ogura, K.; Inagaki, F.

Convenient Method for Resolving Degeneracies due to Symmetry of the Magnetic Susceptibility Tensor and Its Application to Pseudo Contact Shift-Based Protein-Protein Complex Structure Determination. *J. Biomol. NMR* **2012**, *53* (1), 53–63.

(180) Saio, T.; Ogura, K.; Shimizu, K.; Yokochi, M.; Burke, T. R.; Inagaki, F. An NMR Strategy for Fragment-Based Ligand Screening Utilizing a Paramagnetic Lanthanide Probe. *J. Biomol. NMR* **2011**, *51* (3), 395–408.

(181) Guan, J.-Y.; Keizers, P. H. J.; Liu, W.-M.; Loehr, F.; Skinner, S. P.; Heeneman, E. A.; Schwalbe, H.; Ubbink, M.; Siegal, G. Small-Molecule Binding Sites on Proteins Established by Paramagnetic NMR Spectroscopy. *J. Am. Chem. Soc.* **2013**, *135* (15), 5859–5868.

(182) Lescanne, M.; Ahuja, P.; Blok, A.; Timmer, M.; Akerud, T.; Ubbink, M. Methyl Group Reorientation under Ligand Binding Probed by Pseudocontact Shifts. *J. Biomol. NMR* **2018**, *71* (4), 275–285.

(183) Anthis, N. J.; Clore, G. M. Visualizing Transient Dark States by NMR Spectroscopy. *Q. Rev. Biophys.* **2015**, *48* (1), 35–116.

(184) M. Korzhnev, D.; E. Kay, L. Probing Invisible, Low-Populated States of Protein Molecules by Relaxation Dispersion NMR Spectroscopy: An Application to Protein Folding. *Acc. Chem. Res.* **2008**, *41* (3), 442–451.

(185) Baldwin, A. J.; Kay, L. E. NMR Spectroscopy Brings Invisible Protein States into Focus. *Nat. Chem. Biol.* **2009**, *5*, 808.

(186) Vallurupalli, P.; Hansen, D. F.; Stollar, E.; Meirovitch, E.; Kay, L. E. Measurement of Bond Vector Orientations in Invisible Excited States of Proteins. *Proc. Natl. Acad. Sci.* **2007**, *104* (47), 18473–18477.

(187) Vallurupalli, P.; Hansen, D. F.; Kay, L. E. Structures of Invisible, Excited Protein States by Relaxation Dispersion NMR Spectroscopy. *Proc. Natl. Acad. Sci.* **2008**, *105* (33), 11766–11771.

(188) Eichmüller, C.; Skrynnikov, N. R. Observation of **M**s Time-Scale Protein Dynamics in the Presence of $Ln^{3+}$ Ions: Application to the N-Terminal Domain of Cardiac Troponin C. *J. Biomol. NMR* **2007**, *37* (2), 79–95.

(189) Hass, M. A. S.; Liu, W. M.; Agafonov, R. V.; Otten, R.; Phung, L. A.; Schilder, J. T.; Kern, D.; Ubbink, M. A Minor Conformation of a Lanthanide Tag on Adenylate Kinase Characterized by Paramagnetic Relaxation Dispersion NMR Spectroscopy. *J. Biomol. NMR* **2015**, *61* (2), 123–136.

(190) Kato, K.; Yamaguchi, T. Paramagnetic NMR Probes for Characterization of the Dynamic Conformations and Interactions of Oligosaccharides. *Glycoconj. J.* **2015**, *32* (7), 505–513.

(191) Fern, B.; Peng, W.; Thompson, A. J.; Dom, G.; Caçada, F. J.; Javier, P. Ø.; Paulson, J. C. Avenues to Characterize the Interactions of Extended N-Glycans with Proteins by NMR Spectroscopy : the Influenza Hemagglutinin Case. *Angew. Chem. Int. Ed.* **2018**, 15051–15055.

(192) Mallagaray, A.; Domínguez, G.; Peters, T.; Pérez-Castells, J. A Rigid Lanthanide Binding Tag to Aid NMR Studies of a 70 KDa Homodimeric Coat Protein of Human Norovirus. *Chem. Commun.* **2016**, *52* (3), 601–604.

(193) Wu, Z.; Feintuch, A.; Collauto, A.; Adams, L. A.; Aurelio, L.; Graham, B.; Otting, G.; Goldfarb, D. Selective Distance Measurements Using Triple Spin Labeling with $Gd^{3+}$, $Mn^{2+}$, and a Nitroxide. *J. Phys. Chem. Lett.* **2017**, *8* (21), 5277–5282.

# Chapter II

# A double armed, hydrophilic, transition metal complex as paramagnetic NMR probe

Based on the research article: Qing Miao, Wei-Min Liu, Thomas Kock, Anneloes Blok, Monika Timmer, Mark Overhand, Marcellus Ubbink. A double armed, hydrophilic, transition metal complex as paramagnetic NMR probe. *Angew. Chem. Int. Ed.* **2019**, 58, 13093–13100

# *Chapter II*

**Abstract**

Synthetic metal complexes find use as paramagnetic probes for the study of proteins and protein complexes. Here, the synthesis and characterization of two transition metal NMR probes (TraNPs), TraNP1-RR and TraNP1-SS, are reported. TraNPs are attached via two arms to engineered cysteine residues on the surface of a protein to generate pseudocontact shift (PCS) using cobalt (II), or paramagnetic relaxation enhancement (PRE) with manganese (II). The zero net charge and good solubility make the TraNPs compatible with proteins. The PCS analysis of TraNPs attached to three different proteins shows that the size of the anisotropic component of the magnetic susceptibility depends on the probe surroundings at the surface of the protein, contrary to what is observed for lanthanoid based probes. The observed PCSs are relatively smaller than for most lanthanoid probes, making cobalt-based probes suitable for localized studies, such as of an active site. The obtained PREs are stronger than obtained with nitroxide spin labels and the possibility to generate both PCS and PRE with the same probe offers advantages. The properties of TraNPs in comparison with other cobalt based paramagnetic probes are discussed.

**Introduction**

Ever since the determination of first metalloprotein structures using paramagnetic NMR restraints,[1-5] it has been acknowledged that paramagnetism is a powerful tool for the study of biomolecules. The interactions of unpaired electrons with nuclei generate paramagnetic effects that contain structural information.[6-7] Pseudocontact shift (PCS) and paramagnetic relaxation enhancement (PRE) are the paramagnetic effects that most frequently find application. PCS offer long-range distance and conformational information and can be easily measured with high precision. PRE only yield distance information but are strongly distance dependent, making exquisitely sensitive to minor states in which the nuclear-electron distance is reduced.[8-10] In proteins that bind metals naturally, a paramagnetic center is already present or can be introduced by replacing a diamagnetic metal ion, like Ca(II) or Mg(II), with a paramagnetic ion, such as Co(II), Mn(II), or a lanthanoid, Ln(III).[11-15] For other proteins, the introduction of a paramagnetic center is required, either via genetic means or through chemical attachment. To limit the effects on the protein and obtain a single set of paramagnetic effects, the ideal probe has no net charge and is hydrophilic, positioned rigidly relative to the protein and of high symmetry. Over the past years, many paramagnetic NMR probes were designed and synthesized.[16-19] Ln(III) has been the paramagnetic center of choice in many cases because of the range of anisotropic components of the magnetic susceptibilities (described by the $\Delta\chi$-tensor) that these ions display, with sizes of $2\times10^{-32}$ m$^3$ for Eu(III), $8\times10^{-32}$ m$^3$ for Yb(III) and up to 50-84$\times10^{-32}$ m$^3$ for Tm(III), Tb(III) and Dy(III).[20-23] The similarity in coordination chemistry makes it possible to use the same probe with different Ln(III) ions. Fewer probes for transition metals have been reported. Of the transition metal ions, high-spin Co(II) yields among the largest PCS, with tensor sizes in the order of 2-7$\times10^{-32}$ m$^3$,[3] and displays weak PRE, whereas Mn(II) causes strong PRE due to the presence of five unpaired electrons and a long electronic relaxation time.[26] The use of transition metal ions as paramagnetic centers for protein structural studies has already a long history.[27-32] However, only few site-specific transition metal probes have been designed for protein NMR studies. S-(2-pyridylthio)-cysteaminyl-EDTA is a commercially available (TRC, Toronto, Canada) transition metal probe. However, it yields multiple PCS for a nucleus due to the presence of stereoisomers of the complex.[33] Some other probes are attached to the protein via a single arm and require additional coordination by a residue of the protein near the attachment site.[34-35] Recently, two-point attachment was introduced for Co(II) probes to ensure that the metal ion is rigid relative to the protein.[36-37] For one of these probes, metal ion exchange between solvent and probe was observed.[36] This prompted us to develop a double-armed transition metal ion probe that could tightly bind the metal ion and generate a single set of paramagnetic effects. Cyclen (1,4,7,10-tetraazacyclododecane) is a widely used building block for metal ligand design due to its high metal binding affinity. A large number of cyclen derivatives have been developed

for metal ions for the application in biomedicine[38-39] and magnetic resonance imaging (MRI),[40-41] for which high thermodynamic stability and kinetic inertness are required. Among these reported cyclen based complexes, there are, however, few successful Co(II) and Mn(II) complexes, in particular for Mn(II), which can easily be oxidized by air.[42]

Here, we report the design and synthesis of several $C_2$-symmetric cyclen derivatives, which can tightly bind the transition metal ions Co(II) and Mn(II) and are stable in air and buffers. These Transition metal NMR Probes (TraNPs) were tested using three proteins. The TraNPs are linked to the proteins via two disulfide bonds at a specific location on protein surface, yielding single sets of paramagnetic effects in NMR spectra. Interestingly, the size of the $\Delta\chi$-tensor of Co-TraNP ranges from 2 – 5 $\times 10^{-32}$ $m^3$ for different proteins, indicating that the protein environment has an indirect effect on the Co(II) coordination that influences the $\Delta\chi$-tensor. We discuss the TraNP properties and compare them with other reported Co(II) tags.

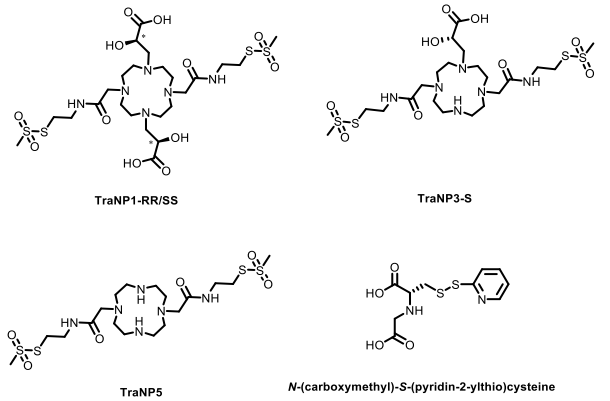


**Figure 2.1** Structures of TraNP1-SS/RR, TraNP3-S, TraNP5, and N-(carboxymethyl)-S-(pyridin-2-ylthio) cysteine (*tag 1*). The asterisks in the structures of TraNP1-SS/RR indicate the asymmetric carbons.

**Results**

**Synthesis of TraNPs.** Derivatives of 1,4,7,10-tetraazacyclododecane (cyclen) have been used extensively for metal binding because of their favorable metal coordination properties.[43-44] For a two-armed transition metal probe, $C_2$-symmetric derivatives that allow attachment to two cysteine residues are required.[21] Selective protection and/or alkylation at the opposing positions of the nitrogens of the cyclen ring can be accomplished because the protonation states of neighboring nitrogens are strongly interdependent, with $pK_a$ values around 1 and 10.[45-46] As judged from the cyclen crystal structure, two opposing nitrogens point outward from the center of the ring, whereas the two others point inward.[47] Here, a selective partial protection and alkylation strategy

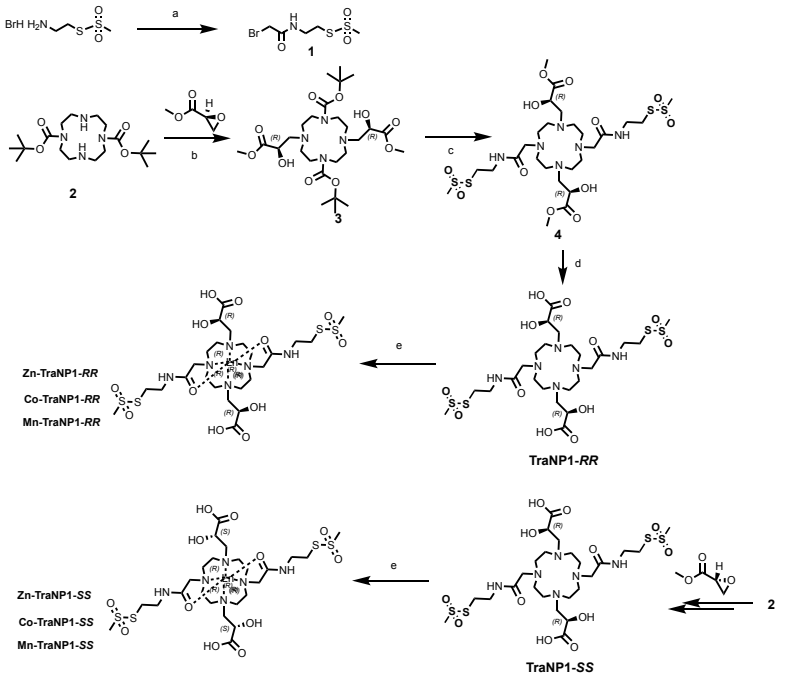


**Scheme 2.1** a) acetyl bromide, $K_2CO_3$, $H_2O$, 0 °C; b) Methyl (2S)-glycidate, MeOH r.t., 48 h; c) i) TFA: DCM (*v/v*) 4:1, r.t., 16 h; ii) compound 1, $K_2CO_3$, ACN, r.t., 12 h; d) 1 M HCl, 50 °C, 4 h; e) ACN, rt, 3 h.

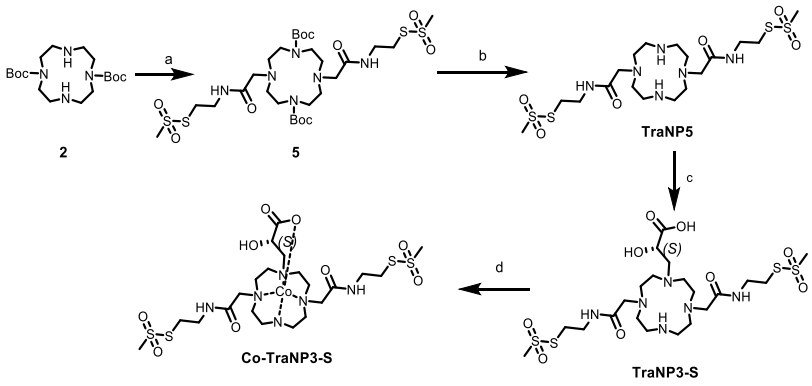


**Scheme 2.2** Synthesis of TraNP3-S and TraNP5. a) compound 2, $K_2CO_3$, ACN; b) i) TFA: DCM (v/v) 3:2, rt; C) i) Methyl (2S)-glycidate, rt, 24 h; ii) 1 M HCl, 50 °C, 4 h; d) ACN, rt, 3 h

was used to synthesize the novel $C_2$ symmetric metal binding ligands TraNP1-SS and TraNP1-RR, as well as the control compounds TraNP3-S and TraNP5 (Figure 2.1). In

addition, N-(carboxymethyl)-S-(pyridine-2-ylthio)cysteine was synthesized (Figure 2.1, *tag 1*). This compound has been described before for the purpose of tagging proteins with Co(II) and was used here for comparison with TraNPs.[36] The synthesis of TraNP1-SS/RR is shown in Scheme 2.1. Cyclen was protected with tert-butoxycarbonyl (Boc) group at positions 1 and 7,[21, 48] and functionalized via a double epoxide ring opening, using the commercially available methyl (S) or (R)-oxirane-2-carboxylate to give compound **3(RR)** and compound **3(SS)** in 61% and 63% yield, respectively. Compound **4(RR)** was obtained by removal of the Boc-groups of compound **3(RR)** with trifluoroacetic acid in dichloromethane, followed by bi-alkylation with compound **1** in the presence of $K_2CO_3$.[49] Analogously, compound **4(SS)** was obtained. Deprotection of the methyl esters with 1 M HCl solution at 50 °C, rather than classical basic solution deprotection, was used because of the lability of the mesityl-groups, and produced TraNP1-SS and TraNP1-RR in 65% and 67% yield, respectively. TraNP3-S and TraNP5 were synthesized using similar approaches, see Scheme 2.2. For the introduction of the metal ions, 1.1 equiv. of Co(II), Mn(II) or Zn(II)) was add to TraNPs ACN solution, followed by stirring at room temperature for 3 h. Except for TraNP5, the metal ion complexes were stable under atmospheric conditions.

**TraNPs attachment.** Three proteins were used to characterize the paramagnetic properties of the TraNP molecules, T4 Lysozyme (T4Lys) with the mutations K147C/T151C, Bacillus circulans xylanase (BCX) with mutations E78Q/T109C/T111C and ubiquitin with the mutations E24C/A28C. The mutation E78Q in BCX abolishes catalytic activity but is otherwise irrelevant for this study. These three proteins contain no cysteines apart from the pair introduced for probe attachment. In T4Lys and ubiquitin, the two cysteines are located in an α-helix, whereas in BCX, the cysteines are in a **β**-strand. The uniformly $^{15}N$ enriched proteins were treated with DTT to reduce possible intermolecular disulfide bonds, the DTT was removed and the proteins were incubated with Co(II)/Zn(II)/Mn(II)-TraNPs. The tagged proteins were purified using size exclusion chromatography and the tagging efficiency was determined by MS and NMR. Mass spectrometry results of Co(II)-TraNP1 T4Lys (19333 ± 2 Da), Co(II)-TraNP1 BCX (21337 ± 2 Da) and Co(II)-TraNP1 ubiquitin (9309 ± 2 Da) agreed with the theoretical values of 19334 Da, 21339 Da and 9311 Da for 98% enrichment of $^{15}N$, respectively, indicating that the probes were attached via two arms (App. Figures A2.1-2.3). No untagged protein was found by MS, suggesting that more than 95% of the protein was tagged. Similar results were found for the complexes containing Zn(II) and Mn(II). These results were confirmed by $^{1}H$-$^{15}N$ HSQC spectra of samples of Co(II)-TraNP tagged proteins, which showed no peaks for untagged protein. An overlay of the NMR spectra of the proteins tagged with Zn(II) and Co(II) loaded TraNP1-RR or TraNP1-SS shows the presence of PCS in the latter spectra (Figure 2.2 and App. Figure A2.4).

**Analysis of the paramagnetic spectra.** The PCS caused by Co(II) on the amides in the proteins were obtained by taking the difference of the $^{1}H^{N}$ chemical shifts in the spectra

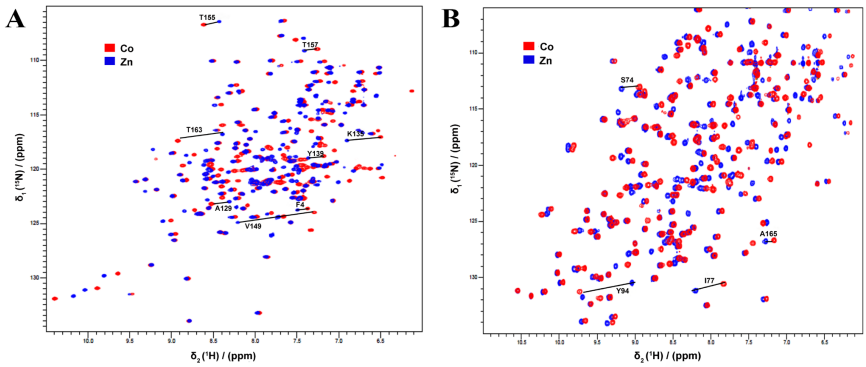


**Figure 2.2.** Overlay of $^{1}$H-$^{15}$N HSQC spectra of Co(II) (red) and Zn(II) (blue) loaded TraNP1-RR attached to T4Lys K147C/T151C (**A**) and BCX E78Q/T109C/T111C (**B**). Several PCS are indicated with solid lines and residue numbers. The NMR spectra were recorded at 14.1 T (600 MHz)

of the Co(II) and Zn(II) tagged proteins. The PCS was fitted to equation 1.1 chapter I to obtain the two components of the anisotropic part of the magnetic susceptibility, $\Delta\chi_{ax}$ and $\Delta\chi_{rh}$, the orientation of the $\Delta\chi$ tensor and the position of the paramagnetic center relative to the protein structure. For TraNP1 T4Lys (K147C/T151C), BCX (E78Q/T109C/T111C) and ubiquitin (E24C/A28C) more than 80, 100 and 40 PCSs were measured, respectively, and fitted against published crystal structures. The results are presented in Tables 2.1 and App. Table A2.1-2.3. A good correlation was found between the experimental and back-calculated PCS (Figure A2.5). The quality of the correlation is expressed with an adjusted Q-value ($Q_a$), defined in eq. 2.1. Only the PCS of the amide of T4Lys residue 163 deviates strongly from the observed value. This residue is located at the C-terminus and its location in the structure may be ill-defined. It was excluded from the calculations. The results for for different crystal structures of the same protein were essentially the same (App. Table A2.1-A2.3). The iso-surfaces of the $\Delta\chi$-tensors, plotted on T4Lys, BCX and ubiquitin, are shown in Figure 2.3 and Figure A2.6. The probes are mostly axial, with only a minor rhombic component. The iso-surfaces of the two enantiomers are very similar. The Co(II) ions are located between the cysteine residues, as expected for a two armed probe, and in line with results obtained for our lanthanoid probes, CLaNP5 and CLaNP7.[21, 48] The distances between the Co(II) and the cysteine $C_\alpha$ atoms are between 7.6 and 9.8 Å (Table 2.1). The distance between Co(II) ions in TraNP1-RR and TraNP1-SS bound to T4Lys is only 1.4 Å and the $\Delta\chi$-tensor orientations are similar (Figure 2.3). However, the $\Delta\chi_{ax}$ of TraNP1-SS is 12% smaller than that of TraNP1-RR (Table 2.1). Also on BCX, TraNP1-RR and TraNP1-SS position the Co(II) in similar locations and the $\Delta\chi$-tensor frame orient in the same way. In this case, $\Delta\chi_{ax}$ of TraNP1-SS is even 32% smaller than for TraNP1-RR. Interestingly, the $\Delta\chi_{ax}$ of TraNP1-RR (SS) attached to BCX is

27% (44%) smaller than for this probe attached to T4Lys Table 2.1). For ubiquitin, the $\Delta\chi$-tensor of Co-TraNP1-SS labeled on ubiquitin was even smaller than for the other two proteins (Table 2.1). These differences will be discussed later.

**Table 2.1** PCS-based $\Delta\chi$-tensor parameters of Co(II)-TraNP1 attached to T4Lys K147C/T151C, BCX E78Q/T109C/ T111C and ubiquitin E24C/A28C.

| **Protein** | **T4Lys** | | **BCX** | | **Ubiquitin** |
|---|---|---|---|---|---|
| **Probes** | **RR** | **SS** | **RR** | **SS** | **SS** |
| $\Delta\chi_{ax}$ [a] | 5.2±0.1 | 4.6±0.1 | 3.8±0.2 | 2.6±0.1 | 2.0±0.1 |
| $\Delta\chi_{rh}$ [a] | 1.2±0.1 | 0.9±0.1 | 0.5±0.1 | 0.6±0.1 | 0.4±0.1 |
| **Restraints** | 81 | 89 | 105 | 100 | 45 |
| $Q_a$ | 0.04 | 0.04 | 0.05 | 0.06 | 0.04 |
| **Co(II)-Cys Cα** | 7.6 (C147) | 7.9 (C147) | 9.8 (C109) | 9.8 (C109) | 8.9 (C24) |
| **distance (Å)** | 8.4 (C151) | 8.3 (C151) | 7.9 (C111) | 8.0 (C111) | 9.3 (C28) |
| **PDB entry** | 2lzm[50] | 2lzm[50] | 2bvv[51] | 2bvv[51] | 2mjb[52] |

[a] in $10^{-32}$ $m^3$

**Paramagnetic relaxation enhancements.** To investigate whether TraNP1 can also be used to generate PREs with a transition metal, TraNP1-SS was loaded with Mn(II) and linked to T4Lys K147C/T151C. PRE was obtained by comparing the intensities of amide resonances in HSQC spectra of Mn(II) and Zn(II) tagged T4Lysles (App. Figure A2.7). Figure 2.4A shows the intensity ratios. From these, the PREs and Mn(II)–$^1H^N$ distances were derived (see Materials and Methods, eq. 2.2 and 2.3). These distances were compared with those obtained from the PCS-based Co(II) position, assuming that Mn(II) and Co(II) in TraNP1-SS sit in the same position relative to T4Lys. A good correlation, with a margin of ±3Å, for distances between 19 and 31 Å was found (Figure 2.4 B). For peaks that broadened beyond detection, the observed distance was set to 19 Å and for the amides with unaffected peak intensities the distance was set to 31 Å, explaining the points on these two horizontal distance lines in Figure 2.4B. Three clear outliers were observed (residues 10, 31 and 32, App. Figure A2.8). It is not clear why these amides give deviating results. The assignments appear correct and the structure is well-defined for these residues. The position of the Mn(II) was also determined by fitting it to the experimental distances (see Material and Methods for details). These calculations place the Mn(II) between the cysteine residues, with distances to the $C_\alpha$ atoms of 7.1 Å (C147) and 8.2 Å (C151). It is 2.5 Å away from the Co(II) position based on the PCS data (App. Figure A2.8A, purple sphere). The experimental and back-calculated distances correlate

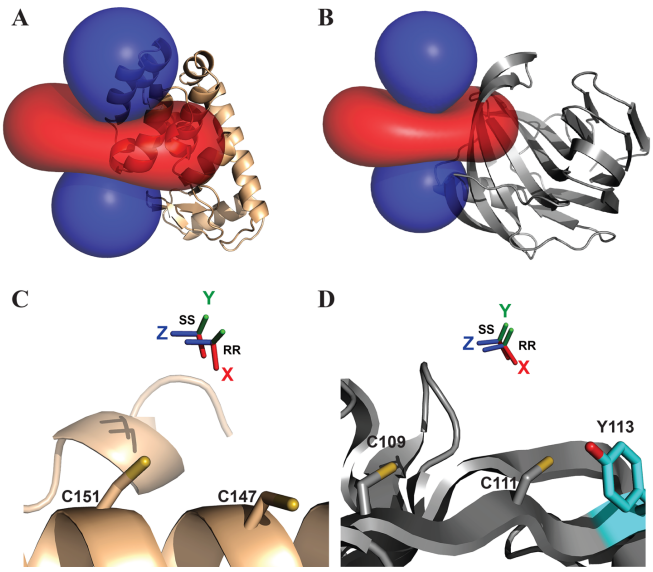


**Figure 2.3** $\Delta\chi$-tensors of TraNP1. A, B) The ±0.2 ppm PCS iso-surfaces of TraNP1-RR are plotted for T4Lys K147C/T151C (PDB entry 2lzm) (**A**) and BCX E78Q/ T109C/T111C (PDB entry 2bvv) (**B**). The backbones of the proteins are drawn in ribbon representation. Positive and negative PCS are indicated by blue and red iso-surfaces, respectively. **C, D**) Co(II) positions and tensor orientations of TraNP1-RR and TraNP1-SS are shown for T4Lys K147C/T151C (**C**) and BCX E78Q/T109C/T111C (**D**). The Cys residues used for attachment have been modelled in the structure and are shown in sticks. Also the sidechain of Tyr113 in BCX is shown in sticks. 3

within the ±3 Å range for most residues, except for residues 10, 31 and 32, which deviate 4-5 Å (App. Figure A2.8B). Exclusion of these three residues yielded a better fit (App. Figure A2.8C). These and other calculations showed that the exact calculated position of the Mn(II) is strongly dependent on the input data set. Even a single violated distance restraint tended to affect the position of the metal (App. Figure A2.8A). It is estimated that the PRE-based position of the metal has a precision of 2-3 Å and is less precise than the location based on the PCS data. However, the metal positions obtained via both approaches are consistent, being in between the two cysteine residues.

**TraNP coordination properties.** To determine which of the pending arms coordinate the metal in TraNP1, TraNP3-S and TraNP5 were synthesized, lacking one or both hydroxy-propionic acid groups, respectively. TraNP5 failed to bind metals, whereas TraNP3-S was capable of coordinating Co(II). When this complex was linked to T4Lys, two sets of PCS were observed for each amide and the PCS was smaller than those observed for TraNP1 (App. Figure A2.9A). As compared to TraNP1, the $C_2$-symmetry is

broken in TraNP3, resulting in two isomers upon attachment to the protein, which could be the cause of the double resonances. It suggests that the amide groups in the other two pending arms are incapable of coordinating the Co(II), so these arms have additional rotational freedom compared to the eight coordination arms of the lanthanoids binding counterparts, CLaNP5 and CLaNP7.[21, 48] Lanthanoids require eight or nine ligands, so all pending arms are involved in metal coordination. We also tested lanthanoids binding to TraNP1. The affinity for these metals is poor. TraNP1 forms six membered rings upon coordination of the metal to the carboxy, whereas in DOTA or the DOTA based CLaNP3,[53] a five membered ring is formed between metal and carboxy group.

**Table 2.2** PCS-based Δχ-tensor parameters of *tag 1* and TraNP1-SS attached to ubiquitin E24C/A28C (PDB entry 2mjb)[52] and T4Lys K147C/T151C (PDB entry 2lzm)[50].

| Protein Probes | Ubiquitin | | | T4Lys | |
|---|---|---|---|---|---|
| | *tag 1* [b] | *tag 1* [c] | TraNP1-SS | *tag 1* | TraNP1-SS |
| $\Delta\chi_{ax}$ [a] | -7.4±0.04 | -7.2±0.1 | 2.2±0.1 | -6.8±0.2 | 4.6±0.1 |
| $\Delta\chi_{rh}$ [a] | -1.4±0.04 | -1.3±0.1 | 0.2±0.1 | -0.46±0.1 | 0.9±0.1 |
| **Restraints** | 66 | 45 | 43 | 53 | 89 |
| $Q_a$ | 0.02 | 0.02 | 0.04 | 0.04 | 0.04 |
| **Co(II)-Cys $C_\alpha$ distance (Å)** | 7.0 (C24)<br>7.4 (C28) | 8.0 (C24)<br>7.4 (C28) | 9.0 (C24)<br>8.8 (C28) | 8.0 (C147)<br>7.0 (C151) | 7.9 (C147) 8.3 (C151) |

[a] in $10^{-32}$ $m^3$; [b] Tensor parameters based on PCSs reported in [36]; [c] Tensor parameters based on work performed in this study.

**Comparison with 'tagging agent 1'.** To compare TraNP1 with another two armed Co(II)-tag, we synthesized the published Co(II) probe named tagging agent 1 (*tag 1*), (S)-2-((pyridin-2-yldisulfaneyl)methyl)succinic acid, Figure 2.1. In this case, the two cysteines on the protein each react with one probe molecule and the Co(II) ion is sandwiched in between the two attached groups. Swarbrick *et al.*[36] attached this probe to ubiquitin E24C/A28C and reported a remarkably large Δχ-tensor ($-7.4 \times 10^{-32}$ $m^3$). We repeated the experiment with the same ubiquitin variant and also attached *tag 1* to T4Lys K147C/T151C. Labeling was checked with mass spectrometry (App. Figure A2.10 and A2.12). For all the samples linked to either tag 1, Co(II)-tag 1 or Zn(II)-tag 1, the same mass was observed, of the free protein plus 409 Da (App. Figure A2.10 and A2.11). This mass difference equals the mass of two attached tag 1 molecule (354 Da) plus an additional 55 Da. As this extra mass was present independent of the presence of either Co(II) or Zn(II) in the sample, we assume that *tag 1* loses these metal ions and picks up another mass in the process of the mass spectroscopy measurement, e.g. Fe(III) or Mn(II) ions. $^{1}H$-$^{15}N$ HSQC spectra of the Co(II) and Zn(II) tagged ubiquitin and T4Lys were recorded and the PCS measured. The size and orientation of the Δχ-tensor of *tag 1*

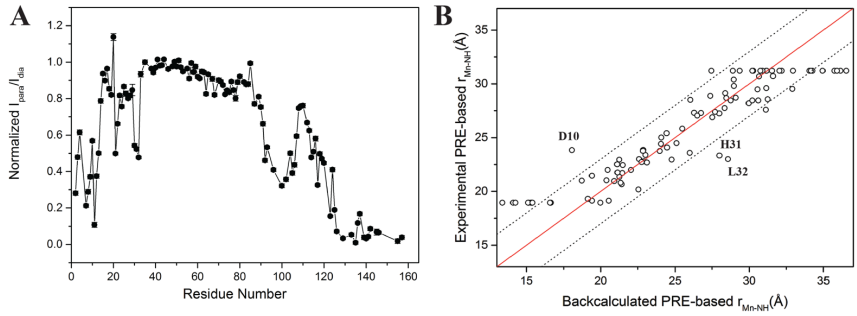


**Figure 2.4** Paramagnetic relaxation enhancement. **A**) $I_{para}/I_{dia}$ ratios of amide resonances in $^{1}$H-$^{15}$N HSQC spectra of T4Lys K147C/T151C tagged with Mn(II)/Zn(II)-TraNP1-SS. **B**) PRE-derived Mn(II)–$^{1}H^{N}$ distances plotted vs. the Co(II)–$^{1}H^{N}$ distances with the Co(II) position derived from PCS data. No fitting was performed. The solid red line represents a perfect correlation and the dotted lines show ±3 Å margin.

derived from the experimental PCS analysis of the ubiquitin NMR spectra were the same as those obtained using the published PCS values (App. Figure 2.7A, Figure A2.12, Table 2.2). In our spectra, some of the residues showed more than a single paramagnetic peak, such as residues K6, T7, L50, Q62, L67 and H68 (App. Figure A2.12). Also, Co(II) loading appeared to be incomplete. In the NMR spectra of ubiquitin tagged with Co(II) loaded *tag1* spectra, diamagnetic peaks were present (App. Figure A2.12B), even if 1.2 equiv. of Co(II) was added, rather than the reported 0.6 equiv.. The tagged, metal-free ubiquitin also behaved curiously, showing many double peaks in the HSQC spectrum, compared to untagged ubiquitin (App. Figure A2.12C). Upon addition of Zn(II), single peaks remain in the HSQC spectrum (App. Figure A2.12C). Thus, the metal free *tag 1* caused the presence of two forms of the protein. Also for T4Lys K147C/T151C, *tag 1* showed partial loading with Co(II) or Zn(II), even with 10 equiv. of the metal ion added. Again, more than one peak with PCS was observed for some of the residues (App. Figure A2.13). From the *tag 1*-T4Lys HSQC spectrum (App. Figure A2.13), around 50 PCSs were measured and used for Co(II) positioning and $\Delta\chi$ tensor calculation. The Co(II) is located between the two cysteine and the distances to the two cysteine C$\alpha$ atoms are around 7 Å (Figure 2.7B), which is similar to the results for the ubiquitin variant. As observed with TraNP1, the size of the tensor was affected by the protein, because the $\Delta\chi_{ax}$ component of Co(II)-*tag 1* was, though still quite large, somewhat smaller than for the ubiquitin variant, and the $\Delta\chi_{rh}$ component was more than three times smaller (Table 2.2).

### Discussion

**Metal coordination and tensor parameters.** The synthesis and characterization of a new two-armed transition metal binding NMR probe, TraNP1, is reported. Loaded with Co(II)

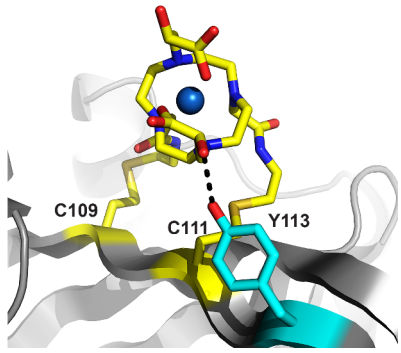


**Figure 2.5** Model of Co-TraNP1-SS attached to BCX E78Q/T109C/T111C. The protein is shown in cartoon representation and the two cysteines and the tag were modelled into the structure (PDB entry 2bvv).[51] The oxygen of Tyr113 (in cyan sticks) can readily be brought into hydrogen bond distance of one of the hydroxy groups of TraNP1-SS. The cysteines and the probe are shown in sticks, with carbons in yellow and the nitrogen, oxygen and sulfurs in blue, red and dark yellow, respectively. The Co(II) ion is shown as a sphere.

and attached to the proteins T4Lys, BCX and ubiquitin via two disulfide bridges, it causes PCS of the resonances of amide nuclei. The PCS can be fitted well and yield the position of the metal relative to the protein as well as the orientation and size of the $\Delta\chi$-tensor. Whereas metal position and tensor orientation are similar, interesting differences are observed in the sizes of the $\Delta\chi_{ax}$ and $\Delta\chi_{rh}$ between the RR and SS enantiomers, as well as between T4Lys, BCX and ubiquitin. We are puzzled by the large variation in these tensor sizes for Co ions that are expected to have the same coordination environments. We attribute these effects are attributed to slight differences in coordination of the cobalt ion. The binding of the probe to the protein and interactions with protein side-chains may introduce slight strain on the Co(II) ligands, leading to changes in the electron distribution and thus in the paramagnetic effect. It is likely that the Co(II) is coordinated by the four ring nitrogens and two carboxy-oxygens in a pseudo-octahedral conformation. Based on the crystal structure of a similar compound,[54] the structure of TraNP1 was modelled using Spartan'14 & Spartan'14 Parallel Suite (www.wavefun.com). The two enantiomers indeed show slight differences (Figure A2.14). The linkage of TraNP1 to the proteins was also modelled, using XPLOR-NIH.[55-56] In this model, the coordination obtained in the Spartan model was constrained and the arms for attachment were free to rotate. The protein backbone was fixed, side chains were allowed to rotate. The position of Co(II) ion was restrained to the experimental position. An acceptable model was obtained in which the plane of the cyclen ring is roughly perpendicular to the surface of the protein and the arms for attachment point away from the ring, relative to the hydroxy-propionic acid groups (Figure 2.5). In the BCX-TraNP1-SS model, Tyr113 is located within hydrogen bonding distance of one of the hydroxy groups. We speculate

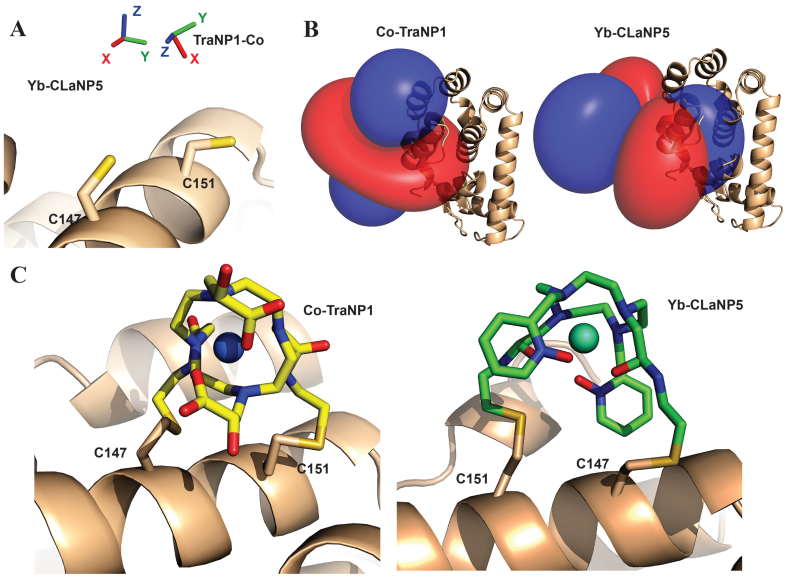


**Figure 2.6** Comparison of Co(II)-TraNP1-SS and Yb(III)-CLaNP5 attached to T4Lys K147C/T151C. **A**) Metal positions and tensor rotations; **B**) PCS iso-surfaces (±0.4 ppm for Yb(III)-CLaNP5, ±0.2 ppm for Co(II)-TraNP1-SS); **C**) Models of the protein-probe structures. The protein is shown in ribbon representation, the probes and cysteines are shown in sticks. The metals are shown as spheres.

that such an interaction with a side chain could affect the ligand coordination of cobalt ion and influence the size of the $\Delta\chi$-tensor. It is concluded that the paramagnetic properties of Co(II) are very sensitive to the environment of the ligands, strongly affecting the size of the anisotropic component of the magnetic susceptibility, in line with the large differences reported for the size of paramagnetic effects in other Co(II)-compounds.[11, 34, 57]

**Comparison between TraNP and CLaNP.** These observations are strikingly different from lanthanoid probes. For rigidly attached probes, such as CLaNP-5 and CLaNP-7, usually similar sizes for $\Delta\chi_{ax}$ and $\Delta\chi_{rh}$ are found, independent of site of attachment.[21, 48] As a consequence, the $\Delta\chi_{ax}$ and $\Delta\chi_{rh}$ need to be determined for TraNP1 in each system, whereas for CLaNP, the sizes can, to first approximation, be estimated on the basis of literature values. Figure 2.6 presents a comparison of the results for Co(II)-TraNP1-SS and Yb(III)-CLaNP5 attached to T4Lys at residues 147 and 151.[58] The positions of the metal are different, with a distance of 2.6 Å between them, although both are located between the two Cys residues. Also, the direction of the main tensor component (z-axis) and the degree of rhombicity differ considerably. Panel C of Figure 2.6 shows the models of the probes attached to T4Lys. In CLaNP, all the four pending arms are involved in the

coordination of the metal and thus are oriented in the same direction, placing them in such a way that the cyclen ring is roughly parallel to the protein surface and the metal in between the cyclen ring and the protein. In TraNP, the cyclen ring is perpendicular to the surface and the metal is thus on one side of the ring, relative to the protein.

**Comparison between TraNP1, *tag 1* and other Co(II) binding motifs**. The comparison of TraNP1 and *tag 1* confirmed that the coordination of the Co(II) has a large effect on the size of the Δχ-tensor. For *tag 1*, four carboxyl groups and two secondary amines are likely involved in the coordination, whereas TraNP1 has two carboxyl groups and four tertiary amines contributing to the coordination. However, both tags are likely to provide a distorted octahedral environment, so it is unclear whether the different type of ligands are the cause of the large Δχ-tensor of *tag 1*, yielding larger PCS than obtained with for TraNP1, approaching those obtained with Yb(III) probes. The metal is roughly located at the same position in both probes, in between the cysteines and 7-8 Å away from the Cα atoms. However, the tensor axes are oriented very differently (Figure 2.7). A disadvantage of *tag 1* is that some amides show more than one resonance in the spectrum of the paramagnetic sample. Furthermore, the metal affinity appears to be relatively low, leading to the presence of peaks of metal-free tagged protein in the spectra of the paramagnetic sample, increasing spectral crowding that could be problematic for larger proteins. Next to the doubly anchored *tag 1*, several tags with a single attachment point were reported, like (2-pyridylthio)-cysteamine-EDTA, 2-vinyl-8-hydroxyquinoline (2V-8HQ)[34] and 3-mercapto-2,6-pyridinedicarboxylic acid (3MDPA)[35]. As a commercially available probe, (2-pyridylthio)-cysteamine-EDTA is widely used in protein paramagnetic NMR after it was first reported with Fe(III) as the paramagnetic center.[59] Further research found that the Co(II) loaded (2-pyridylthio)-cysteamine-EDTA

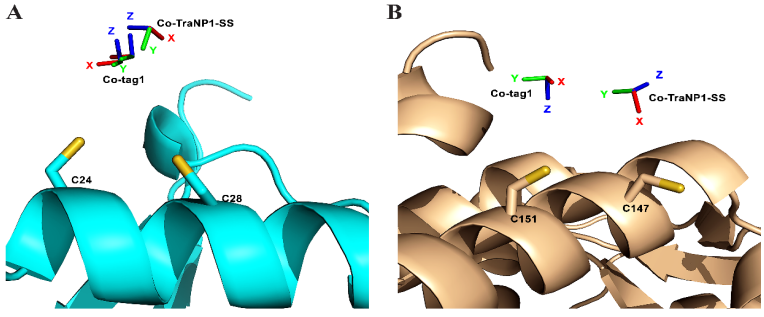


**Figure 2. 7** Metal positions and tensor orientations of Co(II)-TraNP1-SS and Co(II)-tag 1 (attached to ubiquitin E24C/A28C (**A**) and T4Lys K147C/T151C (**B**). In (A) the left tensor of tag 1 is based on fitting the PCS reported in [36]; the right one is based on the PCS observed in the current work. The proteins are shown in ribbons, the cysteines were modelled into the structure and are shown as sticks.

generated two sets of PCS, in one case[33] but not in other[60], due to the presence of stereoisomers of the complex. The 2V-8HQ is a rigid and small probe for the Co(II) and requires additional ligands from a protein side-chains, making the metal location less predictable than for a two-armed probe. Slow exchange of Co(II) ions between the solvent and the 2V-8HQ (chapter I, Figure 1.10) tag on ubiquitin was reported. The affinity and exchange rate depend on the coordinating side chain. For 3MDPA, which can bind Ln(III) and Co(II), the tensor orientations for all the metal ions are similar but the metal affinity is very weak.

To reduce the probe attachment flexibility, genetic incorporation of natural or unnatural amino acids in the protein sequence has been proposed. The unnatural amino acid of bipyridylalanine (BpyAla, chapter 1, Figure 1.4)[61] and 2-amino-3-(8-hydroxyquinolin-3-yl)propanoic acid dihydrochloride (HQA, chapter 1, Figure 1.4)[62] that both side chain strongly chelates transition metal ions were successfully introduced into West Nile virus NS2B-NS3 protease (WNVpro) and membrane proteins (1TM-CXCR1 and p7), respectively. Similar to 2V-8HQ, both require additional ligands provide by protein side chains. HQA was used for not for Co(II) but Mn(II) to measure PRE. Recently, it was reported that also a dihistidine (diHis) motif can be used to bind Co(II).[37] The motif was introduced to ubiquitin at two positions on an α-helix, mutant E24H/A28H and A28H/D32H, as well as a **β**-strand of GB1, mutant E15H/T17H. Also in this study, the dHis motif generated different $\Delta\chi$-tensor values and orientations for the different protein variants.

**Conclusion.** TraNP1 adds a new probe to the range of paramagnetic probes available for NMR on biomolecules.[16, 18] Co(II) has a smaller anisotropic magnetic susceptibility than most lanthanides, placing it close to Pr(III). Its application can lie in studying small and local structural changes in proteins and protein complexes, such as can occur in enzyme active sites during catalysis or in protein pockets upon ligand binding. The stronger effects of lanthanoids are less suitable for studying such small structural changes. The reason is that such probes cannot detect changes close to the probe due to PRE effect and events further away require larger structural changes to cause significant PCS changes. A 1 Å change at a large distance from a paramagnetic metal leads to a small relative change in angle and distance and thus a small change in PCS, both in absolute and relative terms, even for strongly paramagnetic ions. This point is illustrated with an example in App. Table A 2.4. Thus, Yb(III) and the stronger Ho(III), Dy(III), Tm(III) and Tb(III) are suited for studying domain motions and determination of structures of complexes,[18] whereas probes with smaller $\Delta\chi$-tensors are suitable for detection of nearby, small structural changes. The relatively low paramagnetic anisotropy of Co-probes makes the measurement of paramagnetically induced RDC inconvenient at routine fields, such as 14 T (600 MHz), with maximal predicted values for $^{1}H$-$^{15}N$ of 1.7 and 4 Hz for TraNP1 and tag 1, respectively. At the highest fields achievable, obtaining these RDC becomes

realistic (7 and 16 Hz, respectively, at 28 T, 1200 MHz), offering possibilities for the study of protein mobility. Finally, the fact that TraNP1 can also bind Mn(II) to measure PREs is convenient, because PRE derived distances complement the restraints obtained from PCS.

**Materials and Methods**

**General:** cyclen, 2-(aminoethyl)methanethiosulfonate hydrobromide, methyl (S)-oxirane-2-carboxylate, N-(tert-Butoxycarbonyloxy)succinimide, $Ln(OAc)_3$, $CoCl_2{\cdot}6H_2O$, $ZnI_2$, $MnCl_2{\cdot}4H_2O$, methyl (R)-oxirane-2-carboxylate and all other chemicals were purchased and used without further purification. Solvents were purchased from Honeywell, BIOSOLVE or Aldrich and directly used for synthesis. Superdex 75 columns and Sephadex G-25 PD10 desalting columns were purchased from GE Healthcare. Reactions were followed by TLC analysis on silica gel (F 1500 LS 254 Schleicher and Schuell, Dassel, Germany) and visualized by UV and/or ninhydrin, $KMNO_4$. Flash chromatography was performed with Screening Devices silica gel 60 (0.04-0.063 mm). A Waters preparative RP-HPLC system, equipped with a Waters C18-Xbridge 5 µm OBD (30 x 150 mm) column and Äkta Basic FPLC (GE Healthcare Inc.) system were used for purification. NMR spectra were recorded on a Bruker AV-400 (400/100 MHz), AV-500 (500/125 MHz) or AV-600 (600/150 MHz) spectrometer. A LCQ liquid chromatography mass spectrometry system and a Finnigan LTQ Orbitrap system were used for high-resolution mass spectrometry and protein conjugation analysis. A Thermo Finnigan LCQ Advantage MAX was used for liquid chromatography (LC) mass spectrometry (MS) analysis. A Thermo Scientific™ NanoDrop 2000 spectrophotometer was used for protein concentration measurement.

**Protein labeling:** To link TraNPs to $^{15}N$ labelled T4Lys, BCX or ubiquitin, produced as described previously,[64-66] the protein sample (1 mL, 200−400 µM) was treated with DTT (final concentration 10 mM) at 0 °C. After 1 h, the protein solution was loaded on a PD-10 column (GE Healthcare), pre-equilibrated with labeling buffer (20 mM sodium phosphate, 150 mM NaCl, pH 7.0, argon degassed) to remove DTT. The eluted protein was added to a solution of labeling buffer containing TraNP (6 equiv.) under an argon atmosphere. The mixture was stirred at 4 °C for 8 h. Then, the mixture was concentrated to 500 µL and purified by using a Superdex 75 gel filtration column. *Tag 1* attachment to ubiquitin and T4Lys followed the procedure described before.[36] Briefly, the protein solution (200 µM) was incubated with 10 mM of DTT at 4 °C for 1 h. The PD10 column was equilibrated with labelling buffer (50 mM HEPES pH 7.5 for ubiquitin, 20 mM sodium phosphate, 150 mM NaCl pH 7.5 for T4Lys, argon degassed) and the protein solution was loaded to remove the DTT and the eluate was added to 10 equiv. *tag 1* solution in labelling buffer to react at r.t. for 2 h. The labeled proteins were concentrated to 500 µL and purified by using a Superdex 75 gel filtration column. The yield of labeling estimated from the LC/MS and NMR, was more than 95%. The purified *tag 1*-ubiquitin and *tag 1*-T4Lys (120 µM) were treated with 1 mM EDTA and purified by PD10 column, before

incubate with $CoCl_2 \cdot 6H_2O$ (1.2 equiv. or 10 equiv.) and $ZnI_2$ (1.2 equiv.) at 4 °C pH 7.5, for 12 h, respectively. The stock solutions containing 10 mM of the metal salts in the same buffer as the protein solution.

**Protein NMR spectroscopy:** The NMR samples of T4Lys-TraNP (100−200 μM) were prepared in 30 mM sodium phosphate pH 5.5 buffer containg 100 mM NaCl and 6% (*v/v*) $D_2O$. The NMR samples of BCX-TraNP (100−200 μM) contained 25 mM sodium acetate buffer pH 5.5, 6% (*v/v*) $D_2O$. For ubiquitin NMR samples, a buffer of 50 mM HEPES pH 7.5, 6% (*v/v*) $D_2O$ was used. All $^{1}H$-$^{15}N$ HSQC were recorded on a Bruker Avance III 600 MHz (14 T) spectrometer, at 298 K for T4Lys/ubiquitin-TraNP/*tag 1* samples and 293 K for BCX-TraNP samples. Data were processed with Topspin 3.5 and analyzed with CcpNmr Analysis version 2.4.0.[67] T4Lys and BCX resonance assignments were kindly provided by Simon P. Skinner and Fredj Ben Bdira, respectively, based on previous work[68-69]. Ubiquitin resonance assignments were kindly provided by Carlos A. Castañeda and David Fushman.

**PCS data analysis:** The $\Delta\chi$-tensors were calculated using Numbat software.[70] Crystal structures of T4Lys, BCX and ubiquitin (PDB entries 2lzm, 2bvv and 2mjb)[50-52], to which hydrogens had been added, were used. The experimental PCS were fitted to equation 1.1, chapter I. The $Q_a$ factor provides a normalized measure for the agreement between a set of observed and calculated data according to equation 2.1:[71]

$$Q_a = \sqrt{\frac{\sum(\delta_{PCS,i}^{cal} - \delta_{PCS,i}^{exp})^2}{\sum(|\delta_{PCS,i}^{cal}| + |\delta_{PCS,i}^{exp}|)^2}} \qquad 2.1$$

where $\delta_{PCS,i}^{cal}$ and $\delta_{PCS,i}^{exp}$ are the back-calculated and experimentally observed PCS for each residue.

**PRE Data Analysis:** The intensity ratio of amide resonances in the paramagnetic sample spectra (Mn(II)-TraNP1-T4Lys, $I_{para}$) and diamagnetic sample spectra (Zn(II)-TraNP1-T4Lys, $I_{dia}$) was determined and normalized, as described previously.[72-73] The $R_{2,para}$ was calculated using equation 2.2, where the $R_{2,dia}$ was obtained from the width at half-height in Hz ($\Delta\mathbf{v}_{1/2}$) of a Lorentzian fit in the proton dimension by using $R_2 = \pi\Delta\mathbf{v}_{1/2}$ in the diamagnetic spectra, and t is the total INEPT evolution time of the HSQC (9 ms).[72] The standard deviation of the spectrum noise level was determined by CcpNmr.[67] The error of $R_{2,para}$ was calculated as described.[73] The $H^N$-to-metal distance (r) was calculated with equation 2.3[71] (see list of symbols at beginning of thesis for all symbol descriptions)

$$\frac{I_{para}}{I_{dia}} = \frac{R_{2,dia}e^{(-R_{2,para}t)}}{R_{2,dia}+R_{2,para}} \qquad 2.2$$

$$r_{IM} = \sqrt[6]{\frac{1}{R_{2,para}}\frac{\gamma_I^2 g_e^2 \beta^2 \mu_0^2 (S+1)S}{240\pi^2}\left(4\tau_c + \frac{3\tau_c}{1+\omega_I^2\tau_c^2}\right)} \qquad 2.3$$

The observed PREs were sorted into three classes of distance restraints. The first class (16 restraints) were those residues with an intensity ratio < 0.2. These residues were considered to be too close to Mn(II) for accurate distance determination and to this class an upper limit of 19 Å was assigned. The second class (39 restraints) was formed by residues with a ratio > 0.87, which were considered to be too far from Mn(II) to yield significant PREs and to these was assigned a lower distance limit of 31 Å. The third class (62 restraints) contained the residues with an intensity ratio between 0.20 and 0.87, and the distances were determined using equation 2.3. All bounds were allowed an additional error margin of 3 Å. The three classes of distance restraints were employed to position the Mn-ion relative to the protein, by using restrained energy minimization protocol in the program X-PLOR-NIH version 2.9.9,[55] in which the NOE term (used for the PRE distances) was the only applied energy term. The protein was fixed and transparent for the metal ion (no van der Waals forces were used). In this way, the metal position is solely determined by the experimental distances. All the parameters are shown in App..

**Synthesis:**

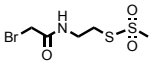

**S-(2-(2-bromoacetamido)ethyl) methanesulfonothioate, 1**

To a solution of S-(2-aminoethyl) methanesulfonothioate-HBr salt (0.5 g, 2.13 mmol) in $H_2O$ (20 mL) $K_2CO_3$ (0.59g, 4.26 mmol) was added. While stirring was continued, the reaction mixture was cooled (0°C) and a solution of acetyl bromide (0.3 mL, 4.26 mmol) in DCM (20 mL) was added drop-wised. The resulting two layers were separated and the water layer was extracted with ethyl acetate (3 x 20 mL). The organic layer (combination of the DCM layer and extracted ethyl acetate layer) was dried ($Na_2SO_4$), concentrated under reduced pressure and purified by silica flash column chromatography (25% of ethyl acetate in pentane), giving compound **1** as a white solid (1 g, 72% yield). $^1$H NMR (400 MHz, $CDCl_3$, 293K): **δ** = 3.31-3.34 (t, 2H, J= 4 Hz), 3.36 (s, 3H), 3.62-3.67 (q, 2H, J=8 Hz), 3.86 (s, 2H), 7.10 (b, 1H). $^{13}$C NMR (400 MHz, $CDCl_3$, 293K): **δ** = 28.89 ($CH_3Br$), 35.38 ($CH_2SO_2$), 37.33 ($CH_2$ $CH_2SO_2$), 39.87 ($CH_2Br$), 50.67 ($CH_3SSO_2$), 166.56 (CONH). HR-MS: m/z 297.9175 $[M+Na]^+$, calcd. $[C_5H_{10}BrO_3S_2]$ 297.9183. FTIR ν ($cm^{-1}$): 1652.7, 1539.7, 1666.4, 1309.3, 1127.6, 957.3, 745.5. mp: 53.2-53.6 °C.

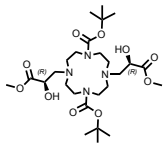

**Di-tert-butyl4,10-bis((*R*)-2-hydroxy-3-methoxy-3-oxopropyl)-1,4,7,10-tetraazacyclododecane-1,7-dicarboxylate, 3*RR***

To a solution of compound **2**[21, 48] (1 g, 2.69 mmol) in methanol (30 mL) methyl (*R*)-oxirane-2-carboxylate (1.4 mL, 16.14 mmol) was added, and stirring was continued for 36 h at room temperature (r.t.), then the product was concentrated under reduced pressure and purified by silica flash column chromatography (40% of ethyl acetate in pentane) to give compound **3 (*RR*)** as an amorphous white solid (1 g, 61% yield). An analogous procedure was used for synthesis of RR-isomer, 2 g (5.4 mmol) of compound **2** and 2.8 mL (16.14 mmol) of (*R*)-oxirane-2-

carboxylate, with a yield of 63% (1.87 g) of compound **3** (***SS***). RR-isomer $^{1}$H NMR (500 MHz, $CDCl_3$, 298 K): **δ** = 1.44 (s, 18H), 2.68-2.67 (br, 6H), 2.85 (br, 2H), 2.99 (br, 4H), 3.32-3.33 (br, 8H), 3.75 (s, 6H) 4.34 (br, 2H). $^{13}$C NMR (500 MHz, $CDCl_3$, 298K): **δ** = 28.57 ($(CH_3)_3C$), 48.73 ($CH_2N$), 52.47 ($CH_3OOC$), 55.10 ($CH_2N$), 58.69 ($CH_2CHOH$), 68.92 (CHOH), 80.26 (C $(CH_3)_3$), 156.47 (COO*t*Bu). The spectroscopic data of the RR-isomer are in accordance with its enantiomer. SS-isomer HR-MS: m/z 577.3450 $[M+H]^+$, calcd. $[C_{26}H_{48}N_4O_{10}]$ 577.3404. RR-isomer HR-MS: m/z 577.3455 $[M+H]^+$, calcd. $[C_{26}H_{48}N_4O_{10}]$ 577.3404. SS-isomer $[\alpha]_D^{20}$= -17.5 (C= 2 mg/mL, methanol), RR-isomer$[\alpha]_D^{20}$= 16.5 (C = 10 mg/mL, methanol). FTIR ν ($cm^{-1}$) SS-isomer: 2923.4, 1734.4, 1054.6, 1033.1, 1013.1.

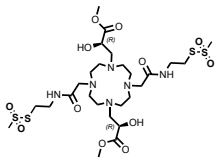

**Dimethyl3,3'-(4,10-bis(2-((2-((methylsulfonyl)thio)ethyl)amino)-2-oxoethyl)-1,4,7,10-tetraazacyclododecane-1,7-diyl)(2S,2'S)-bis(2-hydroxypropanoate), 4*RR***

Compound **3 (*RR*)** (0.5 g, 0.87 mmol) was dissolved in a mixture of dichloromethane and TFA (2.5 mL, 2:3 *v/v*) and stirred for 16 h at room temperature. The reaction mixture was concentrated under reduced pressure and co-evaporated with toluene to remove the TFA. The crude mixture was dissolved in acetonitrile (9 mL), and S-(2-(2-bromoacetamido)ethyl) methanesulfonothioate (0.61 g, 2.61 mmol), $K_2CO_3$ (0.48 g, 3.48 mmol) and a catalytic amount of tetrabutylammonium iodide (TBAI) were added. After stirring for 48 h at r.t., the reaction mixture was filtered and the solid was washed with acetonitrile (50 mL). The filtrate was concentrated under reduced pressure to give a yellow oil which was purified by reverse phase HPLC (0.2% TFA and a 10-20% acetonitrile gradient on a C18 preparative column) obtaining compound **4 (*RR*) (**0.42 g, 63%). A similar procedure was used for the synthesis of the SS-isomer, 1g (1.74 mmol) of compound **3** (***SS*)** and 1.22 g (5.22 mmol), with a yield of 60% (0.8 g) of compound **4** (***SS***). RR-isomer $^{1}$H NMR (500 MHz, $CD_3OD$, 333K): **δ** = 3.13 (br, 8H), 3.36-3.39 (t, 4H, J= 5 Hz), 3.43 (s, 8H), 3.47-3.55 (br, 12H), 3.56-3.63 (m, 10H), 3.80 (s, 6H), 4.77-4.81 (dd, 2H, J= 5 Hz). 13C NMR (500 MHz, $CD_3OD$, 333K): **δ** = 36.44 ($CH_2SO_2$), 40.37 ($CH_2$ $CH_2SO_2$), 50.65 ($CH_2N$), 52.51 ($CH_2N$), 53.35 ($CH_3S$), 55.94 ($CH_2CONH$), 56.97 ($CH_2CHOH$), 67.47 (CHOH), 172.74 ($COOCH_3$). The spectroscopic data of the SS-isomer are in agreement with its enantiomer. HR-MS SS-isomer: m/z 767.2468 $[M+H]^+$, calcd. $[C_{26}H_{50}N_6O_{12}S_4]$ 767.2403; RR-isomer: m/z 767.2466 $[M+H]^+$, calcd. $[C_{26}H_{50}N_6O_{12}S_4]$ 767.2403. SS-isomer $[\alpha]_D^{20}$= -17.4 (C= 5 mg/mL, Methnol), RR-isomer $[\alpha]_D^{20}$= 16.3 (C= 10 mg/mL, Methnol). FTIR ($cm^{-1}$) SS-isomer: 1748.6, 1669.9, 1313.6, 1200.6, 1177.7, 1129.0, 960.2, 831.4, 801.3, 748.4, 719.8.

**Di-tert-butyl4,10-bis(2-((2-((methylsulfonyl)thio)ethyl)amino)-2-oxoethyl)-1,4,7,10-tetraazacyclododecane-1,7-dicarboxylate, 5**

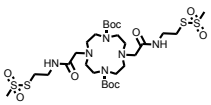

To a solution of compound **2**[48, 63](1 g, 2.69 mmol) in acetonitril (30 mL), compound **1** (3 g, 10.76 mmol) and $K_2CO_3$ (1.5 g, 10.76 mmol) were added. The reaction mixture was stirred at r.t. for 48 h, then filtered and concentrated under reduced pressure and purified by silica flash column chromatography (3% of MeOH in DCM) to give an oily product (1.1 g, 54% yield). $^1$H NMR (500 MHz, $CDCl_3$, 298K): **δ** = 1.45 (s, 18H), 2.84 (s, 8H), 3.23 (s, 4H, $CH_2CONH$), 3.34 (t, 4H), 3.37 (s, 6H), 3.37-3.38 (br, 8H), 3.60-3.64 (dd, 4H); $^{13}$C NMR (500 MHz, $CDCl_3$, 298K): **δ** = 28.71 ($(CCH_3)_3C$), 35.86 ($CH_2SO_2S$), 39.03 ($CH_2CH_2SO_2S$), 80.59 ($C(CH_3)_3$), 156.70 (COO*t*Bu). HR-MS: m/z 763.2850 $[M+H]^+$, calcd. $[C_{28}H_{55}N_6O_{10}S_4]$ 763.2862. FTIR ($cm^{-1}$): 2973.5, 2933.4, 1684.2, 1319.3, 1156.2, 1053.2, 1033.1, 960.2, 831.2, 799.2, 748.4, 721.2.

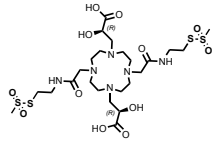

**(2*S*,2'*S*)-3,3'-(4,10-bis(2-((2-((methylsulfonyl)thio)ethyl)amino)-2-oxoethyl)-1,4,7,10-tetraazacyclododecane-1,7-diyl)bis(2-hydroxypropanoic acid), TraNP1**

Compound **4 (*RR*)** (0.2 g, 0.26 mmol) was dissolved in 1 M HCl (6 mL) and heated to 50°C for 8 h. The pH of the reaction mixture was adjusted to 6 by using a solution of sat. $NaHCO_3$ at 0 °C. The solution was concentrated *in vacuo* to give a yellow oil and the crude compound purified by reverse phase HPLC (0.2% TFA and a 11-16% acetonitrile gradient on C18 preparative column), yielding 67% TraNP1-SS (white solid). The synthesis of the TraNP1-SS isomer followed a similar procedure, 6 mL of 1 M HCl solution containing 0.2 g (0.26 mmol) of compound 4 (***SS***) was heated up to 50 °C for 8 h to yield 0.12 g of TraNP1-SS (yield 62%). TraNP1-RR $^1$H NMR (500 MHz, $CD_3OD$, 333 K): **δ** = 3.09-3.19 (br, 8H, $CH_2N$), 3.37-3.38 (t, 4H, J= 5 Hz), 3.42 (s, 6H), 3.50-3.55 (br, 14H), 3.58-3.65 (br, 8H), 4.69-4.72 (dd, 2H, J= 5 Hz). $^{13}$C NMR (500 MHz, $CD_3OD$, 333K): **δ** = 36.45 ($CH_2SO_2$), 40.37 ($CH_2CH_2SO_2$) 50.74 ($CH_2N$), 52.90 ($CH_2N$), 50.97 ($CH_3S$), 56.09 ($CH_2CONH$), 57.64 ($CH_2CHO$) 67.30 (CHOH) 172.53 (COOH), 173.92 (CONH). The spectroscopic data of TraNP1-SS are in agreement with its enantiomer. SS isomer HR-MS: m/z 739.2154 $[M+H]^+$, calcd. $[C_{24}H_{46}N_6O_{12}S_4]$ 739.2050. RR isomer HR-MS: m/z 739.2141 $[M+H]^+$, calcd. $[C_{24}H_{46}N_6O_{12}S_4]$ 739.2050. SS-isomer $[\alpha]_D^{20}$ = -17.8 (C = 10 mg/mL, methanol), RR-isomer $[\alpha]_D^{20}$ = 16.6 (C= 5 mg/mL, methanol). FTIR ($cm^{-1}$) SS-isomer: 1659.9, 1559.7, 1312.2, 1196.3, 1126.2, 1033.1, 958.7, 831.4, 799.9, 747.0, 719.8.

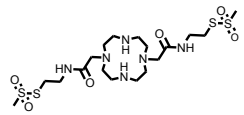

**S,S'-(((2,2'-(1,4,7,10-tetraazacyclododecane-1,7 diyl)bis(acetyl))bis(azanediyl))bis(ethane-2,1-diyl))dimethanesulfonothioate, TraNP5**

Compound **5** (0.5 g, 0.66 mmol) was deprotected with a mixture of DCM:TFA (*v:v*, 2:3) for 6 h at r.t., then concentrated under reduced pressure and co-evaporated with toluene. $^1$H NMR (500 MHz, $CD_3OD$, 298 K): **δ** = 2.99-3.01 (br, 8H), 3.16-3.18 (t, 8H, J=5 Hz), 3.35-3.38 (t, 4H, J= 5 Hz), 3.45-3.46 (s, 10H) 3.58-3.61 (t, 4H, J= 5 Hz). $^{13}$C NMR (500 MHz,

$CD_3OD$, 298K): **δ** = 36.42 ($CH_2SO_2S$), 40.28 ($CH_2CH_2SO_2S$), 44.57 ($CH_2N$), 50.71 ($CH_2N$), 51.47 ($CH_3S$), 57.03 ($CH_2CONH$), 173.60 (CONH). HR-MS SS-isomer: m/z 563.1805 $[M+H]^+$, calcd. $[C_{18}H_{38}N_6O_6S_4]$ 563.1814. FTIR ($cm^{-1}$): 1671.3, 1319.6, 1199.13, 1177.7, 1127.6, 958.7, 831.4, 798.5, 748.4, 721.2.

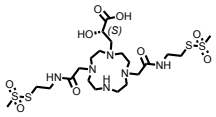

**(*S*)-3-(4,10-bis(2-((2-((methylsulfonyl)thio)ethyl)amino)-2-oxoethyl)-1,4,7,10-tetraazacyclododecan-1-yl)-2-hydroxypropanoic acid, TraNP3-S**

To a solution of TraNP5 (0.2 g, 0.36 mmol) in methanol (3 mL), methyl (*S*)-oxirane-2-carboxylate (31 µL, 0.36 mmol) was added, the mixture stirred at r.t. for 36 h, and concentrated under reduced pressure. Without purification, the crude mixture was deprotected with a 1 M HCl (2 mL) solution at 50 °C and purified by reverse phase HPLC (0.2% TFA and a 15-20% acetonitrile gradient on C18 preparative column). $^1$H NMR (500 MHz, $CD_3OD$, 333 K): **δ** = 3.03 (t, 4H, J= 5Hz), 3.11 (t, 4H, J= 5 Hz), 3.22 (t, 4H, J= 5 Hz), 3.38 (t, 4H, J= 10 Hz), 3.43 (s, 6H), 3.43-3.45 (br, 4H), 3.47 (d, 4H), 3.51-3.56 (m, 2H), 3.59-3.62 (t, 4H, J= 5Hz), 4.53 (m, 1H). $^{13}$C NMR (500 MHz, $CD_3OD$, 343K): **δ** = 36.47 ($CH_2SO_2S$), 40.30 ($CH_2CH_2SO_2S$), 44.65 ($CH_2N$), 50.85 ($CH_2N$), 50.16 ($CH_2N$), 56.96 ($CH_2NH$), 50.89 ($CH_3S$), 53.73 ($CH_2CONH$), 58.03 ($CH_2CHOH$), 67.73 ($CHOHCH_2$), 173.30 (COOH), 174.87 (CONH). HR-MS: m/z 651.1973 $[M+H]^+$, calcd. $[C_{21}H_{42}N_6O_9S_4]$ 651.1896. $[\alpha]_D^{20}$ = -9.1 (C = 2 mg/mL, methanol). FTIR ($cm^{-1}$): 1677.7, 1558.3, 1456.7, 1418.1, 1313.6, 1200.6, 1130.5, 958.7, 832.8, 799.9, 748.4, 712.2.

**Metal complex**: To a solution of TraNP1-SS (20.7 mg, 28 µmol) in 280 µL ACN, 1.1 equiv. $CoCl_2{\cdot}6H_2O$ was added. The mixture was stirred at rt for 3 h and the formation of metal complex was checked by LC/MS. Without further purification, Co-TraNP1-SS was used to protein sample labeling. The other metal ions Zn(II) and Mn(II) were chelated to TraNPs following the same procedure. Co-TraNP1-SS HR-MS: m/z 796.1319 $[M+H]^+$, calcd. $[C_{24}H_{44}CoN_6O_{12}S_4]$ 796.1232; Zn-TraNP1-SS HR-MS: m/z 401.0667 $[M+H]^{2+}$, calcd. $[C_{24}H_{44}ZnN_6O_{12}S_4]$ 401.0596; Mn-TraNP1-SS HR-MS: m/z 792.1354 $[M+H]^+$, calcd. $[C_{24}H_{44}MnN_6O_{12}S_4]$ 791.1282; Co-TraNP1-RR HR-MS: m/z 796.1317 $[M+H]^+$, calcd. $[C_{24}H_{44}CoN_6O_{12}S_4]$ 796.1232; Zn-TraNP1-RR HR-MS: m/z 401.0687 $[M+2H]^{2+}$ calcd. $[C_{24}H_{44}ZnN_6O_{12}S_4]$ 401.0669. Co-TraNP3-S HR-MS: m/z 708.1149 $[M+H]^+$, calcd. $[C_{24}H_{44}CoN_6O_{12}S_4]$ 708.1150.

**References**

(1) Banci, L.; Bertini, I.; Eltis, L. D.; Felli, I. C.; Kastrau, D. H. W.; Luchinat, C.; Piccioli, M.; Pierattelli, R.; Smith, M. The Three-Dimensional Structure in Solution of the Paramagnetic High-Potential Iron-Sulfur Protein I from *Ectothiorhodospira Halophila* through Nuclear Magnetic Resonance. *Eur. J. Biochem.* **1994**, *225*, 715-725.

(2) Bertini, I.; Luchinat, C.; Parigi, G.; Pierattelli, R. NMR Spectroscopy of Paramagnetic Metalloproteins. *ChemBioChem* **2005**, *6*, 1536-1549.

(3) Arnesano, F.; Banci, L.; Piccioli, M. NMR Structures of Paramagnetic Metalloproteins. *Q. Rev. Biophys.* **2005**, *38*, 167-219.
(4) Bertini, I.; Ciurli, S.; Dikiy, A.; Gasanov, R.; Luchinat, C.; Martini, G.; Safarov, N. High-Field NMR Studies of Oxidized Blue Copper Proteins: The Case of Spinach Plastocyanin. *J. Am. Chem. Soc.* **1999**, *121*, 2037-2046.
(5) Banci, L.; Bertini, I.; Bren, K. L.; Gray, H. B.; Sompornpisut, P.; Turano, P. Solution Structure of Oxidized *Saccharomyces Cerevisiae* Iso-1-Cytochrome *c*. *Biochemistry* **1997**, *36*, 8992-9001.
(6) Koehler, J.; Meiler, J. Expanding the Utility of NMR Restraints with Paramagnetic Compounds: Background and Practical Aspects. *Prog. Nucl. Magn. Reson. Spectrosc.* **2011**, *59*, 360-389.
(7) Hass, M. A. S.; Ubbink, M. Structure Determination of Protein–Protein Complexes with Long-Range Anisotropic Paramagnetic NMR Restraints. *Curr. Opin. Struct. Biol.* **2014**, *24*, 45-53.
(8) Volkov, A. N.; Worrall, J. A. R.; Holtzmann, E.; Ubbink, M. Solution Structure and Dynamics of the Complex between Cytochrome *c* and Cytochrome *c* Peroxidase Determined by Paramagnetic NMR. *Proc. Natl. Acad. Sci.* **2006**, *103*, 18945-18950.
(9) Scanu, S.; Foerster, J. M.; Ullmann, G. M.; Ubbink, M. Role of Hydrophobic Interactions in the Encounter Complex Formation of the Plastocyanin and Cytochrome *f* Complex Revealed by Paramagnetic NMR Spectroscopy. *J. Am. Chem. Soc.* **2013**, *135*, 7681-7692.
(10) Schilder, J.; Liu, W. M.; Kumar, P., Wei-Min; Overhand, M.; Huber, M.; Ubbink, M. Protein Docking Using an Ensemble of Spin Labels Optimized by Intra-Molecular Paramagnetic Relaxation Enhancement. *Phys. Chem. Chem. Phys.* **2016**, *18*, 5729-5742.
(11) Cerofolini, L.; Staderini, T.; Giuntini, S.; Ravera, E.; Fragai, M.; Parigi, G.; Pierattelli, R.; Luchinat, C. Long-Range Paramagnetic NMR Data Can Provide a Closer Look on Metal Coordination in Metalloproteins. *J. Biol. Inorg. Chem.* **2018**, *23*, 71-80.
(12) Piccioli, M.; Turano, P. Transient Iron Coordination Sites in Proteins: Exploiting the Dual Nature of Paramagnetic NMR. *Coord. Chem. Rev.* **2015**, *284*, 313-328.
(13) Harper, L. V.; Amann, B. T.; Vinson, V. K.; Berg, J. M. NMR Studies of a Cobalt-Substituted Zinc Finger Peptide. *J. Am. Chem. Soc.* **1993**, *115*, 2577-2580.
(14) Barthelmes, K.; Reynolds, A. M.; Peisach, E.; Jonker, H. R. A.; DeNunzio, N. J.; Allen, K. N.; Imperiali, B.; Schwalbe, H. Engineering Encodable Lanthanide-Binding Tags into Loop Regions of Proteins. *J. Am. Chem. Soc.* **2011**, *133*, 808-819.
(15) Barthelmes, D.; Barthelmes, K.; Schnorr, K.; Jonker, H. R. A.; Bodmer, B.; Allen, K. N.; Imperiali, B.; Schwalbe, H. Conformational Dynamics and Alignment Properties of Loop Lanthanide-Binding-Tags (LBTs) Studied in Interleukin-1β. *J. Biomol. NMR* **2017**, *68*, 187-194.
(16) Liu, W.-M.; Overhand, M.; Ubbink, M. The Application of Paramagnetic Lanthanoid Ions in NMR Spectroscopy on Proteins. *Coord. Chem. Rev.* **2014**, *273-274*, 2-12.
(17) Keizers, P. H. J.; Ubbink, M. Paramagnetic Tagging for Protein Structure and Dynamics Analysis. *Prog. Nucl. Magn. Reson. Spectrosc.* **2011**, *58*, 88-96.
(18) Nitsche, C.; Otting, G. Pseudocontact Shifts in Biomolecular NMR Using Paramagnetic Metal Tags. *Prog. Nucl. Magn. Reson. Spectrosc.* **2017**, *98-99*, 20-49.
(19) Nitsche, C.; Otting, G., Chapter 2 Intrinsic and Extrinsic Paramagnetic Probes. In *Paramagnetism in Experimental Biomolecular NMR*, The Royal Society of Chemistry: 2018; pp 42-84.
(20) Yang, F.; Wang, X.; Pan, B.-B.; Su, X.-C. Single-armed Phenylsulfonated Pyridine Derivative of DOTA is Rigid and Stable Paramagnetic Tag in Protein Analysis. *Chem. Commun.* **2016**, *52*, 11535-11538.

(21) Keizers, P. H. J.; Saragliadis, A.; Hiruma, Y.; Overhand, M.; Ubbink, M. Design, Synthesis, and Evaluation of a Lanthanide Chelating Protein Probe: ClaNP-5 Yields Predictable Paramagnetic Effects Independent of Environment. *J. Am. Chem. Soc.* **2008**, *130*, 14802–14812.

(22) Müntener, T.; Kottelat, J.; Huber, A.; Häussinger, D. New Lanthanide Chelating Tags for PCS NMR Spectroscopy with Reduction Stable, Rigid Linkers for Fast and Irreversible Conjugation to Proteins. *Bioconjugate Chem.* **2018**, *29*, 3344-3351.

(23) Loh, C.-T.; Graham, B.; Abdelkader, E. H.; Tuck, K. L.; Otting, G. Generation of Pseudocontact Shifts in Proteins with Lanthanides Using Small "Clickable" Nitrilotriacetic Acid and Iminodiacetic Acid Tags. *Chem. Eur. J.* **2015**, *21*, 5084-5092.

(24) Lescanne, M.; Ahuja, P.; Blok, A.; Timmer, M.; Akerud, T.; Ubbink, M. Methyl Group Reorientation under Ligand Binding Probed by Pseudocontact Shifts. *J. Biomol. NMR* **2018**, *71*, 275-285.

(25) Guan, J.-Y.; Keizers, P. H. J.; Liu, W.-M.; Löhr, F.; Skinner, S. P.; Heeneman, E. A.; Schwalbe, H.; Ubbink, M.; Siegal, G. Small-Molecule Binding Sites on Proteins Established by Paramagnetic NMR Spectroscopy. *J. Am. Chem. Soc.* **2013**, *135*, 5859-5868.

(26) Dorazio, S. J.; Olatunde, A. O.; Tsitovich, P. B.; Morrow, J. R. Comparison of Divalent Transition Metal Ion Paracest MRI Contrast Agents. *J. Biol. Inorg. Chem.* **2014**, *19*, 191-205.

(27) Epperson, J. D.; Ming, L.-J.; Baker, G. R.; Newkome, G. R. Paramagnetic Cobalt(II) as an NMR Probe of Dendrimer Structure: Mobility and Cooperativity of Dendritic Arms. *J. Am. Chem. Soc.* **2001**, *123*, 8583-8592.

(28) Gochin, M. A High-Resolution Structure of a DNA–Chromomycin–Co(II) Complex Determined from Pseudocontact Shifts in Nuclear Magnetic Resonance. *Structure* **2000**, *8*, 441-452.

(29) Bertini, I.; Fragai, M.; Lee, Y.-M.; Luchinat, C.; Terni, B. Paramagnetic Metal Ions in Ligand Screening: The $Co^{II}$ Matrix Metalloproteinase 12. *Angew. Chem. Int. Ed.* **2004**, *43*, 2254-2256.

(30) Tu, K.; Gochin, M. Structure Determination by Restrained Molecular Dynamics Using NMR Pseudocontact Shifts as Experimentally Determined Constraints. *J. Am. Chem. Soc.* **1999**, *121*, 9276-9285.

(31) Balayssac, S.; Bertini, I.; Bhaumik, A.; Lelli, M.; Luchinat, C. Paramagnetic Shifts in Solid-State NMR of Proteins to Elicit Structural Information. *Proc. Natl. Acad. Sci.* **2008**, *105*, 17284.

(32) Nadaud, P. S.; Helmus, J. J.; Kall, S. L.; Jaroniec, C. P. Paramagnetic Ions Enable Tuning of Nuclear Relaxation Rates and Provide Long-Range Structural Restraints in Solid-State NMR of Proteins. *J. Am. Chem. Soc.* **2009**, *131*, 8108-8120.

(33) Pintacuda, G.; Moshref, A.; Leonchiks, A.; Sharipo, A.; Otting, G. Site-specific Labelling with a Metal Chelator for Protein-Structure Refinement. *J. Biomol. NMR* **2004**, *29*, 351-361.

(34) Yang, Y.; Huang, F.; Huber, T. Site-Specific Tagging Proteins with a Rigid, Small and Stable Transition Metal Chelator, 8-Hydroxyquinoline, for Paramagnetic NMR Analysis. *J. Biomol. NMR* **2016**, *64*, 103-113.

(35) Man, B.; Su, X.-C.; Liang, H.; Simonsen, S.; Huber, T.; Messerle, B. A.; Otting, G. 3-Mercapto-2,6-Pyridinedicarboxylic Acid: A Small Lanthanide-Binding Tag for Protein Studies by NMR Spectroscopy. *Chem. Eur. J.* **2010**, *16*, 3827-3832.

(36) Swarbrick, J. D.; Ung, P.; Dennis, M. L.; Lee, M. D.; Chhabra, S.; Graham, B. Installation of a Rigid EDTA-like Motif into a Protein **α**-Helix for Paramagnetic NMR Spectroscopy with Cobalt(II) Ions. *Chem. Eur. J.* **2015**, *22*, 1228-1232.

(37) Bahramzadeh, A.; Jiang, H.; Huber, T.; Otting, G. Two Histidines in an **α** -Helix : A Rigid $Co^{2+}$ -Binding Motif for PCS Measurements by NMR Spectroscopy. *Angew. Chem. Int. Ed.* **2018**, 6226-6229.

(38) Drewry, J. A.; Gunning, P. T. Recent Advances in Biosensory and Medicinal Therapeutic Applications of Zinc(II) and Copper(II) Coordination Complexes. *Coord. Chem. Rev.* **2011**, *255*, 459-472.

(39) Renfrew, A. K.; O'Neill, E. S.; Hambley, T. W.; New, E. J. Harnessing the Properties of Cobalt Coordination Complexes for Biological Application. *Coord. Chem. Rev.* **2018**, *375*, 221-233.

(40) Wahsner, J.; Gale, E. M.; Rodríguez-Rodríguez, A.; Caravan, P. Chemistry of MRI Contrast Agents: Current Challenges and New Frontiers. *Chem. Rev.* **2019**, *119*, 957-1057.

(41) Woods, M.; Kovacs, Z.; Zhang, S.; Sherry, A. D. Towards the Rational Design of Magnetic Resonance Imaging Contrast Agents: Isolation of the Two Coordination Isomers of Lanthanide DOTA-type Complexes. *Angew. Chem. Int. Ed.* **2003**, *42*, 5889-5892.

(42) Wang, S.; Westmoreland, T. D. Correlation of Relaxivity with Coordination Number in Six-, Seven-, and Eight-coordinate Mn(II) Complexes of Pendant-arm Cyclen Derivatives. *Inorg. Chem.* **2009**, *48*, 719-727.

(43) Meyer, M.; Dahaoui-Gindrey, V.; Lecomte, C.; Guilard, R. Conformations and Coordination Schemes of Carboxylate and Carbamoyl Derivatives of the Tetraazamacrocycles Cyclen and Cyclam, and the Relation to Their Protonation States. *Coord. Chem. Rev.* **1998**, *178-180*, 1313-1405.

(44) Alexander, V. Design and Synthesis of Macrocyclic Ligands and Their Complexes of Lanthanides and Actinides. *Chem. Rev.* **1995**, *95*, 273-342.

(45) Rohovec, J.; Gyepes, R.; Císařová, I.; Rudovský, J.; Lukeš, I. Nucleophilic Reactivity of Perhydro-3,6,9,12-Tetraazacyclopenteno[1,3-*f,g*]Acenaphthylene. A Unified Approach to N-Monosubstituted and N,N″-Disubstituted Cyclene Derivatives. *Tetrahedron Lett.* **2000**, *41*, 1249-1253.

(46) Izatt, R. M.; Pawlak, K.; Bradshaw, J. S.; Bruening, R. L. Thermodynamic and Kinetic Data for Macrocycle Interactions with Cations and Anions. *Chem. Rev.* **1991**, *91*, 1721-2085.

(47) Reibenspies, J. Structure of 1,4,7,10-Tetraazacyclododecane Trihydrate. *Acta Crystallogr C* **1992**, *48*, 1717-1718.

(48) Liu, W.-M.; Keizers, P. H. J.; Hass, M. A. S.; Blok, A.; Timmer, M.; Sarris, A. J. C.; Overhand, M.; Ubbink, M. A pH-Sensitive, Colorful, Lanthanide-Chelating Paramagnetic NMR Probe. *J. Am. Chem. Soc.* **2012**, 17306−17313.

(49) Leonov, A.; Voigt, B.; Rodriguez-Castañeda, F.; Sakhaii, P.; Griesinger, C. Convenient Synthesis of Multifunctional EDTA-Based Chiral Metal Chelates Substituted with an S-Mesylcysteine. *Chem. Eur. J.* **2005**, *11*, 3342-3348.

(50) Weaver, L. H.; Matthews, B. W. Structure of Bacteriophage T4 Lysozyme Refined at 1.7 Å Resolution. *J. Mol. Biol.* **1987**, *193*, 189-199.

(51) Sidhu, G.; Withers, S. G.; Nguyen, N. T.; McIntosh, L. P.; Ziser, L.; Brayer, G. D. Sugar Ring Distortion in the Glycosyl-Enzyme Intermediate of a Family G/11 Xylanase. *Biochemistry* **1999**, *38*, 5346-5354.

(52) Maltsev, A. S.; Grishaev, A.; Roche, J.; Zasloff, M.; Bax, A. Improved Cross Validation of a Static Ubiquitin Structure Derived from High Precision Residual Dipolar Couplings Measured in a Drug-Based Liquid Crystalline Phase. *J. Am. Chem. Soc.* **2014**, *136*, 3752-3755.

(53) Vlasie, M. D.; Comuzzi, C.; van den Nieuwendijk, A. M. C. H.; Prudêncio, M.; Overhand, M.; Ubbink, M. Long-Range-Distance NMR Effects in a Protein Labeled with a Lanthanide–DOTA Chelate. *Chem. Eur. J.* **2007**, *13*, 1715-1723.

(54) Esteves, C. V.; Lima, L. M. P.; Mateus, P.; Delgado, R.; Brandão, P.; Félix, V. Cyclen Derivatives with Two Trans-Methylnitrophenolic Pendant Arms: A Structural Study of Their Copper(II) and Zinc(II) Complexes. *Dalton Trans.* **2013**, *42*, 6149-6160.

(55) Schwieters, C. D.; Kuszewski, J. J.; Tjandra, N.; Marius Clore, G. The Xplor-NIH NMR Molecular Structure Determination Package. *J. Magn. Reson.* **2003**, *160*, 65-73.
(56) Schwieters, C. D.; Kuszewski, J. J.; Marius Clore, G. Using Xplor–NIH for NMR Molecular Structure Determination. *Prog. Nucl. Magn. Reson. Spectrosc.* **2006**, *48*, 47-62.
(57) Ostrovsky, S. M.; Falk, K.; Pelikan, J.; Brown, D. A.; Tomkowicz, Z.; Haase, W. Orbital Angular Momentum Contribution to the Magneto-Optical Behavior of a Binuclear Cobalt(II) Complex. *Inorg. Chem.* **2006**, *45*, 688-694.
(58) Skinner, S. P. Classical and Paramagnetic NMR Spectroscopy Techniques Applied to Different Protein Systems. Doctoral Thesis, Leiden University, Leiden, Netherlands, 2013.
(59) Ebright, Y. W.; Chen, Y.; Pendergrast, P. S.; Ebright, R. H. Incorporation of an EDTA-Metal Complex at a Rationally Selected Site within a Protein: Application to EDTA-Iron DNA Affinity Cleaving with Catabolite Gene Activator Protein (CAP) and Cro. *Biochemistry* **1992**, *31*, 10664-10670.
(60) Gaponenko, V.; Altieri, A. S.; Li, J.; Byrd, R. A. Breaking Symmetry in the Structure Determination of (Large) Symmetric Protein Dimers. *J. Biomol. NMR* **2002**, *24*, 143-148.
(61) Nguyen, T. H. D.; Ozawa, K.; Stanton-Cook, M.; Barrow, R.; Huber, T.; Otting, G. Generation of Pseudocontact Shifts in Protein NMR Spectra with a Genetically Encoded Cobalt(II)-Binding Amino Acid. *Angew. Chem. Int. Ed.* **2011**, *50*, 692-694.
(62) Park, S. H.; Wang, V. S.; Radoicic, J.; De Angelis, A. A.; Berkamp, S.; Opella, S. J. Paramagnetic Relaxation Enhancement of Membrane Proteins by Incorporation of the Metal-Chelating Unnatural Amino Acid 2-Amino-3-(8-Hydroxyquinolin-3-yl)Propanoic Acid (HQA). *J. Biomol. NMR* **2015**, *61*, 185-196.
(63) Keizers, P. H. J.; Desreux, J. F.; Overhand, M.; Ubbink, M. Increased Paramagnetic Effect of a Lanthanide Protein Probe by Two-Point Attachment. *J. Am. Chem. Soc.* **2007**, *30*, 9292-9293.
(64) Castañeda, C. A.; Spasser, L.; Bavikar, S. N.; Brik, A.; Fushman, D. Segmental Isotopic Labeling of Ubiquitin Chains to Unravel Monomer-Specific Molecular Behavior. *Angew. Chem. Int. Ed.* **2011**, *50*, 11210-11214.
(65) Liu, W.-M.; Skinner, S. P.; Timmer, M.; Blok, A.; Hass, M. A. S.; Filippov, D. V.; Overhand, M.; Ubbink, M. A Two-Armed Lanthanoid-Chelating Paramagnetic NMR Probe Linked to Proteins via Thioether Linkages. *Chem. Eur. J.* **2014**, *20*, 6256-6258.
(66) Ludwiczek, M. L.; Heller, M.; Kantner, T.; McIntosh, L. P. A Secondary Xylan-Binding Site Enhances the Catalytic Activity of a Single-Domain Family 11 Glycoside Hydrolase. *J. Mol. Biol.* **2007**, *373*, 337-354.
(67) Vranken, W. F.; Boucher, W.; Stevens, T. J.; Fogh, R. H.; Pajon, A.; Llinas, M.; Ulrich, E. L.; Markley, J. L.; Ionides, J.; Laue, E. D. The CCPN Data Model for NMR Spectroscopy: Development of a Software Pipeline. *Proteins: Struct., Funct., Bioinf.* **2005**, *59*, 687-696.
(68) McIntosh, L. P.; Wand, A. J.; Lowry, D. F.; Redfield, A. G.; Dahlquist, F. W. Assignment of the Backbone Proton and Nitrogen-15 NMR Resonances of Bacteriophage T4 Lysozyme. *Biochemistry* **1990**, *29*, 6341-6362.
(69) Plesniak, L. A.; McIntosh, L. P.; Wakarchuk, W. W. Secondary Structure and Nmr Assignments of Bacillus Circulans Xylanase. *Protein Sci.* **1996**, *5*, 1118-1135.
(70) Schmitz, C.; Stanton-Cook, M. J.; Su, X.-C.; Otting, G.; Huber, T. Numbat: An Interactive Software Tool for Fitting $\Delta\chi$-Tensors to Molecular Coordinates Using Pseudocontact Shifts. *J. Biomol. NMR* **2008**, *41*, 179-189.
(71) Bashir, Q.; Volkov, A. N.; Ullmann, G. M.; Ubbink, M. Visualization of the Encounter Ensemble of the Transient Electron Transfer Complex of Cytochrome *c* and Cytochrome *c* Peroxidase. *J. Am. Chem. Soc.* **2010**, *132*, 241-247.

(72) Battiste, J. L.; Wagner, G. Utilization of Site-Directed Spin Labeling and High-Resolution Heteronuclear Nuclear Magnetic Resonance for Global Fold Determination of Large Proteins with Limited Nuclear Overhauser Effect Data. *Biochemistry* **2000**, *39*, 5355-5365.
(73) Schilder, J.; Löhr, F.; Schwalbe, H.; Ubbink, M. The Cytochrome *c* Peroxidase and Cytochrome *c* Encounter Complex: The Other Side of the Story. *FEBS Lett.* **2014**, *588*, 1873-1878.
(74) García de la Torre, J.; Huertas, M. L.; Carrasco, B. HydroNMR: Prediction of NMR Relaxation of Globular Proteins from Atomic-Level Structures and Hydrodynamic Calculations. *J. Magn. Reson.* **2000**, *147*, 138-146.

# Chapter III

# A hydrophilic paramagnetic NMR probe for lanthanoid ions and 3d-block ions

# *Chapter III*


**Abstract**

A new DOTA based transition metal ion paramagnetic NMR probe (TraNP2) was designed and synthesized. TraNP2 can tightly chelate both lanthanoids and 3d-block metal ions. Its paramagnetic properties were studied after attachment to T4 Lysozyme mutant K147C/T151C. NMR spectra of the amide groups of T4Lys tagged with Yb(III)-TraNP2 showed two sets of PCS, suggesting presence of at least two conformers. Surprisingly, Co(II) loaded TraNP2 linked to the T4Lys mutant induces only very small PCS. The paramagnetic properties of Co(II)-TraNP2 complex were studied by measuring the effective magnetic moment ($\mu_{B,\ eff}$). The results showed that Co(II)-TraNP2 is indeed paramagnetic. The reason why the PCS are so small remains unclear.

**Introduction**

The use of small ligands able to bind paramagnetic metal ions that can be applied as probes in paramagnetic NMR is becoming an important strategy to study protein dynamics.[1–3] With different metal ions, various paramagnetic effects can be obtained. Lanthanoids are the common metal ions used for paramagnetic NMR, due to their similar chemical properties and variable paramagnetic effects.[4,5] 3d-Block metal ions can also be used to generate somewhat weaker paramagnetic effects. For example, cobalt (II) generates an anisotropic magnetic tensor from 2 to 10 x $10^{-32}$ $m^3$ with a weak PRE effect, which is suitable to study small proteins or localized effects in bigger systems.[6–9] Manganese (II) does not induce PCS but can produce a strong PRE effect, due to five unpaired electrons and a long electronic relaxation time.[7,10,11] The coordination requirements in terms of numbers and geometry differ considerably between these two groups of ions.

According to Werner's coordination theory,[12] two types of valence contribute to metal ion coordination, one related to the oxidation state of the ion and another related to its coordination numbers. Satisfying both valences leads to the lowest energy structure. Commonly, 3d-block ions have various oxidation states and require four to six coordination donors.[13] Their geometries, which are well explained by crystal field theory[14,15], are tetrahedral, square pyramidal and octahedral (Figure 1.4, Chapter I). Lanthanoid ions are stable in +3 oxidation state and need seven to nine coordination sites.[16] Different from 3d-block ions, the coordination geometries of Ln(III) are less studied.[17] Few reported paramagnetic NMR probes are able to coordinate both Ln(III) and 3d-block ions. Among these probes, multiple sets of PCS were detected or additional coordination from a protein side chain was required.[10,18] As described in chapter I, sections 3.3.4.1 and 3.3.4.2, probe **46** and probe **51** (Figure 1.10, Chapter I) are the only two that can chelate both group ions. Probe **46** needs additional coordination of a protein side chain, and Co(II) loaded probe **51** generated two sets of PCS. Also, the metal ion binding affinity was poor.

Here, we describe a probe that is able to bind to both 3d-block ions and lanthanoid ions. In Leiden, several successful Ln(III) based probes, such as CLaNP5[19] and CLaNP7[20], were designed and synthesized. However, these probes are not suitable for 3d-blok ions, like Co(II) and Mn (II). In chapter II, the design and synthesis of TraNP1 (transition metal NMR probe # 1) was described. It coordinates Co(II) and generates a single set of paramagnetic effects in a tagged protein, but it is not a good chelator for Ln(III). As part of that effort, we also designed an isomer of TraNP1 with different coordination arms (Figure 3.1). The effect of the branching of the carbons of two opposing arms is anticipated to reduce the number of conformers. Previously, branched side-arms having methyl-groups have been reported.[21,22] We introduced methylene hydroxyl groups to ensure a more hydrophilic probe, to avoid precipitation of the tagged

proteins. According to the NMR spectra, TraNP2 is a good ligand for both Co(II) and Yb(III). However, multiple PCS were observed for Yb(III)-TraNP2 attached protein, whereas small PCS were detected for a protein tagged with Co(II)-TraNP2.

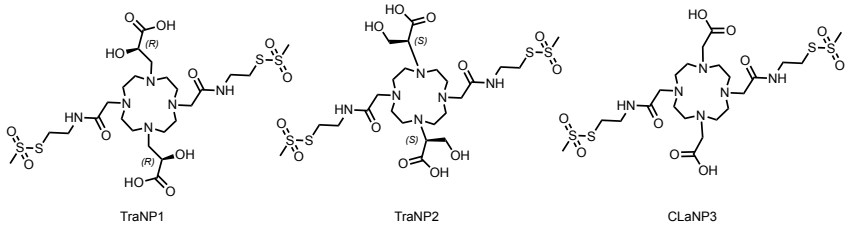


**Figure 3.1** Structure of TraNP1, TraNP2 and CLaNP3

**Results and Discussion**

**Design and synthesis of TraNP2.** The most used and well-studied cyclen based chelator is DOTA (chapter 1, Figure 1.8), which has high metal binding affinity to form thermodynamically stable complexes.[23,24] Instead of using acetate groups as coordination arms, a pair of methyl hydroxyl groups substituted analogous was used as coordination arms for TraNP2 with the aim to reduce the number of conformers (Figure 3.1). These two chiral groups were incorporated at the opposing nitrogens to ensure a $C_2$ symmetry. A frequently applied strategy to synthesize a $C_2$ symmetric cyclen derivative is via a selective protection and alkylation strategy. However, this strategy proved unsuccessful for the synthesis of TraNP2. The synthetic route of TraNP2 is shown in Scheme 3.1. Cyclen was first alkylated with two equiv. of **1**, readily obtained from the amino acid serine via its diazonium salt[25], in the presence of DIPEA. LC-MS, showed that after 48 h at rt, no starting compound was detected and that the main product was the desired di-alkylated compound (only small amounts of mono and tri-alkylated products were observed). The obtained crude product was used to react with excess S-(2-(2-bromoacetamido)ethyl)

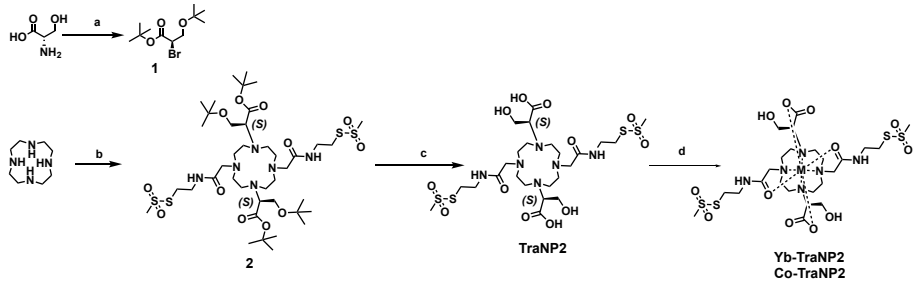


**Scheme 3.1** Synthesis route of TraNP2 a). i) D-Serine, KBr, HBr, $NaNO_2$, $H_2O$, -15 °C, 16 h; ii) *p*-toluenesulfonic acid monohydrate, 2-methylprop-1-ene, rt, 72 h; b) i) compound 1, DIPEA, ACN, rt, 48 h; ii) S-(2-(2-bromoacetamido)ethyl) methanesulfonothioate, $K_2CO_3$, ACN, rt, 48 h; c) TFA: DCM (2:3, *v*:*v*), rt, 10 h; d) ACN, rt, 3 h.

methanesulfonothioate in the presence of $K_2CO_3$ to give **2** in 55% yield after purification. For the deprotection of all the *t*Bu groups, a mixture of TFA:DCM (2:3, *v:v*) was used and the crude product was purified by HPLC with 0.2% TFA and a 15-20% acetonitrile gradient on C18 preparative column, yielding 63% of TraNP2.

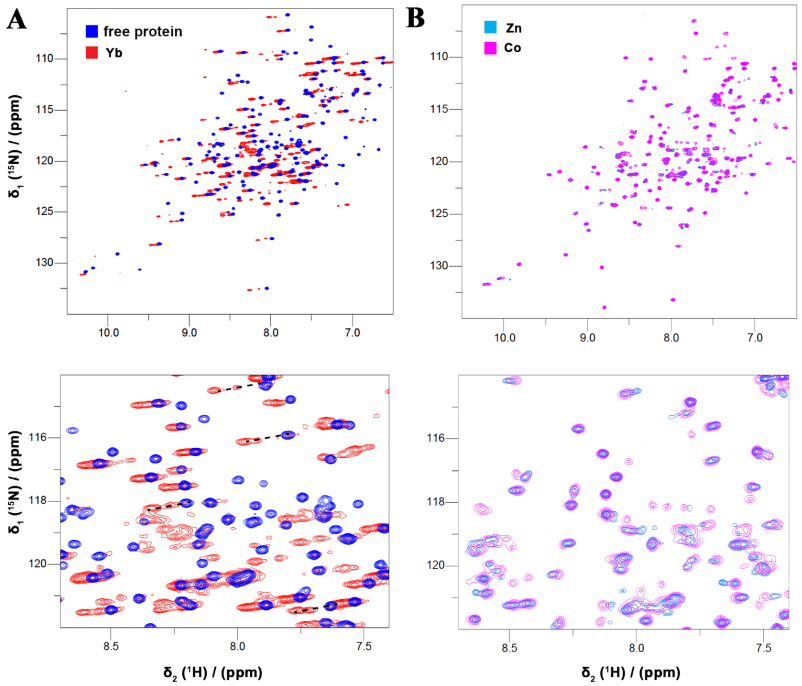


**Figure 3.2** Overlay of $^{1}H$-$^{15}N$ HSQC spectra of T4Lys K147C/T151C (blue) linked to Yb(III) (red) loaded TraNP2 ((**A**), full spectrum (top), zoom in spectrum (bottom)), or Co(II) (magenta) and Zn(II) (sky blue) loaded TraNP2 (**B**), full spectrum (top), zoom in spectrum (bottom)). The NMR spectra were recorded at 14.1 T (600 MHz).

**Protein labeling and NMR spectroscopy.** The uniformly $^{15}N$ enriched T4Lys K147C/T151C were treated with DTT to reduce possible intermolecular disulfide bonds, the DTT was removed and the proteins were incubated with Co(II)/Zn(II)/Yb(III)-TraNP2. The tagged proteins were purified using size exclusion chromatography and the tagging efficiency was determined by MS and NMR. Mass spectrometry results of Co(II)-TraNP2 T4Lys (19333 ± 2 Da) and Yb(III)-TraNP2 T4Lys (19445 ± 2 Da) agreed with the theoretical values of 19334 Da and 19446 Da, respectively, for 98% enrichment of $^{15}N$, suggesting that the probes were attached via two arms and the metal ion was tightly bound and more than 95% of the protein was labeled (App. Figure A3.1). The labeled proteins were used for NMR measurements at a concentration of 100-200 μM. Figure 3.2 shows the overlay HSQC spectra of two pairs samples. For Yb(III)-TraNP2 labeled and free T4Lys, two sets of PCS were detected for most cross peaks in the spectra (Figure 3.2 A). This indicates that at least two conformers of Yb(III)-TraNP2 were present with a different Δχ-

tensor, causing double resonances for an amide spin. Similar results were reported for a published probe-CLaNP3 (Caged Lanthanoid NMR Probe # 3, Figure 3.1).[26] Thus, two chiral branched side-arms cannot effectively reduce the number of conformers of DOTA based complexes. In the spectra of T4Lys tagged with Co(II)/Zn(II)-TraNP2 (Figure 3.2 B), small PCS were observed.

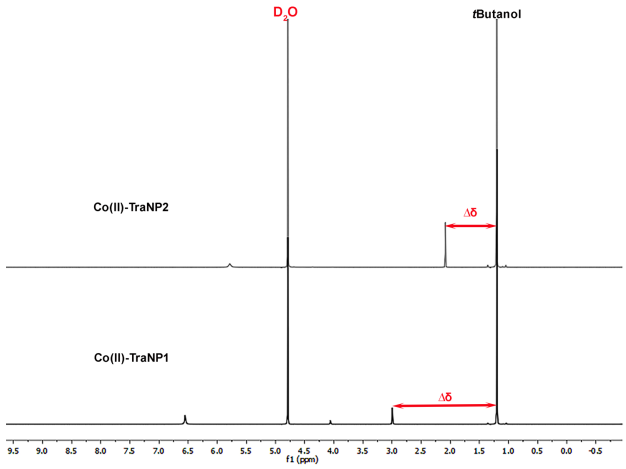


**Figure 3.3** $^{1}$H NMR spectra of Co(II)- TraNP2 and Co(II)-TraNP1 measured by Evans' method. The NMR spectra were recorded at 9.4 T (400 MHz) and 293K.

**Evans' method**. It is surprising that the Co(II) sample showed so few paramagnetic effects. We tested how paramagnetic the sample actually was. In 1953, D. F. Evans proposed a method to determine magnetic susceptibility of paramagnetic molecules in solution using a NMR approach.[27] It is based on bulk magnetic susceptibility shifts (BMS)[28,29] of an inert compound caused by the presence of the paramagnetic molecule. This method has frequently been applied in coordination chemistry to detect the spin-states and effective magnetic moments.[30–33] Here, we use this method to investigate the paramagnetic properties of Co(II)-TraNP1 and Co(II)-TraNP2. Both of the complexes generated BMS for the inert compound tertiary butanol, 720 Hz for TraNP1 and 352 Hz for TraNP2, respectively, indicating the Co(II) ions in both complexes are paramagnetic (Figure 3.3). Using equation 3.1 to 3.3 (Materials and Methods), the effective magnetic moment in Bohr magnetons ($\mu_{B,\,eff}$) of TraNP2 is 5.05. For TraNP1, it is 3.31.

It is remarkable that the Co(II)-TraNP2 probe does not cause significant PCS, despite having a large magnetic moment. The results suggest that the coordination is such that the magnetic susceptibility is isotropic, effectively cancelling the pseudocontact effect. Note that Evans' method measure the total magnetic susceptibility $\chi$, whereas the

PCS is a result of the anisotropy of $\chi$. As was reported in chapter II, the size of the anisotropy varies widely for different Co(II) complexes and can even be different between enantiomers and for one and the same probe tagged to different proteins.

In conclusion, modification of DOTA coordination arms with chiral carbons with methylene hydroxy groups as substituents can modulate the coordination properties to make them suitable for binding to both Ln(III) and 3d-block ions. Unfortunately, TraNP2 is not suitable as a probe for protein NMR because the Yb(III) complex yields double resonances, whereas the Co(II) complex displays an isotropic magnetic susceptibility.

**Materials and Methods**

**General**: cyclen, 2-(aminoethyl)methanethiosulfonate hydrobromide, methyl (S)-oxirane-2-carboxylate, N-(tert-Butoxycarbonyloxy)succinimide, $Ln(OAc)_3$, $CoCl_2{\cdot}6H_2O$, $ZnI_2$, $MnCl_2{\cdot}4H_2O$, methyl (R)-oxirane-2-carboxylate and all other chemicals were purchased and used without further purification. Solvents were purchased from Honeywell, BIOSOLVE or Aldrich and directly use for synthesis. Superdex 75 columns and Sephadex G-25 PD10 desalting columns were purchased from GE Healthcare. Reactions were followed by TLC analysis on silica gel (F 1500 LS 254 Schleicher and Schuell, Dassel, Germany); visualized by UV and/or ninhydrin, $KMNO_4$. Flash chromatography was performed with Screening Devices silica gel 60 (0.04-0.063 mm). A Waters preparative HPLC system, equipped with a Waters C18-Xbridge 5 µm OBD (30 x 150 mm) column and Äkta Basic FPLC (GE Healthcare Inc.) system were used for purification. NMR spectra were recorded on a Bruker AV-400 (400/100 MHz), AV-500 (500/125 MHz) or AV-600 (600/150 MHz) spectrometer. A LCQ liquid chromatography mass spectrometry system and a Finnigan LTQ Orbitrap system were used for high-resolution mass spectrometry and protein conjugation analysis. Thermo Finnigan LCQ Advantage MAX used for liquid chromatography (LC)-mass spectrometry (MS) analysis. Thermo Scientific™ NanoDrop 2000 spectrophotometers were used for protein concentration measurement.

**Protein labeling:** To link M-TraNP2 to $^{15}N$ labelled T4Lys produced as described in chapter II. The yield of labeling estimated from the LC-MS and NMR, was more than 95%.

**Protein NMR spectroscopy:** The NMR samples of T4lys-Metal-TraNP2 (100–200 µM) were prepared in 30 mM sodium phosphate pH 5.5 buffer containg 100 mM NaCl, and 6% (*v/v*) $D_2O$. All $^1H$-$^{15}N$ HSQC were recorded on a Bruker AV-600 (600 MHz) spectrometer, at 298 K. Data were processed with Topspin 3.5 and analyzed with CcpNmr Analysis version 2.4.0. T4Lys resonances assignments were provided by Dr. Simon P. Skinner based on previous work.

**Evans' method:** A pair of coaxial NMR tubes with different diameter was required for this method. A melting point capillary was used as inter tube and a 5 mm NMR tube was used as an outer tube. Co(II)-TraNP2 (2.5 mg, 3.15 µmol) was dissolved in $D_2O$ (157 µL,

containing 2% (*v/v*) tertiary butanol). This solution (100 μL) was carefully transferred into a melting point capillary (inter tube) before it was zipped. The 5 mm NMR tube contained 500 μL of $D_2O$ with 2% (*v/v*) tertiary butanol. The above zipped melting point capillary was transferred into the 5 mm NMR tube at the bottom. The spectra were acquired at 9.4 T (400 MHz) on a Bruker NMR spectrometer. For Co(II)-TraNP1 the sample contained 13.5 μmol in 116 μL $D_2O$ with 2% (*v/v*) tertiary butanol. By measuring the chemical shifts difference of an inert compound, the tertiary butanol, in the presence and absence of a paramagnetic compound, the effective magnetic moment in Bohr magnetons ($\mu_{eff}$) of the paramagnetic compound can be calculated with equation 3.1 to 3.3.[27,31,32,34]

$$\mu_{eff} = 2.84\sqrt{\chi_p T} \quad 3.1$$

$$\chi_p = \frac{3\times10^3\Delta f}{4\pi f_m C} - \chi_D \quad 3.2$$

$$\chi_D \approx -\frac{M}{2}\times 10^{-6} \quad 3.3$$

$\chi_P$ (in emu/mol) is the corrected paramagnetic molar susceptibility defined by equation 3.2; T (in K) is the absolute temperature for the measurement. $\Delta f$ (in Hz) is the chemical shift difference of the inert compound in the presence and absence of the paramagnetic compound; $f_m$ (in Hz) is external magnetic field, C (in mole/L) is the concentration of the paramagnetic compound; $\chi_D$ (in emu/mol) is the diamagnetic susceptibility and M (in g/mol) is the molecular mass.

**Synthesis**

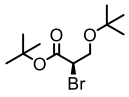

**Tert-butyl (*R*)-2-bromo-3-(tert-butoxy) propanoate, compound 1**

To a three necked flask equipped with a magnetic stirring bar and gas inlet tube, KBr (11.4 g, 96.9 mmol) and D-Serine (3 g, 28.5 mmol) were dissolved in $H_2O$ (50 mL), and cooled to -15 °C. A wash bottle containing 1 M KOH solution connected to the flask and $N_2$ gas pass through it. Then HBr solution (48%, 7 mL) was added to the reaction mixture, followed by six portions of $NaNO_2$ (2.4 g, 34.8 mmol) added (~0.4 g every 20 mins). The reaction mixture was allowed to warm to 0 °C and stirring was continued for 16 h. The reaction mixture was flushed with $N_2$ and extracted with diethyl ether (3 x 20 mL), dried ($Na_2SO_4$) and concentrated under reduced pressure. Without further purification, 1 g (~6.57 mmol) of the crude compound was dissolved in DCM (50 mL) in a DURAN bottle and at 0 °C treated with *p*-toluenesulfonic acid monohydrate (1.25 g, 6.57 mmol) and with 2-methylprop-1-ene (10 mL). After 72 h at rt, the reaction mixture was washed with sat. $NaHCO_3$ solution (25 mL) and water (25 mL), dried ($Na_2SO_4$) and concentrated. The residue was purified with silica flash column chromatography (10% of diethyl ether in pentane) to give 1.62 g (88 %) compound **1** as a slightly yellow oil. The spectroscopic data were in agreement with those reported in the literature: $^1$H NMR (400 MHz, $CDCl_3$, 293K): **δ** = 1.16 (s, 9H), 1.46 (s, 9H), 3.57-3.60 (d, 1H), 3.75-3.79 (t, 1H), 4.05-4.09 (d, 1H). $^{13}$C NMR (400 MHz, $CDCl_3$, 293K): **δ** = 27.41 ($CH_3C$), 27.74 ($CH_3C$), 63.69

($CH_2OtBu$) 74.00 ($C(CH_3)_3$), 82.23 ($C(CH_3)_3$), 167.83 (COOtBu). $[\alpha]_D^{20}$= -3.1 (C= 10 mg/mL, Methanol). FTIR ($cm^{-1}$): 2982.1, 2923.4, 2844.7, 1054.6, 1033.1, 1010.3.

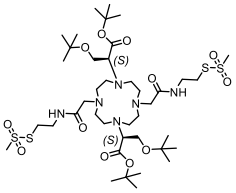

**Di-tert-butyl2,2'-(4,10-bis(2-((2-((methylsulfonyl)thio)ethyl)amino)-2-oxoethyl)-1,4,7,10-tetraazacyclododecane-1,7-diyl)(2S,2'S)-bis(3-(tert-butoxy)propanoate), compound 2**

Cyclen (0.5 g, 2.9 mmol) in acetonitrile (30 mL) was mixed with compound **1** (1.65 g, 5.8 mmol) and DIPEA (1.5 mL, 8.7 mmol) and stirring was continued at rt for 48 h. Without purification, the resulting mixture was mixed with S-(2-(2-bromoacetamido)ethyl) methanesulfonothioate (3.22 g, 11.6 mmol) and $K_2CO_3$ (1.6 g, 11.6 mmol). After stirring at rt for 48 h, $K_2CO_3$ was removed by filtration, the mixture concentrated and the residue purified by silica gel flash column chromatography (7% of MeOH in DCM) to give the title compound as a white solid, 0.79 g (31% yield). $^1$H NMR (500 MHz, MeOD, 298K): **δ** = 1.20-1.21 (d, 18H), 1.52-1.54 (d, 18H), 1.99-2.09 (m, 4H), 2.26-2.34 (d, 2H), 2.48-2.56 (d, 2H), 2.62-2.77 (m, 4H), 3.34-3.39 (m, 2H), 3.41-3.42 (q, 6H), 3.50-3.57 (m, 3H), 3.60-3.72 (m, 4.5H), 3.75-3.89 (m, 5.5 H), 3.34-3.39 (m, 2H). $^{13}$C NMR (500 MHz, MeOD, 298 K): **δ** = 27.76, 28.56, 37.07, 39.78, 47.06, 50.93, 57.49, 82.55, 200.77. HR-MS: m/z 963.4626 $[M+H]^+$, calcd. $[C_{40}H_{78}N_6O_{12}S_4]$ 963.4639. $[\alpha]_D^{20}$= 8.1 (C= 1 mg/mL, methanol). FTIR ($cm^{-1}$): 1682.8, 1204.9, 1186.3, 1136.2, 1033.1, 844.3, 802.8, 724.1.

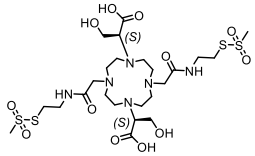

**(2S,2'S)-2,2'-(4,10-bis(2-((2-((methylsulfonyl)thio)ethyl)amino)-2-oxoethyl)-1,4,7,10-tetraazacyclododecane-1,7-diyl)bis(3-hydroxypropanoic acid), TraNP2**

Compound **2** (0.1 g, 0.11 mmol) was dissolved in TFA:DCM (2:3, *v:v*) while stirring at rt for 10 h. The reaction mixture was concentrated and the residue purified by reverse phase HPLC (0.2% TFA and a 10-15% acetonitrile gradient on C18 preparative column), yielding 0.05 g (63% yield) TraNP2. $^1$H NMR (500 MHz, MeOD, 343 K): **δ** = 3.22 (br, 6H), 3.38 (m, 4H), 3.36-3.43 (br, 2H), 3.54-3.64 (m, 8H), 3.43 (s, 6H), 3.41-3.56 (br, 8H), 3.69-3.87 (dd, 4H), 4.12-4.16 (m, 4H). $^{13}$C NMR (500 MHz, MeOD, 343 K): **δ** = 36.45 ($CH_2SO_2$), 40.29 ($CH_2CH_2SO_2$) 51.83 ($CH_2N$), 50.96 ($CH_3S$), 56.19 ($CH_2CONH$), 60.05 ($CH_2OH$), 64.63 ($CHCH_2OH$). $[\alpha]_D^{20}$= 8.0 (C= 2 mg/mL, methanol). HR-MS: m/z 739.2145 $[M+H]^+$, calcd. $[C_{24}H_{46}N_6O_{12}S_4]$ 739.2050. FTIR (ν $cm^{-1}$): 1684.2, 1203.4, 1130.5, 1054.6, 1033.1, 1013.11, 835.7, 801.3, 748.3, 721.2.

**Metal complexes**: To a solution of TraNP2 (20.7 mg, 28 µmol) in 280 µL ACN, 1.1 equiv. $CoCl_2{\cdot}6H_2O$ or $ZnI_2{\cdot}6H_2O$ or $Yb(CH_3COO)_3{\cdot}4H_2O$ was added. The mixture stirred at rt for 3 h and the formation of metal complex was checked by LC/MS. Without further purification, Co-TraNP2 was used to protein sample labeling. The other metal ions $Zn^{2+}$

and $Yb^{3+}$ were chelated to TraNP2 following the same procedure. Co-TraNP2 HR-MS: m/z 796.1319 $[M+H]^+$, calcd. $[C_{24}H_{44}CoN_6O_{12}S_4]$ 796.1232; Zn-TraNP2 HR-MS: m/z 401.0667 $[M+2H]^{2+}$, calcd. $[C_{24}H_{44}ZnN_6O_{12}S_4]$ 401.0596; Yb-TraNP2-SS HR-MS: m/z 913.1520 $[M+H]^+$, calcd. $[C_{24}H_{44}YbN_6O_{12}S_4]$ 913.1523.

**References**


(1) Nitsche, C.; Otting, G. Pseudocontact Shifts in Biomolecular NMR Using Paramagnetic Metal Tags. *Prog. Nucl. Magn. Reson. Spectrosc.* **2017**, *98–99*, 20–49.

(2) Su, X. C.; Otting, G. Paramagnetic Labelling of Proteins and Oligonucleotides for NMR. *J. Biomol. NMR* **2010**, *46* (1), 101–112.

(3) Keizers, P. H. J.; Ubbink, M. Paramagnetic Tagging for Protein Structure and Dynamics Analysis. *Prog. Nucl. Magn. Reson. Spectrosc.* **2011**, *58* (1–2), 88–96.

(4) Liu, W. M.; Overhand, M.; Ubbink, M. The Application of Paramagnetic Lanthanoid Ions in NMR Spectroscopy on Proteins. *Coord. Chem. Rev.* **2014**, *273–274*, 2–12.

(5) Otting, G. Prospects for Lanthanides in Structural Biology by NMR. *J. Biomol. NMR* **2008**, *42* (1), 1–9.

(6) Nguyen, T. H. D.; Ozawa, K.; Stanton-Cook, M.; Barrow, R.; Huber, T.; Otting, G. Generation of Pseudocontact Shifts in Protein NMR Spectra with a Genetically Encoded Cobalt(II)-Binding Amino Acid. *Angew. Chemie. Int. Ed.* **2011**, *123*, 718–720.

(7) Yang, Y.; Huang, F.; Huber, T. Site-Specific Tagging Proteins with a Rigid , Small and Stable Transition Metal Chelator, 8-Hydroxyquinoline, for Paramagnetic NMR Analysis. *J. Biomol. NMR* **2016**, *64* (2), 103–113.

(8) Bahramzadeh, A.; Jiang, H.; Huber, T.; Otting, G. Two Histidines in an **α**-Helix: A Rigid $Co^{2+}$-Binding Motif for PCS Measurements by NMR Spectroscopy. *Angew. Chemie. Int. Ed.* **2018**, *57* (21), 6226–6229.

(9) Dvoretsky, A.; Gaponenko, V.; Rosevear, P. R. Derivation of Structural Restraints Using a Thiol-Reactive Chelator. *FEBS Lett.* **2002**, *528* (1–3), 189–192.

(10) Moshref, A.; Otting, G.; Sharipo, A.; Pintacuda, G.; Leonchiks, A. Site-Specific Labelling with a Metal Chelator for Protein-Structure Refinement. *J. Biomol. NMR* **2004**, *29* (3), 351–361.

(11) Park, S. H.; Wang, V. S.; Radoicic, J.; De Angelis, A. A.; Berkamp, S.; Opella, S. J. Paramagnetic Relaxation Enhancement of Membrane Proteins by Incorporation of the Metal-Chelating Unnatural Amino Acid 2-Amino-3-(8-Hydroxyquinolin-3-yl)Propanoic Acid (HQA). *J. Biomol. NMR* **2015**, *61* (3–4), 185–196.

(12) Kauffman, G. B. Theories of Coordination Compounds. *J. Chem. Educ.* **1986**, 63(4), A116.

(13) Venkataraman, D.; Du, Y.; Wilson, S. R.; Hirsch, K. A.; Zhang, P.; Moore, J. S. A Coordination Geometry Table of the d-Block Elements and Their Ions. *J. Chem. Educ.* **1997**, *74* (8), 915–918.

(14) Van Vleck, J. H. Theory of the Variations in Paramagnetic Anisotropy among Different Salts of the Iron Group. *Phys. Rev.* **1932**, *41* (2), 208–215.

(15) Newman, D. J; Ng, B. K. C. *Crystal Field Handbook*; Cambridge University Press: Cambridge, 2000.

(16) Nielsen, L. G.; Junker, A. K. R.; Sørensen, T. J. Composed in the F-Block: Solution Structure and Function of Kinetically Inert Lanthanide(III) Complexes. *Dalt. Trans.* **2018**, *47* (31), 10360–10376.

(17) Chau, O.; Goeleven, D.; Oujja, R. Variational Inequality Models Arising in the Study of

Viscoelastic Materials. *Coord. Chem. Rev.* **2000**, *196*, 165–195.

(18) Man, B.; Su, X. C.; Liang, H.; Simonsen, S.; Huber, T.; Messerle, B. A.; Otting, G. 3-Mercapto-2, 6-Pyridinedicarboxylic Acid: A Small Lanthanide-Binding Tag for Protein Studies by NMR Spectroscopy. *Chem. Eur. J.* **2010**, *16* (12), 3827–3832.

(19) Keizers, P. H. J.; Saragliadis, A.; Hiruma, Y.; Overhand, M.; Ubbink, M. Design, Synthesis, and Evaluation of a Lanthanide Chelating Protein Probe: CLaNP-5 Yields Predictable Paramagnetic Effects Independent of Environment. *J. Am. Chem. Soc.* **2008**, *130* (44), 14802–14812.

(20) Liu, W.-M.; Keizers, P. H. J.; Hass, M. A. S.; Blok, A.; Timmer, M.; Sarris, A. J. C.; Overhand, M.; Ubbink, M. A pH-Sensitive, Colorful, Lanthanide-Chelating Paramagnetic NMR Probe. *J. Am. Chem. Soc.* **2012**, *134* (41), 17306–17313.

(21) Brittain, H. G.; Desreux, J. F. Luminescence and NMR Studies of the Conformational Isomers of Lanthanide Complexes with an Optically Active Polyaza Polycarboxylic Macrocycle. *Inorg. Chem.* **1984**, *23* (26), 4459–4466.

(22) Suchý, M.; Li, A. X.; Milne, M.; Bartha, R.; Hudson, R. H. E. DOTMA-Based Amides (DOTMAMs) as a Platform for the Development of PARACEST MRI Contrast Agents. *RSC Adv.* **2016**, *6* (67), 62647–62655.

(23) Meyer, M.; Dahaoui-Gindrey, V.; Lecomte, C.; Guilard, R. Conformations and Coordination Schemes of Carboxylate and Carbamoyl Derivatives of the Tetraazamacrocycles Cyclen and Cyclam, and the Relation to Their Protonation States. *Coord. Chem. Rev.* **1998**, *178–180*, 1313–1405.

(24) Gilsoul, D.; Jacques, V.; Mesbahi, M.; Hermann, M.; Desreux, J. F.; Sauvage, C.; Humblet, V.; Comblin, V. Designing New MRI Contrast Agents: A Coordination Chemistry Challenge. *Coord. Chem. Rev.* **2002**, *185–186*, 451–470.

(25) C. Eichenauer, N.; Tschersich, R.; Pietruszka, J. Total Synthesis of Solandelactone I. *J. Nat. Prod.* **2015**, *78* (11), 2782–2790.

(26) Vlasie, M. D.; Comuzzi, C.; Van Den Nieuwendijk, A. M. C. H.; Prudêncio, M.; Overhand, M.; Ubbink, M. Long-Range-Distance NMR Effects in a Protein Labeled with a Lanthanide-DOTA Chelate. *Chem. Eur. J.* **2007**, *13* (6), 1715–1723.

(27) Evans, D. F. 400. The Determination of the Paramagnetic Susceptibility of Substances in Solution by Nuclear Magnetic Resonance. *J. Chem. Soc.* **1959**, *0*, 2003–2005.

(28) Dickinson, W. C. The Time Average Magnetic Field at the Nucleus in Nuclear Magnetic Resonance Experiments. *Phys. Rev.* **1951**, *81* (5), 717–731.

(29) Chu, K. -. C.; Xu, Y.; Balschi, J. A.; Springer, C. S. Bulk Magnetic Susceptibility Shifts in Nmr Studies of Compartmentalized Samples: Use of Paramagnetic Reagents. *Magn. Reson. Med.* **1990**, *13* (2), 239–262.

(30) Evans, D. F.; James, T. A. Variable-Temperature Magnetic-Susceptibility Measurements of Spin Equilibria for Iron(III) Dithiocarbamates in Solution. *J. Chem. Soc. Dalt. Trans.* **1979**, 4, 723–726.

(31) Loliger, J.; Scheffold, R. Paramagnetic Moment Measurements by NMR A Micro Technique. *J. Chem. Educ.* **2009**, *49* (9), 646.

(32) De Buysser, K.; Herman, G. G.; Bruneel, E.; Hoste, S.; Van Driessche, I. Determination of the Number of Unpaired Electrons in Metal-Complexes. A Comparison between the Evans' Method and Susceptometer Results. *Chem. Phys.* **2005**, *315* (3), 286–292.

(33) Nataro, C.; Fosbenner, S. M. Synthesis and Characterization of Transition-Metal Complexes Containing 1,1′-Bis(Diphenylphosphino)Ferrocene. *J. Chem. Educ.* **2009**, *86* (12), 1412.

(34) Schubert, E. M. Utilizing the Evans Method with a Superconducting NMR Spectrometer in

the Undergraduate Laboratory. *J. Chem. Educ.* **1992**, *69* (1), 62.

# Chapter IV

# Rigidified and hydrophilic DOTA-like lanthanoid ligands: Design, synthesis, NMR studies and molecular modeling

# *Chapter IV*


**Abstract**

In this chapter, two enantiomeric hydrophilic rigid DOTA-like lanthanoid complexes were designed and synthesized, following a strategy that allows the incorporation of two sets of two adjacent substituents. Via this strategy we obtained a more hydrophilic and rigid macrocyclic ring, featuring four chiral hydroxyl-methylene substituents. EXSY NMR spectroscopy was used to investigate the conformational behavior of the novel macrocycles as compared to DOTA and DOTA derivatives. One dimensional $^{1}H$ NMR spectra of these novel macrocyclic ring based lanthanoid complexes indicate that TSAP and SAP conformers coexist, but they favor TSAP geometry, which is different from DOTA. According to the 2D $^{1}H$ EXSY spectra of Eu(III) loaded complexes, ring flipping of the cyclen-ring was completely suppressed by the presence of the four chiral hydroxyl-methylene substituents at proximate positions. These results are in agreement with conformational modelling. The reorientation of the pendent arms still causes conformational exchange, giving rise to only two conformers. This indicates that these novel complexes are suitable scaffolds to develop rigid probes for paramagnetic NMR of proteins. Due to their hydrophilic nature, it is anticipated that they are less likely to cause protein precipitation than their more hydrophobic counterparts.

**Introduction**

Due to their physical and chemical properties, trivalent lanthanoid ion complexes are widely used in MRI as contrast agents, in NMR as resonance shift or line-broadening agents, and in luminescence.[1–3] DOTA (1,4,7,10-tetraazacyclododecane-1,4,7,10-tetraacetic acid) and DOTA derivatives are one of the most applied lanthanoids chelators, valued for their high metal binding affinity and the stability of the formed complexes.[4,5]

As it was discovered from DOTA lanthanoid complex crystal structures, four nitrogen atoms of the cyclen ring and four oxygen atoms of the pendent arms are involved in the metal ion coordination to form a nearly perfect square antiprism.[6–8] The coordinating nitrogen- and oxygen atoms are defined as the N- and O- plane, respectively. In DOTA lanthanoid complexes, the metal ion is sandwiched between these two planes. It was demonstrated that the relative torsion of the two planes yields two distinct coordination geometries of the complexes, referred to as square antiprismatic (SAP) and twisted square antiprismatic (TSAP) (Figure 1.8, Chapter I).[6–8] Contrary to the TSAP, which has a torsion angle between the two planes of about 25°, the SAP geometry features a torsion angle of about 39°, and thus, forms a smaller metal coordination cavity and a more compact structure.[9–11] As was determined by NMR, the ratio of these two conformers of DOTA and DOTA derivatives is dependent on the nature of the lanthanoid ion and the structure of the ligands.[12,13]

Furthermore, complexes of lanthanoids having a large radius, such as Gd(III) and Eu(III), can coordinate water at a ninth coordination site. In MRI, the exchange rate of the coordinated water is one of the important factors to evaluate the efficiency of a contrast agent.[1] A number of studies illustrated that the water exchange rate of the TSAP conformer is about two orders of magnitude faster than that of SAP, thus providing evidence that these geometries exhibit quite different properties.[14–17] The complexes have four states, two SAP enantiomers and two TSAP enantiomers. These conformers show chemical exchange, indicating that they can interconvert on a timescale of 10 – 100 ms.[10,18] In $^{1}$H NMR spectra the pairs of enantiomers have identical resonance positions, but the SAP and TSAP conformers have very distinct spectra. The presence of the TSAP and SAP conformers hampers the application of lanthanoid complexes based on DOTA-like ligands in many fields. For example, protein structure determination and dynamics characterization by using paramagnetic probes in NMR can give rise to multiple sets of resonances[19] or exchange between the resonances of the conformers,[20] as described in chapter I. This drawback of DOTA and DOTA derivatives can also not be ignored in other applications, such as MRI,[21,22] luminescence[23,24] and dynamic nuclear polarization.[25]

Many efforts have been reported to decrease the number of preferred conformers of DOTA-like complexes, rigidification being the most efficient and frequently employed way. Incorporation of bulky groups or chiral carbons, on the

pendent arms, on the macrocyclic ring or both, have been reported in the literature.[26–35] It should be noted that with the introduction of more bulk on the ligand metal ions coordination of the lanthanoid becomes more difficult. In comparison with the modification or replacement of the acetate arms, substitution of specific protons on the tetraaza ring to force a ring flip are rare. Most of the reported examples of chiral cyclen placed chiral carbons on each of the four ethylenediamines, resulting in a complex with $C_4$ symmetry.[31,35,36] Among them, tetramethylated cyclen (4MDOTA, Chart 4.1) was the most studied and provided increased rigidity,[36] while, even with additional chiral methyl modifications on the arms (4MDOTMA, chart 4.1), both isomers are still observed.[37,38] In a recent work, the methyl substituents on the ring were replaced with various other alkyl groups (such as ethyl, benzyl, isobutyl and butylamine), but no groups on the pendent arms were added.[31] According to the reported results, the substituted groups could occupy either at the corner or side positions on the ring, yielding two conformers, and it was shown that the ratio of the two conformers depends on the size of the substituens.[31] It should be pointed out that the incorporation of methyl and related substituents such as described above makes the DOTA derivatives more hydrophobic, which enhances the chance of protein precipitation once used them as a probe to study paramagnetic NMR.

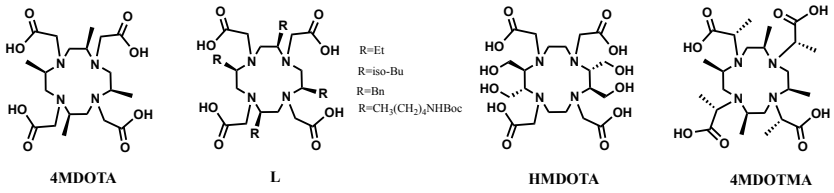


**Chart 4.1** Structures of DOTA-like rigid ligands.

Here, we report the design, synthesis and conformational analysis using NMR and modeling of several novel DOTA-derivatives. We designed a $C_2$ symmetric chiral cyclen-like ring with two pairs of hydroxyl-methylene substituents. For the hydroxy-methylene substituted ligands (Chart 4.1), both enantiomers were prepared. To investigate only the influence of the substituents on the ring flip, the regular pendent arms were used. Two sets of chemical shifts were observed in the 1D $^1$H spectrum of these new DOTA-like lanthanoid complexes, which were identified as the SAP and TSAP conformers. The main species for these complexes is the TSAP conformer. The 2D EXSY NMR results indicated that in these complexes ring flipping is not observable at a rate matching the NMR time scale. Exchange is only observed due to reorientation of the pendent arms.

**Results and Discussion**

**HMDOTA design and synthesis.** In our design, we anticipated that the introduction of two substituents on adjacent carbons of the cyclen-ring system with the appropriate

stereochemistry relative to each other would position them both "equatorial". To ensure $C_2$ symmetry (see Chapter I, section 3), a second set of substituents on the opposite site of the cyclen-ring system was incorporated. We selected hydroxyl-methylene groups to render the resulting complex more hydrophilic. This novel cyclen derivative is referred to as **cyclenol**, compound **9**. (Scheme 4.1). To investigate the effects of a larger substituent on the conformational exchange we also prepared the O-benzyl derivative (BnMDOTA). A previously reported cyclization method was applied with improvements.[35,39] Both enantiomers of tartaric acid as the starting compounds were modified to obtain the precursors **6** and **7**, amenable to cyclization (Scheme 4.1). To decrease side products formed due to intermolecular reactions, the base, concentration and temperature of the cyclization reaction were optimized.

The chance of intermolecular reactions was reduced by performing the cyclization at a low concentration. It was found that concentrations below 0.03 mol/L did not result in a further increase of the yield of the desired cyclized product. According to the LC-MS, the main side product was the intermolecular N-alkylation product formed between cyclized compound **8** and compound **7** (Scheme 4.3). The effects of temperature and acid scavenger were evaluated as shown in Table 4.1. When the reaction was performed at room temperature, with $NaHCO_3$ as base, the lowest yield for

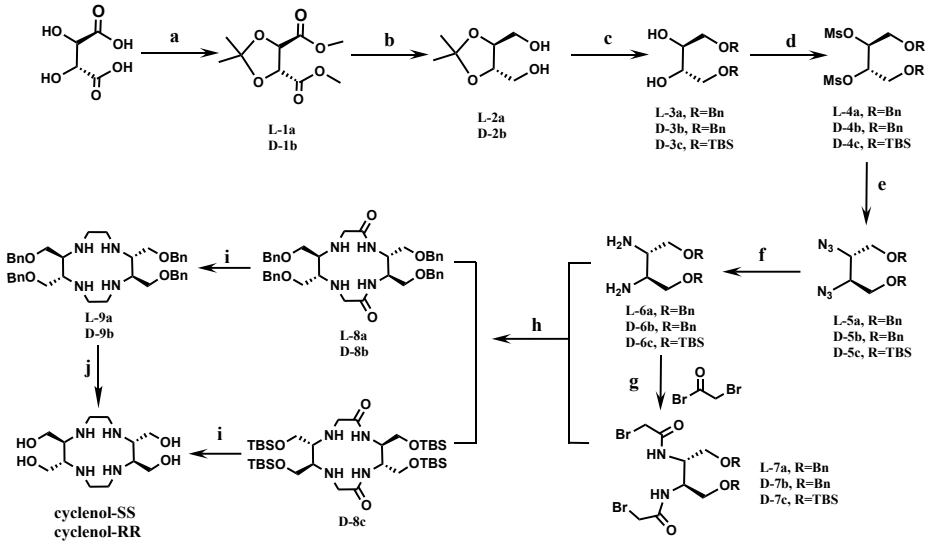


**Scheme 4.1** a) I) $SOCl_2$, MeOH, reflex; II) *p*-TsOH•$H_2O$, DMP, DCM, 50 °C, 6 h; b) $NaHB_4$, MeOH, rt, o/n; c) I) BnBr, NaH, DMF, 0 °C, 16 h; II) 1 mol/L HCl in EtOH, 80 °C, 6 h, 80 °C, d) MsCl, $Et_3N$, DCM, rt, 3 h; e) $NaN_3$, DMSO, 80 °C, 24 h; f) Pd/C, $H_2$, MeOH, 24 h; g) 2-bromoacetyl bromide, $K_2CO_3$, DCM/$H_2O$ (1:1), 0 °C, 10 h; h) $NaHCO_3$, ACN, 80 °C, 24 h; i) Red-Al, toluene, 80 °C, 24 h; j). Pd/C, $H_2$, EtOH, 24 h.

both products was obtained, while at 80 °C, most cyclized compound was produced. In comparison with the other acid scavengers, $NaHCO_3$ is a weak base and it may be that both alkylation reactions are slow at rt, whereas at high temperature, the intramolecular N-alkylation is preferred over the intermolecular alkylation of the secondary amine group. Therefore, the cyclization was performed at a concentration of 0.03 mol/L, a temperature of 80 °C and using $NaHCO_3$ as base. The TBS or benzyl protective groups did not affect the cyclization outcome in any way.

Before deprotection of the benzyl or TBS groups, the acquired **8** was treated with the reagent Red-Al to reduce the two amide groups to amines. The TBS protection groups were lost at this step to directly give **cyclenol**. The benzyl groups remained attached, yielding **9**. Both products, with or without protection of the hydroxyls, were alkylated with *tert*-butyl bromoacetate in the present of $K_2CO_3$ at room temperature. Under this condition, the **cyclenol** formed a side product in which one of the hydroxyls had also reacted. Both purified products **10** and **11** were deprotected to give the final ligands. Compound **10a** afforded BnMDOTA in one step with a yield 69% or in two steps

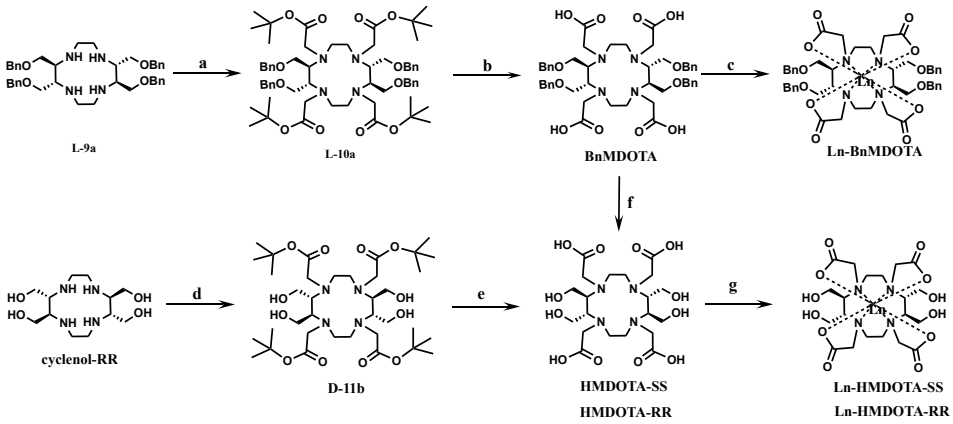


**Scheme 4.2** a) tert-butyl 2-bromoacetate, $K_2CO_3$, ACN, rt, 16 h; b) TFA/DCM (4:1), rt, 16 h; c) $LnCl_3$, DMSO, 80 °C, pH=8; d) tert-butyl 2-bromoacetate, DIPEA, ACN, rt, 16 h; e) TFA/DCM (4:1), rt, 16 h; f) Pd/C, EtOH, $H_2$, rt, 72 h; g) $LnCl_3$, $D_2O$, pH=8, rt.

**Scheme 4.3** The intermolecular side reaction discussed in the text.

given HMDOTA (SS enantiomer) with a yield of 60 %. After deprotection of the *tert*-butyl groups of **11b**, the RR enantiomer of HMDOTA was produced.

**Table 4.1** Yield of cyclization under different conditions

| *Temp./base* | $K_2CO_3$ | | $Ce_2CO_3$ | | $Na_2CO_3$ | | $NaHCO_3$ | |
|---|---|---|---|---|---|---|---|---|
| | **a** | **b** | **a** | **b** | **a** | **b** | **a** | **b** |
| ***rt (72 h)*** | 15% | 30% | 14% | 30% | 16% | 30% | 10% | 8% |
| ***50 °C (24 h)*** | 13% | 32% | 12% | 28% | 15% | 30% | 16% | 14% |
| ***80 °C (24 h)*** | 14% | 40% | 15% | 35% | 23% | 35% | 30% | 15% |

**a** aimed cyclized product, **b** detected side product.

**Preparation and stability of metal complexes.** Chlorate salts of lanthanoids were used for preparation of all metal complexes. For HMDOTA, the formation of the complexes was performed in $D_2O$ at pH 8 under rt for 12 h. Harsher condition were necessary to obtain complexes of the BnDOTA ligand, the metal complexes being formed in DMSO at pH 8 and 80 °C for 10 h. The stability of Eu(III) loaded HMDOTA was investigated at different temperatures and pD values (pD=pH+0.4), as shown in Figure 4.1A and B. For comparison, lanthanoids complexes of DOTA (commercially purchased) and another reported rigid DOTA derivate (referred to as PyDOTA, synthetical details see chapter V, Materials and Methods) were prepared as well. Figure 4.2 shows the structures of the four complexes.

**1D $^1$H spectra.** The relative torsion of the two N- and O-planes as discussed above causes conformational exchange of the complex, represented as reorientations of the pendent arms and the flip of the cyclen ring. The coordination of the carboxylic pendent arms can rotate either in clockwise (**Λ**) or anticlockwise (Δ), and the tetra-aza macrocyclic ring can adopt **λλλλ** or **δδδδ** conformations. This results in four conformations present as two enantiomeric pairs, Δ(**λλλλ**) and **Λ**(**δδδδ**) in one, **Λ**(**λλλλ**) and Δ(**δδδδ**) in another (Figure 4.3 A). The Δ(**λλλλ**) or **Λ**(**δδδδ**) are the SAP conformers, whereas the **Λ**(**λλλλ**) and Δ(**δδδδ**) are the TSAP conformers.[10,11] These two geometries generate different magnetic properties if the bound metal ion is paramagnetic (Figure 4.3B), enabling the isomers to be distinguished by NMR spectroscopy.

The 1D $^1$H spectra of the four ligands shown in Figure 4.1, loaded with Eu(III) or Yb(III) were recorded at 20 °C and 14.1 T. The spectra of Eu(III)-DOTA and Yb(III)-DOTA was in agreement with previously reported results (Figure 4.1 C and D).[11,40] Two sets of six peaks with different intensity were observed for both samples, corresponding to the resonance shifts of the two diastereoisomers, SAP and TSAP. The peak set with higher intensity and larger resonance shift rang are assigned as SAP. The assignment of the peaks is shown in Figure 4.3B

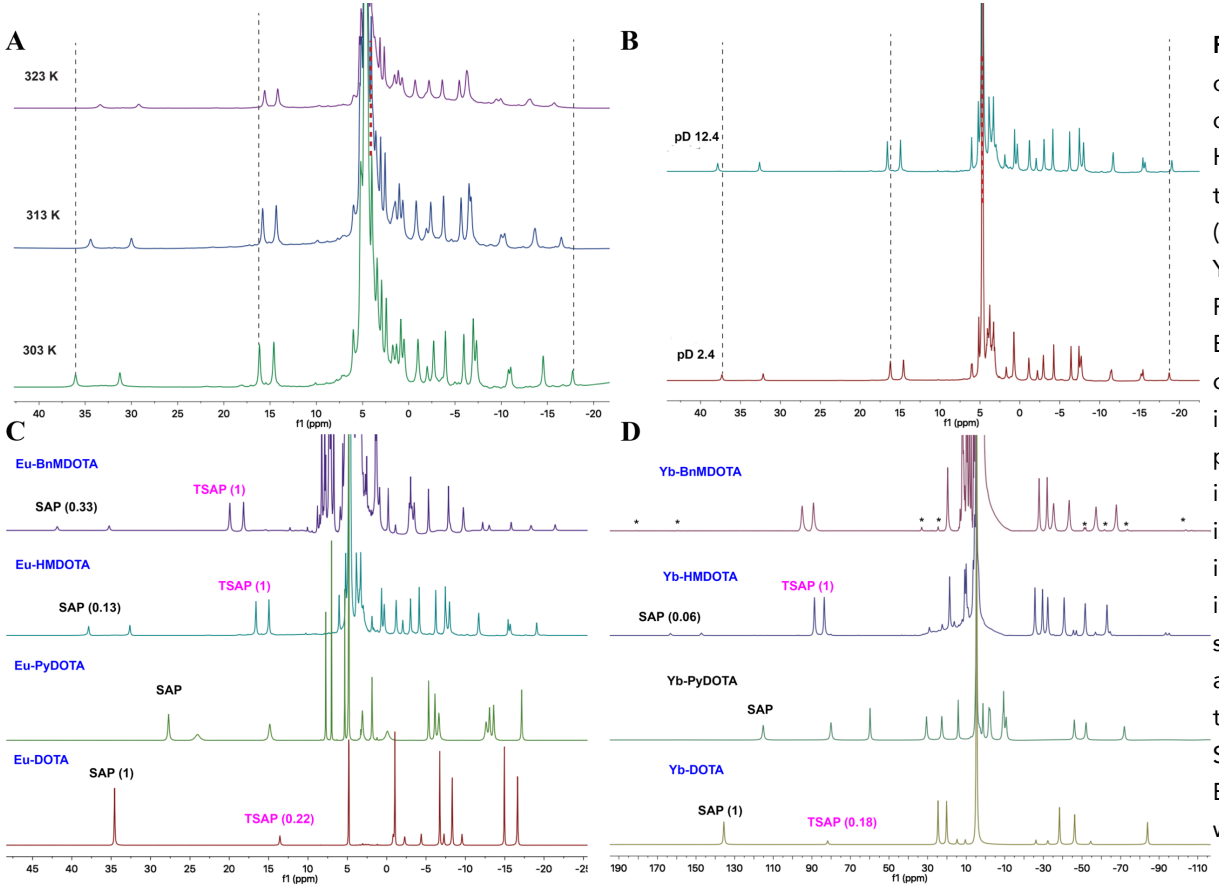


**Figure 4.1** 1D $^{1}$H spectra of DOTA and DOTA-like complexes. (**A, B**) Eu(III)-HMDOTA at different temperatures (**A**) and pD (**B**); (**C, D**) Eu(III) (**C**) and Yb(III) (**D**) loaded DOTA, PyDOTA, HMDOTA, BnMDOTA at 293 K. Red dashed lines in **A** and **B** indicate the reference peaks of methanol. The integrations of both isomer peaks are listed in brackets with the integration of the main species set to 1. The asterisks in **D** indicate the chemical shifts of SAP conformer of Yb-BnMDOTA. Spectra were recorded at 14.1 T.

The introduction of pyridine-N-oxide arms, in PyDOTA, reduces number of observable conformers.[20,41] This was demonstrated by the 1D $^1$H spectra in this work as well. In the spectra (Figure 4.1 C and D), 12 peaks (exclude the peaks of the pyridine-N-oxide ring) are expected per conformer for this $C_2$ symmetric compound. Twelve are observed (the peak at $\delta$ ($^1$H)=14.85 ppm show no cross peaks in COSY and EXSY with other peaks), both in the spectra of Eu(III)-Py-DOTA and Yb(III)-PyDOTA, indicating that only one conformation is present, which was reported as SAP,[20] was present. The increased linewidths indicate that a chemical exchange process is occurring, reflecting the conversion of one SAP enantiomer into another, which consists of a correlated ring flip and arm rotation.

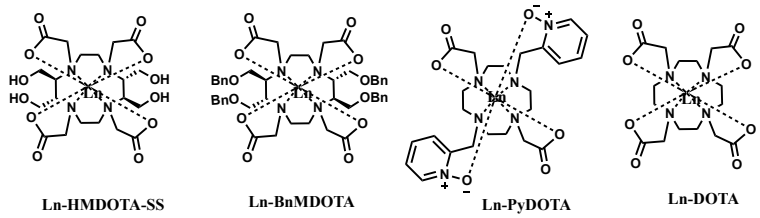


**Figure 4.2** Structures of lanthanoid complexes of HMDOTA, BnMDOTA, PyDOTA and DOTA.

The HMDOTA features four hydroxyl-methyl substituents on the tetraaza ring in the SSSS or RRRR configurations. The two pairs of substituents are located at the opposite ethylenic groups and the pairs are next to each other, resulting in a $C_2$ symmetry. The main set of chemical shifts of fourteen peaks was assigned to the TSAP conformer, based on the positions of the peaks in comparison to those of Eu(III)-DOTA. The assignment of other peaks was carried out based on 2D EXSY and COSY spectra (Figure 4.4 and App. Figure A4.1). Furthermore, both Eu(III) loaded chiral complexes (SSSS/RRRR) generated exactly the same chemical shifts in 1D $^1$H spectra (Figure 4.5), as expected. A very obvious difference between Eu(III)-DOTA and Eu(III)-HMDOTA is that in the former SAP is the favorable conformer, whereas in the latter, it is TSAP. Similar results were found for Yb(III) loaded DOTA and HMDOTA. The ratio was determined by taking the ratio of integrals of protons resonances at the lowest field in SAP and TSAP conformers (Figure 4.1C and D). A comparison of the ratios for the Yb(III) and Eu(III) compounds indicates that the population of the minor isomer depends on the ionic radius, as well as on the compound.

BnMDOTA has larger and more hydrophobic groups at the four substituent positions and its complexes may be expected to be more rigid. It was found that there still were two sets of peaks in the 1D $^1$H spectra of both Eu(III) and Yb(III) loaded

BnMDOTA complexes (Figure 4.1 C and D) but the TSAP conformer is even more favorable than in HMDOTA.

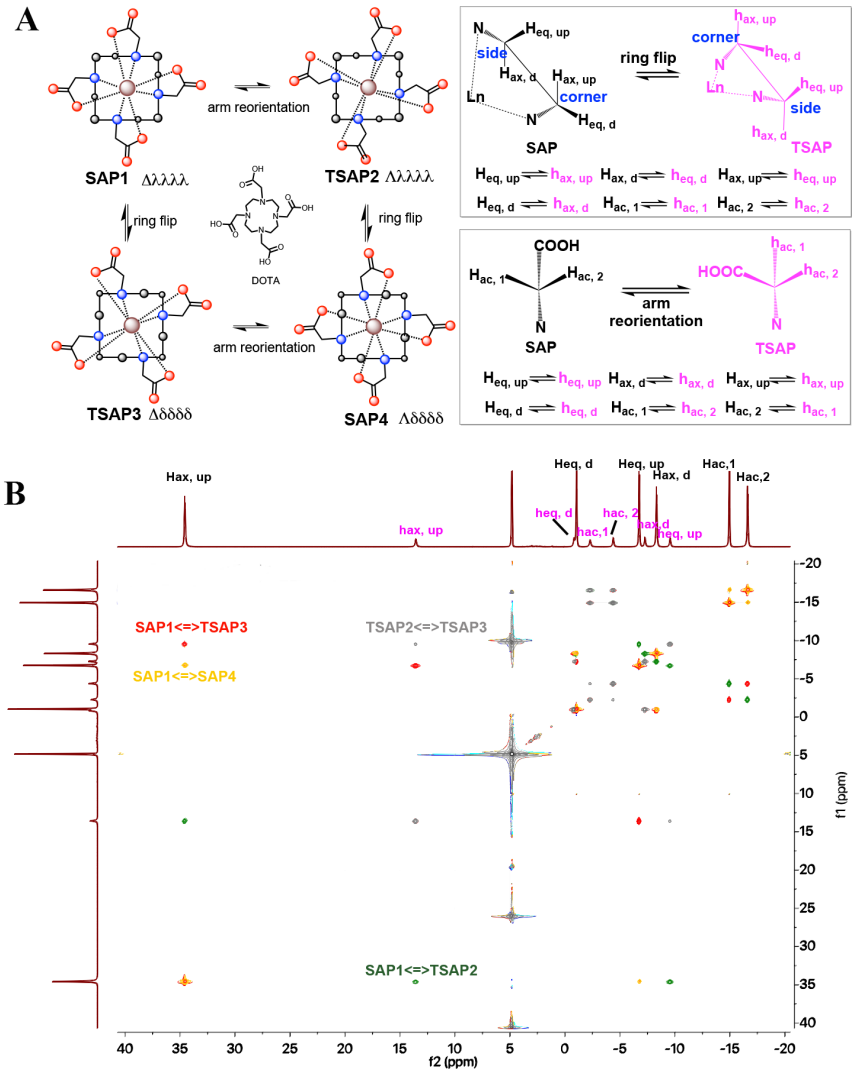


**Figure 4.3 A**) Schematic representation of DOTA lanthanoid complex conformational exchange (left) (see also **Chapter 1, Figure 1.8**) and the effect of the two exchange processes on the different protons (right). **B**) 2D 1H EXSY spectrum of Eu(III)-DOTA, peaks in red and green indicate the conformational exchange of ring flip and arm reorientation, respectively; peaks in orange and grey indicate the two-step conformational exchange between enantiomers. Peak assignments were shown in H (SAP) and h (TSAP).

**2D $^1$H EXSY spectra.** To study the exchange process between the conformers in the different compounds, EXSY experiments were recorded with a mixing time of 8 ms. It is known that exchange occurs in DOTA with rates of about 100 $s^{-1}$ [10,18] and with this mixing time, such exchange processes can be detected, while minimizing NOE build-up. In the spectra of the paramagnetic Eu(III) and Yb(III) compounds, the dispersion of the resonances is so large that for most of the peaks exchange will be in the slow regime. The conformational exchange process of the DOTA conformers is illustrated in Figure 4.3. The inversion of the cyclen ring generates the exchange between the axial protons of SAP1(SAP4) and equatorial protons of TSAP3(TSAP2). The reorientation of the pendent arms causes the exchange between axial protons of SAP1(SAP4) and axial protons TSAP2(TSAP3). It is also possible that during the mixing both ring flip and arm rotation occur, causing exchange between enantiomers, for example, between the axial proton of SAP1 and the equatorial proton of SAP4. Similarly, exchange between TSAP2 and TSAP3 can occur. Thus, the appearance of the various cross-peaks in the EXSY spectrum is indicative for presence or absence of exchange on the millisecond time scale between conformers. This conformational exchange was investigated for the four Eu(III) complexes by 2D $^1$H EXSY. The results are shown in Figure 4.3 and 4.4.

Four sets of exchanging cross peaks were observed in the Eu(III)-DOTA spectrum, demonstrating the exchange between the four isomers (Figure 4.3B). For the other three complexes, only one set of exchange cross peaks was found. Although the spectrum of Eu(III)-PyDOTA, shows only the presence of the SAP conformers, conformational exchange between two SAP enantiomers is still detected. This result indicates that reorientation of the pendent arms and flipping of the cyclen ring occurs in a correlated fashion, with the intermediate TSAP form being very lowly populated, similar to what was reported for CLaNP5.[20]

Interestingly, in the Eu(III)-HMDOTA and Eu(III)-BnMDOTA EXSY spectra, only exchange due to arm rotation was detected. Ring flipping does not occur on the time scale of the EXSY experiment, so the rate must be much less than 100 $s^{-1}$. Clearly, the substituents hinder the ring flipping process significantly.

**Molecule conformational modulation.** It was reported that the substituents on the cyclen ring prefer to adopt an equatorial position.[36] As shown in Figure 4.3 A, there are two equatorial positions relative to the macrocyclic ring, referred to as "eq, up" or "eq, down". In the case of HMDOTA and BnMDOTA, the substituents are located at adjacent positions and both of them will prefer to adopt equatorial positions, as was supported by lack of exchange in the EXSY experiments. To further understand the arrangement of these substituents relative to the tetraaza ring, conformer distributions of Ln(III)-HMDOTA were calculated using Spartan'14 & Spartan'14 Parallel Suite (www.wavefun.com).

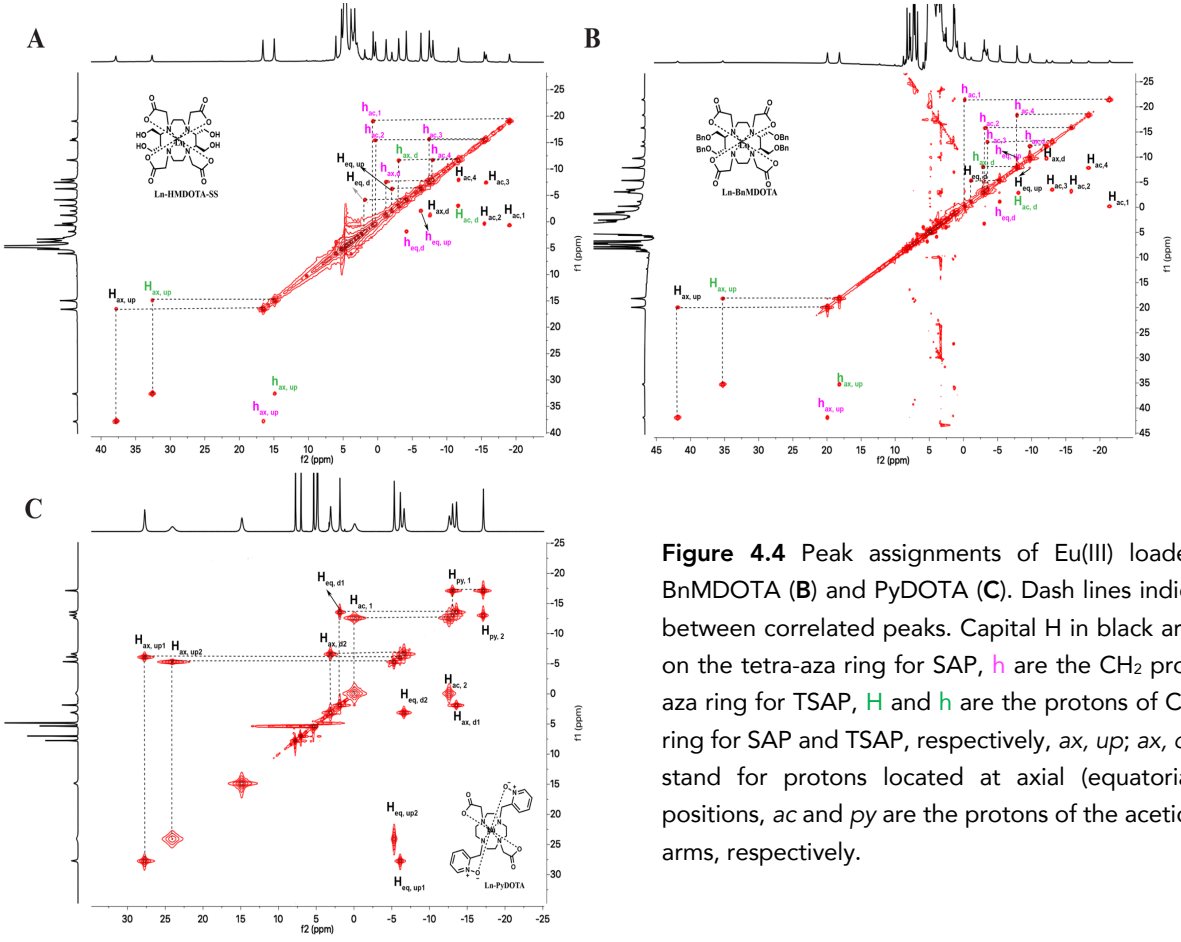


**Figure 4.4** Peak assignments of Eu(III) loaded HMDOTA (**A**), BnMDOTA (**B**) and PyDOTA (**C**). Dash lines indicate the exchange between correlated peaks. Capital H in black are the $CH_2$ protons on the tetra-aza ring for SAP, h are the $CH_2$ protons on the tetra-aza ring for TSAP, H and h are the protons of CH on the tetra-aza ring for SAP and TSAP, respectively, *ax, up*; *ax, d*; *eq, up* and *eq, d* stand for protons located at axial (equatorial) up and down positions, *ac* and *py* are the protons of the acetic acid and pyridine arms, respectively.

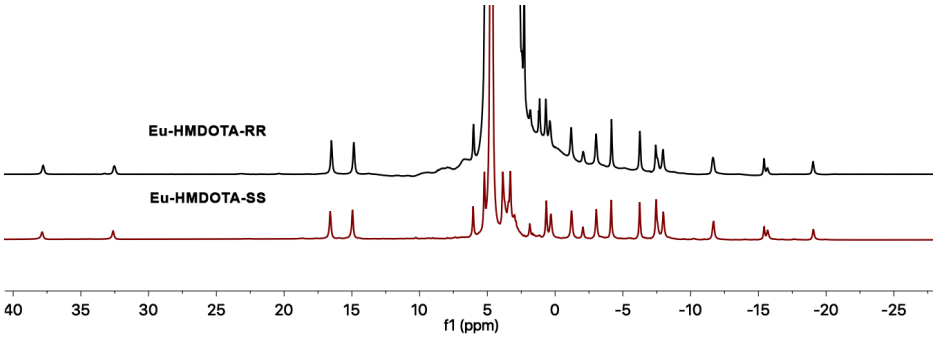


**Figure 4.5** 1D $^{1}$H spectra of Eu(III)-HMDOTA-SS/RR.

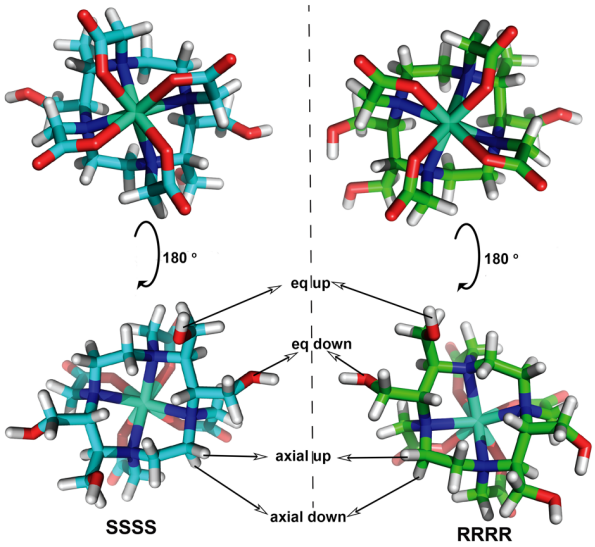


**Figure 4.6** Models of the most stable coordination of Eu(III)-HMDOTA-SS/RR, as deduced from NMR studies and molecular conformational distribution calculations. Carbons are shown in cyan (S configuration) and green (R configuration), and the nitrogen, oxygen and proton in blue, red and light grey, respectively.

A crystal structure of Gd(III)-DOTA[7] was modified with four hydroxyl-methyl groups on the cyclen ring and used for molecular structure modeling. The substituents of Eu(III)-HMDOTA were located at equatorial positions for both configurations and adopted TSAP geometry (Figure 4.6), in agreement with the NMR results. It is interesting that for both configurations, the substituents on the corner carbons always adopt the 'eq up' geometry whereas on the side carbons they take the 'eq down' position. Therefore, the teraaza ring of Eu(III)-HMDOTA-SSSS is in a **λλλλ** conformation, while **δδδδ**

conformation is found for Eu(III)-HMDOTA-RRRR. The arm rotation of Eu(III)-HMDOTA-SSSS is Δ, but R configuration is **Λ**.

In conclusion, a synthetic strategy was described that allows the synthesis of novel functionalized DOTA derivatives with substituents on the tetraaza ring at adjacent positions. Using this method, two DOTA-like $C_2$-symmetric enantiomers were obtained. With the substituents, these novel ligands are more hydrophilic and rigid. Both SAP and TSAP conformers exist but with a higher abundance of TSAP after ligation to medium- or small size lanthanoids. Calculations indicate that the most stable isomer is indeed TSAP. EXSY experiments confirmed the rigidity of these ligands. Conformational exchange was still observed but only due to rotation of the flexible acetate arms. Therefore, to further reduce the number of isomers, modification on the pendent arms, such as replacement of the acetic acid arms by pyridine or the introduction of chiral centers on the arms, is a good option. It will be very interesting to link such compounds to proteins and test the ability to detect protein dynamics.

**Materials and methods**

**General:** All the chemicals were purchased from Sigma-Aldrich, Merk, Fisher Scientific and VWR and used as received. DOTA was purchased from Macrocyclics. Solvents were purchased from Honeywell, BIOSOLVE or Aldrich and stored over 3 Å molecular sieves before use. Traces of water from reagents were removed by co-evaporation with toluene in reactions that required anhydrous conditions. Flash chromatography was performed on Screening Devices silica gel 60 (40-63 μm) and $C_{18}$-reversed phase silica gel (fully endcapped, 40-63 μm). Liquid chromatography-mass spectrometry (LC-MS) analysis was performed on a Surveyor HPLC system (Thermo Finnigan) equipped with a $C_{18}$ column (Gemini, 4.6 mm x 50 mm, 5 μm particle size, Phenomenex), coupled to a LCQ Adventage Max (Thermo Finnigan) ion-trap spectrometer ($ESI^+$). TLC analysis was performed on a silica gel (F 1500 LS 254 Schleicher and Schuell, Dassel, Germany) in which visualized by UV and/or ninhydrin, $KMnO_4$. Reaction was monitored by LC-MS analysis and TLC analysis. Waters preparative HPLC system, equipped with a Waters C18-Xbridge 5 μm OBD (30 x 150 mm) column, was used for purification and the applied buffers were $H_2O$ (2% TFA) and ACN. High-resolution mass spectrometry (HRMS) analysis was performed with an LTQ Orbitrap mass spectrometer (Thermo Finnigan), equipped with an electronspray ion source in positive mode (source voltage 3.5 kV, sheath gas flow 10 mL/min, capillary temperature 250 °C) with resolution R = 60000 at m/z 400 (mass range m/z = 150–2000) and dioctyl phthalate (m/z = 391.28428) as a "lock mass". NMR spectra were recorded on a Bruker AV-400 (400/100 MHz), AV-500 (500/125 MHz) or AV-600 (600/150 MHz) spectrometer. Chemical shifts (**δ**) are reported in ppm relative to the residual signal of the deuterated solvent.

**Metal complex preparation:** Compound HMDOTA-SS (3 mg, 5.7 μmol) was dissolved in $D_2O$ at rt and the pH was adjusted to around 8 by adding 1 mol/L NaOD. To this solution was added equal amount of $LnCl_3 \bullet nH_2O$ and the pH value adjust again to 8 by using 1 mol/L NaOD. After reacted at rt for 12 h, above solutions were directly used for NMR measurements. Same procedure was used for Ln-DOTA and Ln-PyDOTA complexes preparation.

Ln-BnMDOTA complexes were prepared in DMSO solution containing BnMDOTA (3 mg, 3.4 μmol) and equal amount of $LnCl_3 \bullet nH_2O$. The pH value of this solutions was adjust to around 8 by adding 1 mol/L NaOD and hearted up to 80 °C for 10 h. Before NMR measurement, DMSO was removed and the complexes were dissolved in MeOD/$D_2O$ (*v*:*v* =4:1).

**NMR spectroscopy:** All EXSY experiment were recorded on a Bruker AV 600 MHz NMR spectrometer at 293 K. The mixing time was 8 ms. Data were processed using Bruker Topspin software.

**Molecule conformational modulation:** A 3D structure was obtained by conformational distribution calculation with molecular mechanic of MMFF (Merck Molecular Force Field).[42]

**Synthesis**

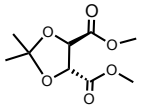

**Dimethyl (4*R*,5*S*)-2,2-dimethyl-1,3-dioxolane-4,5-dicarboxylate, compound 1a and 1b**

To L-(+)-Tartaric acid (15 g, 0.1 mole) in methanol (0.5 L) was added $SOCl_2$ (14.6 mL, 0.2 mole) while cooling with an ice bath. After the addition, the ice bath was removed and the reaction mixture heated under reflux and the reaction progress monitored by TLC. After 16 h, the reaction mixture was treated by the addition of trimethylamine (circa 40 mL) until the pH of the reaction mixture was around 6. The reaction mixture was filtrated and concentrated under reduced pressure using a rotary evaporator. The crude product was dissolved in DCM (1 L) and washed with water (2 x 1 L) and brine (1 L). The organic layer was dried with anhydrous $Na_2SO_4$, filtrated and concentrated under reduced pressure to give a colorless oily product. Without further purification, above crude product was dissolved in DCM (0.5 L) followed by addition of *p*-toluenesulfonic acid monohydrate (p-TsOH$\bullet H_2O$, 9.5 g, 0.05 mol) and 2,2-dimethoxypropane (DMP, 15 mL, 0.2 mole), respectively. This mixture was hearted up to 50 °C and the reaction followed by TLC. The organic solvent was removed after 6 h and the product was purified by flash silica gel column chromatography (6 % of ether in pentane, $R_f$= 0.2) yielding 85% (18.5 g, 0.085 mole) of compound **1a** as a white solid. Similar procedure was applied for the synthesis of the compound **1b**. D-(-)-Tartaric acid (15 g, 0.1 mol) yield 80% (17.4 g, 0.080 mole) of Compound **1a**. The spectroscopic data

of **1a** are in agreement with those reported in the literature: $^{1}$H NMR (400 MHz, $CCl_3D$, 293K): **δ** = 1.10 (s, 6H, $2CH_3$), 3.81 (s, 6H, $2OCH_3$), 4.75 (s, 2H, 2OCHCO). $^{13}$C NMR (400 MHz, $CCl_3D$, 293K): **δ** = 27.12 ($CH_3$), 52.85 (2CHCOOMe), 78.35 ($2OCH_3$), 110.52 ($C(CH_3)_2O_2$), 170.56 (2COOMe). HR-MS compound **1a**: m/z 219.0863 $[M+H]^+$, calcd. $[C_4H_6O_6]$ 219.0869. FTIR ($cm^{-1}$): 1677.7, 1558.3, 1456.7, 1418.1, 1313.6, 1200.6, 1130.5, 958.7, 832.8, 799.9, 748.4, 712.2. NMR, HRMS and IR data of the compound **1b** are in agreement with compound **1a**. Compound **1a** $[\alpha]_D^{20}$ =-17.7° (C= 1 mg/mL, $CHCl_3$). Compound **1b** $[\alpha]_D^{20}$=13.3° (C = 1 mg/mL, $CHCl_3$).

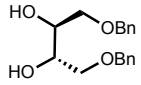


**((4*R*,5*R*)-2,2-dimethyl-1,3-dioxolane-4,5-diyl)dimethanol, compound 2a and 2b**

A solution of compound **1a** (10 g, 46 mmol) in methanol (460 mL) was cooled down to 0 °C and $NaBH_4$ (3.5 g, 92 mmol) was added in small portions. The reaction mixture was allowed to warm to rt and stirring was continued for 16 h. The reaction solution was quenched by adding $H_2O$ under ice bath condition and the solution was removed under reduced pressure using a rotary evaporator. The crude product was dissolved in DCM (0.5 L) and washed with water (2 x 0.5 L) and brine (0.5 L). The organic layer was dried with anhydrous $Na_2SO_4$, filtrated and concentrated under reduced pressure to give a slight yellow oily product. This product was purified by flash silica gel column chromatography with a gradient of 0-30% ethyl acetate in pentane to yield 91% (8.38 g, 41.9 mmol) compound **2a** as a colorless liquid. Similar procedure was applied for the synthesis of the compound **2b**. Compound **1b** (10 g, 46 mmol) yield 93% (8.56 g, 42.8 mmol) of compound **2b**. The spectroscopic data of **2a** are in agreement with those reported in the literature: Compound **2a** $^{1}$H NMR (400 MHz, $CCl_3D$, 293K): **δ** = 1.39 (s, 6H, $2CH_3$), 3.00 (b, 2H, 2OH), 3.67-3.75 (q, 4H, $^{2}J$= 8 Hz, $2CH_2OH$), 3.94 (s, 2H, $2CHOCCH_3$). $^{13}$C NMR (400 MHz, $CCl_3D$, 293K): **δ** = 27.07 ($2CH_3$), 62.19 ($CH_2OH$), 78.35 ($CHCH_2$), 109.38 ($C(CH3)_2O_2$). HR-MS: m/z 163.0978 $[M+H]^+$, calcd. $[C_7H_{14}O_4]$ 163.0970. FTIR ($cm^{-1}$): 3281.2, 2934.9, 2883.4, 2368.2, 1654.2, 1423.8, 1319.3, 1223.5, 1074.6, 1038.9, 1008.8, 881.5. NMR, HRMS and IR data of compound **2b** are in agreement with compound **2a**. Compound **2a** $[\alpha]_D^{20}$= -2.3° (C = 2.2 mg/mL, $CHCl_3$). Compound **2b** $[\alpha]_D^{20}$= +1.1° (C = 1.2 mg/mL, $CHCl_3$).

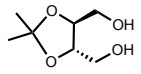


**(2R,3R)-1,4-bis(benzyloxy)butane-2,3-diol, compound 3a and 3b**

To a DMF solution (50 mL) of compound **2a** (1.62 g, 10 mmol) was added NaH (0.72 g, 30 mmol) in small portions at 0 °C. The mixture was stirred for 30 min, then benzylbromide (2.6 mL, 22 mmol) was added at 0 °C. The reaction mixture was allowed to warm to rt and stirring was continued for 16 h ensuing that no starting compound was present and a double protected compound was formed as evidenced by TLC analysis. Then $H_2O$ (10 mL) was added to quench the reaction at 0 °C. The reaction mixture was partially concentrated under reduced pressure. Then the residual solvent was diluted with

ethyl acetate (0.5 L) to extract with water (2 x 0.5 L) and brine (.0.5 L). The organic layer was dried with anhydrous $Na_2SO_4$, filtrated and evaporated under reduced pressure. Without further purification, the crude product was dissolved in ethanol (50 mL) containing 1mol/L HCl (1.66 mL) and the reaction mixture was heated up to 80 °C under continuous stirring. After 6 h, the reaction mixture was neutralized by adding saturated aqueous $NaHCO_3$ (circa 3 mL) and concentrated under reduced pressure. The crude product was purified by flash silica gel column chromatography with a gradient of 0-20% of ethyl acetate in pentane (ethyl acetate/pentane=1:1, $R_f$= 0.45) to yield 85% of compound **3a** (2.6 g, 8.5 mmol) as a white solid. Similar procedure was applied for the synthesis of the compound **3b**. Compound **2b** (2.00 g, 12.3 mmol) yield 83% of compound **3b** (3.12 g, 10.2 mmol). The spectroscopic data of **3a** are in agreement with those reported in the literature: Compound **3a** $^1$H NMR (400 MHz, $CCl_3D$, 293K): **δ** = 2.85 (s, 2H, 2OH), 3.55-3.63 (m, 4H, $2CH_2OBn$), 3.86-3.88 (t, 2H, $^3$J= 4 Hz, 2CHOH), 4.50-4.58 (q, 4H, $^3$J= 12 Hz, $2CH_2Ph$), 7.25-7.36 (m, 10H, $2(CH)_5C$). $^{13}$C NMR (400 MHz, $CCl_3D$, 293K): **δ** = 70.67 (2CHOH), 72.09 ($2CH_2OBn$), 73.70 ($CH_2Ph$), 127.91 ($(CH)_5C$), 127.98 ($(CH)_5C$), 128.60 ($(CH)_5C$), 128.96 ($(CH)_5C$), 137.82 ($C(CH)_5$). HR-MS: m/z 303.1602 $[M+H]^+$, calcd. $[C_{18}H_{22}O_4]$ 303.1596. FTIR ($cm^{-1}$): 3371.3, 30.9.3, 2844.7, 2351.0, 2024.8, 1750.1, 1684.2, 1453.8, 1362.3, 1313.6, 1206.3, 1096.1, 1054.6, 1033.1, 950.2, 721.1, 696.9. NMR, HRMS and IR data of compound **3b** are in agreement with compound **3a**. Compound **3a** $[\alpha]_D^{20}$= -10.2° (C = 3.5 mg/mL, $CHCl_3$). Compound **3b** $[\alpha]_D^{20}$= 8.5° (C = 2 mg/mL, $CHCl_3$).

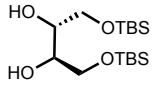


**(2R,3R)-butane-1,2,3,4-tetraol, compound 3c**

Compound **2b** (2 g, 12 mmol) was dissolved in ethanol (50 mL) containing 1mol/L HCl (1.66 mL) and the solution was heated up to 80 °C under continuous stirring. After 6 h, the reaction mixture was neutralized by adding saturated aqueous $NaHCO_3$ (3 mL) and concentrated under reduced pressure. Above crude product was dissolved in DCM (100 mL) and washed with water (2 x 100 mL) and brine (100 mL) and the organic layer was dried with anhydrous $Na_2SO_4$ and concentrated under reduced pressure. Without further purification, the crude product was dissolved in DMF (60 mL). To this solution was added imidazole (1.85 g, 27 mmol) under continuous stirring, cooled down to 0 °C and slowly added TBDMCl (0.38 mL, 27 mmol). After the addition, the reaction was allowed to warm up to rt and stirring was continued for 16 h. The reaction mixture was diluted with DCM (500 mL) and washed with saturated aqueous $NaHCO_3$ (500 mL), water (2 x 500 mL), brine (500 mL) and the organic layer dried with anhydrous $Na_2SO_4$, filtrated and concentrated under reduce pressure. The crude product was purified by flash silica gel column chromatography with a gradient of 0-20% of ether in pentane (ether/pentane=10:1, $R_f$= 0.35) to give compound **3c** as a light yellow colored liquid. The spectroscopic data of **3c** are in agreement with those reported in the literature: $^1$H NMR (300 MHz, $CDCl_3$) **δ**= 0.02 (s, 12H, $2CH_3Si$), 0.90 (s, 18H, $2C(CH_3)_3$), 2.8 (m, 2H, $CHCH_2OTBS$), 3.75 (m, 4H, $2CH_2CH$); $^{13}$C NMR (300 MHz, $CDCl_3$) **δ**= -5.47 ($2CH_3Si$),

(2($CH_3$)$_3$C), 25.82 , 65.03 (2$CH_2$OTBS), 71.45 (2CH$CH_2$O). -5.41 (2$CH_3$Si), -5.31 (2$CH_3$Si), 25.90 (2($CH_3$)$_3$C), 38.62 (2($CH_3$)$SO_2$), 62.02 (2$CH_2$OTBS), 79.90 (2CH$CH_2$O). HR-MS: m/z 351.2391 $[M+H]^+$, calcd. [$C_{16}H_{38}O_4Si_2$] 351.2387. $[\alpha]_D^{20}$= +9.5° (C = 2.2 mg/mL, $CHCl_3$).

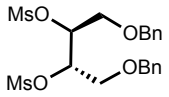


**(2R,3R)-1,4-bis(benzyloxy)butane-2,3-diyl dimethanesulfonate, compound 4a and 4b/c**

Compound **3a** (1.5 g, 5 mmol) in DCM (50 mL), Hünig base (2.08 mL, 15 mmol) was added in one portion at 0 °C to this solution. Followed by dropwise addition of methanesulfonyl chloride (0.93 mL, 12 mmol) under continuous stirring. The reaction mixture was allowed to warm to rt and stirring was continued for 3 h and the reaction was quenched by adding $H_2O$ (15 mL) at 0 °C. The crude product was diluted with DCM (100 mL) and washed with water (2 x 150 mL) and brine (150 mL). The organic layer was dried with anhydrous $Na_2SO_4$, filtrated and concentrated under reduce pressure. Flash silica gel column chromatography with a gradient of 0-20% of ethyl acetate in pentane as eluent (ethyl acetate/pentane=1:2, $R_f$= 0.35) was applied to yield 91% of compound **4a** (2.1 g, 4.6 mmol) as a white solid. Similar procedure was used for compound **4b** and **4c**. Compound **3b** (1.0 g, 3.3 mmol) yielding 88% of compound **4b** (1.3 g, 2.9 mmol). Compound **3c** (2 g, 5.7 mmol) yielding 80% of compound **4c** (2.31 g, 4.56 mmol). The spectroscopic data of **4a** are in agreement with those reported in the literature: Compound **4a** $^1$H NMR (400 MHz, $CCl_3D$, 293K) **4a**: **δ** = 3.04 (s, 6H, 2$CH_3SO_2$), 3.76-3.79 (t, 4H, $^3$J= 4 Hz, 2$CH_2$O), 4.46-4.58 (t, 4H, $^3$J= 12 Hz, 2$CH_2$Ph), 4.46-4.58 (m, 2H, 2CH$CH_2$O), 7.26-7.37 (m, 10H, 2(CH)$_5$C). $^{13}$C NMR (400 MHz, $CCl_3D$, 293K): **δ** = 38.83 (2$CH_3SO_2$), 68.70 (2$CH_2$O), 73.69 (2$CH_2$Ph) 78.80 (2CH$CH_2$O), 128.10-130.16 (2(CH)$_5$C), 136.99 (2C(CH)$_5$). HR-MS: m/z 459.1145 $[M+H]^+$, calcd. [$C_{20}H_{26}O_8S_2$] 459.1147. FTIR ($cm^{-1}$): 3853.5, 3734.8, 3676.1, 2973.5, 2937.7, 2866.2, 2844.7, 2352.5, 2329.6, 1362.3, 1174.8, 1116.1, 1054.6, 1033.1, 1013.1, 917.2, 824.2, 798.5, 738.4, 701.2. The NMR, IR and HRMS date of the compound 4b are in agreement with compound 4a. Compound 4c $^1$H NMR (400 MHz, $CCl_3D$, 293K): **δ** = 0.1 (s, 12H, 2$CH_3$Si), 0.9 (s, 18H, 2C($CH_3$)$_3$), 3.10 (s, 6H, 2($CH_3$)$SO_2$), 3.92-3.94 (t, 4H, $^3$J= 4 Hz, 2$CH_2$OTBS), 4.80-4.83 (m, 2H, 2CH$CH_2$O). $^{13}$C NMR (400 MHz, $CCl_3D$, 293K): **δ** = -5.41 (2$CH_3$Si), -5.31(2$CH_3$Si), 25.90 (2($CH_3$)$_3$C), 38.62 (2($CH_3$)$SO_2$), 62.02 (2$CH_2$OTBS), 79.90 (2CH$CH_2$O). HR-MS: m/z 529.1747 $[M+Na]^+$, calcd. [$C_{18}H_{42}O_8S_2Si_2$] 529.1757. FTIR ($cm^{-1}$): 3680.4, 2936.3, 2371.1, 2321.0, 1362.3, 1257.8, 1176.2, 1109.0, 1054.61, 1033.1, 1013.1, 917.2, 835.7, 779.9, 732.6, 668.3. Compound **4a** $[\alpha]_D^{20}$= -6.8 (C = 6 mg/mL, $CH_2Cl_2$). Compound **4b** $[\alpha]_D^{20}$=13.6 (C = 5 mg/mL, $CH_2Cl_2$). Compound **4c** $[\alpha]_D^{20}$= 15.4 (C = 7.2 mg/mL, MeOH).

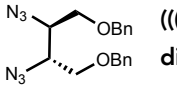


**((((2*S*,3*S*)-2,3-diazidobutane-1,4-diyl)bis(oxy))bis(methylene))dibenzene, compound 5a and 5b/c**

Compound **4a** (1 g, 2.2 mmol) was dissolved in DMSO (15 mL). To the reaction mixture was added $NaN_3$ (1 g, 15.3 mmol) in portions and the reaction mixture was heated at 80

°C for 24 h. The reaction mixture was diluted with DCM (100 mL) and washed with water (2 x 100 mL) and brine (100 mL). The organic layer was dried with anhydrous $Na_2SO_4$, filtrated and concentrated under reduced pressure. Further purification was acquired with flash silica gel column chromatography with a gradient of 0-10% of ether in pentane to yield 95 % of compound **5a** (0.9 g, 2.7 mmol) as a slight yellow liquid. $R_f$= 0.35 (ester/pentane =1:12) A similar procedure was used to obtain compound **5b** and **5c**. Compound **4b** (1 g, 2.2 mmol) yielding 93% of compound **5b** (0.7 g, 2.0 mmol). Compound **4c** (1.5 g, 3.0 mmol) yielding 95% of compound **5c** (1.12 g, 2.81 mmol). The spectroscopic data of **5a** are in agreement with those reported in the literature: $^1$H NMR (400 MHz, $CCl_3D$, 293K) compound 5a: **δ** = 3.68-3.70 (t, 4H, $^3$J= 2 Hz, $2CH_2Ph$), 3.75-3.79 (m, 2H, $2CHCH_2O$), 4.57 (s, 4H, $2CH_2O$), 7.26-7.42 (m, 10H, $2(CH)_5C$). $^{13}$C NMR (400 MHz, $CCl_3D$, 293K): **δ** = 61.00 ($2CHCH_2O$), 69.640 ($2CH_2O$), 73.58 ($2CH_2Ph$) 127.51-128.57 ($2(CH)_5C$) 137.41 ($2C(CH)_5$). HR-MS: m/z 353.1721 $[M+H]^+$, calcd. $[C_{18}H_{20}N_6O_2]$ 353.1726. FTIR ($cm^{-1}$): 3853.3, 2955.5, 2100.1, 1357.2, 1180.5, 1116.2, 1054.1 1033.1, 1013.1, 824.2, 775.2. The NMR, IR and HRMS date of the compound **5b** are in agreement with compound **5a**. Compound **5c** $^1$H NMR (400 MHz, $CCl_3D$, 293K): **δ** = 0.02 (s, 12H, $2CH_3Si$), 0.82 (s, 18H, $2C(CH_3)_3$), 2.52 (s, 6H, $2(CH_3)SO_2$), 3.46-3.49 (t, 2H, $^3$J= 4 Hz, $2CHCH_2O$), 3.73-3.74 (d, 4H, 4H, $^2$J= 4 Hz, $2CH_2OTBS$). $^{13}$C NMR (400 MHz, $CCl_3D$, 293K): **δ** = -5.71 ($2CH_3Si$), -5.64 ($2CH_3Si$), 25.63 ($2(CH_3)_3C$), 62.24 ($2CHCH_2O$), 63.14 ($2CH_2OTBS$). HR-MS: m/z 423.2331 $[M+Na]^+$, calcd. $[C_{16}H_{36}N_6O_2Si_2]$ 423.2336. FTIR ($cm^{-1}$): 2953.5, 2860.5, 2100.6, 1257.8, 1177.7, 1111.8, 1054.6, 1033.1, 1008.8, 837.1, 778.4. Compound **5a** $[\alpha]_D^{20}$= -4.9 (C=3 mg/mL, MeOH). Compound **5b** $[\alpha]_D^{20}$=10.3° (C=5 mg/mL, MeOH). Compound **5c** $[\alpha]_D^{20}$= 9.8 ° (C=2 mg/mL, MeOH).

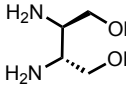


**(2*R*,3*R*)-1,4-bis(benzyloxy)butane-2,3-diamine, compound 6a and 6b/c**

Compound **5a** (1 g, 2.8 mmol) in methanol (30 mL) was treated with a catalytic amount of Pd/C (10% palladium on carbon) (circa 10 mg) and stirred for 24 h under an hydrogen atmosphere. The reaction mixture was filtered and concentrated in vacuo. A light yellow colored oily of compound **6a** was obtained and used for further reaction without purification. Similar procedure was used to obtain compound **6b** and **6c**. The spectroscopic data of **6a** are in agreement with those reported in the literature: Compound **6a** $^1$H NMR (400 MHz, $CCl_3D$, 293K): $^1$H NMR (400 MHz, $CCl_3D$, 293K): **δ** = 3.50-3.65 (q, 4 H, $^3$J= 7.2 Hz, $2CH_2O$), 3.63 (s, 2H, $2CHCH_2O$), 4.29-4.50 (q, 4H, $^3$J= 18 Hz, $2CH_2Ph$), 6.59 (s, NH), 7.20-7.33 (m, 10H, $5(CH)_5C$). $^{13}$C NMR (400 MHz, $CCl_3D$, 293K): **δ** = 51.69 ($2CHCH_2O$), 68.65 ($2CH_2O$), 73.38 ($2CH_2Ph$), 127.93-128.52 ($5(CH)_5C$), 137.42 ($C(CH)_5$). HR-MS: m/z 301.1922 $[M+H]^+$, calcd. $[C_{18}H_{24}N_2O_2]$ 301.1916. FTIR ($cm^{-1}$): 2949.2, 2864.8, 2368.2, 2322.4, 1456.7, 1362.3, 1054.6, 1033.1, 1013.1, 736.9, 696.9. The NMR, IR and HRMS date of the compound **6b** are in agreement with compound **6a**. Compound **6c** $^1$H NMR (400 MHz, $CCl_3D$, 293K): **δ** = 0.04 (s, 12H, $2Si(CH_3)_2$), 0.87 (s, 18H, $2C(CH_3)_3$),

2.82 (s, 2H, $2CHCH_2O$), 3.54-3.64 (m, 4H, $2CH_2OTBS$). $^{13}C$ NMR (400 MHz, $CCl_3D$, 293K): **δ** = -5.33 ($2CH_3Si$), -5.31 ($2CH_3Si$), 25.99 ($2(CH_3)_3C$), 54.21 ($2CHCH_2O$), 66.08 ($2CH_2OTBS$). HR-MS: m/z 349.2696 $[M+H]^+$, calcd. $[C_{16}H_{40}N_2O_2Si_2]$ 349.2707. FTIR ($cm^{-1}$): 2929.1, 2844.7, 2368.2, 2322.4, 1472.4, 1362.3, 1255.0, 1054.6, 1033.1, 1006.0, 835.7, 775.6, 668.3. Compound **6a** $[\alpha]_D^{20}$ = -18.5 ° (C = 4.2 mg/mL, MeOH). Compound **6b** $[\alpha]_D^{20}$=26.0 ° (C = 4.8 mg/mL, MeOH). Compound **6c** $[\alpha]_D^{20}$= 17.2 (C = 9 mg/mL, MeOH).

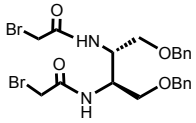

**N,N'-((2R,3R)-1,4-bis(benzyloxy)butane-2,3-diyl)bis(2-bromoacetamide), compound 7a and 7b/c**

Compound **6a** (3 g, 10 mmol) in DCM (100 mL) was treated with $K_2CO_3$ aqueous solution (0.4 mol/L, 50 mL). This mixture was cooled down to 0 °C and bromoacetyl bromide (2.9 mL, 22 mmol) in DCM (20 mL) was added. After 10 h stirring at 0 °C, the two layers mixture were separated and the water layer was extracted with DCM (3 x 50 mL). The combined organic layer was dried with anhydrous $Na_2SO_4$, filtrated and concentrated under reduce pressure. The crude product was purified by flash silica gel column chromatography with a gradient of 0-10% of ethyl acetate in DCM (ethyl acetate/DCM=1:5, $R_f$= 0.42) to give compound **6a** as white solid (3.8 g, 7 mmol) in 70 % yield. A similar procedure was used to obtain compound **7b** and **7c**: Compound **6b** (3 g, 10 mmol) yielding 74% of compound **7b** (4 g, 7.4 mmol). Compound **6c** (2 g, 5.7 mmol) yielding 72% of compound **7c** (2.4 g, 4.1 mmol), $R_f$= 0.3 (ethyl acetate/pentane =1:4). Compound **7a** $^1H$ NMR (400 MHz, $CCl_3D$, 293K): **δ** = 3.46-3.55 (m, 4H, $2CH_2O$), 3.77 (s, 4H, $2CH_2Br$), 4.35-4.39 (m, 2H, $2CHCH_2O$), 4.57 (s, 4H, $2CH_2Ph$), 6.59 (s, NH), 7.20-7.33 (m, 10H, $2(CH)_5C$). $^{13}C$ NMR (400 MHz, $CCl_3D$, 293K): **δ** = 51.69 ($2CHCH_2O$), 68.65 ($2CH_2O$), 73.38 ($2CH_2Ph$), 127.93-128.52 ($2(CH)_5C$), 137.42 ($2C(CH)_5$), 166.06 (2CONH). HR-MS: m/z 541.0322 $[M+H]^+$, calcd. $[C_{22}H_{26}Br_2N_2O_4]$ 541.0338. FTIR ($cm^{-1}$): 3711.9, 3279.7, 2982.1, 2864.8, 2844.7, 2826.1, 1652.7, 1559.7, 1054.6, 1033.1, 1013.1, 747.0, 698.3. The NMR, IR and HRMS date of the compound **7b** are in agreement with compound **7a**. Compound **7c** $^1H$ NMR (500 MHz, $CCl_3D$, 293K): **δ** = 0.08 (s, 12H, $2CH_3Si$), 0.91 (s, 18H, $2C(CH_3)_3$), 3.72-3.81 (d, 4H, $^3J$= 3 Hz, $2CH_2OTBS$), 3.83 (4H, $2CH_2Br$), 4.22-4.24 (d, 2H, $^3J$= 2 Hz, $2CHCH_2O$), 7.71 (2H, 2NHCO). $^{13}C$ NMR (500 MHz, $CCl_3D$, 293K): **δ** = -5.37 ($2CH_3Si$), 25.91 ($2(CH_3)_3C$), 29.05 ($2CH_2Br$), 52.13 ($2CHCH_2O$), 61.94($2CH_2OTBS$), 166.12 (2CONH). HR-MS: m/z 589.1118 $[M+H]^+$, calcd. $[C_{22}H_{26}Br_2N_2O_4Si_2]$ 589.1128. FTIR ($cm^{-1}$): 3751.9, 3689.0, 2950.6, 2894.8, 2827.6, 2378.2, 2312.4, 1647.0, 1559.7, 1254.9, 1116.1,1054.6, 1033.1, 1013.1, 835.7, 777.0. Compound **7a** $[\alpha]_D^{20}$ = -42.27 (C = 7.5 mg/mL, $CH_2Cl_2$). Compound **7b** $[\alpha]_D^{20}$ =25.3 ° (C = 7 mg/mL, $CH_2Cl_2$). Compound **7c** $[\alpha]_D^{20}$= 35.9 ° (C = 4.5 mg/mL, MeOH).

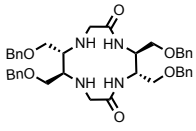

**(5R,6R,11R,12R)-5,6,11,12-tetrakis((benzyloxy)methyl)-1,4,7,10-tetraazacyclododecane-2,9-dione, compound 8a and 8b/c**

Compound **5a** (0.5 g, 1.67 mmol) and compound **7a** (0.9 g, 1.67 mmol) were dissolved in ACN (550 mL) containing $NaHCO_3$ (1.4 g, 16.67 mmol). The mixture was heated at 80 °C and stirring was continued for 24 h. The reaction mixture was filtrated and concentrated under reduced pressure. The crude product was purified with silica gel column chromatography with a gradient of 0-3% of methanol in DCM to yield 30% of compound **8a** (0.26 g, 0.38 mmol) as a white solid. $R_f$= 0.45 (DCM/MeOH= 10:1). A similar procedure was used to obtain compound **8b** and **8c**: Compound **5b** (0.6 g, 1.85 mmol) and compound **7b** (1.0 g, 1.85 mmol) yielding 27% of compound **8b** (0.25 g, 0.37 mmol). Compound **5c** (0.7 g, 1.7 mmol) and compound **7c** (1.0 g, 1.7 mmol), yielding 29% of compound **8c** (0.26 g, 0.34 mmol), $R_f$= 0.3 (methanol/DCM =15:1). Compound **8a** $^1$H NMR (400 MHz, $CD_3OD$, 293K): **δ** = 3.34-3.54 (m, 6H, $2CH_2NH$, $2CHCH_2O$), 3.60-3.78 (m, 8H, $4CH_2O$), 4.33-4.56 (m, 10H, $2CHCH_2O$, $4CH_2Ph$), 4.57 (s, 4H, $2CH_2O$), 6.59 (S, 4NH), 7.28-7.38 (m, 20H, $4(CH)_5C$). $^{13}$C NMR (400 MHz, $CD_3OD$, 293K): **δ** = 52.68 ($2CH_2O$), 52.95 ($2CHCH_2O$), 61.80 ($2CHCH_2O$), 67.22 ($2CH_2O$), 69.80 ($2CH_2NH$), 74.35 ($2CH_2Ph$), 74.68 ($2CH_2Ph$), 128.99-129.62 ($2(CH)_5C$), 138.34 ($C(CH)_5$), 138.99 ($C(CH)_5$), 168.79 (2CONH). HR-MS: m/z 681.3655 $[M+H]^+$, calcd. $[C_{40}H_{48}N_4O_6]$ 681.3652. FTIR ($cm^{-1}$): 3650.3, 2982.1, 2844.7, 1652.7, 1054.6, 1033.1, 1013.1, 736.9, 696.9, 668.3. The NMR, IR and HRMS date of the compound **8b** are in agreement with compound **8a**. Compound **8c**: $^1$H NMR (500 MHz, $CD_3OD$, 293K): **δ** = 0.10 (s, 12H, $2CH_3Si$), 0.11 (s, 12H, $2CH_3Si$), 0.93 (s, 18H, $2C(CH_3)_3$), 0.94 (s, 18H, $2C(CH_3)_3$), 2.71-2.73 (t, 2H, $^3$J=4 Hz, 2CHNH), 3.16-3.27 (d, 4H, $^3$J=4 Hz, $2CH_2CO$), 3.76-3.86 (m, 4H, $2CH_2CHNCO$), 3.79 (s, 4H, $2CH_2CHNH$), 4.14 (s, 2H, 2CHNCO). $^{13}$C NMR (500 MHz, $CD_3OD$, 293K): **δ** = -5.31 ($2CH_3Si$), -5.27 ($2CH_3Si$), 26.44 ($2(CH_3)_3C$), 26.49 ($2(CH_3)_3C$), 53.16 ($2CH_2CO$), 53.65 (2CHNH), 63.02 (CHNCO), 63.74 ($2CH_2CHNH$), 64.14 ($CH_2CHNCO$), 174.96 (2CONH). HR-MS: m/z 777.5221 $[M+H]^+$, calcd. $[C_{37}H_{80}N_4O_6Si_4]$ 777.5233. FTIR ($cm^{-1}$): 3736.2, 2982.1, 1652.7, 1521.1, 1506.8, 1456.7, 1033.1, 1013.1. Compound **8a** $[\alpha]_D^{20}$= -24.33 ° (C = 3 mg/mL, MeOH). Compound **8b** $[\alpha]_D^{20}$=7.86 (C = 1.4 mg/mL, MeOH). Compound **8c** $[\alpha]_D^{20}$= 8.0 ° (C = 2.3 mg/mL, MeOH).

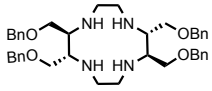


**(2R,3R,8R,9R)-2,3,8,9-tetrakis((benzyloxy)methyl)-1,4,7,10-tetraazacyclododecane, compound 9a**

Compound **8a** (0.1 g, 147 µmol) was co-evaporated with dried toluene three times and dissolved in dried toluene (2 mL). Above mixture was cooled down to 0 °C and Red-All (3.5 M in toluene, 0.42 mL) was dropwise added. After the addition, the reaction mixture was allowed to warm to rt for 1 h, then heated at 80 °C under a $N_2$ atmosphere. After 24 h, no starting compound was detected by the LC-MS. Water (circa 5 mL) was slowly added to quench the reaction at 0 °C. The reaction solution was extracted with $CHCl_3$ (3 x 50 mL) dried with anhydrous $Na_2SO_4$ and the solution was concentrated under reduce pressure. Further purification was done with self-packed $C_{18}$ revers phase silica gel column chromatography with a gradient of 10-30% of methanol in

$H_2O$ (0.2 % of TFA) to give compound 9a as white solid (69 mg, 106 µmol, 72% yield). $^1H$ NMR (400 MHz, $CD_3OD$, 293K): **δ** = 2.90 (s, 8H, $4CH_2NH$), 3.23 (b, 4H, $4CHCH_2O$), 3.41-3.67 (q, 8H, $4CH_2O$), 4.40-4.52 (q, 8H, $4CH_2Ph$), 7.30-7.37 (m, 20H, $4(CH)_5C$). $^{13}C$ NMR (400 MHz, $CD_3OD$, 293K): **δ** = 42.16 ($4CH_2NH$), 65.68 ($4CH_2O$), 74.35 ($4CH_2Ph$), 129.19-129.59 ($4(CH)_5C$), 138.63 ($4C(CH)_5$). HR-MS: m/z 681.3655 $[M+H]^+$, calcd. $[C_{40}H_{52}N_4O_4]$ 681.3652. FTIR ($cm^{-1}$): 3853.5, 3736.2, 3628.9, 2982.1, 2923.4, 2376.8, 1496.8, 1339.4, 1202.0, 1123.3, 1054.6, 1033.1, 1013.1, 741.2. $[\alpha]_D^{20}$= -9.09 ° (C = 2.2 mg/mL, $CH_2Cl_2$).

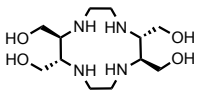


**Cyclenol-RR and Cyclenol-SS**

Compound **9a** (50 mg, 77 µmol) in ethanol (3 mL) was treated with Pd/C (10%wt Pd on carbon, circa 20 mg) at rt. Then the reaction flask was equipped with a $H_2$ gas balloon and the reaction monitored by LC-MS. After 72 h, no starting material was detected by LC-MS. The mixture was filtrated through Celite and concentrated. The crude product was purified by gel filtration to afford cyclenol (20 mg, 68 µmol, 88%) as a white solid. $^1H$ NMR (500 MHz, $D_2O$, 293K): **δ** = 2.92 (m, 8H, $4CH_2NH$), 3.03 (b, 4H, $4CHCH_2O$), 3.58-3.91 (q, 8H, $^3J$ = 12.5 Hz, $4CH_2OH$). $^{13}C$ NMR (400 MHz, $D_2O$, 293K): **δ** = 40.85 ($4CH_2NH$), 55.74 ($4CHCH_2OH$), 57.39 ($4CH_2OH$). HR-MS: m/z 293.2188 $[M+H]^+$, calcd. $[C_{12}H_{28}N_4O_4]$ 293.2189. FTIR ($cm^{-1}$): 2982.1, 2844.7, 2378.2, 2351.0, 2313.4, 1054.6, 1033.1, 1013.1. Cyclenol-SS $[\alpha]_D^{20}$= -17.9 ° (C = 2.3 mg/mL, MeOH), cyclenol-RR $[\alpha]_D^{20}$= 27.0 ° (C = 2.0 mg/mL, MeOH).

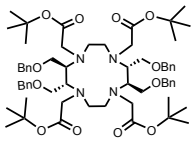


**Tetra-*tert*-butyl 2,2',2'',2'''-((2*S*,3*S*,8*S*,9*S*)-2,3,8,9-tetrakis((benzyloxy)methyl)-1,4,7,10-tetraazacyclododecane-1,4,7,10-tetrayl)tetraacetate, compound 10a**

Compound **9a** (50 mg, 77 µmol) and *tert*-butyl 2-bromoacetate (120 mg, 616 µmol) was dissolved in dried ACN (0.8 mL). To the stirred above mixture was added $K_2CO_3$ (85 mg, 616 µmol) and stirring was continued for 16 h. Then the solution was filtrated through Celite, concentrated and followed by purification of the crude product on silica gel column chromatography to give compound **10** (60 mg, 54 µmol, 80%) as a white solid. $^1H$ NMR (400 MHz, $CD_3OD$, 293K): **δ** = 1.48 (s, 18H, $2(CH_3)_3C$), 1.49 (s, 18H, $2(CH_3)_3C$), 2.25-2.28 (d, 2H, $^3J$= 12 Hz, $CH_2N$), 2.51-2.58 (t, 2H, $^3J$= 12 Hz, $CH_2N$), 2.63-2.70 (t, 2H, $^3J$= 12 Hz, $CH_2N$), 2.84-2.88 (q, 2H, $2CHCH_2O$), 3.00-3.05 (d, 2H, $^3J$= 12 Hz, $CH_2COOtBu$), 3.00-3.10 (2H, $CH_2N$), 3.00-3.10 (2H, $2CHCH_2O$), 3.36-3.78 (m, 6H, $2CH_2COOtBu$, $CH_2OBn$), 3.52-3.56 (m, 2H, $CH_2OBn$), 3.62-3.65 (d, 2H, $^3J$= 12 Hz, $CH_2COOtBu$), 3.71-3.77 (t, 4H, $^3J$= 12 Hz, $2CH_2OBn$), 4.19-4.40 (m, 8H, $4CH_2Ph$). $^{13}C$ NMR (400 MHz, $CD_3OD$, 293K): **δ** = 28.34 ($2C(CH_3)$), 28.40 ($2C(CH_3)$), 45.84 ($2CH_2N$), 50.52 ($2CH_2N$), 54.14 ($2CH_2COOtBu$), 54.69 ($2CH_2COOtBu$), 56.00 ($CHCH_2O$), 60.22 ($CHCH_2O$), 65.71 ($2CH_2OBn$), 67.15 ($2CH_2OBn$), 73.00 ($CH_2Ph$), 74.18 ($CH_2Ph$), 82.75 ($2C(CH_3)_3$), 82.81 ($2C(CH_3)_3$), 128.90-129.47 ($4(CH)_5C$), 139.11 ($2C(CH)_5$), 139.15 ($2C(CH)_5$), 174.68 ($2COOtBu$), 175.45 ($2COOtBu$). HR-MS: m/z 1109.6785 $[M+H]^+$, calcd.

$[C_{64}H_{92}N_4O_{12}]$ 1109.6790. FTIR ($cm^{-1}$): 3853.5, 3736.2, 3628.9, 2982.1, 2923.4, 2376.8, 1496.8, 1339.4, 1202.0, 1123.3, 1054.6, 1033.1, 1013.1, 741.2. $[\alpha]_D^{20}$= -8.1° (C = 1 mg/mL, $CH_2Cl_2$).

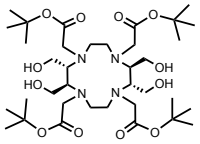

**Compound 11a**

Compound **10a** (0.2 g, 0.18 mmol) in ethanol (3 mL) was added Pd/C (10%wt Pd on carbon, 20 mg) at rt. Then the reaction flask was equipped with a $H_2$ gas balloon and the reaction monitored by LC-MS. After 72 h, no starting material was detected by LC-MS. The mixture was filtrated through Celite and concentrated. The crude product was purified by gel filtration to afford compound **11b** (0.13 mg, 0.14 mmol, 79%) as a white solid. $^1$H NMR (500 MHz, $D_2O$, 293K): **δ** =1.50 (s, 18H, 2$(CH_3)_3$C), 1.51 (s, 18H, 2$(CH_3)_3$C) 2.31-2.34 (d, 2H, $^3$J=14.4 Hz, $CH_2$N), 2.57-2.62 (t, 2H, $^3$J= 10 Hz, $CH_2$N), 2.72-2.77 (m, 2H, $CH_2$N), 2.72-2.77 (m, 2H, 2CHC$H_2$OH), 2.84-2.88 (q, 2H, 2CHC$H_2$O), 3.01-3.04 (m, 2H, 2CHC$H_2$O), 3.08-3.12 (d, 2H, $^3$J=20 Hz, $CH_2$O), 3.08-3.17 (m, 2H, $CH_2$N), 3.42-3.56 (q, 4H, $CH_2$Ph), 3.64-3.68 (d, 2H, $^3$J=20 Hz, $CH_2$O), 3.70-3.72 (dd, 2H, $^3$J= 3 Hz, $CH_2$O), 3.94-3.97 (dd, 2H, $^3$J= 3 Hz, $CH_2$O), 3.85-3.94 (m, 4H, $CH_2$Ph). $^{13}$C NMR (500 MHz, $CD_3OD$, 293K): **δ** = 28.40 (2$(CH_3)_3$C), 28.41 (2$(CH_3)_3$C), 45.39 (2$CH_2$N), 50.33 (2$CH_2$N), 53.92 (2$CH_2$Ph), 54.31 (2$CH_2$O), 57.62 (2$CH_2$O), 57.83 (2CH$CH_2$O), 58.97 (2$CH_2$Ph), 62.20 (2CH$CH_2$O), 82.82 (2C$(CH_3)_3$), 82.84 (2C$(CH_3)_3$), 174.66 (2COO*t*Bu), 175.46 (2COO*t*Bu). HR-MS: m/z 749.4921 $[M+H]^+$, calcd. $[C_{36}H_{68}N_4O_{12}]$ 749.4912. FTIR ($cm^{-1}$): 2983.4, 2923.4, 2866.2, 2380.2, 2310.8, 1555.4, 1506.8, 1456.7, 1054.6, 1033.1, 1013.1. $[\alpha]_D^{20}$= -9.8 ° (C = 1 mg/mL, $CH_2Cl_2$).

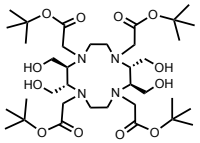

**Compound 11b**

Cyclenol-RR (20 mg, 68 µmol) and *tert*-butyl 2-bromoacetate (53 mg, 272 µmol) were dissolved in dried ACN (1 mL). To the stirred above mixture was added $K_2CO_3$ (38 mg, 272 µmol) and reacted for 72 h. Then the solution was filtrated through Celite and concentrated followed by purification of the crude produce on C18 reverse phase silica gel column chromatography to give compound **11b** (27 mg, 36 µmol, 53%) as a white solid. The NMR, IR and HRMS date of the compound **11b** are in agreement with compound **11a**. $[\alpha]_D^{20}$= 21.4 ° (C = 2.4 mg/mL, MeOH). NMR, HRMS and FTIR analysis data are in agreement with compound 11a.

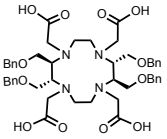

**2,2',2'',2'''-((2S,3S,8S,9S)-2,3,8,9-tetrakis((benzyloxy)methyl)-1,4,7,10-tetraazacyclododecane-1,4,7,10-tetrayl)tetraacetic acid, BnMDOTA**

Compound **10** (50 mg, 45 µmol) was dissolved in DCM/TFA (*v*:*v* =1:4, 1 mL) mixture at 0 °C under inert atmosphere and stirring was continued. After 1 h, the

reaction mixture was allowed to warm to rt and traced by LC-MS. The reaction was quenched after 16 h by adding toluene and concentrated after no starting and intermediate compound was observed by LC-MS. Further purification of the crude product was achieved by self-packed $C_{18}$ reverse phase silica gel column chromatography with a gradient of 10-35% of methanol in $H_2O$ (0.2 % of TFA) to afford BnMDOTA (27.5 mg, 31 µmol) as white solid. $^1$H NMR (500 MHz, $CD_3OD$, 293K): **δ** = 3.045-3.07 (d, 2H, $^3$J= 14 Hz, $CH_2N$), 3.21-3.23 (t, 2H, $^3$J= 5 Hz, $CH_2N$), 3.38-3.49 (m, 6H, $CH_2O$, $CH_2N$, $2CHCH_2O$), 3.54-3.64 (m, 6H, $2CHCH_2O$, $CH_2O$, $CH_2N$), 3.70-3.73 (m, 2H, $CH_2O$), 3.87-3.92 (m, 4H, $2CH_2O$), 4.27-4.51 (m, 12H, $4CH_2Ph$, $2CH_2COOH$). $^{13}$C NMR (500 MHz, $CD_3OD$, 293K): **δ** = 50.38 ($2CH_2N$), 52.44 ($2CH_2N$), 57.31 ($CHCH_2O$), 73.15 ($CHCH_2O$), 64.39 ($2CH_2OBn$), 65.53 ($2CH_2OBn$), 52.40 ($2CH_2OBn$), 53.13 ($2CH_2COOtBu$), 74.32 ($CH_2Ph$), 74.56 ($CH_2Ph$), 128.90-129.47 ($4(CH)_5C$), 138.01 ($2C(CH)_5$), 138.57 ($2C(CH)_5$). HR-MS: m/z 885.4281 $[M+H]^+$, calcd. $[C_{48}H_{60}N_4O_{12}]$ 885.4284. FTIR ($cm^{-1}$): 2982.1, 2973.5, 2967.8, 1830.2, 1559.7, 1506.8, 1456.7, 1339.4, 1054.6, 1033.1, 1013.1. $[\alpha]_D^{20}$= -12.4 ° (C = 2.5 mg/mL, MeOH).

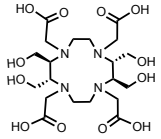

**Compound HMDOTA-SS**

Compound **11a** (30 mg, 40 µmol) was dissolved in 1 mol/L HCl (4 mL) and heated at 50 °C under continuous stirring. After 5 h, the reaction mixture was quenched by adding $NaHCO_3$ (saturated aq., cirta 3 mL) to adjust the pH to neutral once no staring and intermediate products was detected by LC-MS. Followed purification by gel filtration to give compound HMDOTA-SS as a white solid. Similar procedure was used for compound HMDOTA-RR. Compound **11b** (0.6 g, 1.85 mmol) yield 75% of compound **8b** (0.25 g, 0.37 mmol). $^1$H NMR (600 MHz, $D_2O$, 293K): **δ** = 2.69-2.72 (d, 2H, $^3$J= 14 Hz, $CH_2NH$), 2.94-2.96 (t, 2H, $^3$J= 11 Hz, $CH_2N$), 3.07-3.08 (b, 2H, $2CHCH_2OH$), 3.22-3.36 (m, 8H, $2CH_2N$, $2CHCH_2OH$, $CH_2COOH$), 3.56-3.59 (d, $^3$J= 16 Hz, $CH_2COOH$), 3.82-4.10 (m, 12H, $4CH_2OH$, $2CH_2COOH$). $^{13}$C NMR (600 MHz, $D_2O$, 293K): **δ** = 45.47 ($2CH_2N$), 51.16 ($2CH_2N$), 57.22 ($2CH_2OH$), 57.38 ($2CH_2OH$), 57.89 ($4CH_2COOH$), 58.50 ($2CHCH_2OH$), 64.15 ($2CHCH_2OH$), 180.50 (COOH), 180.86 (COOH). HR-MS: m/z 525.2406 $[M+H]^+$, calcd. $[C_{20}H_{36}N_4O_{12}]$ 525.2408. $[\alpha]_D^{20}$= -4.3 ° (C = 1 mg/mL, MeOH). FTIR ($cm^{-1}$): 2983.5, 2923.3, 2866.2, 2380.2, 2310.8, 1555.4, 1506.8, 1456.7, 1054.6, 1033.1, 1013.1. The NMR, IR and HRMS date of the compound HMDOTA-RR are in agreement with compound **8a**. $[\alpha]_D^{20}$= 5.12 ° (C = 1.6 mg/mL, MeOH).

**References**

(1) Wahsner, J.; Gale, E. M.; Rodríguez-Rodríguez, A.; Caravan, P. Chemistry of MRI Contrast Agents: Current Challenges and New Frontiers. *Chem. Rev.* **2019**, *119* (2), 957–1057.

(2) Liu, W. M.; Overhand, M.; Ubbink, M. The Application of Paramagnetic Lanthanoid Ions in NMR Spectroscopy on Proteins. *Coord. Chem. Rev.* **2014**, *273–274*, 2–12.

(3) Heffern, M. C.; Matosziuk, L. M.; Meade, T. J. Lanthanide Probes for Bioresponsive Imaging.

*Chem. Rev.* **2014**, *114* (8), 4496–4539.

(4) Cacheris, W. P.; Nickle, S. K.; Sherry, A. D. Thermodynamic Study of Lanthanide Complexes of 1,4,7-Triazacyclononane-N,N′,N"-Triacetic Acid and 1,4,7,10-Tetraazacyclododecane-N,N′,N",N‴-Tetraacetic Acid. *Inorg. Chem.* **1987**, *26* (6), 958–960.

(5) Baranyai, Z.; Brücher, E.; Iványi, T.; Király, R.; Lázár, I.; Zékány, L. Complexation Properties of N,N′,N″,N‴-[1,4,7,10-Tetraazacyclododecane-1,4,7,10-Tetrayltetrakis(1-Oxoethane-2,1-Diyl)]Tetrakis[Glycine] (H4dotagl). Equilibrium, Kinetic, and Relaxation Behavior of the Lanthanide(III) Complexes. *Helv. Chim. Acta* **2005**, *88* (3), 604–617.

(6) Spirlet, M. R.; Rebizant, J.; Desreux, J. F.; Loncin, M. F. Crystal and Molecular Structure of Sodium Aqua(1,4,7,10-Tetraazacyclododecane-1,4,7,10-Tetraacetato)Europate(III) Tetrahydrate $Na^+(EuDOTA \cdot H_2O)^- \cdot 4H_2O$, and Its Relevance to NMR Studies of the Conformational Behavior of the Lanthanide Complexes Formed by the Lanthanide Complexes formed by the Macrocyclic Ligand DOTA. *Inorg. Chem.* **1984**, *23* (3), 359–363.

(7) Chang, C. A.; Francesconi, L. C.; Malley, M. F.; Kumar, K.; Gougoutas, J. Z.; Tweedle, M. F.; Lee, D. W.; Wilson, L. J. Synthesis, Characterization, and Crystal Structures of M(DO3A) (M = Iron, Gadolinium) and Na[M(DOTA)] (M = Fe, Yttrium, Gd). *Inorg. Chem.* **1993**, *32* (16), 3501–3508.

(8) Aime, S.; Barge, A.; Benetollo, F.; Bombieri, G.; Botta, M.; Uggeri, F. A Novel Compound in the Lanthanide(III) DOTA Series. X-Ray Crystal and Molecular Structure of the Complex $Na[La(DOTA)La(HDOTA)] \cdot 10H_2O$. *Inorg. Chem.* **1997**, *36* (19), 4287–4289.

(9) Meyer, M.; Dahaoui-Gindrey, V.; Lecomte, C.; Guilard, R. Conformations and Coordination Schemes of Carboxylate and Carbamoyl Derivatives of the Tetraazamacrocycles Cyclen and Cyclam, and the Relation to Their Protonation States. *Coord. Chem. Rev.* **1998**, *178–180*, 1313–1405.

(10) Aime, S.; Botta, M.; Fasano, M.; Marques, M. P. M.; Geraldes, C. F. G. C.; Pubanz, D.; Merbach, A. E. Conformational and Coordination Equilibria on DOTA Complexes of Lanthanide Metal Ions in Aqueous Solution Studied by $^1$H-NMR Spectroscopy. *Inorg. Chem.* **1997**, *36* (10), 2059–2068.

(11) Aime, S.; Botta, M.; Ermondi, G. NMR Study of Solution Structures and Dynamics of Lanthanide(III) Complexes of DOTA. *Inorg. Chem.* **1992**, *31* (21), 4291–4299.

(12) Kucera, B. E.; Aime, S.; Woods, M.; Tircso, G.; Botta, M.; Young, V. G.; Garda, Z. Properties, Solution State Behavior, and Crystal Structures of Chelates of DOTMA. *Inorg. Chem.* **2011**, *50* (17), 7955–7965.

(13) Kumas, C.; Fernando, W. S.; Zhao, P.; Regueiro-Figueroa, M.; Kiefer, G. E.; Martins, A. F.; Platas-Iglesias, C.; Sherry, A. D. Unexpected Changes in the Population of Coordination Isomers for the Lanthanide Ion Complexes of DOTMA-Tetraglycinate. *Inorg. Chem.* **2016**, *55* (18), 9297–9305.

(14) Woods, M.; Aime, S.; Botta, M.; Howard, J. A. K.; Moloney, J. M.; Navet, M.; Parker, D.; Port, M.; Rousseaux, O. Correlation of Water Exchange Rate with Isomeric Composition in Diastereoisomeric Gadolinium Complexes of Tetra(Carboxyethyl)Dota and Related

Macrocyclic Ligands. *J. Am. Chem. Soc.* **2000**, *122* (40), 9781–9792.

(15) Woods, M.; Kovacs, Z.; Zhang, S.; Sherry, A. D. Towards the Rational Design of Magnetic Resonance Imaging Contrast Agents: Isolation of the Two Coordination Isomers of Lanthanide DOTA-Type Complexes. *Angew. Chemie. Int. Ed.* **2003**, *42* (47), 5889–5892.

(16) Ratnakar, S. J.; Woods, M.; Lubag, A. J. M.; Kovács, Z.; Sherry, A. D. Modulation of Water Exchange in Europium(III) DOTA−Tetraamide Complexes via Electronic Substituent Effects. *J. Am. Chem. Soc.* **2008**, *130* (1), 6–7.

(17) Zhang, S.; Kovacs, Z.; Burgess, S.; Aime, S.; Terreno, E.; Sherry, A. D. {DOTA-Bis(Amide)}lanthanide Complexes: NMR Evidence for Differences in Water-Molecule Exchange Rates for Coordination Isomers. *Chem. Eur. J.* **2001**, *7* (1), 288–296.

(18) Jacques, V.; Desreux, J. F. Quantitative Two-Dimensional EXSY Spectroscopy and Dynamic Behavior of a Paramagnetic Lanthanide Macrocyclic Chelate: YbDOTA(DOTA = 1,4,7,10-Tetraazacyclododecane-N,N′,N″,N‴-Tetraacetic Acid). *Inorg. Chem.* **1994**, *33* (18), 4048–4053.

(19) Vlasie, M. D.; Comuzzi, C.; Van Den Nieuwendijk, A. M. C. H.; Prudêncio, M.; Overhand, M.; Ubbink, M. Long-Range-Distance NMR Effects in a Protein Labeled with a Lanthanide-DOTA Chelate. *Chem. Eur. J.* **2007**, *13* (6), 1715–1723.

(20) Hass, M. A. S.; Liu, W. M.; Agafonov, R. V.; Otten, R.; Phung, L. A.; Schilder, J. T.; Kern, D.; Ubbink, M. A Minor Conformation of a Lanthanide Tag on Adenylate Kinase Characterized by Paramagnetic Relaxation Dispersion NMR Spectroscopy. *J. Biomol. NMR* **2015**, *61* (2), 123–136.

(21) Clough, T. J.; Jiang, L.; Wong, K.-L.; Long, N. J. Ligand Design Strategies to Increase Stability of Gadolinium-Based Magnetic Resonance Imaging Contrast Agents. *Nat. Commun.* **2019**, *10* (1), 1420.

(22) Benetollo, F.; Bombieri, G.; Calabi, L.; Aime, S.; Botta, M. Structural Variations across the Lanthanide Series of Macrocyclic DOTA Complexes: Insights into the Design of Contrast Agents for Magnetic Resonance Imaging. *Inorg. Chem.* **2003**, *42* (1), 148–157.

(23) Bonnet, C. S.; Buron, F.; Caillé, F.; Shade, C. M.; Drahoš, B.; Pellegatti, L.; Zhang, J.; Villette, S.; Helm, L.; Pichon, C.; et al. Pyridine-Based Lanthanide Complexes Combining MRI and NIR Luminescence Activities. *Chem. Eur. J.* **2012**, *18* (5), 1419–1431.

(24) Faulkner, S.; Pope, S. J. A.; Burton-Pye, B. P. Lanthanide Complexes for Luminescence Imaging Applications. *Appl. Spectrosc. Rev.* **2005**, *40* (1), 1–31.

(25) Lumata, L.; Jindal, A. K.; Merritt, M. E.; Malloy, C. R.; Sherry, A. D.; Kovacs, Z. DNP by Thermal Mixing under Optimized Conditions Yields >60 000-Fold Enhancement of 89Y NMR Signal. *J. Am. Chem. Soc.* **2011**, *133* (22), 8673–8680.

(26) Aime, S.; Botta, M.; Ermondi, G.; Fedeli, F.; Uggeri, F. Synthesis and NMRD Studies of Gadolinium(3+) Complexes of Macrocyclic Polyamino Polycarboxylic Ligands Bearing **β**-Benzyloxy-**α**-Propionic Residues. *Inorg. Chem.* **1992**, *31* (6), 1100–1103.

(27) Polasek, M.; Kotek, J.; Hermann, P.; Cisauova, I.; Binnemans, K.; Lukes, I. Lanthanide(III) Complexes of Pyridine-N-Oxide Derivatives of DOTA in Solution and in the Solid State. A

New Kind of Isomerism in Complexes of DOTA-like Ligands. *Inorg. Chem.* **2008**, *48* (2), 466-475.

(28) Jacques, V.; Gilsoul, D.; Comblin, V.; Desreux, J. F. Rigidified Macrocyclic Lanthanide Chelates for Magnetic Resonance Imaging. *J. Alloys Compd.* **1997**, *249* (1–2), 173–177.

(29) Gilsoul, D.; Jacques, V.; Mesbahi, M.; Hermann, M.; Desreux, J. F.; Sauvage, C.; Humblet, V.; Comblin, V. Designing New MRI Contrast Agents: A Coordination Chemistry Challenge. *Coord. Chem. Rev.* **2002**, *185–186*, 451–470.

(30) Brittain, H. G.; Desreux, J. F. Luminescence and NMR Studies of the Conformational Isomers of Lanthanide Complexes with an Optically Active Polyaza Polycarboxylic Macrocycle. *Inorg. Chem.* **1984**, *23* (26), 4459–4466.

(31) Dai, L.; Jones, C. M.; Chan, W. T. K.; Pham, T. A.; Ling, X.; Gale, E. M.; Rotile, N. J.; Tai, W. C. S.; Anderson, C. J.; Caravan, P.; et al. Chiral DOTA Chelators as an Improved Platform for Biomedical Imaging and Therapy Applications. *Nat. Commun.* **2018**, *9* (1), 1-10.

(32) Lee, M. D.; Loh, C. T.; Shin, J.; Chhabra, S.; Dennis, M. L.; Otting, G.; Swarbrick, J. D.; Graham, B. Compact, Hydrophilic, Lanthanide-Binding Tags for Paramagnetic NMR Spectroscopy. *Chem. Sci.* **2015**, *6* (4), 2614–2624.

(33) Geraldes, C. F. G. C.; Sherry, A. D.; Kiefer, G. E. The Solution Structure of Ln (DOTP)$^{5-}$ Complexes. A Comparison of Lanthanide-Induced Paramagnetic Shifts with the MMX Energy-Minimized Structure. *J. Magn. Reson.* **1992**, *97* (2), 290–304.

(34) Vanasschen, C.; Bouslimani, N.; Thonon, D.; Desreux, J. F. Gadolinium DOTA Chelates Featuring Alkyne Groups Directly Grafted on the Tetraaza Macrocyclic Ring: Synthesis, Relaxation Properties, "Click" Reaction, and High-Relaxivity Micelles. *Inorg. Chem.* **2011**, *50* (18), 8946–8958.

(35) Lucio, P.; Beltrami, A.; Franzini, M.; Paoli, P.; Rossi, P.; Uggeri, F.; Virtuani, M. Gd ( III ) Complexes of Poly ( Hydroxymethyl ) Substituted Derivatives of 1,4,7,10-tetraazacyclododecane-1,4,7,10-tetraacetic acid. *Inorganica Chim. Acta* **2001**, *317*, 218–229.

(36) Ranganathan, R. S.; Raju, N.; Fan, H.; Zhang, X.; Tweedle, M. F.; Desreux, J. F.; Jacques, V. Polymethylated DOTA Ligands . 2 . Synthesis of Rigidified Lanthanide Chelates and Studies on the Effect of Alkyl Substitution on Conformational Mobility and Relaxivity. *Inorg. Chem.* **2002**, *41* (25), 515–520.

(37) Opina, A. C. L.; Strickland, M.; Lee, Y. S.; Tjandra, N.; Andrew Byrd, R.; Swenson, R. E.; Vasalatiy, O. Analysis of the Isomer Ratios of Polymethylated-DOTA Complexes and the Implications on Protein Structural Studies. *Dalt. Trans.* **2016**, *45* (11), 4673–4687.

(38) Strickland, M.; Schwieters, C. D.; Göbl, C.; Opina, A. C. L.; Strub, M. P.; Swenson, R. E.; Vasalatiy, O.; Tjandra, N. Characterizing the Magnetic Susceptibility Tensor of Lanthanide-Containing Polymethylated-DOTA Complexes. *J. Biomol. NMR* **2016**, *66* (2), 125–139.

(39) Bradshaw, J. S.; Krakowiak, K. E.; Izatt, R. M.; Zamecka-Krakowiak, D. J. New High Yield Syntheses of Cyclams Using the Crab-like Cyclization Reaction. *Tetrahedron Lett.* **1990**, *31* (8), 1077–1080.

(40) Blahut, J.; Hermann, P.; Tošner, Z.; Platas-Iglesias, C. A Combined NMR and DFT Study of Conformational Dynamics in Lanthanide Complexes of Macrocyclic DOTA-like Ligands. *Phys. Chem. Chem. Phys.* **2017**, *19* (39), 26662–26671.

(41) Polášek, M.; Rudovský, J.; Hermann, P.; Lukeš, I.; Elst, L. Vander; Muller, R. N. Lanthanide(III) Complexes of a Pyridine N-Oxide Analogue of DOTA: Exclusive M Isomer Formation Induced by a Six-Membered Chelate Ring. *Chem. Commun.* **2004**, 22, 2602–2603.

(42) Halgren, T. A. Merck Molecular Force Field. I. Basis, Form, Scope, Parameterization, and Performance of MMFF94. *J. Comput. Chem.* **1996**, *17* (5-6), 490–519.

# Chapter V

# A two-armed probe for in-cell DEER measurements on protein

# *Chapter V*

**Abstract**

The double electron-electron resonance (DEER) technique combined with site-directed spin labeling (SDSL) is a popular method for bio-molecular structure studies. The application of DEER to protein systems within living cells puts rigorous restraints on the spin-label. The probe needs to be immobiled relative to the protein and both the linkage and the paramagnetic state need to be stable under the reducing conditions inside the cell. Here, three two-armed Gd(III) complexes, Gd(III)-CLaNP13a/b/c, were synthesized and applied as site-specific spin-labels for protein DEER measurements. The three probes differ in the length of the arms that link the Gd(III) chelating cage to the protein. Rather than the disulphide linkage employed for protein attachment in other most CLaNP molecules, carbon-sulfur bonds are used to link the probe to the protein. DEER experiments for spin-labeled variants of T4 lysozyme were performed in *vitro*, in cell lysate and in *D. discoideum* cells. A narrow distance distribution was detected for all the spin-labels with the different linkers. The DEER derived distances are on the order of 4 nm and are in agreement with the expected values based on the metal positions derived from paramagnetic NMR results. The results indicate that the probes are mostly rigid relative to the protein due to the dual attachment sites. The carbon-sulfur linkages make the probes suitable for in-cell protein studies.

**Introduction**

Structural studies are generally performed *in vitro*, on isolated and purified protein samples. However, protein functions in a complex environment, interacting with a range of large and small molecules under conditions that differ strongly from a diluted aqueous solution. Hence, it can be of relevance to study protein structures and interactions also in cell lysates or within a cell. EPR spectroscopy offers a method to measure accurate distances in biomolecular systems at relatively low sample concentrations, especially at Q and W band frequencies.[1,2] The double electron−electron resonance (DEER, also named PELDOR) technique measures the magntitude of the dipolar interaction between two electron spins,[3–5] which is strongly distance-dependent and yields distance information in the range of 2 - 8 nm.[6] However, unpaired electrons are rare in biological systems and thus, for DEER experiments, spin-labels need to be introduced at specific sites, using site-directed spin labeling (SDSL). Two probes need to be introduced in the system at a distance suitable to obtain a DEER signal. The electron spins should have minimal motional freedom relative to the protein to reduce the width of the distance distribution obtained from the DEER experiment. In-cell measurements introduce further requirements for the spin-label. The cellular environment is strongly reducing, so both the spin-label itself and the bond linking the probe to the protein need to be resistant to reduction.[7,8]

Nitroxide compounds are the most commonly applied spin-labels in EPR spectroscopy, for a large variety of distance measurements, due to their small size and handling ease.[9,10] The first in-cell DEER measurement of a protein-protein distance was obtained by injection of 3-maleimido-PROXYL labeled human ubiquitin into oocytes. The maleimide functional group was conjugated to a cysteine residue.[11] Unlike a disulphide bridge, the C-S bond between the cysteine and maleimide group is resistant to reduction, but the unpaired electron of the nitroxide radical can readily react under reducing conditions, making it less useful for in-cell studies.[11] Gd(III), with a spin state of S=2/7, shows both higher sensitivity and stability than a nitroxide compound and, especially at high magnetic field, is a good candidate for in-cell DEER measurements.[12–14] A DOTA (1,4,7,10-tetraazacyclododecane-1,4,7,10-tetraacetic acid) based Gd(III) complex functionalized with a maleimide group, was successfully used for in-cell DEER on a protein, although a wide distance distribution (about 15 Å at half-height) was found, due to the flexibility of the linker.[15] Different strategies have been applied to reduce the mobility of the tag. One is to employ tags with a rigid attachment group.[16] Alternatively, the probe can be anchored via two arms to the protein.[17,18] To our best knowledge, no probes have been reported that are equipped with two arms using the maleimide groups for attachment for DEER measurement *in vitro* or in-cells.

Here, we report three two-armed Gd(III) complexes, CLaNP13a/b/c, as spin labels for EPR experiments *in vitro*, in cell lysate and in *Dictyostelium discoideum* cells.

Narrow distance distributions are found and the distances are in good agreement with distances derived from paramagnetic NMR experiments.

**Results and Discussion**

**Design and synthesis of Gd(III)-CLaNP13.** The caged lanthanoid NMR probe #5 (CLaNP5) is a well-studied two-armed Ln(III) probe for paramagnetic NMR spectroscopy on proteins. The cyclen based molecule is equipped with two pyridine N-oxide coordination arms that reduce the arm rotation (Figure 5.1).[17, 19] Using CLaNP5 as a building block, Gd-CLaNP13 was designed, in which the arms for protein attachment were functionalized with maleimide groups. The length of the spacer was varied from 2 to 4 methylene groups (Figure 5.1). Maleimide can readily and specifically react with the thiolate group of a cysteine side chain, forming a carbon-sulfur bond, which is not prone to reduction.[15] Following the synthesis route of CLaNP5, the tetra-N-alkylated compound **3** was obtained with good yield (Scheme 5.1). The carboxy groups were coupled to amino alkanes of different lengths, carrying the maleimide groups, to afford **4**, which tightly chelates Gd(III), giving **5.**

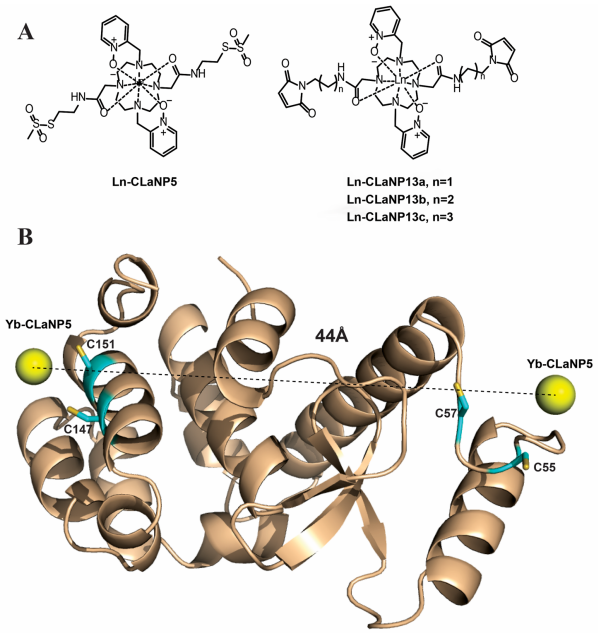


**Figure 5.1 A**) Structures of Ln(III)-CLaNP5 and Ln(III)-CLaNP13; **B**) Model of the structure of T4Lys based on PDB entry 3dke[20] with two Cys pairs for the attachment of two probes. The positions of the metals are based on PCS analysis using Yb(III)-CLaNP5 as a paramagnetic probe. The backbone is drawn in ribbon representation. The Cys residues used for attachment have been modelled into the structure and are shown in sticks. The metal ions are shown as yellow spheres.

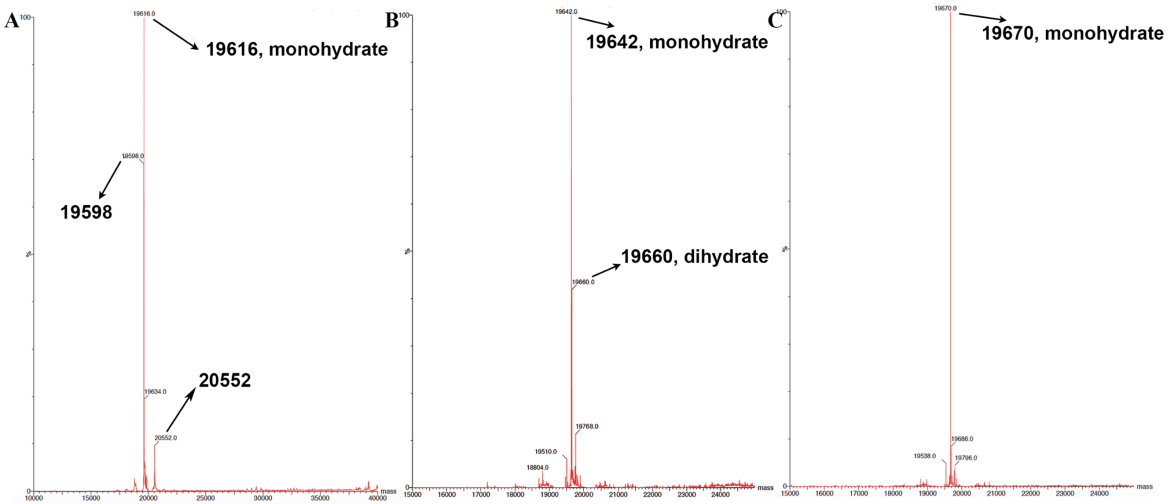


**Figure 5.2** ESI-TOF MS spectra of CLaNP13a (**A**), CLaNP13b (**B**) and CLaNP13c (**C**) linked to $^{15}N$ enriched T4lys T147C/N151C mutant.

**Table 5.1** Mass spectrometry results (in Da).

| Sample | Mutant 1[a] | Mutant 2[b] | CLaNP13a[c] | | CLaNP13b[c] | | CLaNP13c[c] | |
|---|---|---|---|---|---|---|---|---|
| | | | Mutant 1[a] | Mutant 2[b] | Mutant 1[a] | Mutant 2[b] | Mutant 1[a] | Mutant 2[b] |
| **Calcd.** | 18697 | 18426 | 19600 | 20250[d] | 19646[d] | 20306[d] | 19674[d] | 20344 |
| **Experm.** | 18697±4 | 18428±4 | 19598±4 | 20248[d] ±4 | 19642[d]±4 | 20304[d] ±4 | 19670[d]±4 | 20341±4 |

[a] $^{15}N$ enriched (96.5%) T4Lys K147C/N151C, [b] T4Lys N55C/V57C/K147C/T151C (natural isotope abundance), [c] CLaNP13 linked to T4Lys mutants, [d] monohydrate results (+18).

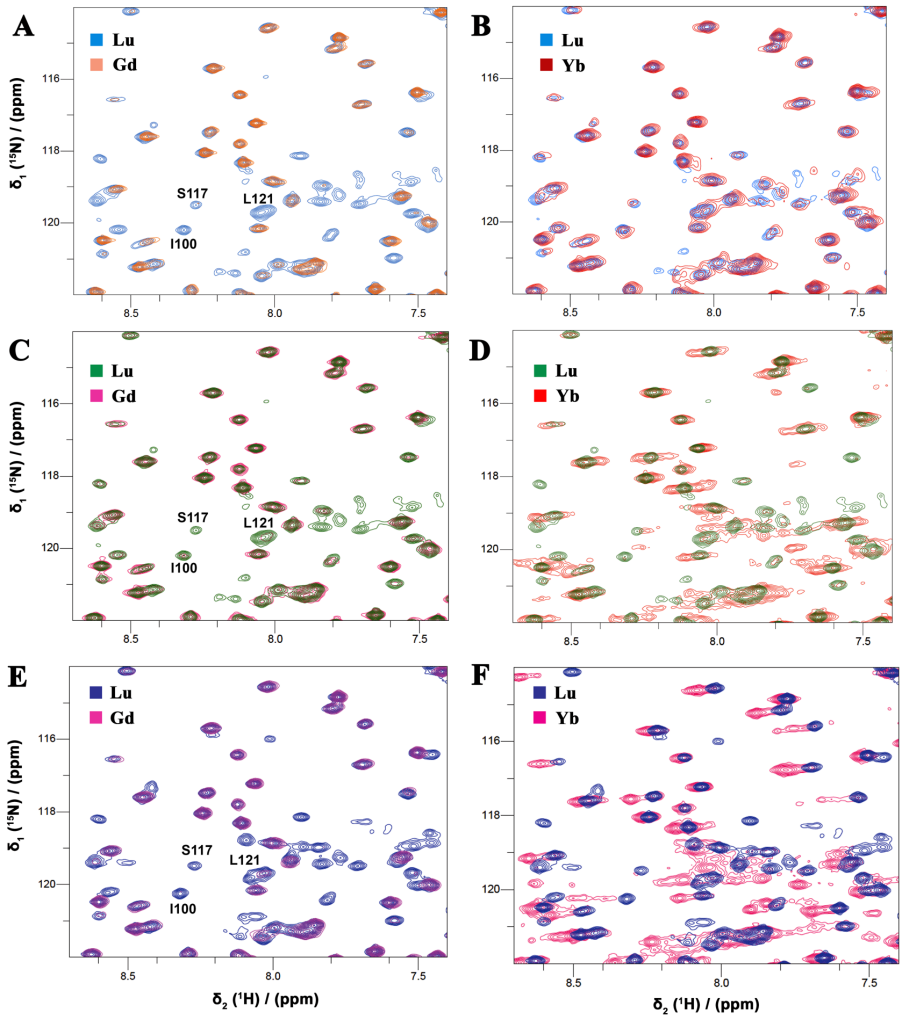


**Figure 5.3** Overlay of $^{1}H$-$^{15}N$ HSQC (detail) spectra of Lu(III), Gd(III) and Yb(III) loaded CLaNP13a (**A, B**), CLaNP13b (**C, D**), or CLaNP13c (**E, F**) attached to T4Lys K147C/T151C. The NMR spectra were recorded at 14.1 T (600 MHz). Peaks of residues mentioned in the text are labeled.

**Protein labeling and paramagnetic NMR studies.** A $^{15}N$ enriched variant of T4 lysozyme (T4Lys) with the substitutions K147C/T151C was used to determine optimal conditions for protein labeling on the basis of LC-MS and NMR results. The best result for double maleimide reactions with the cysteines was using a buffer with pH 7.8, at 4 °C for 6 h. To test whether free thiolates remained after the reaction, iodoacetamide was added. The LC-MS results, obtained by Dr. Bogdan Florea, yielded masses that match those expected for probes attached via two arms, assuming that one or two water molecules

remained bound to the protein-probe complexes (Figure 5.2 and Table 5.1). No peaks with additional mass of 58 Da were detected, which would be expected for protein with one-arm attached probe and an additional acetamide group linked to the second cysteine sulfur atom, and also no free protein was detected, suggesting that the protein labelling efficiency was more than 95%. In the MS spectrum of the CLaNP13a, a very small peak (20552 Da) is observed that represents T4Lys with two probes bound, each via a single arm. After attachment of the first maleimide group, the reaction with the second will generally be efficient because it is intramolecular. The limited length of the linker in CLaNP13a may allow for some competition with the second-order reaction of the protein-probe complex with a second probe molecule. However, according to the MS spectrum, the fraction of this species is very small. Paramagnetic NMR spectra also provide evidence for complete labeling. An overlay of $^{1}H$-$^{15}N$ HSQC spectra of CLaNP13 loaded with Lu(III) or Gd(III) shows that in the spectrum of the latter sample some peaks completely disappear, such as the resonances of the amides of I100, S117 and L121, due to strong paramagnetic relaxation broadening. Figure 5.3 shows in detail, the full spectra are shown in Appendix Figure 5.1. If untagged protein was present, residual intensities would be expected. $^{15}N$ enriched T4Lys K147C/T151C was also tagged with Yb(III) loaded CLaNP13 to generate pseudocontact shifts (PCS). As expected, in the $^{1}H$-$^{15}N$ HSQC spectra more than one PCS was observed for many amide groups (Figure 5.3). The PCS is dependent on the position of the nucleus within the frame of the tensor that describes the anisotropic components of the magnetic susceptibility ($\Delta\chi$ tensor), which is

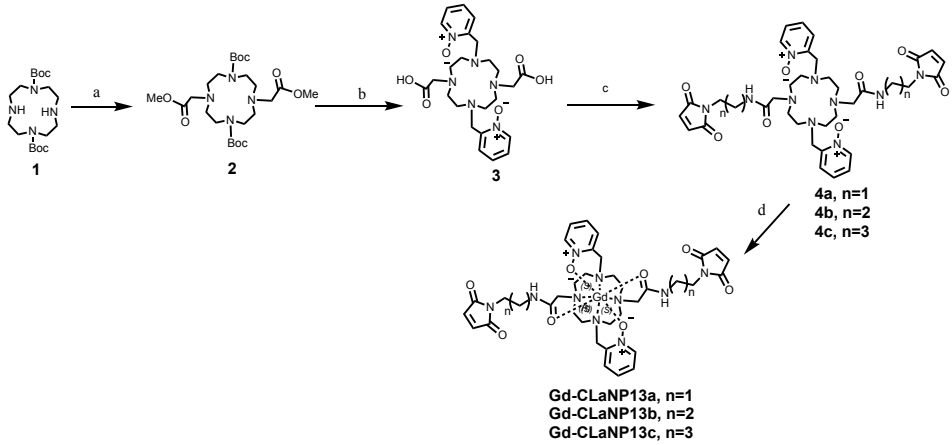


**Scheme 5.1** Synthesis route of Gd-CLaNP13. a) methyl 2-bromoacetate, $K_2CO_3$, ACN, rt, 16 h; b) i) TFA/DCM (4:1, *v*:*v*); ii) 2-(chloromethyl)pyridine 1-oxide, $K_2CO_3$, ACN, rt, 16 h; c) N-hydroxysuccinimide, N-(3-Dimethylaminopropyl)-N′-ethylcarbodiimide hydrochloride, 1-(2-aminopropyl)-1H-pyrrole-2,5-dione, DMF, rt, 24 h. d) $Gd(OAc)_3{\cdot}4H_2O$, DMF, rt, overnight.

determined by electronic distribution over the molecular orbitals of around the metal ion. The reaction of the maleimide ring can lead to two enantiomers, and thus, the probe can bind in slightly different ways to the protein, causing the lanthanoid cage to be in different orientations and resulting in multiple PCS. However, it is expected that the different forms have the metal in almost the same position, so the effect of having different forms on the DEER distance measurements is expected to be small. To estimate the metal positions relative to the T4Lys protein structure, $^{15}$N enriched T4Lys K149C/T151C and T4Lys N55C/V57C (data provided by Dr. Simon Skinner) were tagged with Yb(III)- or Lu(III)-CLaNP5 and PCS obtained from $^{1}$H-$^{15}$N HSQC spectra (Figure 5.4, App. Figure A5.2). In both cases, single set of PCS were found and the PCS fitted very well to equation 1.1 (chapter I), yielding the $\Delta\chi$ tensor sizes and orientations as well as the metal positions (Figure 5.5; Table 5.2, Figure 5.1). The magnetitude of the $\Delta\chi_{ax}$ differ between the two variants. The value for T4Lys N55C/V57C is somewhat lower than the one usually obtained (8.5 x $10^{-32}$ $m^3$).[19,21,22] The two cysteine residues are located in a loop, so the reduced $\Delta\chi_{ax}$ value could point to a limited degree of flexibility of the probe due to loop motions. The $\Delta\chi$ is very sensitive to motion, so the amplitude of the motion is expected to be small, compared to, for example, a single armed probe.[17] The $\Delta\chi_{ax}$ for the other variant, T4Lys K149C/T151C, is large, suggesting the probe is rigid relative to the protein. The metal positions were combined in a model shown in Figure 5.1B, yielding a distance of 44 Å between the two lanthanoids.

**Table 5.2** PCS-based $\Delta\chi$-tensor parameters of Yb(III)-CLaNP5 attached to T4Lys variants.

| **Protein** | **T4Lys** | |
|---|---|---|
| **Probes** | **N55C/V557C** | **K147C/T151C** |
| $\Delta\chi_{ax}$ [a] | 6.3±0.1 | 9.9±0.1 |
| $\Delta\chi_{rh}$ [a] | 3.6±0.1 | 4.3±0.1 |
| **Restraints** | 91 | 78 |
| $Q_a$ | 0.03 | 0.02 |
| **PDB entry** | 3dke[20] | 3dke[20] |

[a] in $10^{-32}$ $m^3$

**DEER experiments.** These experiments were performed by Enrico Zurlo and Dr. Martina Huber. For the EPR experiments, the quadruple cysteine mutant T4Lys N55C/V57C/K147C/T151C was labeled with Gd(III)-CLaNP13, variants a, b or c. LC-MS results showed that the samples were labeled with two probes and the labeling efficiency was more than 95% (App. Figure 5.3 and Table 5.1). The Gd(III) EPR spectrum at 95 GHz, the DEER traces and derived distance distributions are shown in Figure 5.6. A similarly narrow distance distribution, a width of about 8 Å (the distribution at half-height), was determined for all three probes. The mean of the distance distribution was slightly

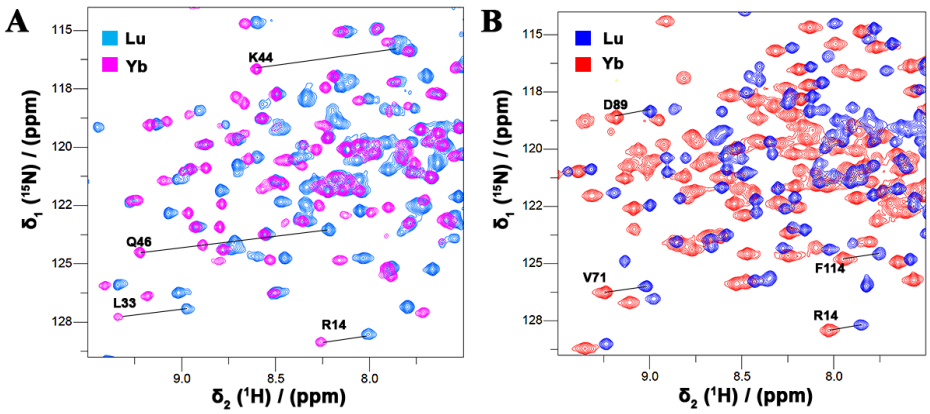


**Figure 5.4** Overlay of $^{1}$H-$^{15}$N HSQC (in detail) spectra of Yb(III) and Lu(II) loaded CLaNP5 attached to T4Lys N55C/V57C (**A**) and T4Lys K147C/T151C (**B**). Several PCS are indicated with solid lines and residue numbers. The NMR spectra were recorded at 14.1 T (600 MHz).

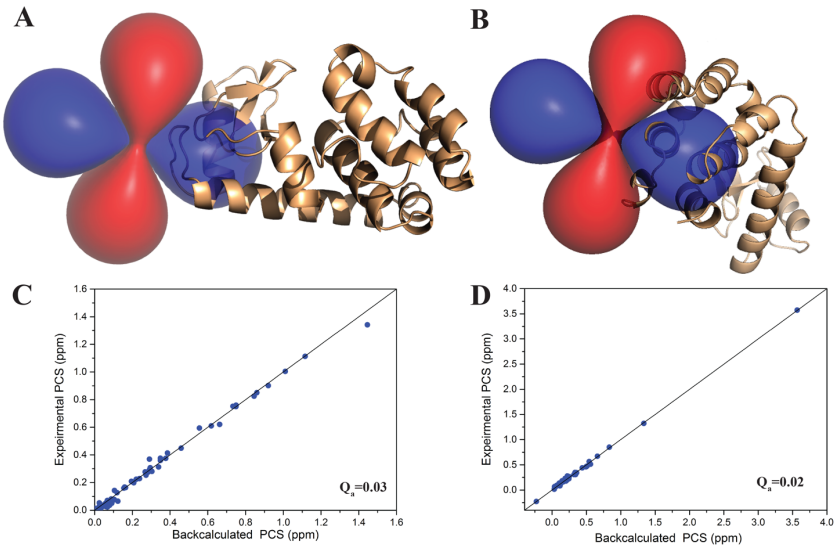


**Figure 5.5** PCS isosurfaces of Yb(III)-CLaNP5 plotted on the structures of T4Lys (PDB entry 3dke)[20] N55C/V57C (**A**) and K147C/T151C (**B**). The protein backbones are drawn in wheat ribbon representation. The iso-surfaces correspond to PCSs of ±0.4 ppm. Positive and negative PCS are indicated by blue and red, respectively. (**C, D**) The experimental $^{1}H^{N}$ PCS (ppm) of Yb(III)-CLaNP5 were plotted against the back-calculated values after fitting to eq. 1.1. for T4Lys N55C/V57C (**C**) and T4Lys K147C/T151C (**D**).

different between the three probes, probably due to the difference in linker length.

CLaNP13a showed the shortest mean distance, 42 Å, CLaNP13b exhibited the longest, 46 Å. These results are in agreement with the metal ion distance based on PCS data (44 Å), for which Yb(III)-CLaNP5 was tagged at the two attachment sites of T4Lys. For a single arm attached Gd(III) probe (Gd(III)-DOTA-M) a half-height distribution width of about 15 Å was reported,[15] indicating that the two-arm attachment limits the mobility of the paramagnetic center considerably.

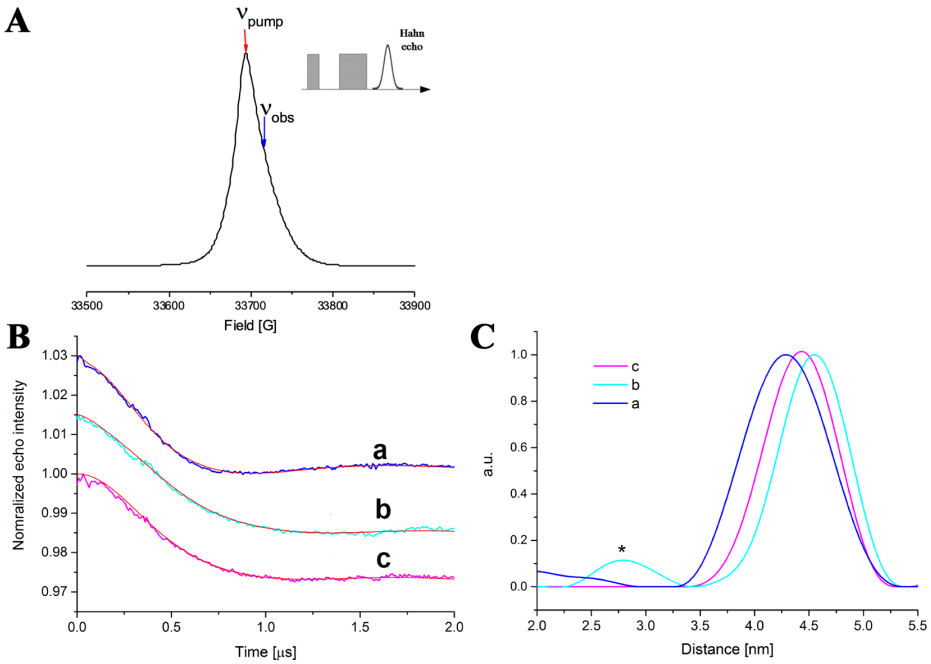


**Figure 5.6 A)** 95 GHz field-swept electron-spin echo spectrum (FSESE) of the central transition region of the Gd(III) EPR signal, Inset: A two-pulse echo sequence (π/2−**τ**−π) was used with a 32 ns π/2 pulse and **τ** = 360 ns. Arrows: positions of pump pulse (red) and observer pulses (blue) in the DEER measurements. Background corrected DEER time traces (**B**) and distance distributions (**C**) for Gd-CLaNP13a (a, blue), Gd-CLaNP13b (b, cyan) and Gd-CLaNP13c (c, magenta) linked to T4Lys N55C/V57C/K147C/T151C *in vitro*. In **(B)** Traces are shifted vertically for clarity. Measurements were performed at 10 K for 12 hours. Red lines: fit obtained with the distance-distributions calculations shown in **(C)** from Tikhonov regularization (**α** = 1000). Peaks marked with asterisks do not contribute significantly to the data, as shown by the DeerAnalysis suppression tool.[24]

To mimic a cellular environment and the reducing conditions, CLaNP13b tagged T4Lys was mixed with a lysate of *Escherichia coli* cells, incubated for up to 24 h and the DEER experiments were repeated. A similar distance distribution was observed as for the

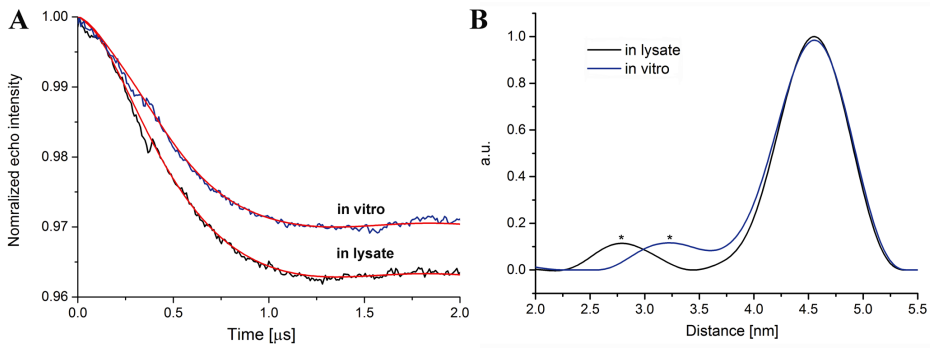


**Figure 5.7** Background corrected DEER time traces (**A**) and distance distributions (**B**) for Gd-CLaNP13b tagged T4Lys N55C/V57C/ K147C/T151C samples *in vitro* (blue), in *E. coli* lysate (black) after 24 h. Traces are shifted vertically for clarity. Red lines: fit obtained with the distance-distribution calculations shown in (**B**) obtained after Tikhonov regularization (**α** = 1000). Peaks marked with asterisks do not contribute significantly to the data, as shown by the DeerAnalysis suppression tool.[24]

*in vitro* measurement (Figure 5.7). This agreement demonstrated that Gd(III)-CLaNP13b is stable in a reducing environment. Encouraged by these results, we wanted to test whether DEER experiments could be performed in live cells. First, uptake of T4Lys was tested using fluorescently labeled protein by mixing ATTO-647-maleimide tagged T4Lys K147C/T151C with *Dictyostelium discoideum* cells (Figure 5.8). These experiments were carried out by Donny de Bruin and Joeri Wondergem. LC-MS results showed that T4Lys K147C/T151C was tagged with only a single ATTO-647-amleimide per protein molecule. *D. discoideum* is known to take up proteins spontaneously.[23] After 30 min incubation, almost all cells have taken up fluorescent protein and it was present in cell body in vesicles (Figure 5.8). The protein was washed away from the medium after 60 min, but the fluorescent protein can still be detected inside the cells and the concentration was estimated to be 5 µM. The protein can still be detected in 3 h after the start of the incubation (Figure 5.8).

Similar experiments were conducted with doublely CLaNP13b tagged T4Lys for in-cell DEER experiments. After incubation, the cells were washed, concentrated and cooled on ice. Before the cells were frozen for EPR measurement, 10% (*v*/*v*) DMSO was added to the medium. DEER experiments were performed at 10 K for 48 h. The in-cell DEER trace has a shape that is consistent with the shape of the trace in vitro and in cell lysate, indication that doubly tagged protein is present in the cells. However, the signal-to-noise was insufficient to allow for a reliable distance distribution to be obtained (Figure A5.4).

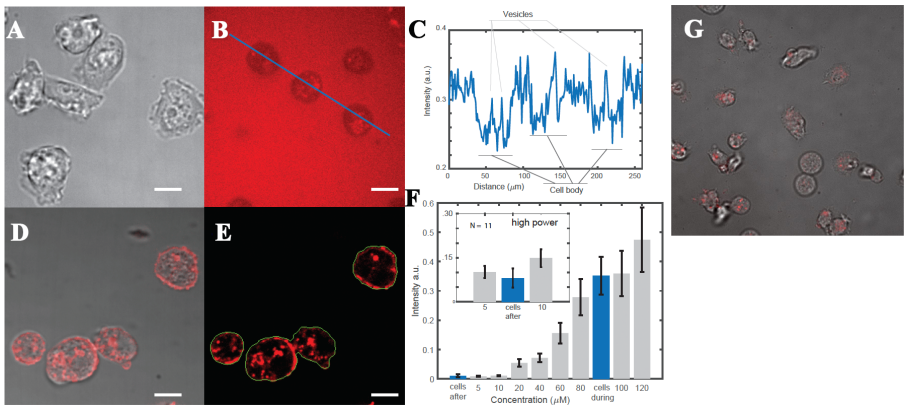


**Figure 5.8** Different stages of the internalization process of T4-ATTO-647 in vegetative *D. discoideum*. **A**) Just prior (t = 0 min) to incubation, cells are adhered to the substrate; **B**). Incubation and subsequent internalization results in a shock response and cell rounding. Confocal fluorescence image (red) shows cells after t = 30 min of incubation. Blue line marks the direction of intensity profile in plot; **C**)**.** Intensity profile of three cells during incubation, the protein is ubiquitous in cell body and surrounding medium; **D**). After washing with PBS (t = 60 min) the cells recover and start spreading. T4-ATTO-647 remains in the cell after washing with phosphate buffered saline (t = 75 min); **E**). To determine the protein concentration inside cells after incubation, cell edges are recognized (green) and mean fluorescence (red) intensities measured; **F**). Mean intensity histogram of various concentrations of T4-ATTO-647 in PBS (grey) versus mean fluorescence inside cells (blue) during and after incubation, measurements were repeated with higher power (inset); **G**). After washing with PBS (t = 3 h) the cells recover and start spreading.

**Conclusion.** In this chapter, the design and synthesis of three Gd(III) based spin labels, CLaNP13a/b/c, was described. Double maleimide groups were introduced to link the probes to the protein via two C-S bonds. *In vitro* DEER measurements yield narrow distance distributions, indicating that the probes display low mobility. The mean observed distance for CLaNP13b is 46 Å, close to the distance calculated on the basis of paramagnetic NMR results (44 Å). The NMR data were based on CLaNP5 probes, whereas the CLaNP13 probes have slightly different arms that link the Ln(III) cage to the protein, which may explain the 2 Å difference in distance. Very similar results were found of a sample in lysate of *E. coli* cells, indicating that the probe is stable in such an environment. The in-cell experiments yielded a very noisy DEER signal, suggesting that the spontaneous protein uptake in *D. discoideum* is insufficient to yield good quality data. Also, the protein is found accumulated in vesicles, perhaps endosomes. In other studies, protein has been introduced via injection or electroporation, leading to a more even distribution of the protein in the cytosol. These approaches could be tested for CLaNP13 as well.

**Materials and Method**

**General:** 1-(2-aminoethyl)-1H-pyrrole-2,5-dione, 1-(3-aminoethyl)-1H-pyrrole-2,5-dione, 1-(4-aminoethyl)-1H-pyrrole-2,5-dione and cyclen were purchased from Abosyn Chemical Inc. and CheMatech. $Gd(OAc)_3{\cdot}4H_2O$, $Yb(OAc)_3{\cdot}4H_2O$, N-(tert-butoxycarbonyloxy)succinimide and methyl 2-bromoacetate were purchased and used without further purification. Solvents were purchased from Honeywell, BIOSOLVE or Aldrich and directly used for synthesis. ATTO-647 maleimide was obtained from ATTO-TEC GmbH. Superdex 75 columns and Sephadex G-25 PD10 desalting columns were purchased from GE Healthcare. Reactions were followed by liquid chromatography-mass spectrometry (LC-MS), TLC analysis on silica gel (F 1500 LS 254 Schleicher and Schuell, Dassel, Germany) in which compounds were visualized by UV and/or ninhydrin, $KMnO_4$. Flash chromatography was performed on Screening Devices silica gel 60 (0.04-0.063 mm). A Waters preparative RP-HPLC system, equipped with a Waters C18-Xbridge 5 µm OBD (30 x 150 mm) column and an Äkta Basic FPLC (GE Healthcare Inc.) were used for purification. NMR spectra were recorded on a Bruker AV-400 (400/100 MHz), AV-500 (500/125 MHz) or AV-600 (600/150 MHz) spectrometer. A LCQ liquid chromatrography mass spectrometry system and a Finnigan LTQ Orbitrap system were used for high-resolution mass spectrometry and protein conjugation analysis. A Thermo Scientific™ NanoDrop 2000 spectrophotometer was used for protein concentration measurements.

**Protein expression and purification:** T4Lys mutant K147C/T151C was produced as described in previous work.[25] The tetra-cysteine mutant N55C/ V57C/K147C/T151C was generated by the Quikchange method (Agilent). After confirming the successful mutations by DNA sequencing, the gene was expressed in *Escherichia coli* BL21 (DE3). Transformed cells were incubated overnight at 37°C on LB agar plates with kanamycin and chloramphenicol (100 µl/mL and 34 µl/mL, respectively). Single colonies were transferred to 2 mL LB medium with kanamycin and chloramphenicol and incubated at 37°C, 250 rpm for 6 h. The precultures were used to inoculate 50 mL (1:1000) for overnight incubation in minimal medium (M9, 37°C, 250 rpm). The 50 mL culture was diluted 100 times and incubated at 37 °C, 250 rpm. When the $OD_{600}$ value reached 1, gene expression was induced by addition of 1 mM isopropyl **β**-D-thiogalactoside (IPTG). The temperature was reduced to 30 °C and the cells were harvested 18 h after induction by centrifugation. The T4Lys N55C/V57C/K147C/T151C was purified according to the method described by Georgieva et al.[26] with some modifications. Cells were lysed using a French press and cleared by centrifugation (45 min, 2500 rpm). The supernatant was loaded on a 5 mL HiTrap CM column equilibrated with 25 mM Tris pH 7.5. The column was washed with 0- 40% linear gradient of buffer B (25 mM Tris pH 7.5, 500 mM NaCl). T4Lys N55C/V57C/K147C/ T151C was eluted in one step with 100 % buffer B.

**Protein labeling:** To label T4Lys mutants with Gd-CLaNP13/ ATTO-647-maleimide, the protein sample (1 mL, 200−300 µM) was treated with DTT (final concentration 10 mM) at

0 °C. After 1 h, the protein buffer solution was loaded on a PD-10 column pre-equilibrated with labeling buffer (25 mM sodium phosphate, 100 mM NaCl, pH 7.8, argon degassed) to remove DTT. The eluted protein was mixed immediately with labeling buffer containing Gd-CLaNP13 (6 equiv.) or ATTO-647-maleimide (4 equiv.) under an argon atmosphere. The mixture was stirred at 4 °C for 6 h. Then the sample volume was reduced to 500 µL by ultrafiltration and purified by using a Superdex 75 gel filtration column, respectively. The yield of labeling for Gd-CLaNP13 labeled T4Lys sample estimated from the LC-MS and NMR, was more than 95%. Labeling with Yb(III)/Lu(III)-CLaNP5 followed a similar procedure except that the labeling buffer was 20 mM sodium phosphate, 100 mM NaCl, pH 7.5 and Yb(III)/Lu(III)-CLaNP5-labeled protein was purified from excess CLaNP-5 with a HiTrap SP column using 30 column volumes for a 0-500 mM NaCl gradient.

**Protein LC-MS sample preparation:** Gd(III)-CLaNP13 labelled T4Lys (10-15 µM) in labelling buffer was incubated with DTT (final concentration 10 mM) on ice for 1h. Iodoacetamide (final concentration 5 mM) was added and the solution was incubated for another 1 h under protection from light. A Bio-rad 6 desalting column was used for buffer exchange before loading the sample on a C4 polymeric reversed phase UPLC column and analyzing it using either an LTQ-Orbitrap mass spectrometer (ThermoScientific) or Synapt G2-Si mass spectrometer (Waters), 10−25 min after thawing.

**DEER sample preparation:** The samples for *in vitro* and in lysate DEER measurements contained 100-150 µM of Gd(III)-CLaNP13 labeled N55C/V57C/K147C/ T151C T4Lys in 20 mM sodium phosphate, pH = 5.5, 150 mM NaCl, 20% (*v*/*v*) glycol and *E. coli* cell lysate (20% (*v*/*v*) glycol), respectively. The sample for in-cell DEER measurement was obtained by incubating *D. discoideum* medium with the protein labelled with Gd(III)-CLaNP13b at a concentration of 115 µM for 90 mins. The cells were recovered, and washed three times in medium to remove excess protein, and to concentrate the cell suspension. The sample was cooled to approx. 4 °C on ice, and 10% (*v*/*v*) DMSO was added to the medium to prepare the cells for freezing and EPR measurement.

**Protein NMR spectroscopy:** All protein NMR spectra were recorded at 298 K on a 600 MHz Bruker Avance III spectrometer. A $^{1}H$-$^{15}N$ HSQC spectrum was acquired for each sample. The final NMR samples contained 100-200 µM of labeled T4Lys in 20 mM sodium phosphate, pH = 5.5, 150 mM NaCl and 5% $D_2O$ for lock.

**PCS data analysis:** The same procedure was applied as described in chapter II (PCS data analysis).

**EPR measurements conditions:** The 95 GHz DEER measurements were recorded using an ELEXSYS E680 spectrometer (Bruker, Rheinstetten, Germany) with a home-built probe head. The measurements were done at a temperature of 10 K. The DEER spectra were recorded using the standard four pulse DEER sequence[29]. The pump pulse duration was

40 ns and the observer pulses durations were 32 and 64 ns, respectively. The pump pulse power was adjusted to invert the echo maximally. The separation between the pump and observer frequencies ($\Delta\mathbf{v}$) was 60 MHz, with the pump pulse adjusted to irradiate at the maximum of the EPR spectrum. To make optimum use of the resonator bandwidth, the pump and observer frequencies were set to 30 MHz higher and lower frequencies respectively with respect to the resonance frequency of resonator. The full sequence for the observer was $\pi/2$–$\boldsymbol{\tau}$– $\pi$ –$\Delta$t- $\pi$ –echo with a delay time $\boldsymbol{\tau}$ of 360 ns and time steps for DEER evolution of 8 ns. The DEER data were analyzed with the program DeerAnalysis 2018.[24]

**Cell culture and live cell imaging:** Axenic *D. discoideum* (Ax2) was obtained from Dr. Günther Gerisch (MPI for Biochemistry, Martinsried, Germany). Cells were grown at 20 °C in HL5 medium and cultured in 100 mm Petridishes (TC-treated culture dish, Corning, USA) and confluency was kept below 70%. For microscopy experiments, cells were harvested and centrifuged at 1500 rpm for 3 min followed by three successive washing steps of the cellular pellet with 17 mM K-Na-phosphate buffered saline (PBS), adjusted to pH = 6.0. After resuspension in PBS, the cells were pipetted into a 70 µL well inside a 35 mm imaging dish (Insert and dish, Ibidi GmbH, Martinsried, Germany) and left to adhere for 30 min. While imaging, T4Lys K147C/T151C linked to ATTO-647 (ATTO-TEC GmbH) was added to a final concentration of 100 µM. Cells were left to incubate for 60 min and were imaged every 30 seconds in two channels (BF and 647) with a Nikon Eclipse Ti microscope, equipped with a Yokogawa confocal spinning disk unit operated at 10,000 rpm (Nikon, Tokyo, Japan). ATTO-647 was excited by a 647 nm solid state diode laser (Coherent, Santa Clara, U.S.A.), supported in an Agilent MLC4 unit (Agilent Technologies, Santa Clara, U.S.A.). Images were captured (50 ms) by an Andor iXon Ultra 897 High Speed EM-CCD (Andor Technology, Belfast, Northern Ireland) through a Cy5 HYQ filter (Nikon, Tokyo, Japan). After incubation, the well was carefully washed with PBS five times (50 µL each step) and imaged for another 15 min.

**Quantification of the in-cell T4-ATTO-647 concentration.** Known concentrations of T4Lys K147C/T151C linked to ATTO-647 in PBS were imaged in the same condition as described for cells. The data were averaged over all images and pixels to find mean intensities per concentration. For the cell data, all pixels belonging to each cell were determined using an in-house Matlab (The Mathworks, Inc., Natick, MA, U.S.A.) script for cell edge recognition (see Figure 5.9 E). In-cell pixels were averaged and subsequently compared to the concentration calibration measurements (see Figure 5.9 F) for two laser powers. All images were pre-processed by flat-field correction and dark-field subtraction.

**Synthesis**

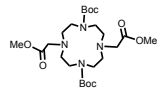


**Di-tert-butyl4,10-bis(2-methoxy-2-oxoethyl)-1,4,7,10-tetraazacyclododecane-1,7-dicarboxylate, compound 2**

To a compound 1[30] (1 g, 2.68 mmol) in 30 mL of acetonitrile (ACN) solution was added four equiv. of $K_2CO_3$ (1.5 g, 10.7 mmol) and methyl 2-bromoacetate (1.64 g, 10.7 mmol) and stirring was continued for 16 h at rt. Then the salt was removed by filtration over a workman filter paper, the organic phase was concentrated under reduced pressure using a rotary evaporator and purified by silica gel flash column chromatograpy (using 40 % of ethyl acetate in pentane as eluent) to give an amorphous white solid (1g, 72% yield). $^1$H NMR (400 MHz, $CDCl_3$, 293K): **δ** = 1.42 (s, 18H), 2.84 (s, 8H), 3.36 (s, 8H), 3.43 (s, 4H), 3.67 (s, 6H); $^{13}$C NMR (400 MHz, $CDCl_3$, 293K): **δ** = 28.59 ($(CH_3)_3C$), 46.66 ($CH_2N$), 51.46 ($CH_3O$) 54.39 ($CH_2N$), 79.57 ($C(CH_3)$), 155.99 ($COOCH_3$). HR-MS: m/z 517.3232 $[M+H]^+$, calcd. $[C_{24}H_{46}N_4O_8]$ 517.3237.

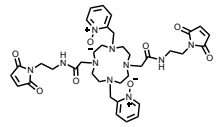

**2,2'-((4,10-bis(carboxymethyl)-1,4,7,10-tetraazacyclododecane-1,7-diyl)bis(methylene))bis(pyridine 1-oxide), compound 3**

Compound 2 (0.5 g, 0.96 mmol) was dissolved in a mixture of DCM and TFA (10 mL, DCM:TFA= 1:4, *v*:*v*) and stirring was continued for 16 h. The reaction mixture was concentrated by co-evaporation with toluene to obtain a yellow oily residue. The residue was dissolved in ACN (10 mL) and 2-(chloromethyl)pyridine 1-oxide [19] (0.35g, 2.4 mmol) and $K_2CO_3$ (0.4 g, 2.9 mmol) were added and stirring was continued at rt for 16 h. The salt was removed by filtration over a workman filtrating paper and the organic layer was concentrated under reduced pressure on a rotary evaporator to yield a brown oily residue. This brown oily product was dissolved in a dioxane water mixture (*v*/*v*= 1:1, 10 mL) where containing 0.25 M of NaOH to obtain compound 3. The crude product purified by reverse phase HPLC (0.2% TFA and a 11-16% acetonitrile gradient on C18 preparative column), yielding 40% of compound 4 (0.19 g, 0.38 mmol). $^1$H NMR (500 MHz, $D_2O$, 343K): **δ** = 3.78-3.90 (m, 18H), 5.14 (s, 4H), 8.18-8.21 (t, 2H), 8.24-8.27 (t, 2H), 8.35 (d, 2H), 8.96 (d, 2H). $^{13}$C NMR (500 MHz, $D_2O$, 343K): **δ** = 49.5 ($CH_2N$), 51.69 ($CH_2N$), 53.76 ($NCH_2COOH$), 54.4 ($CH_2C$), 129.11 (CH) 130.61 (CH) 131.83 (CH), 140.79 (CH), 166.54 (COOH), 166.52 ($CCH_2$). HR-MS: m/z 503.2604 $[M+H]^+$, calcd. $[C_{24}H_{34}N_6O_6]$ 503.2618. FTIR ($cm^{-1}$): 3089.4, 2358.2, 2341.0, 1684.2, 1458.1, 1312.2, 1196.3, 1130.5, 799.9, 772.7, 719.8, 668.3.

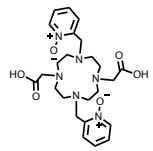

**2,2'-((4,10-bis(2-((2-(2,5-dioxo-2,5-dihydro-1*H*-pyrrol-1-yl)ethyl)amino)-2-oxoethyl)-1,4,7,10-tetraazacyclododecane-1,7-diyl)bis(methylene))bis(pyridine 1-oxide), compound 4a**

Compound 3 (0.1 g, 0.2 mmol) was dissolved in dried DMF (3 mL) and treated with N-hydroxysuccinimide (0.09g, 0.8 mmol) and N-(3-Dimethylaminopropyl)-N′-ethylcarbodiimide hydrochloride (0.15g, 0.8 mmol). After 10 mins with continues stirring was added 1-(2-aminoethyl)-1*H*-pyrrole-2,5-dione (0.12 g, 0.8 mmol) to the reaction mixture and stirring was continued at rt. The reaction was followed by LC-MS. After 24 h, no more compound 3 was detected by LC-MS and the reaction mixture was

concentrated under reduced pressure using a rotary evaporator. For purification, HPLC (0.2% TFA and a 15-25% acetonitrile gradient on C18 preparative column) was employed to yield 70% of compound 4 (0.1 g, 0.14 mmol). A similar procedure was used for synthesis compound 4b and 4c with 1-(3-aminopropyl)-1*H*-pyrrole-2,5-dione (0.1 mg, 0.53 mmol) and 1-(4-aminobutyl)-1H-pyrrole-2,5-dione (0.1 mg, 0.5 mmol), respectively. $^{1}$H NMR (500 MHz, MeOD, 323K): compound 4a **δ** = 3.27 (s, 8H), 3.33-3.35 (t, 4H), 3.46 (s, 8H), 3.54 (s, 4H), 3.61-3.63 (t, 4H), 4.45 (s, 4H), 6.80 (s, 4H), 7.60-7.66 (m, 4H), 7.88-7.90 (t, 2H), 8.45-8.46 (t, 2H). $^{13}$C NMR (500 MHz, MeOD, 323K): **δ** = 38.10 ($CH_2NHCO$), 39.47 ($CH_2NCOCO$), 51.95 ($CH_2N$), 53.96 ($NCH_2C$) 55.81 ($CH_2CONH$), 128.65 (CH) 130.09 (CH) 130.71 (CH), 135.56 (CHCON), 141.78 (CH), 172.69 (CO). Compound 4b $^{1}$H NMR (500 MHz, MeOD, 333K) **δ** = 1.77-1.82 (m, 4H), 3.16-3.17 (t, 4H), 3.25 (br, 8H), 3.47-3.53 (br, 12H), 3.66 (s, 4H), 4.39 (s, 4H), 6.78 (s, 4H), 7.56-7.63 (m, 4H), 7.84-7.86 (dd, 2H), 8.41-8.42 (d, 2H). $^{13}$C NMR (500 MHz, MeOD, 323K): **δ** = 29.11 ($CH_2CH_2NH$), 36.19 ($CH_2NHCO$), 37.98 ($CH_2NCO$), 51.29 ($CH_2CH_2N$), 52.24 ($CH_2CH_2N$), 53.88 ($CH_2C$), 56.12 ($NCH_2CONH$), 128.48 (CH) 129.88 (CH) 130.60 (CH), 135.46 (CHCON), 141.76 (CH), 172.60 (CO). Compound 4c $^{1}$H NMR (500 MHz, MeOD, 333K) **δ** = 1.47-1.53 (m, 4H), 1.57-1.63 (m, 4H), 3.20-3.23 (br, 12H), 3.46-3.50 (br, 12H), 3.66 (s, 4H), 4.36 (s, 4H), 6.77 (s, 4H), 7.56-7.63 (m, 4H), 7.82-7.84 (dd, 2H), 8.41-8.42 (d, 2H). $^{13}$C NMR (500 MHz, MeOD, 323K): **δ** = 26.85 ($CH_2CH_2NHCO$), 27.46 ($CH_2CH_2NCOCO$), 38.21 ($CH_2NHCO$), 40.05 ($CH_2NCO$), 51.08 ($CH_2CH_2N$), 52.34 ($CH_2CH_2N$), 53.74 ($CH_2C$), 56.19 ($NCH_2CONH$), 128.44 (CH) 129.81 (CH) 130.59 (CH), 135.40 (CHCON), 141.79 (CH), 172.64 (CO).HR-MS: compound 4a m/z 747.3577 $[M+H]^+$, calcd. $[C_{36}H_{46}N_{10}O_8]$ 747.3578; compound 4b m/z 775.3892 $[M+H]^+$, calcd. $[C_{38}H_{50}N_{10}O_8]$ 775.3851; compound 4c 803.4217 $[M+H]^+$, calcd. $[C_{40}H_{54}N_{10}O_8]$ 803.4204. FTIR ($cm^{-1}$) compound 4a: 3080.8, 2359.6, 2332.4, 1705.7, 1684.2, 1443.8, 1410.9, 1200.6, 1173.4, 1130.5, 1054.61, 1033.1, 830.0, 799.9, 777.0, 719.8, 696.9, 668.3. Compound 4b and 4c showing the same spectra as 4a.

**Metal complex**: To a solution of compound 4a (30 mg, 40 µmol) in 400 µL dried DMF, 1.2 equiv. of $Gd(OAc)_3{\cdot}4H_2O$ was added. The mixture was stirred at rt for 16 h and the formation of the metal complex was checked by LC-MS. Without further purification, Gd-CLaNP13a was used for protein sample labeling. Gd-CLaN13a/b/c were prepared following the same procedure. HR-MS: Gd-CLaNP13a m/z 301.4252 $[M]^{3+}$, calcd. $[C_{36}H_{46}GdN_{10}O_8]$ 301.4253; Gd-CLaNP13b m/z 310.7687 $[M]^{3+}$, calcd. $[C_{38}H_{50}GdN_{10}O_8]$ 310.7679; Gd-CLaNP13c m/z 320.1129 $[M]^{3+}$, calcd. $[C_{40}H_{54}GdN_{10}O_8]$ 320.1117.

### Reference

(1) Schiemann, O.; Prisner, T. F. Long-Range Distance Determinations in Biomacromolecules by EPR Spectroscopy. *Q. Rev. Biophys.* **2007**, *40* (1), 1–53.

(2) Jeschke, G.; Polyhach, Y. Distance Measurements on Spin-Labelled Biomacromolecules by Pulsed Electron Paramagnetic Resonance. *Phys. Chem. Chem. Phys.* **2007**, *9* (16), 1895–1910.

(3) Kaminker, I.; Tkach, I.; Manukovsky, N.; Huber, T.; Yagi, H.; Otting, G.; Bennati, M.; Goldfarb, D. W-band Orientation Selective DEER Measurements on a $Gd^{3+}$/Nitroxide Mixed-labeled Protein Dimer with a Dual Mode Cavity. **2013**, 227, 66-71.

(4) Dias, D. M.; Ciulli, A. NMR Approaches in Structure-Based Lead Discovery: Recent Developments and New Frontiers for Targeting Multi-Protein Complexes. *Prog. Biophys. Mol. Biol.* **2014**, *116* (2), 101–112.

(5) Clayton, J. A.; Keller, K.; Qi, M.; Wegner, J.; Koch, V.; Hintz, H.; Godt, A.; Han, S.; Jeschke, G.; Sherwin, M. S.; et al. Quantitative Analysis of Zero-Field Splitting Parameter Distributions in Gd(III) Complexes. *Phys. Chem. Chem. Phys.* **2018**, *20* (15), 10470–10492.

(6) Drescher, M. BT-EPR Spectroscopy: Applications in Chemistry and Biology EPR in Protein Science. **2012**, 91–119.

(7) Goldfarb, D. $Gd^{3+}$ Spin Labeling for Distance Measurements by Pulse EPR Spectroscopy. *Phys. Chem. Chem. Phys.* **2014**, *16* (21), 9685–9699.

(8) Yang, Y.; Yang, F.; Li, X. Y.; Su, X. C.; Goldfarb, D. In-Cell EPR Distance Measurements on Ubiquitin Labeled with a Rigid PyMTA-Gd(III) Tag. *J. Phys. Chem. B* **2019**, *123* (5), 1050–1059

(9) Kaminker, I.; Bye, M.; Mendelman, N.; Gislason, K.; Sigurdsson, S. T.; Goldfarb, D. Distance Measurements between Manganese(II) and Nitroxide Spin-Labels by DEER Determine a Binding Site of $Mn^{2+}$ in the HP92 Loop of Ribosomal RNA. *Phys. Chem. Chem. Phys.* **2015**, *17* (23), 15098–15102.

(10) Azarkh, M.; Okle, O.; Eyring, P.; Dietrich, D. R.; Drescher, M. Evaluation of Spin Labels for In-Cell EPR by Analysis of Nitroxide Reduction in Cell Extract of Xenopus Laevis Oocytes. *J. Magn. Reson.* **2011**, *212* (2), 450–454.

(11) Igarashi, R.; Sakai, T.; Hara, H.; Tenno, T.; Tanaka, T.; Tochio, H.; Shirakawa, M. Distance Determination in Proteins inside Xenopus Laevis Oocytes by Double Electron−Electron Resonance Experiments. *J. Am. Chem. Soc.* **2010**, *132* (24),

(12) Clayton, J. A.; Qi, M.; Godt, A.; Goldfarb, D.; Han, S.; Sherwin, M. S. $Gd^{3+}$-$Gd^{3+}$ Distances Exceeding 3 nm Determined by Very High Frequency Continuous Wave Electron Paramagnetic Resonance. *Phys. Chem. Chem. Phys.* **2017**, *19* (7), 5127–5136.

(13) Matalon, E.; Huber, T.; Hagelueken, G.; Graham, B.; Frydman, V.; Feintuch, A.; Otting, G.; Goldfarb, D. Gadolinium(III) Spin Labels for High-Sensitivity Distance Measurements in Transmembrane Helices. *Angew. Chemie. Int. Ed.* **2013**, *52* (45), 11831–11834.

(14) Feintuch, A.; Otting, G.; Goldfarb, D. $Gd^{3+}$ Spin Labeling for Measuring Distances in Biomacromolecules: Why and How? *Methods Enzymol.* **2015**, *563*, 415–457.

(15) Bellapadrona, G.; Martorana, A.; Goldfarb, D.; Aime, S.; Feintuch, A.; Di Gregorio, E. Probing Protein Conformation in Cells by EPR Distance Measurements Using $Gd^{3+}$ Spin Labeling . *J. Am. Chem. Soc.* **2014**, *136* (38), 13458–13465.

(16) Yang, Y.; Yang, F.; Gong, Y.-J.; Chen, J.-L.; Goldfarb, D.; Su, X.-C. A Reactive, Rigid Gd(III) Labeling Tag for In-Cell EPR Distance Measurements in Proteins. *Angew. Chemie. Int. Ed.* **2017**, *56* (11), 2914–2918.

(17) Keizers, P. H. J.; Desreux, J. F.; Overhand, M.; Ubbink, M. Increased Paramagnetic Effect of a Lanthanide Protein Probe by Two-Point Attachment. *J. Am. Chem. Soc.* **2007**, *129* (30), 9292–9293.

(18) Fleissner, M. R.; Bridges, M. D.; Brooks, E. K.; Cascio, D.; Kalai, T.; Hideg, K.; Hubbell, W. L. Structure and Dynamics of a Conformationally Constrained Nitroxide Side Chain and Applications in EPR Spectroscopy. *Proc. Natl. Acad. Sci.* **2011**, *108* (39), 16241–16246.

(19) Keizers, P. H. J.; Saragliadis, A.; Hiruma, Y.; Overhand, M.; Ubbink, M. Design, Synthesis,

and Evaluation of a Lanthanide Chelating Protein Probe: CLaNP-5 Yields Predictable Paramagnetic Effects Independent of Environment. *J. Am. Chem. Soc.* **2008**, *130* (44), 14802–14812.

(20) Liu, L.; Quillin, M. L.; Matthews, B. W. Use of Experimental Crystallographic Phases to Examine the Hydration of Polar and Nonpolar Cavities in T4 Lysozyme. *Proc. Natl. Acad. Sci.* **2008**, *105* (38), 14406–14411.

(21) Bertini, I.; Calderone, V.; Cerofolini, L.; Fragai, M.; Geraldes, C. F. G. C.; Hermann, P.; Luchinat, C.; Parigi, G.; Teixeira, J. M. C. The Catalytic Domain of MMP-1 Studied through Tagged Lanthanides. *FEBS Lett.* **2012**, *586* (5), 557–567.

(22) Camacho-Zarco, A. R.; Munari, F.; Wegstroth, M.; Liu, W.-M.; Ubbink, M.; Becker, S.; Zweckstetter, M. Multiple Paramagnetic Effects through a Tagged Reporter Protein. *Angew. Chemie. Int. Ed.* **2015**, *54* (1), 336–339.

(23) Clarke, M. Recent Insights into Host-Pathogen Interactions from Dictyostelium. *Cell. Microbiol.* **2010**, *12* (3), 283–291.

(24) Jeschke, G.; Chechik, V.; Ionita, P.; Godt, A.; Zimmermann, H.; Banham, J.; Timmel, C. R.; Hilger, D.; Jung, H. DeerAnalysis2006 - A Comprehensive Software Package for Analyzing Pulsed ELDOR Data. *Appl. Magn. Reson.* **2006**, *30* (3–4), 473–498.

(25) Liu, W.-M.; Skinner, S. P.; Filippov, D. V.; Blok, A.; Ubbink, M.; Timmer, M.; Overhand, M.; Hass, M. A. S. A Two-Armed Lanthanoid-Chelating Paramagnetic NMR Probe Linked to Proteins via Thioether Linkages. *Chem. Eur. J.* **2014**, *20* (21), 6256–6258.

(26) Georgieva, E. R.; Roy, A. S.; Grigoryants, V. M.; Borbat, P. P.; Earle, K. A.; Scholes, C. P.; Freed, J. H. Effect of Freezing Conditions on Distances and Their Distributions Derived from Double Electron Electron Resonance (DEER): A Study of Doubly-Spin-Labeled T4 Lysozyme. *J. Magn. Reson.* **2012**, *216*, 69–77.

(27) Schmitz, C.; Stanton-Cook, M. J.; Su, X. C.; Otting, G.; Huber, T. Numbat: An Interactive Software Tool for Fitting $\Delta\chi$ -Tensors to Molecular Coordinates Using Pseudocontact Shifts. *J. Biomol. NMR* **2008**, *41* (3), 179–189.

(28) Bashir, Q.; Volkov, A. N.; Ullmann, G. M.; Ubbink, M. Visualization of the Encounter Ensemble of the Transient Electron Transfer Complex of Cytochrome *c* and Cytochrome *c* Peroxidase. *J. Am. Chem. Soc.* **2010**, *132* (1), 241–247.

(29) Pannier, M.; Veit, S.; Godt, A.; Jeschke, G.; Spiess, H. Dead-Time Free Measurement of Dipole–Dipole Interactions between Electron Spins. *J. Magn. Reson.* **2000**, *142* (2), 331–340.

(30) Liu, W.-M.; Keizers, P. H. J.; Hass, M. A. S.; Blok, A.; Timmer, M.; Sarris, A. J. C.; Overhand, M.; Ubbink, M. A pH-Sensitive, Colorful, Lanthanide-Chelating Paramagnetic NMR Probe. *J. Am. Chem. Soc.* **2012**, *134* (41), 17306–17313.

*Chapter V*

# Chapter VI

# General discussion, conclusions and prospects

# *Chapter VI*

The main subject of this thesis is the design and synthesis of paramagnetic molecules for protein studies with NMR and EPR spectroscopy. With the development of paraNMR and DEER experiments, synthetic paramagnetic centers are becoming popular. About half of the current paramagnetic probes were described in the past five years, reflecting this popularity. Several of them improved the stability and rigidity of the probes, mainly by introducing novel attachment groups forming thioether and triazole linkers.[1–3] Such linkages help to extend the application of the probes to in-cell measurements.[4,5] Some small probes were designed for 3d-block metal ions as well, but these probes show low metal ion binding affinity.[6,7] The research described in this thesis contributed to the development of paramagnetic probes. Hereafter, the properties of these new probes are discussed, and some general conclusions and prospects are given.

**Development of synthetic paramagnetic NMR probes for 3d-block metal ions**

The advantage of a chemically attached paramagnetic center is that it can be specifically directed to the protein domain of interest.[8,9] 3d-Block metal ions are one of the three main types of paramagnetic centers, as described in chapter I section 2. In contrast to what is the case for lanthanoid ions, few synthetic paramagnetic NMR probes for 3d-block metal ions have been reported, especially for cyclen based probes. In chapter II and chapter III, two cyclen-based two-armed hydrophilic 3d-blocked protein paramagnetic probes, referred to as TraNP1 (Chapter II, Figure 2.1) and TraNP2 (Chapter III, Figure 3.1), were developed. TraNP1 was successfully ligated to Co(II) and Mn(II), giving complexes with relative high hydrophilicity and zero net charge. Single sets of PCS were observed with Co(II)-TRaNP1 linked proteins. Its Mn(II) complex caused PRE. It was interesting to note that TraNP2, being an isomer of TraNP1, exhibited very different paramagnetic properties. TraNP2 coordinated both 3d-block ions and lanthanoids, resulting in small and double sets of PCS with Co(II)-TraNP2 and Yb(III)-TraNP2, respectively. This indicates that the magnetic properties of 3d-block metal ions are highly dependent on their ligands.

The comparison between TraNP1 and another pseudo-two-armed probe (*tag 1*)[6] was performed using two proteins (chapter II). The results of this NMR study strongly indicate that the cyclen based probe complexed to 3d-block metal ions, (i.e. TraNP1), has a higher rigidity and metal binding affinity than *tag 1,* producing less complex NMR spectra. Moreover, TraNP1 avoids the binding of free metal ions to the probe.

**Next generation of paramagnetic NMR probes: more rigid and hydrophilic**

Studies of protein dynamics are crucial to understand protein function at atomic level. Potentially, one of the most suitable methods for these types of studies is paraNMR. It was found that the acquired paramagnetic effects in a dynamic protein can be modulated by the movement of the paramagnetic center, yielding inaccurate structural information.[10] This was confirmed by relaxation dispersion experiments that were

performed on proteins linked to CLaNP5 (chapter I, Figure 1.9). The observed dispersion effects were due to the movement of the probe, showing the presence of a minor state of the probe. DOTA, the basis of CLaNP5, is an outstanding metal ion binding ligand, especially for lanthanoids. With four carboxyl groups and octadentate coordination, its complexes possess high symmetry, solubility and thermal stability in aqueous solution. Therefore, DOTA and its derivatives are often applied as paramagnetic NMR probes. However, conformational exchange is a general property of lanthanoid DOTA and DOTA-like complexes. In chapter IV, the core structure of CLaNP5, Ln(III)-PyDOTA (Figure 4.2), was found to undergo a conformational exchange between two SAP conformers, due to the simultaneously flip of the cyclen ring and reorientation of the pendent arms. When CLaNP5 is linked to a (chiral) protein, its symmetry will be broken. It is also possible that the conformation change slightly reorients the probe relative to the protein. In either case, the two conformers can cause non-equivalent $\Delta\chi$ tensors, which, under milliseconds exchange, result in relaxation dispersion effects, as reported in the literature.[11] Also the attachment of this probe via a $CONHCH_2CH_2S$ linkage could contribute to the mobility of the tag.[11] Thus, an extensively rigid paramagnetic center is required to perform protein dynamic studies. Besides rigidity, several other requirements need to be considered for the design of the ultimate paramagnetic NMR probe, as was discussed in chapter I, section 3, including hydrophilicity, stability, symmetry and reactivity with the two functional groups (such as thiols) of the target protein. A rigid cyclen-like macrocyclic ring was designed and synthesized in chapter IV (Scheme 4.2, compound 9). Equipped with pendent arms, conformation exchange of its lanthanoid loaded complex was studied by NMR. The introduction of four chiral hydroxyl-methylene groups on the tetraaza ring froze the conformation of the macrocyclic ring to one state. The remaining observed conformational exchange was due only to the reorientation of the pendent arms.

CLaNP5 (chapter I, Figure 1.9), in which one pair of the acetate acid pendent arms is replaced by a pair of pyridyl-N-oxide ones, is recognized as one of the most rigid

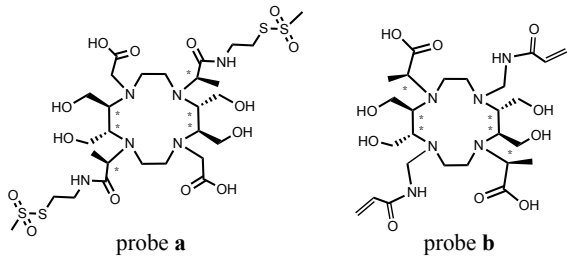


**Figure 6.1** Structures of potential next generation DOTA-like paramagnetic probe. The asterisks identify the chiral carbons.

DOTA-like paramagnetic probe. However, the high hydrophobicity and charge make CLaNP5 not generally applicable for all proteins. An alternative approach would be the introduction rigidity by the use of pendent arms having chiral carbons with small substituents.[1] Thus, using the hydroxyl-methylene substituted cyclenol as coordination ring and the chiral centers modified linker as attachment arms (Figure 6.1, probe a) could force the probe in a single conformation. Although MST attachment group has high selectivity, the disulfide bound is less stable compared to a thioether linkage and the $CONHCH_2CH_2S$ linkage could contribute to the mobility of the probe. In this case, probe b (Figure 6.1) with a short chiral vinyl groups could be another choice.

**Development of paramagnetic probes for in cell EPR measurement**

EPR combined with site-specific spin labels has been applied for the investigation of distances between two labels.[12] In this case, paramagnetic NMR probes with a suitable paramagnetic center, such as Gd(III), Mn(III) or a free radical, are candidates for EPR measurements on proteins. Recently, this method was successfully extended to protein in-cell distance measurements. The cellular conditions require a spin label that is inert in a reductive environment. In chapter V, the two-armed CLaNP13 was designed and synthesized for this purpose. A narrow distance distribution was obtained for Gd(III)-CLaNP13 labeled proteins in cell lysate, demonstrating the stability and rigidity of the probe, which is thus potentially suitable for distance measurements under cellular conditions. As mentioned in chapter V, the introduced maleimide groups caused multiple sets PCS for using it as an NMR probe. Thus, probe b (Figure 6.1) can match the requirements for both NMR and in-cell EPR measurements.

**References**

(1) Yang, F.; Wang, X.; Pan, B. Bin; Su, X. C. Single-Armed Phenylsulfonated Pyridine Derivative of DOTA is Rigid and Stable Paramagnetic Tag in Protein Analysis. *Chem. Commun.* **2016**, *52* (77), 11535–11538.

(2) Müntener, T.; Kottelat, J.; Huber, A.; Häussinger, D. New Lanthanide Chelating Tags for PCS NMR Spectroscopy with Reduction Stable, Rigid Linkers for Fast and Irreversible Conjugation to Proteins. *Bioconjug. Chem.* **2018**, *29* (10), 3344–3351.

(3) Jiang, W.-X.; Gu, X.-H.; Dong, X.; Tang, C. Lanthanoid Tagging via an Unnatural Amino Acid for Protein Structure Characterization. *J. Biomol. NMR* **2017**, *67* (4), 273–282.

(4) Müntener, T.; Häussinger, D.; Selenko, P.; Theillet, F.-X. In-Cell Protein Structures from 2D NMR Experiments. *J. Phys. Chem. Lett.* **2016**, *7* (14), 2821–2825.

(5) Yang, Y.; Yang, F.; Gong, Y.-J.; Chen, J.-L.; Goldfarb, D.; Su, X.-C. A Reactive, Rigid Gd(III) Labeling Tag for In-Cell EPR Distance Measurements in Proteins. *Angew. Chemie. Int. Ed.* **2017**, *56* (11), 2914–2918.

(6) Swarbrick, J. D.; Ung, P.; Dennis, M. L.; Lee, M. D.; Chhabra, S.; Graham, B. Installation of a Rigid EDTA-like Motif into a Protein **α**-Helix for Paramagnetic NMR Spectroscopy with Cobalt(II) Ions. *Chem. Eur. J.* **2016**, *22* (4), 1228–1232.

(7) Yang, Y.; Wang, J.-T.; Pei, Y.-Y.; Su, X.-C. Site-Specific Tagging Proteins via a Rigid, Stable and Short Thiolether Tether for Paramagnetic Spectroscopic Analysis. *Chem. Commun.*

**2015**, *51* (14), 2824–2827.

(8) Nitsche, C.; Otting, G. Pseudocontact Shifts in Biomolecular NMR Using Paramagnetic Metal Tags. *Prog. Nucl. Magn. Reson. Spectrosc.* **2017**, *98–99*, 20–49.

(9) Liu, W. M.; Overhand, M.; Ubbink, M. The Application of Paramagnetic Lanthanoid Ions in NMR Spectroscopy on Proteins. *Coord. Chem. Rev.* **2014**, *273–274*, 2–12.

(10) Eichmüller, C.; Skrynnikov, N. R. Observation of **M**s Time-Scale Protein Dynamics in the Presence of $Ln^{3+}$ Ions: Application to the N-Terminal Domain of Cardiac Troponin C. *J. Biomol. NMR* **2007**, *37* (2), 79–95.

(11) Hass, M. A. S.; Liu, W. M.; Agafonov, R. V.; Otten, R.; Phung, L. A.; Schilder, J. T.; Kern, D.; Ubbink, M. A Minor Conformation of a Lanthanide Tag on Adenylate Kinase Characterized by Paramagnetic Relaxation Dispersion NMR Spectroscopy. *J. Biomol. NMR* **2015**, *61* (2), 123–136.

(12) Schiemann, O.; Prisner, T. F. Long-Range Distance Determinations in Biomacromolecules by EPR Spectroscopy. *Q. Rev. Biophys.* **2007**, *40* (1), 1–53.

## *Chapter VI*

# English summary

Paramagnetic NMR spectroscopy (paraNMR) is a powerful technique for biomolecular studies, due to a variety of paramagnetic effects, such as the pseudocontact shift (PCS) and paramagnetic relaxation enhancement (PRE), that contain long-range structural information. Most proteins do not have a paramagnetic center or metal binding site. Thus, it is required to introduce a paramagnetic center with minimal effects on the protein. Synthetic paramagnetic centers are commonly applied for protein structure investigations in paraNMR. The main subject of this thesis is to design, synthesize and apply novel paramagnetic NMR probes for such studies.

An overview of paramagnetic NMR spectroscopy, types of paramagnetic centers, reported paramagnetic probes and applications of paraNMR in protein studies is provided in **Chapter I**.

A novel paramagnetic NMR probe, TraNP1 (transition metal NMR probe # 1), for 3d-block ions is reported in **Chapter II**. The magnetic properties of Co(II) and Mn(II) loaded TraNP1 are investigated by linking these probes via two attachment arms to three different proteins. Paramagnetic NMR spectra show that the probe places the metal ion in a well-defined location relative to the protein. The medium size of the anisotropy of the magnetic susceptibility tensor makes Co(II)-TraNP1 suitable for small proteins and localized studies. In contrast to CLaNP5 (caged lanthanoid NMR probe # 5), the size of the anisotropic components of the magnetic susceptibility of Co(II)-TraNP1 is influenced by its surroundings on the surface of the proteins.

**Chapter III** describes the design and synthesis of a paramagnetic probe, TraNP2, which is a good ligand for both 3d-block and lanthanoid ions. For lanthanoid loaded TraNP2, even with double-arm attachment, multiple sets of PCS are detected in NMR spectra of proteins. Surprisingly, Co(II)-loaded TraNP2 generates almost negligible PCS. Thus, surprisingly, TraNP2 generates clearly different results as protein paramagnetic probe from those for TraNP1, despite being an isomer. This observation confirms the sensitivity of the anisotropic magnetic properties of Co(II) for its environment.

In **Chapter IV**, a rigid DOTA derivative, HMDOTA, is produced as lanthanoid ligand. The strategy that is used for rigidification is to introduce chiral centers into the cyclen ring. The conformational exchange of these lanthanoid complexes is investigated by 1D $^{1}$H and 2D $^{1}$H EXSY NMR. According to the EXSY spectra, the conformational exchange caused by cyclen ring flip is eliminated by the substituents. Therefore, as a rigidified lanthanoid ligand, HMDOTA is a promising building block for the design of rigid paramagnetic probes for proteins that can be used for dynamic studies.

## *English summary*

In **Chapter V**, a rigid Gd(III) probe, CLaNP13, is designed and synthesized for in-cell protein distance measurements using EPR spectroscopy. Rather than the disulphide linkage employed for protein attachment in other CLaNP molecules, more stable carbon-sulfur bonds are used to link the probe to the protein. A good agreement is found between the data from measurements *in vitro* and in cell lysate, showing the stability of CLaNP13 under reductive conditions. DEER derived distances are in the order of 4 nm and are in agreement with the expected values based on the metal positions derived from paramagnetic NMR results.

**Chapter VI** contains a general discussion about the work described in this thesis and an outlook for the next generation of chemical synthetic paramagnetic NMR probes.

# Nederlandse samenvatting

Paramagnetische kernspinspectroscopie (paraNMR) is een krachtige techniek om biomoleculen te bestuderen, dankzij verschillende paramagnetische fenomenen, zoals de pseudocontact shift (PCS) en paramagnetische relaxatieversterking (PRE), die structurele informatie geven over lange afstanden. De meeste eiwitten hebben geen paramagnetische centrum of en binden geen metaalionen. Dan is het nodig om een paramagnetische centrum te introduceren, met minimale verstoring van het eiwit. Doorgaans worden synthetische paramagnetische centra gebruikt voor het onderzoeken van eiwitstructuren met paraNMR. Het ontwerp, de synthese en de toepassing van nieuwe paramagnetische NMR probes voor eiwitstructuuronderzoek vormen het onderwerp van dit proefschrift.

Een overzicht van paramagnetische NMR-spectroscopie, verschillende types paramagnetische centra, gepubliceerde paramagnetische probes en toepassingen van paraNMR in eiwitstructuuronderzoek wordt besproken in **Hoofdstuk I**.

Een nieuwe paramagnetische NMR sonde, TraNP1 (overgangsmetaal NMR sonde # 1), voor 3d-blok ionen wordt gerapporteerd in **Hoofdstuk II**. De magnetische eigenschappen van TraNP1 geladen met Co(II) en Mn(II) worden onderzocht door ze via twee armen aan drie verschillende eiwitten te koppelen. De paramagnetische NMR-spectra laten zien dat de sondes het metaalion in een goed gedefinieerde locatie plaatsen ten opzichte van het eiwit. De grootte van de anisotropie van de magnetische susceptibiliteitstensor maakt Co(II)-TraNP1 geschikt voor kleine eiwitten en gelokaliseerd eiwitonderzoek. In tegenstelling tot CLaNP5 (caged lanthanide NMR probe # 5) wordt de grootte van de anisotrope componenten van het magnetische susceptibiliteit van Co(II)-TraNP1 beïnvloed door de omgeving op het oppervlakte van het eiwit.

**Hoofdstuk III** beschrijft het ontwerp en synthese van een paramagnetische probe, TraNP2, een goed ligand voor 3d-blok- en lanthanoïde-ionen. Voor TraNP2 geladen met een lanthanoïde ion, zelfs met een dubbele linker, worden meerdere sets PCS gevonden in NMR spectra van eiwitten. Verrassend genoeg genereerd TraNP2 geladen met Co(II) bijna verwaarloosbare PCS. Alhoewel TraNP2 een isomeer van TraNP1 is, geeft het duidelijk andere resultaten als paramagnetische eiwitprobe. Dit bevestigt de gevoeligheid van de anisotrope magnetische eigenschappen van Co(II).

In **Hoofdstuk IV** wordt een rigide DOTA derivaat, HMDOTA, geproduceerd als lanthanoïdeligand. De manier waarop dit wordt bewerkstelligd is door de introductie van chirale centra aan de cycleenring. De conformatieuitwisseling van lanthanoïdecomplexen wordt onderzocht door 1D $^{1}$H en 2D $^{1}$H EXSY NMR. De EXSY spectra geven aan dat de conformatieuitwisseling verzoorzaakt door cycleenring flip geëlimineerd is door de substituenten. Hierdoor belooft het rigide lanthanoïdeligand HMDOTA een zeer

geschikte uitgangsstof te zijn voor het ontwerp van paramagnetische eiwitsondes voor het onderzoeken van eiwitdynamiek.

In **Hoofdstuk V** wordt CLaNP13, een rigide Gd(III) sonde, ontworpen en gesynthetiseerd voor het uitvoeren van eiwitafstandsmetingen in de cel met EPR spectroscopie. In tegenstelling tot de disulfidebruggen die worden gebruikt voor andere CLaNP moleculen, worden stabielere koolstof-zwavelbindingen gebruikt om de sonde aan het eiwit te bevestigen. De resultaten van experimenten uitgevoerd *in vitro* en in cellysaat komen sterk overeen, wat aangeeft dat de CLaNP13 stabiel is in een reducerende omgeving. Verder leveren de DEER-afstandsmetingen een afstand op in de orde van 4 nm, wat overeen komt met de waarden die verwacht worden op basis van de metaalposities afgeleid uit de paramagnetische NMR resultaten.

**Hoofdstuk VI** is een algemene discussie over het werk beschreven in dit proefschrift en beschrijft de mogelijke volgende generatie van synthetische paramagnetische NMR sondes.

# Appendices

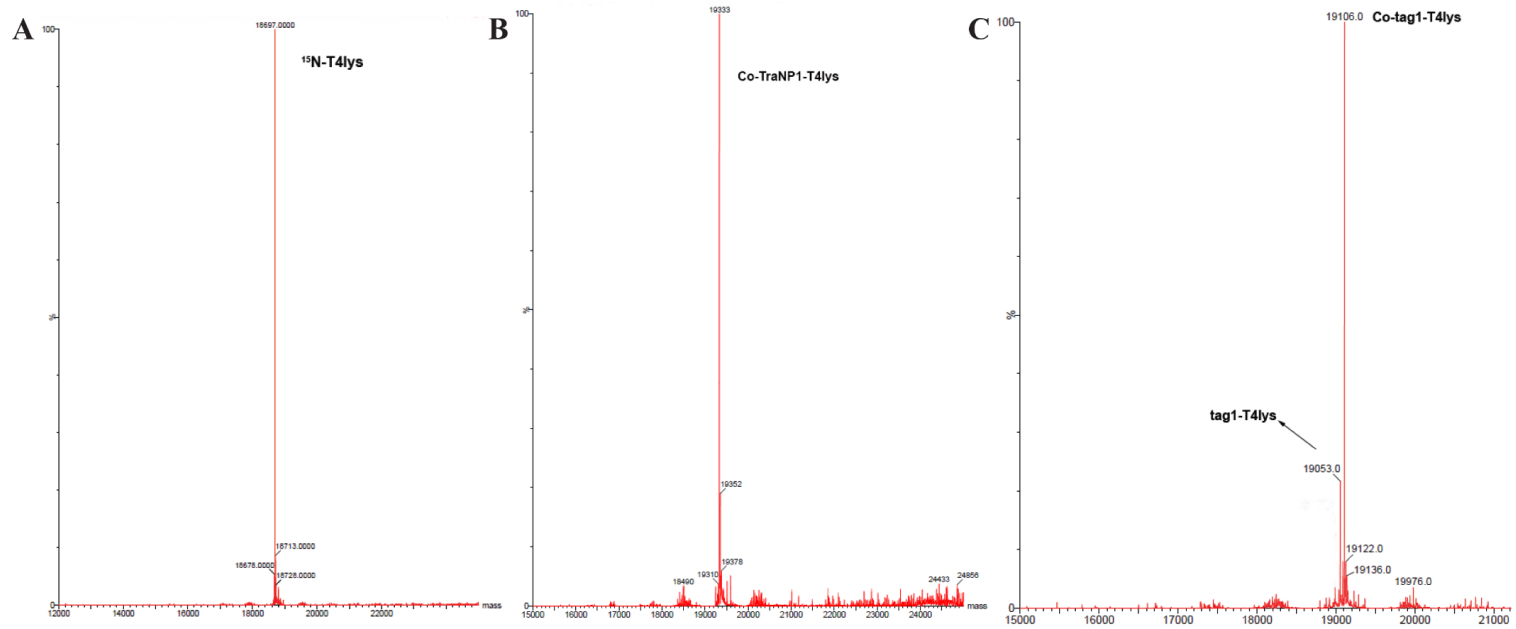


**App. Figure A2.1** MALDI-TOF mass spectra of $^{15}$N-riched T4Lys mutant (**A**), Co-TraNP1 (**B**) and *tag 1*(**C**) labeled $^{15}$N-riched T4Lys mutant.

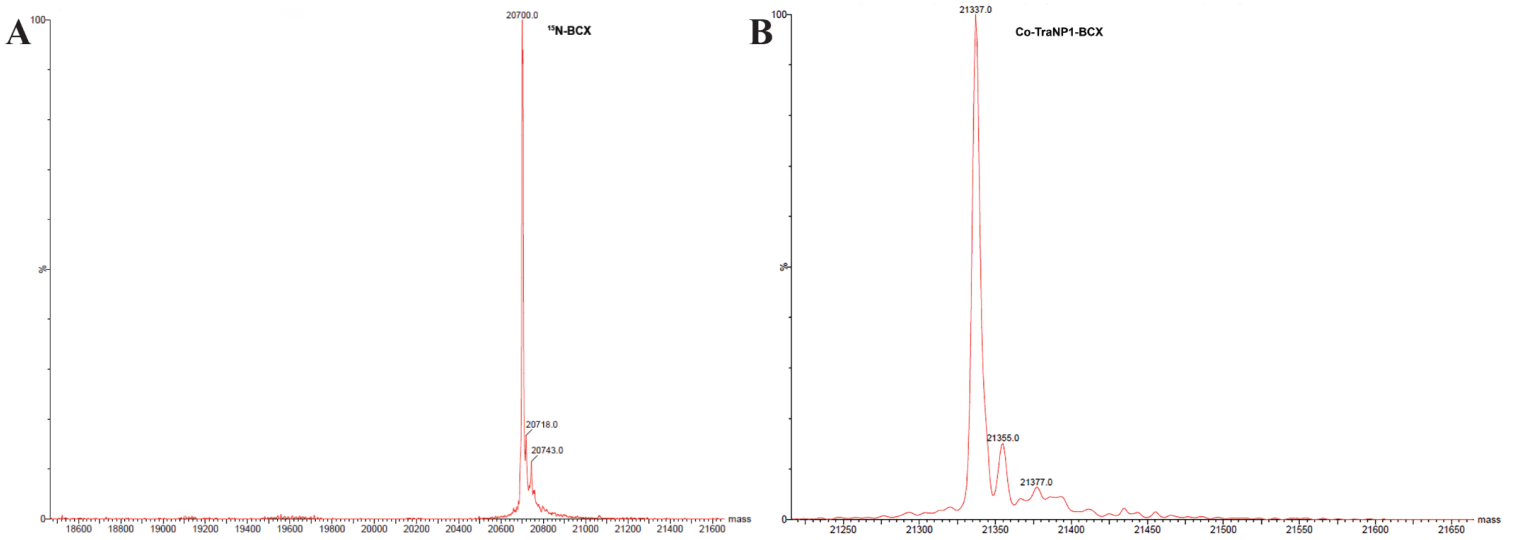


**App. Figure A2.2** MALDI-TOF mass spectra of $^{15}$N-riched BCX mutant (**A**) and Co-TraNP1 (**B**) labeled $^{15}$N-riched BCX mutant.

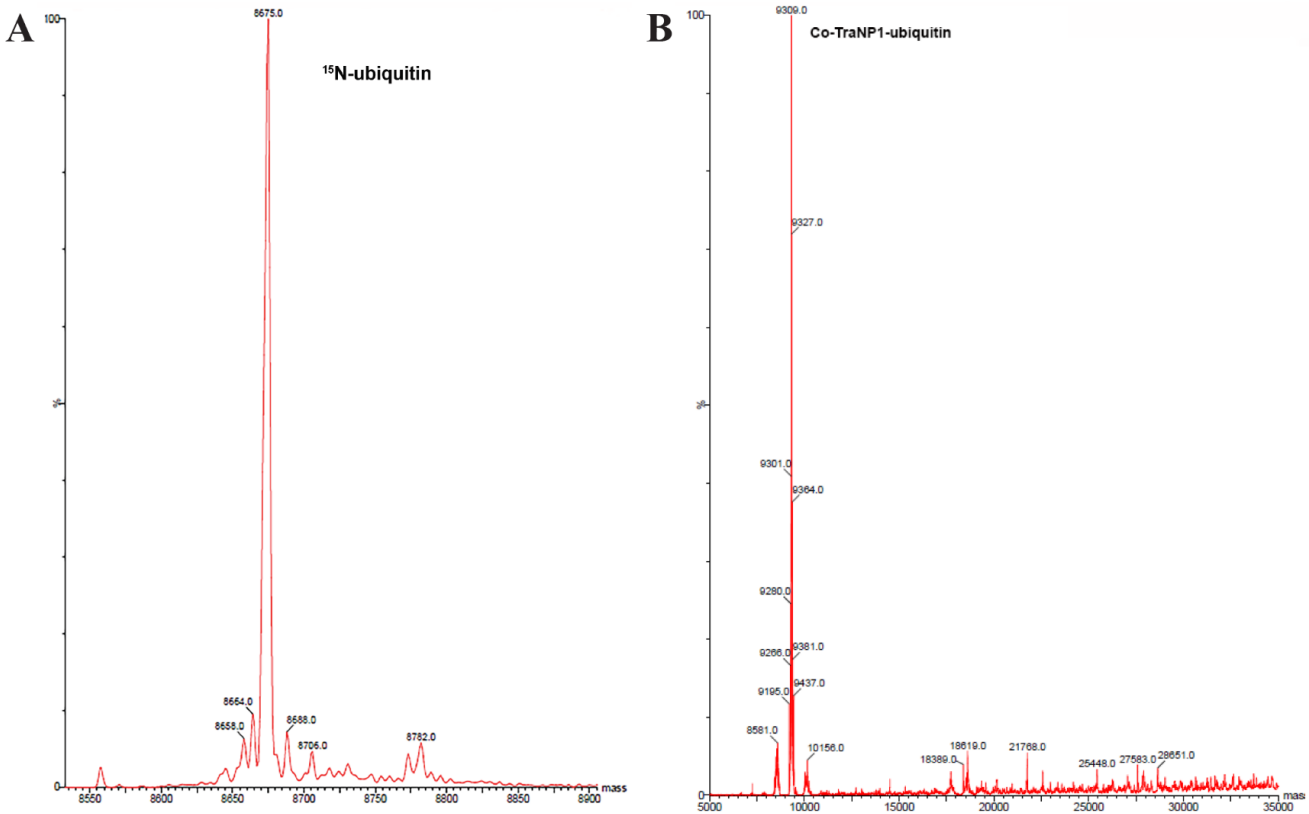


**App. Figure A2.3** MALDI-TOF mass spectra of $^{15}$N-riched ubiquitin mutant (**A**), Co-TraNP1 labeled $^{15}$N-riched ubiquitin mutant (**B**).

**Table A2.1** PCS-based Δχ-tensor parameters of Co(II)-TraNP1 attached to T4Lys K147C/T151C, fitted to three crystal structures.

| PDB | 2lzm [1] | | 3dke [2] | | 1l68 [3] | |
|---|---|---|---|---|---|---|
| Probes | RR | SS | RR | SS | RR | SS |
| $\Delta\chi_{ax}$ [a] | 5.2±0.1 | 4.6±0.1 | 5.2±0.2 | 4.7±0.1 | 5.2±0.2 | 4.6±0.1 |
| $\Delta\chi_{rh}$ [a] | 1.2±0.1 | 0.9±0.1 | 1.3±0.1 | 0.9±0.2 | 1.3±0.1 | 0.9±0.2 |
| X (Å) [b] | 3.4±0.1 | 3.9±0.1 | 43.7±0.2 | 44.2±0.2 | 43.9±0.1 | 44.4±0.1 |
| Y (Å) [b] | -3.6±0.1 | -4.3±0.1 | 8.3±0.2 | 7.5±0.2 | 8.8±0.1 | 8.0±0.2 |
| Z (Å) [b] | -4.4±0.1 | -4.2±0.1 | -8.9±0.1 | -8.6±0.1 | -9.1±0.1 | -9.0±0.1 |
| α (°) | 57±1 | 57±4 | 56±1 | 56±5 | 58±1 | 58±1 |
| β (°) | 68±1 | 69±1 | 68±1 | 69±2 | 68±1 | 69±2 |
| γ (°) | 118±1 | 103±3 | 119±1 | 105±4 | 118±1 | 103±1 |
| Restraints | 81 | 89 | 78 | 84 | 78 | 89 |
| $Q_a$ | 0.04 | 0.04 | 0.04 | 0.04 | 0.04 | 0.04 |

**Table A2.2** PCS-based Δχ-tensor parameters of Co(II)-TraNP1 attached to T109C/T111C BCX, fitted to three crystal structures.

| PDB | 2bvv[4] | | 3vzm[5] | | 1bvv[4] | |
|---|---|---|---|---|---|---|
| Probes | RR | SS | RR | SS | RR | SS |
| $\Delta\chi_{ax}$ [a] | 3.8±0.2 | 2.6±0.1 | 3.8±0.2 | 2.6±0.1 | 3.8±0.2 | 2.6±0.1 |
| $\Delta\chi_{rh}$ [a] | 0.5±0.1 | 0.6±0.1 | 0.5±0.1 | 0.6±0.2 | 0.5±0.1 | 0.6±0.1 |
| X (Å) [b] | 17.3±0.2 | 17.1±0.1 | 17.2±0.2 | 17.4±0.1 | 17.4±0.2 | 17.1±0.1 |
| Y (Å) [b] | 13.9±0.2 | 14.1±0.2 | 13.8±0.2 | 14.1±0.2 | 13.6±0.2 | 14.5±0.2 |
| Z (Å) [b] | 39.3±0.1 | 39.4±0.1 | 39.6±0.1 | 39.4±0.1 | 39.2±0.1 | 39.7±0.2 |
| α (°) | 2.7±1 | 173±2 | 4.5±4 | 169±3 | 177±4 | 176±2 |
| β (°) | 18±2 | 156±1 | 18±2 | 155±1 | 161±2 | 157±1 |
| γ (°) | 137±1 | 37±4 | 134±1 | 31±1 | 38±1 | 41±1 |
| Restraint | 105 | 100 | 105 | 99 | 104 | 99 |
| $Q_a$ | 0.05 | 0.06 | 0.05 | 0.06 | 0.05 | 0.07 |

**Table A2.3** PCS-based Δχ-tensor parameters of Co(II)-TraNP1-SS attached to E24C/A28C ubiquitin, fitted to three crystal structures.

| PDB | 2mjb[6] | 1d3z[7] | 3onz[8] |
|---|---|---|---|
| $\Delta\chi_{ax}$ [a] | 2.0±0.1 | 2.0±0.1 | 1.8±0.1 |
| $\Delta\chi_{rh}$ [a] | 0.4±0.1 | 0.6±0.1 | 0.3±0.1 |
| X (Å) [b] | 4.2±0.6 | 5±0.6 | 3.9±0.4 |
| Y (Å) [b] | 3.6±0.3 | 4.2±0.5 | 2.4±0.4 |
| Z (Å) [b] | -14.4±0.3 | -14.1±0.4 | -14.1±0.2 |
| α (°) | 71±16 | 71±12 | 73±22 |
| β (°) | 56±2 | 50±4 | 65±2 |
| γ (°) | 96±13 | 88±11 | 93±20 |
| Restraint | 45 | 45 | 45 |
| $Q_a$ | 0.04 | 0.05 | 0.04 |

[a] $\Delta\chi_{ax}$ and $\Delta\chi_{rh}$ are in $10^{-32}$ $m^3$; [b] the coordinates of the Co(II) are in the frame defined by the PDB file;

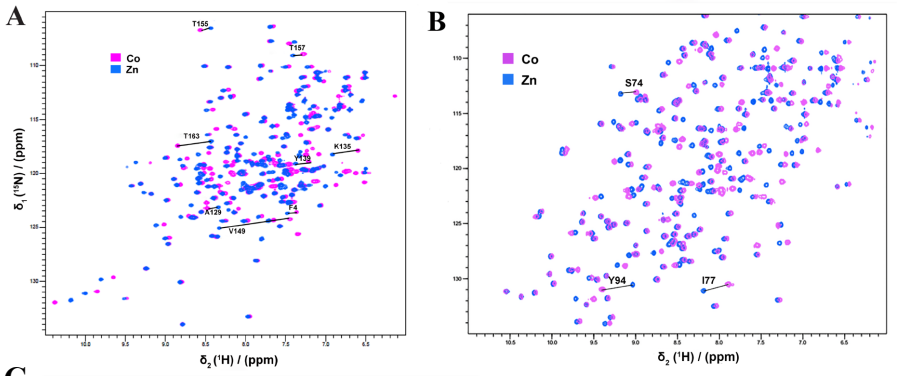


**App. Figure A2.4** Overlay of $^{1}H$-$^{15}N$ HSQC spectra of Co(II) (magenta) and Zn(II) (blue) loaded TraNP1-SS attached to T4Lys K147C/T151C (**A**) BCX E78Q/T109C/T111C (**B**) and ubiquitin E24C/A28C. Several PCSs are indicated with solid lines and residue numbers. The NMR spectra were recorded at 14.1 T (600 MHz).

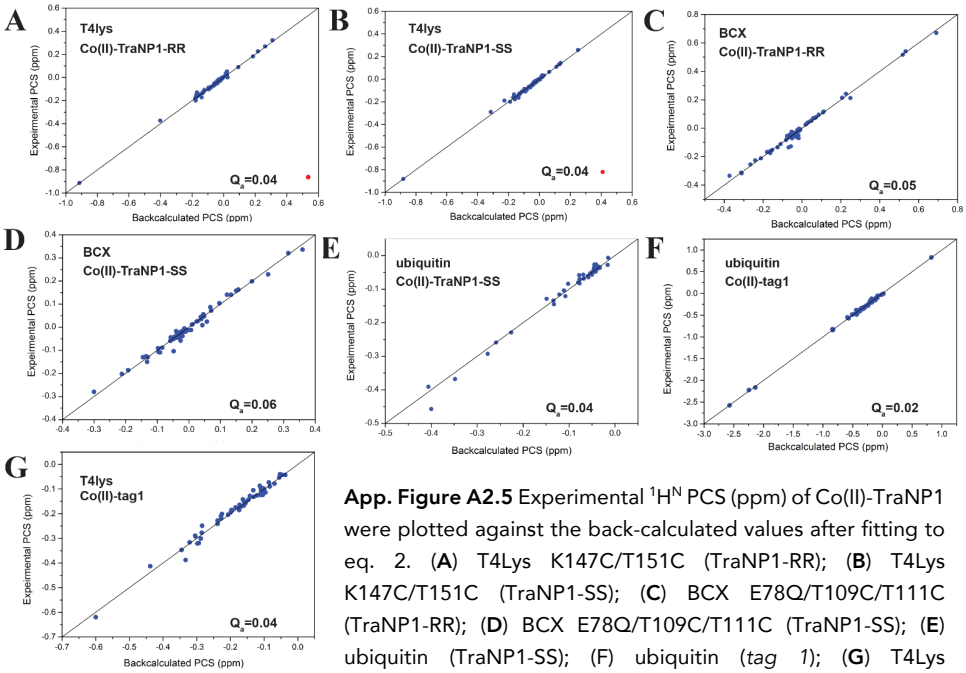


**App. Figure A2.5** Experimental $^{1}H^{N}$ PCS (ppm) of Co(II)-TraNP1 were plotted against the back-calculated values after fitting to eq. 2. (**A**) T4Lys K147C/T151C (TraNP1-RR); (**B**) T4Lys K147C/T151C (TraNP1-SS); (**C**) BCX E78Q/T109C/T111C (TraNP1-RR); (**D**) BCX E78Q/T109C/T111C (TraNP1-SS); (**E**) ubiquitin (TraNP1-SS); (F) ubiquitin (*tag 1*); (**G**) T4Lys K147C/T151C (*tag 1*). The solid line represent a perfect correlation.

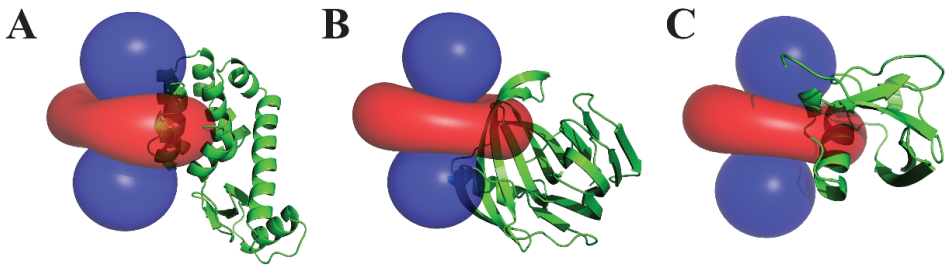


**App. Figure A2.6** PCS isosurfaces of TraNP1-SS plotted on the structures of T4Lys K147C/T151C (PDB entry 2zlm)[1] (**A**), BCX E78Q/T109C/ T111C (PDB entry 2bvv)[4] (**B**) and ubiquitin E24C/A28C (PDB entry 2mjb)[6] (**C**). The protein backbones are drawn in green ribbon representation. The iso-surfaces correspond to PCSs of ±0.2 ppm. Positive and negative PCSs are indicated by blue and red, respectively.

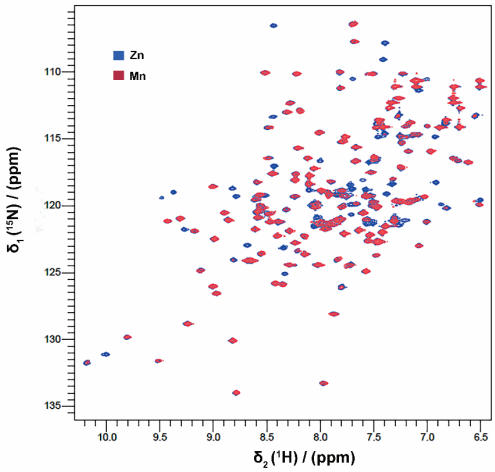


**App. Figure A2.7** Overlay of $^{1}H$-$^{15}N$ HSQC spectra of Mn(II)-TraNP1-SS (red) and Zn(II)-TraNP1-SS (blue) attached to T4Lys K147C/T151C. The NMR spectra were recorded at 14.1 T (600 MHz).

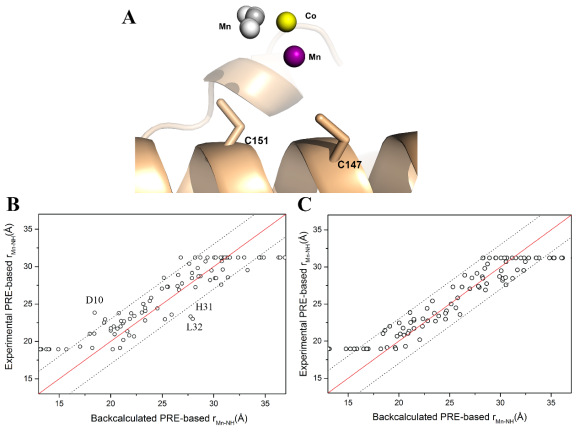


**App. Figure A2.8** Analysis of PRE data. (**A**) The positions obtained for the metal in TraNP1-SS relative to the T4Lys K147C/T151C backbone (wheat, PDB entry 2lzm) are shown as spheres. The PCS-based Co(II) position is in yellow. The position of purple sphere is found when including all Mn(II) PRE data. The grey spheres are found when the PRE for residues 10, 31 and 32 are left out, in five fits with random starting positions of the metal; (**B+C**) Experimental amide proton-to-Mn(II) distances plotted against the back-calculated values, including (**B**) or excluding (**C**) the distances for residues 10, 31 and 32. The red solid lines represent a perfect correlation and the dotted lines indicate a ±3 Å range.

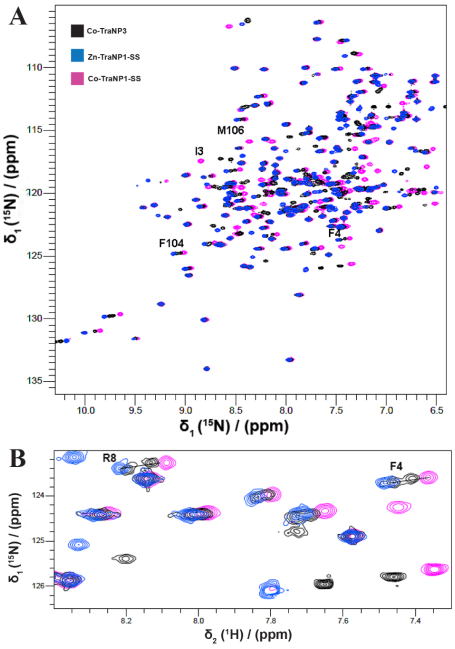


**App. Figure A 2.9** Overlays of $^{1}$H-$^{15}$N HSQC spectra for various TraNPs attached to T4Lys K147C/T151C. **A**) Co/Zn-TraNP1 and Co-TraNP3-S; **B**) Detail. Several PCS are indicated with residue numbers. The NMR spectra were recorded at 14.1 T (600 MHz).

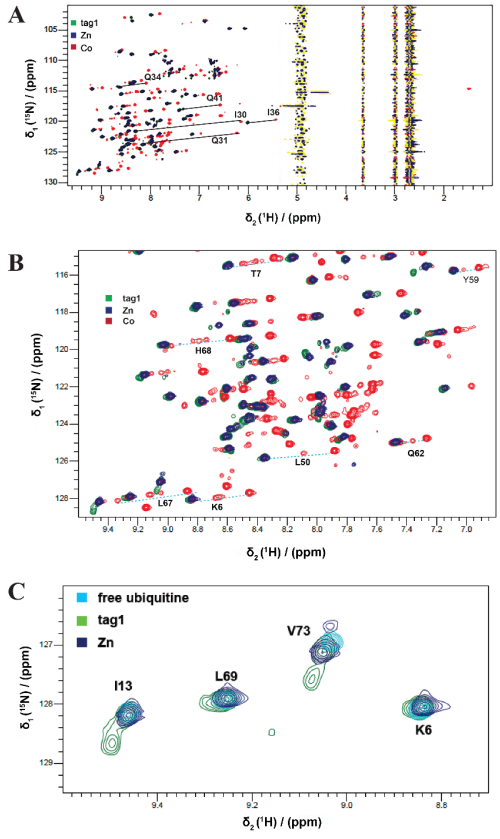


**App. Figure A2.12** Overlay of $^{1}$H-$^{15}$N HSQC spectra of Co(II)-*tag 1* (red), Zn(II)-*tag1* (dark blue), metal-free *tag 1* (green) linked to ubiquitin E24C/A28C and untagged ubiquitin E24C/A28C (cyan). (**A**) Full spectrum, several PCSs are indicated with black solid lines and residue numbers; (**B**) Detail, showing some amides for which multiple PCS were observed (cyan dashed lines). (**C**) Detail, showing the double peaks that appear in ubiquitin linked to *tag 1* but not in the untagged protein or when *tag 1* is bound to Zn(II). The NMR spectra were recorded at 14.1 T (600 MHz).

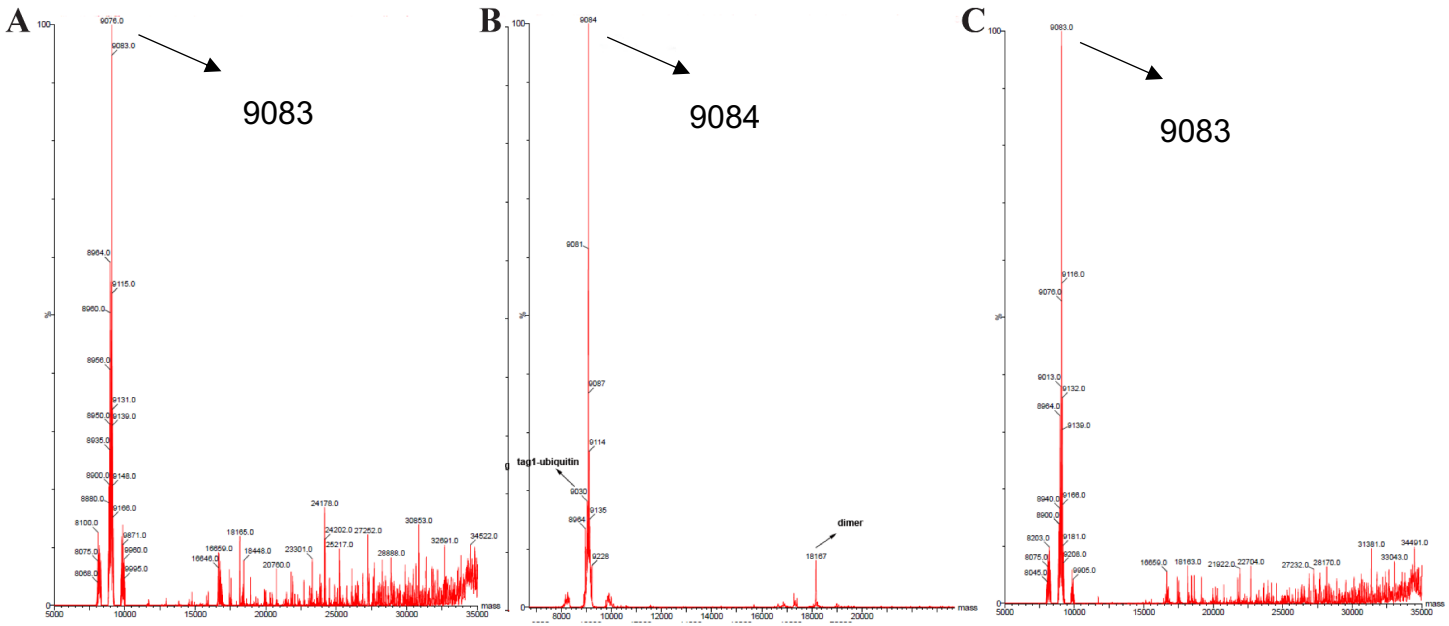


**App. Figure A2.10** MALDI-TOF mass spectra of $^{15}$N-riched *tag 1* (**A**), Co-*tag 1* (**B**) and Zn-*tag 1* (**C**) labeled $^{15}$N-riched ubiquitin mutant

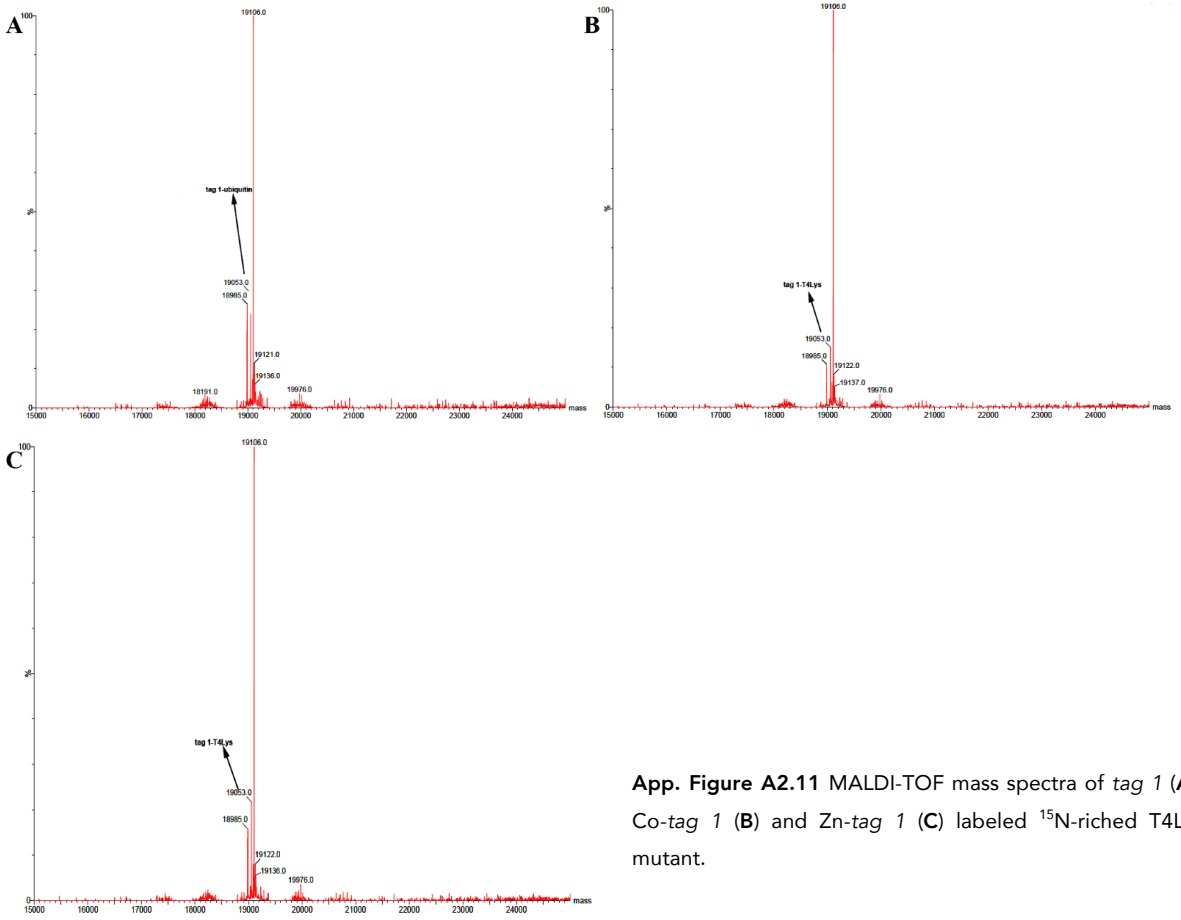


**App. Figure A2.11** MALDI-TOF mass spectra of *tag 1* (**A**), Co-*tag 1* (**B**) and Zn-*tag 1* (**C**) labeled $^{15}$N-riched T4Lys mutant.

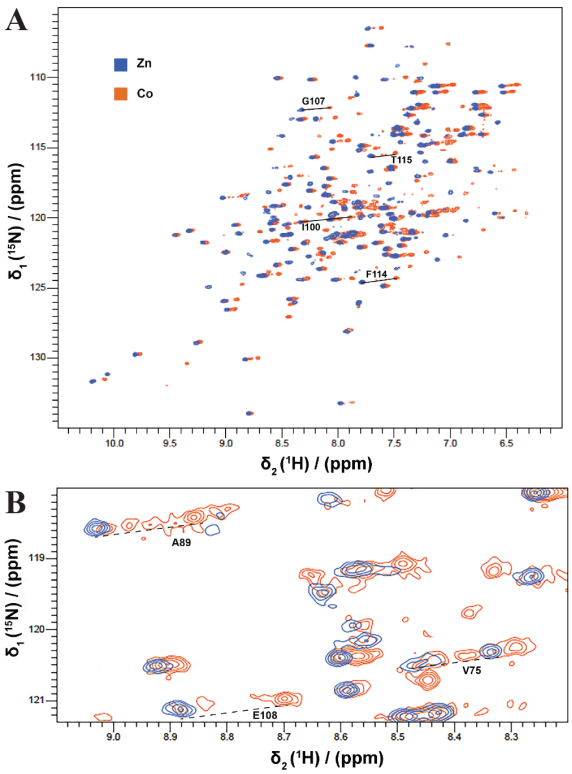


**App. Figure A2.13** Overlay of $^{1}H$-$^{15}N$ HSQC spectra of T4Lys K147C/T151C linked to Co(II) (orange, 10 eq.) or Zn(II) (blue, 1.2 eq.) loaded *tag 1*. (**A**) full spectrum, (**B**) Detail. Several PCSs are indicated with dash lines and residue numbers. The NMR spectra were recorded at 14.1 T (600 MHz).

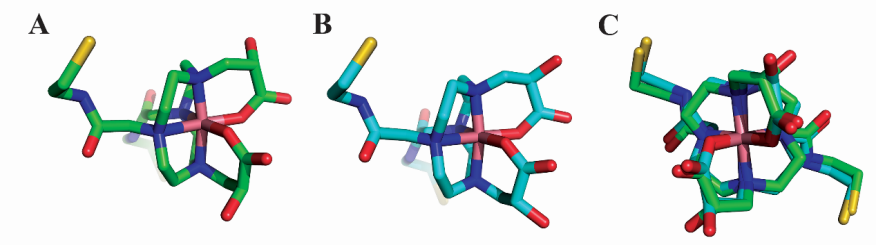


**App. Figure A2.14** Structure models of TraNP1. (**A**) Co-TraNP1-SS, side view; (B) Co-TraNP1-RR, side view; (**C**) overlay of Co-TraNP1-RR and -SS, view along the symmetry axis.

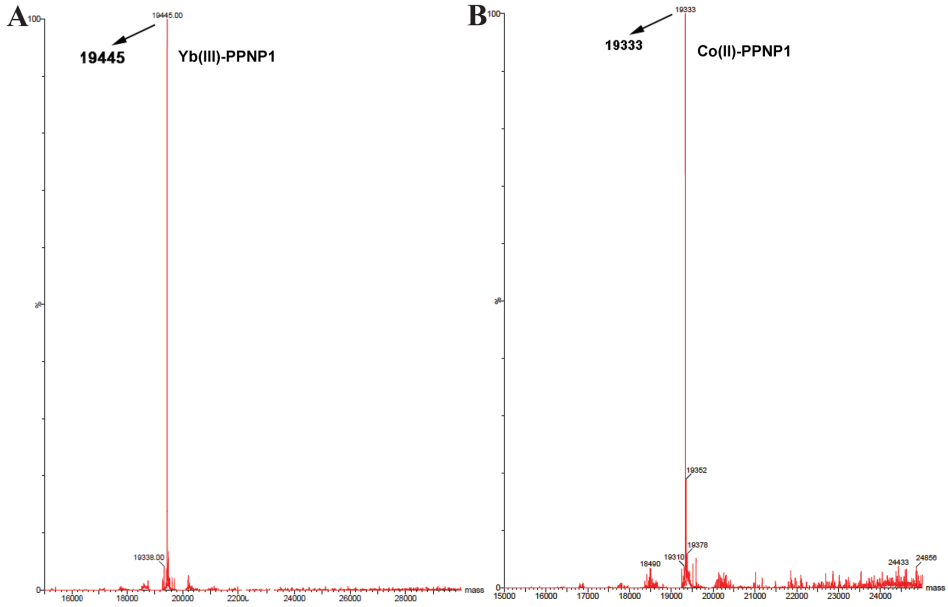


**App. Figure A3.1** MALDI-TOF mass spectra of Yb(III)-TraNP2 (**A**) and Co(II)-TraNP2 (**B**) labeled $^{15}N$-enriched T4Lys mutant

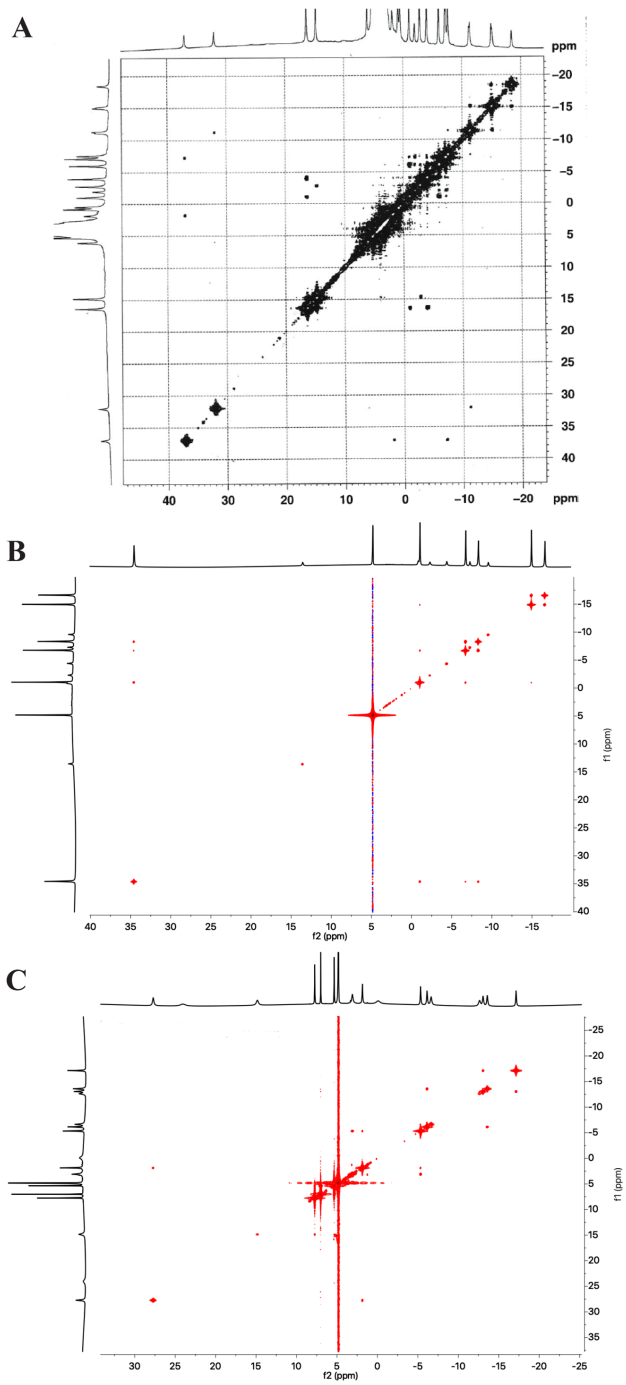


**App. Figure A4.1** 2D $^{1}$H COSY spectra of Eu(III)-HMDOTA (**A**), Eu(III)-DOTA, (**B**) and Eu(III)-PyDOTA (**C**).

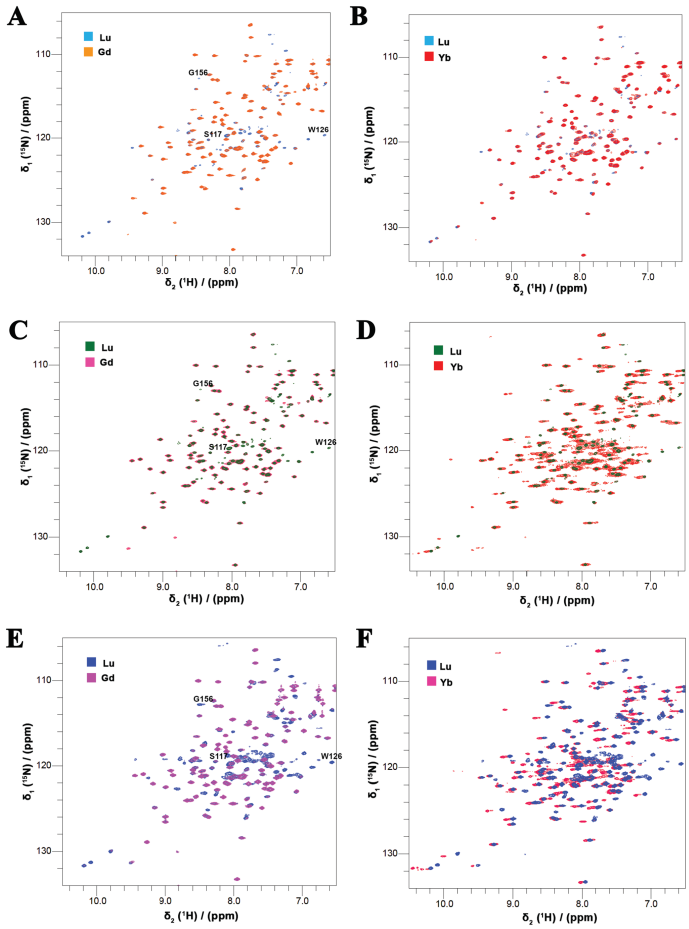


**App. Figure A5.1** Overlay of $^{1}$H-$^{15}$N HSQC spectra of Lu(III), Gd(III) and Yb(III) loaded CLaNP13a (**A, B**), CLaNP13b (**C, D**), or CLaNP13c (**E, F**) attached to T4Lys K147C/T151C. The NMR spectra were recorded at 14.1 T (600 MHz). Peaks of residues mentioned in the text are labeled.

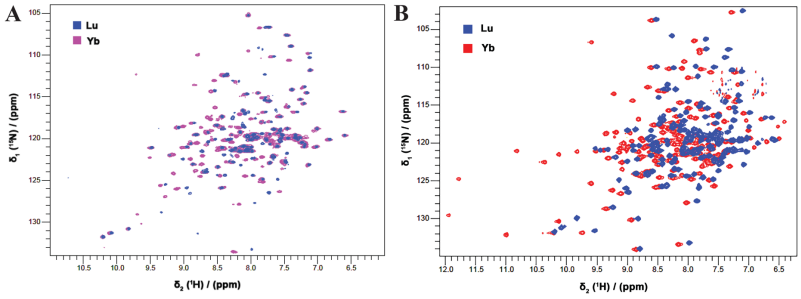


**App. Figure A5.2** Overlay of $^{1}$H-$^{15}$N HSQC spectra of Yb(III) and Lu(II) loaded CLaNP5 attached to T4Lys N55C/V57C (**A**) and T4lys K147C/T151C (**B**). The NMR spectra were recorded at 14.1 T (600 MHz).

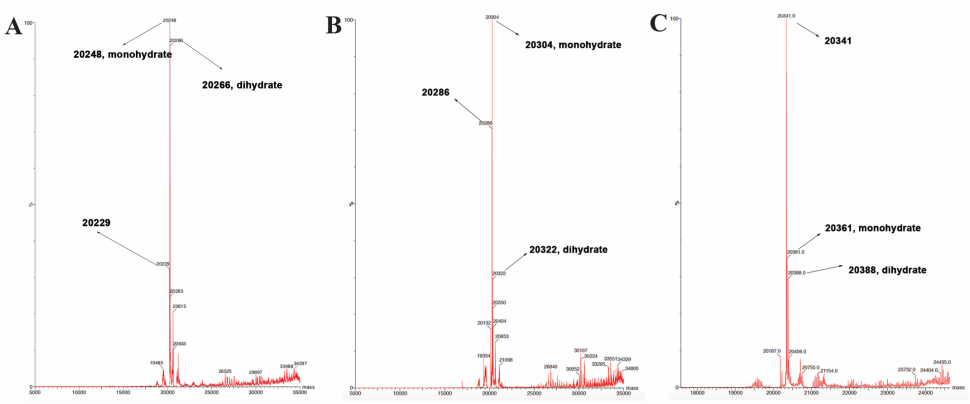


**App. Figure A5.3** ESI-TOF MS spectra of CLaNP13a (**A**), CLaNP13b (**B**) and CLaNP13c (**C**) linked to T4Lys N55C/V57C/T147C/N151C mutant.

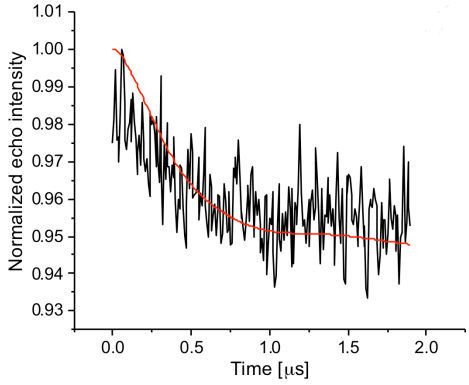


**App. Figure A5.4** Background corrected DEER time traces for Gd-CLaNP13b linked to T4Lys N55C/V57C/K147C/T151C in-cell.

## References

(1) Weaver, L. H.; Matthews, B. W. Structure of Bacteriophage T4 Lysozyme Refined at 1.7 Å Resolution. *J. Mol. Biol.* **1987,** *193*, 189-199.

(2) Liu, L.; Quillin, M. L.; Matthews, B. W. Use of Experimental Crystallographic Phases to Examine the Hydration of Polar and Nonpolar Cavities in T4 Lysozyme. *Proc. Natl. Acad. Sci.* **2008,** *105*, 14406.

(3) Heinz, D. W.; Baase, W. A.; Matthews, B. W. Folding and Function of a T4 Lysozyme Containing 10 Consecutive Alanines Illustrate the Redundancy of Information in an Amino Acid Sequence. *Proc. Natl. Acad. Sci.* **1992,** *89*, 3751-3755.

(4) Sidhu, G.; Withers, S. G.; Nguyen, N. T.; McIntosh, L. P.; Ziser, L.; Brayer, G. D. Sugar Ring Distortion in the Glycosyl-Enzyme Intermediate of a Family G/11 Xylanase. *Biochemistry* **1999,** *38*, 5346-5354.

(5) Ludwiczek, M. L.; D'Angelo, I.; Yalloway, G. N.; Brockerman, J. A.; Okon, M.; Nielsen, J. E.; Strynadka, N. C. J.; Withers, S. G.; McIntosh, L. P. Strategies for Modulating the pH-Dependent Activity of a Family 11 Glycoside Hydrolase. *Biochemistry* **2013,** *52*, 3138-3156.

(6) Maltsev, A. S.; Grishaev, A.; Roche, J.; Zasloff, M.; Bax, A. Improved Cross Validation of a Static Ubiquitin Structure Derived from High Precision Residual Dipolar Couplings Measured in a Drug-Based Liquid Crystalline Phase. *J. Am. Chem. Soc.* **2014,** *136*, 3752-3755.

# List of publications

***Related to this thesis***

1. **Qing Miao**, Wei-Min Liu, Thomas Kock, Anneloes Blok, Monika Timmer, Mark Overhand, Marcellus Ubbink. A double armed, hydrophilic, transition metal complex as paramagnetic NMR probe. ***Angew. Chem. Int. Ed*, 2019,** 58, 13093–13100.

2. **Qing Miao**, Enrico Zurlo, Simon Peter Skinner, Donny de Bruin, Joeri Wondergem, Anneloes Blok, Monika Timmer, Mark Overhand, Martina Huber, Marcellus Ubbink. A two-armed probe for in-cell DEER measurements on proteins. (To be submitted)

3. **Qing Miao**, Mark Overhand, and Marcellus Ubbink. Rigidified and hydrophilic DOTA-like lanthanoid ligands: Design, synthesis, NMR studies and molecular modelling. (In preparation)

***Other publications***

4. Xuwei Fu, Pei Wang, **Qing Miao**, Kaiqiang Liu, Huijing Liu, Jianfei Liu and Yu Fang. Polymerizable organo-gelator-stabilized gel-emulsions toward the preparation of compressible porous polymeric monoliths. ***J. Mater. Chem. A,* 2016**, 4, 15215–15223.

5. Xiangli Chen, Lingling Liu, Kaiqiang Liu, **Qing Miao**, Yanchao Lv and Yu Fang. Compressible porous hybrid monoliths: preparation via a low molecular mass gelators-based gel-emulsion approach and exceptional performances. ***J. Mater. Chem. A,* 2015**, 3, 24322-24332.

6. **Qing Miao**, Xiangli Chen, Lingling Liu, Yu Fang. Synergetic effect based gel-emulsions and their utilization for the template preparation of porous polymeric monoliths. ***Langmuir,* 2014,** 30, 13680−13688.

7. Xiangli Chen, Lingling Liu, Kaiqiang Liu, **Qing Miao** and Yu Fang. Facile preparation of porous polymeric composite monoliths with superior performances in oil–water separation-a low-molecular mass gelators-based gel emulsion approach. ***J. Mater. Chem. A*, 2014**, 2, 10081-10089.

8. Xue Min, **Miao Qing**, Fang Yu. Synthesis and gelation properties of cholesterol-based new low-molecular-mass gelators. ***Acta Phys. Chim. Sin.*, 2013**, 29, 2005-2012.

# Curriculum vitae

Qing Miao was born on 28th of December 1988 in Xi'an, China. She began her Bachelor education in Chemistry in 2008 at Xi'an University. For her Bachelor's thesis, she joined Prof. Dr. Yu Fang's group in Shaanxi Normal University. In 2012, she obtained her Bachelor diploma and received the "JiXue" scholarship for three years of Master education at Shaanxi Normal University. During her Master research, she was supervised by Prof. Dr. Yu Fang to develop new porous polymer materials for volatile organic compounds (VOCs) for adsorption and storage of oily matters. At that time, she discovered the power of fundamental research and the charm of physical chemistry by the guidance of Prof. Dr. Yu Fang. In 2015, she graduated with Honours and decided to further extend her research abroad. In the same year, she was funded by the Chinese Scholarship Council (CSC) to start her doctoral research under the supervision of Prof. Dr. Marcellus Ubbink at Leiden University. During her PhD, she became attracted to the power of paramagnetic NMR and design and synthesis several paramagnetic NMR probes for proteins with the help of Dr. Mark Overhand in the Bio-organic synthesis group. The results of this research are presented in this thesis.